UNIVERSITAT POLITÈCNICA
DE CATALUNYA
BARCELONATECH

CFD studies of reactive flow with thermal and mass diffusional effects in a supercritical packed bed catalytic reactor

by

Samuel J. Mekala

CFD studies of reactive flow with thermal and mass diffusional effects in a supercritical packed bed catalytic reactor

Doctoral Thesis

by

Samuel J. Mekala

Submitted to the Department of Chemical Engineering of the

Universitat Politècnica de Catalunya

in partial fulfillment of the requirements for the

Degree of Doctor of Philosophy

In Chemical Process Engineering

Supervised by:

Prof. Alfredo Guardo Zabaleta

Department of Chemical Engineering

Universitat Politècnica de Catalunya

Barcelona, September 2016

Ad Dei Gloriam

Summary

Packed bed reactors are widely used in various chemical processes. Fundamental understanding of the heat and mass transfer phenomena in the packed beds is essential for better modelling of these processes. Theoretical models used to describe the flow in packed beds generally assume an effectively homogeneous systems ignoring the complexities of flow in the void spaces of the packed beds. These details may however be influencing significantly the various phenomena in the system. To enhance this understanding, Computational Fluid Dynamics (CFD) is used to obtain detailed flow, temperature and concentration profiles in packed bed with multiple species undergoing heat and mass transfer with accompanying reaction in a heterogeneous catalytic reactor model. CFD is a simulation tool that through solving of momentum, mass and energy balances around complex geometries gives advanced view of fluid flow and transport mechanisms in the catalytic reactor.

In this thesis work, fluid flow and heat and mass transfer phenomena in packed beds is solved using CFD codes, developing a modelling strategy to design heterogeneous reaction packed bed equipment. Supercritical transesterification reaction process, for which experimental data was available, was taken as a reference for simulation models. Due to the complexity of this process which involves various transport phenomena, and extreme operating conditions, each of the transfer process occurring in the packed bed is studied distinctly.

A state-of-the art and a literature review is presented for CFD applications in packed beds, supercritical fluids and transesterification reaction. The governing equations and accompanying complementary models used in the simulations are presented. Physical properties of the reaction components methanol, triolein, diglyceride, mono-glyceride, fatty acid methyl esters, and glycerol at supercritical conditions are estimated. A geometrical model of reactor, which is a cylindrical tube filled with cylindrical particles arranged randomly, is developed. A 120-degree segment of packed bed tube is generated and validated against a complete wall-segment bed. Mesh influence over the flow is checked for different mesh refinement and a mesh of optimal refinement, independent of the mesh is selected for further study.

As the packed bed is heated from the walls, wall-to-fluid heat transfer in packed beds is analysed, and CFD obtained results are used to assess the flow and thermal effects in packed bed. Free and forced convection effects are comparatively analysed on axial lines and radial planes, identifying the regions of mixed convection. Heat transfer coefficients are obtained from CFD data using established theoretical models. The results are also related with empirical correlations analysing comparable trends.

Particle-to-fluid mass transfer in packed beds is also studied with the triolein diffusion from particles to analyse the diffusional effects in the bed. For an analogous energy transfer, particle-to-fluid heat transfer is also studied. Flow effects resulting from density, temperature, concentration gradients are analysed. Free/forced heat and mass convection for these situations is comparatively analysed on axial lines and radial planes, identifying the areas of mixed convection and compared against reported data. Heat and mass transfer coefficients are obtained from the CFD data using theoretical models. Numerical results obtained are presented and compared against empirical correlations on mass transfer for supercritical extraction. And correspondingly for the particle to fluid heat transfer simulations.

Applicability of available reaction kinetics for transesterification reaction is studied. Packed bed models are prepared for one-step irreversible and three-step reversible reaction kinetics, for different temperatures and space-times. Flow effects resulting from density, temperature, concentration gradients and changes in velocity are analysed. The yield of FAME, conversion of triolein for different temperature or space times are comparatively analysed. Free/forced mass convection for these situations is analysed on axial lines and radial plane. Reaction rates numerically obtained results are compared against experimental results, and flow, concentration and conversion profiles are obtained and analysed. Effects of the two kinetic models is studied for the simulated conditions.

Transesterification reaction in supercritical packed bed reactor is modelled along with heat and mass transfer effects. The obtained numerical results for heat transfer and mass transfer simulations were validated against empirical correlations. The obtained results in reaction simulations show good agreement with experimental results for smaller lengths of the reactor and lower space times. However intra-particle simulations are necessary in reaction simulations in order to account for the mass-transfer resistance observed in experiments which reduced the conversions as compared to simulations, with the increase in reactor length and space-time. Conclusively, the applicability of CFD in modelling heat and mass transfer with reaction at supercritical conditions is ascertained.

Resumen

Los reactores de lecho empacado son ampliamente utilizados en diversos procesos químicos. La comprensión de los fenómenos de transferencia de calor y masa en estos equipos es esencial para una mejor modelización de sus procesos. Los modelos teóricos utilizados para describir el flujo en lechos de relleno generalmente asumen sistemas homogéneos haciendo caso omiso de las complejidades de flujo en el espacio intersticial del relleno. Estos detalles pueden sin embargo influir significativamente en los diversos fenómenos que ocurren en el sistema. La Dinámica de Fluidos Computacional (CFD) puede utilizarse para profundizar en el conocimiento de estos fenomenos obteniendo información detallada del flujo, la temperatura y la concentración de reactivos y productos en el interior del relleno, resultado de los fenómenos de transferencia de calor y masa con reacción química en un modelo de reactor catalítico heterogéneo.

En este trabajo de tesis, los fenómenos de flujo y transferencia de calor y masa en lechos empaquetados se resuelve mediante códigos CFD, desarrollando una estrategia de modelado utiles para diseñar reactores de lecho empacado. Se seleccionó como referencia del modelo computacional un proceso de reacción de transesterificación supercrítica, para el que se disponía de resultados experimentales previamente obtenidos. Debido a la complejidad de este proceso que implica varios fenómenos simultáneos, y las condiciones de funcionamiento extremas del proceso seleccionado, cada uno de los fenómenos de transferencia fueron estudiados individualmente.

Este trabajo incluye un estado de la técnica y revisión de la literatura para aplicaciones de CFD en lechos empacados, fluidos supercríticos y procesos de transesterificación. Se presentan las ecuaciones fundamentales y los modelos complementarios utilizados en el modelado numérico. Se estiman las propiedades físicas de reactivos y productos participantes en el proceso (metanol, trioleína, diglicérido, monoglicérido, ésteres metílicos de ácidos grasos y glicerol) en condiciones supercríticas. Se presenta un modelo geométrico de reactor catalítico heterogéneo, que es un tubo cilíndrico lleno de partículas cilíndricas dispuestas al azar, basado en el reactor la planta piloto usada en el estudio experimental previo. Se generó un modelo de 120º de la circunferencia del reactor de lecho empacado, en el cual se llevaron a cabo estudios de independencia de malla sobre los resultados.

Se estudian los efectos de la trasnferencia calor pared-fluido, y los resultados obtenidos con CFD son utilizados para revisar los efectos de flujo radial sobre el flujo dentro del lecho empacado. Los resultados obtenidos son comparados contra correlaciones empiricas,

obteniendo tendencias similares. También se estudió la transferencia de materia partícula-fluido a través de comparación contra correlaciones empíricas y análisis de la convección mixta (natural+forzada) a alta presión. La reacción de transesterificación fue implemetada en el modelo computacional usando un modelo cinético de un paso y un modelo cinético de tres pasos, para diferentes temperaturas y tiempos de residencia. Los reusltados son comparados con datos experimentales previamente otenidos por el grupo de investigación.

Acknowledgements

I would like to express my sincere gratitude and respect to my thesis supervisor Prof. Alfredo Guardo Zabaleta for his guidance throughout my research work. I would like to thank Prof. M. A. Larrayoz the thesis supervisor during the early period of the thesis development. Their encouragement made the initiation of this work possible and whose patient supervision was essential during the course of this research work. Their technical, moral and economic support is very much esteemed.

I would also like thank Prof. Francesc Recasens head of the supercritical fluids research group for offering me the possibility to work in the group. His comments on my work and advise were helpful in having new insights in my research. Special thanks to Prof. Joachim Casal, director of the PhD program, for accepting me into the PhD, and his helping me to adjust to the university processes early at my arrival.

To all the administration staff of the Chemical Engineering Department, especially Irene Perez and Conchi Gonzalez my sincere thanks. I would like to thank IT staff Mr. Jose Luis for his support regarding the PC and software during my PhD work.

I would like to acknowledge the Erasmus Mundus External Cooperation Window, for the scholarship provided through the Willpower program.

I would like to my lab mates, Edresi, Miguel, Dr. Santana, and my friends in Barcelona for making my stay pleasant, Brent C., John C., Brandi, Gèrman, Cesar, Pau, Dwight, Austin, Tony, Rachael Tyler, Vinoth, Shrikanth, Nikhil, Salvador, Rafa … And my friends in India, who keep me up with the things Rajesh, Venu, Gipson, Ravi B., Santhi, Divya… Special thanks to my dear friend and mentor Dr. Agile Mathew, for his moral support and direction.

I want to express my deep gratitude to my father, mother, brother and sister for their love, prayers and support all through my life. They made me who I am today.

Above all, I am grateful to God, who gave me everything.

-Samuel

TABLE OF CONTENTS

List of Figures

List of Tables

Nomenclature

C_p	Specific heat	J / kg·K
D, D_{AB}	Diffusion coefficient	m^2 / s
P	Pressure	Pa
d,	Packed bed diameter	M
D_p	Particle diameter	M
g	Acceleration due to gravity	m / s^2
h	Heat transfer coefficient	W / m^2·K
k	Thermal conductivity	W / m·K
k_c	Mass transfer coefficient	m / s
L	Packed bed height	m
m	Mass	kg
$\dot{m}$	Mass flow rate	kg / s
M_w	Molecular weight	kg / kmol
P	Pressure	Pa
p	Static pressure	Pa
r	Reaction rate	mol / m^3 · s
R	Packed bed radius	m
T	Temperature	K
t	Time	s
U, u	Velocity	m / s
V	Volume	m^3
x, y, z	Cartesian coordinates	m
x	Axial coordinate	m
X	Species mass fraction	Dimensionless
y	Distance to the wall	m
Y_i	Mass fraction of species	Dimensionless
z	Compressibility factor	Dimensionless

Subscripts, Superscripts,

0	Referred to initial conditions / reference values
ax	Referred to axial property
c	Referred to critical property
eff	Referred to effective quantity
f	Referred to a fluid
i, j, k	Referred to Cartesian coordinates
	Referred to species
n	Referred to normal vector
p	Referred to particle
r	Referred to radial property
	Referred to reduced property
w	Referred to the wall
$\bar{}$	Referred to mean component of a variable
∞	Referred to a bulk property

Greek symbols

$\boldsymbol{\alpha_{ax}}$	Axial (fluid or thermal) diffusion coefficient	m^2/s
$\boldsymbol{\beta}$	Volumetric thermal expansion coefficient	1/K
$\boldsymbol{\gamma}$	Ratio of specific heats (C_p / C_v)	Dimensionless
$\boldsymbol{\varepsilon}$	Bed void fraction	Dimensionless
$\boldsymbol{\mu}$	Molecular dynamic viscosity	kg / m·s
$\boldsymbol{\nu}$	Molecular kinematic viscosity	m^2/s
$\boldsymbol{\rho}$	Density	kg / m^3
$\boldsymbol{\sigma}$	Dipole moment	C·.m

Dimensionless numbers

Bi	Biot number
Gr	Grashof number
Nu	Nusselt number
Pe	Peclet number
Pr	Prandtl number

Re	Reynolds number
Sh	Sherwood number
Sc	Schmidt number

Acronyms

CAD	Computer aided design
CAE	Computer aided engineering
CFD	Computational Fluid Dynamics
CP	Critical point
CSTR	Continuous stirred tank reactor
DG	Diglyceride
EOS	Equation of state
FAME	Fatty acid methyl ester
FD	Finite differences
FE	Finite elements
FV	Finite volumes
GL	Glycerol
MG	Monoglyceride
MRI	Magnetic resonance imaging
PDE	Partial differential equations
RANS	Reynolds-averaged Navier-Stokes
SCE	Supercritical extraction
SCF	Supercritical fluid(s)
TP	Triple point
TG	Triglyceride
UDE	User-defined equation
UDF	User-defined function

CHAPTER I

1. INTRODUCTION

1.1 MOTIVATION AND PROBLEM STATEMENT

Packed bed reactors are extensively used in the chemical process industries in wide range of applications due to their simplicity in structure and effectiveness in terms of providing abundant contact area for surface reaction or for heat or mass transfer area. Because of the packing structure which facilitates easy flow of fluid through the packings and having low pressure drop makes the packed beds basically advantageous in many applications.

Many mass transfer operations and catalytic processes are performed in packed beds. Mass transfer operations like leaching, extraction, adsorption/desorption involve packed beds. And catalytic processes in chemical industry, for example, steam reforming, CO conversion, ammonia synthesis, methanol synthesis and in petroleum refining, isomerization, polymerization, hydrocracking cracking, catalytic reforming all involve packed beds for heterogeneous catalytic reactions.

Packed beds are preferred due to their ease of operation, thermal and reactive efficiency. In the design of packed beds multiple factors come into consideration. The fluid dynamics study is essential to the design of the packed bed design for studying its flow regimes, pressure drop mass and momentum balance. The main considerations in the design of a packed bed are its, energy conservation (efficient use of energy), pressure drop, catalyst packing structure and shape to enhance catalyst effectiveness by providing adequate reaction surface area.

Catalysts were discovered in the early 20^{th} century which led to a breakthrough in the chemical industry. In packed bed reactors reactions occur on the catalyst particles which are placed inside the reactor tube randomly or structurally. The reactants enter from one end of the reactor and the products flow out from the other end. The catalyst tubes are heat exchanged form the walls wither by burners or heating/cooling jackets.

Catalytic reactors involve interactions of various chemical and physical processes. Which are broadly heat and mass transfer for physical process and the chemical reaction. Each involving a wide range of mathematical models, kinetic rate expressions for various configurations. The understanding of the influence of dispersion, momentum and energy transfers around the

catalyst with generation and dissolution of chemical components in the reactor is crucial in designing an effective reactor.

Various theoretical models were developed by many researchers over the decades explaining the various phenomena: heat transfer through the tube wall, convection of fluid, heat and mass transfer between the bulk fluid and catalyst pellets, flows involving reactions in the packed beds. Most of these models which are based on simplifying assumptions like simple geometric structure, pseudo-homogeneity, using correlation based effective transport parameters, unidirectional velocity field, using effectiveness factors in the reaction source terms, for the packed bed do not effectively represent the overall phenomena in the packed bed.

In case of supercritical transesterification catalytic reaction temperature in the bed (tube wall temperature is controlled using a heating jacket) is an important parameter in design and operation of the catalytic reactor determining the conversion in the bed. Having an optimal temperature for higher conversion is a design objective. The heat and mass transfer effects between the fluid and particle in supercritical conditions are an important aspects influencing the catalytic transesterification, as the reaction occurs on the particle surface. Ensuring proper transfer gradients between particles and fluid in necessary for reaction progress in the packed bed.

Several kinetic models for the supercritical transesterification reaction were proposed by researchers. Each of them adequate for particular reaction conditions. Studying the validity of these kinetic models is necessary for tweaking the reaction parameters for necessary output.

With the increase in the computational capabilities, computational fluid dynamics (CFD) has become robust tool in modelling the packed beds for the various situations addressed above. Unlike the conventional simplifying mathematical models, CFD models can be capable of having a more accurate model. CFD can provide a detailed flow structure along with mass, heat and reaction effects in the reactor, which is a remarkable improvement over traditional approach of obtaining flow and heat transfer data by sampling points in the packed bed by intrusive methods.

Many researchers have found the CFD as a reliable, accurate method for chemical equipment. Significant amount of information can be obtained for packed beds by using the CFD simulations. In the current research work the use and accuracy of CFD simulations has been studied for catalysed transesterification reaction under supercritical conditions. The packed bed wall-to fluid heat transfer, particle-to-fluid mass transfer, particle-to-fluid heat transfer and two

kinetic models, with one step irreversible and a three step irreversible kinetic model of transesterification have been studied for a packed bed of cylindrical catalyst particles.

In the following sections the nature of supercritical fluids, the development and advantages of computational fluid dynamics are presented. Transesterification reaction with supercritical CO_2 and methanol cosolvents is discussed along with packed bed equipment modelling using CFD.

1.2 PACKED BEDS

The extensive use of packed beds in chemical industry is attributed to their structural simplicity and effectiveness in providing abundant contact area for surface reaction or for heat or mass transfer area. A wide variety of chemical processes are facilitated by the packed beds including solid extraction, distillation, absorption, adsorption/desorption, catalytic heterogeneous reactions. Packed bed reactors are one of the most common reactors due to their high conversion rate per catalyst weight used in synthesis, effluent treatment and catalytic combustion. The reactors are becoming increasingly powerful due to the more sophisticated and wholly new catalysts being invented. The numerous processes employing the packed bed result in a variety of are equipment.

The main characteristics of the packed bed equipment are height to diameter ratio (L/D) of the packed tube, tube to particle diameter ratio (N), packing type and structure. Packing types range from catalyst pellets, for heterogeneous reactions, to seeds, largely used for oil extraction. Inert pellets are also used for providing contact area especially in counter current liquid-liquid operations. The geometrical characteristics (L/D) of the packed tube/reactor together with the packing structure (which includes particle's size, shape, porosity, the packing distribution and its void fraction) influence the radial and axial flow behaviour, conditioning also heat and mass transfer mechanisms. And with low N, the wall effects are present across the entire radius of the bed. These factors play a significant role in reaction rates in the packed bed reactors.

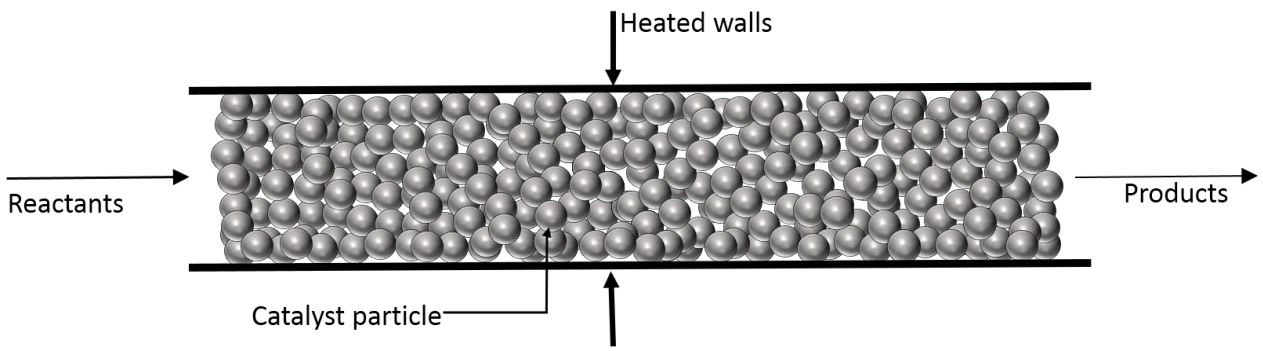

Figure 1-1 Packed bed reactor schematic with randomly packed spherical catalysts

As multiple factors influence the effectiveness of a packed bed, its modelling is a complex task. In the designing of a packed bed reactor, the design must include the mass and heat transfer effects as well as the chemical reactions. The packed catalyst is also critically important to the modelling of the device. Most theoretical models for packed bed heat and mass transfer lump several transport mechanisms into an effective parameter, making the models not so descriptive. Depending on the need, a variety of variations can be designed, by having, for example different temperature and reactant concentrations.

1.2.1 Packed bed modelling

A good qualitative description of the various physical and chemical processes taking place in the packed bed reactor is required for its effective design. With the various factors influencing the operation as described above, accurate modelling of these packed beds is complicated. Typically, the models provide grouped parameters for the easy description of the physical processes. These methods lack generality, resulting in multiple parameters for a specific equipment.

For the understanding of the processes taking place in the packed bed, it is necessary to obtain accurate data from inside the packed bed.

1.3 SUPERCRITICAL FLUIDS

A chemical element or compound or mixture is called a supercritical fluid (SCF) when its temperature and pressure are higher than its corresponding critical temperature (T_c) and critical pressure (P_c), but below the pressure required to condense it into solid. The critical point (CP in Figure 1-2) is the highest temperature and pressure at which the vapour and liquid co-exist at equilibrium.

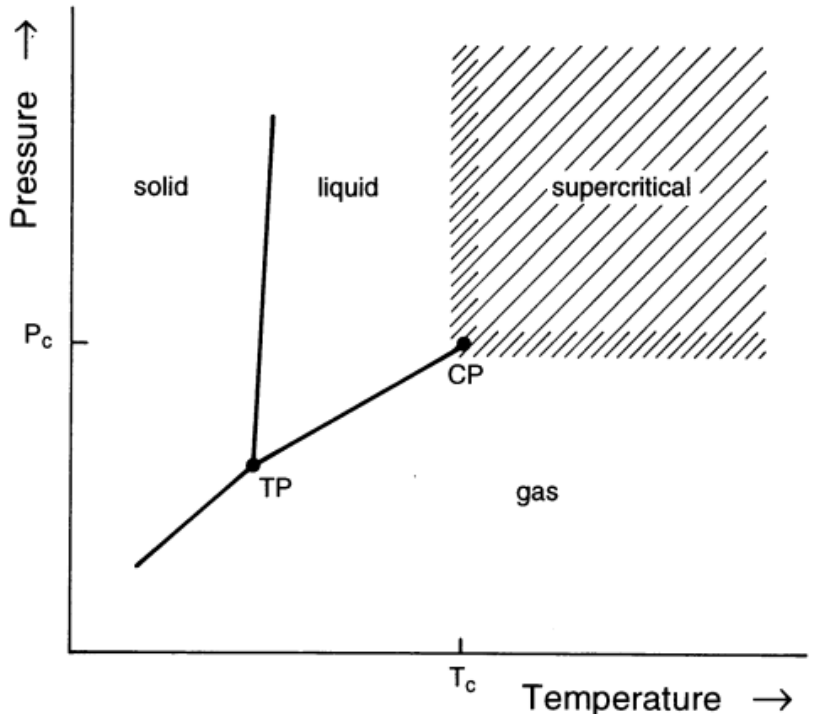

Figure 1-2 Supercritical state for a pure component. CP critical point, TP triple point, T_c critical temperature, P_c critical pressure (Brunner, 1994)

The properties of SCFs vary generally between those of liquids and gases. This is due to the fact that gaseous phase and liquid phases merge together and become indistinguishable at critical point. These properties, (especially density) are highly sensitive to small changes in the temperature and pressure near the critical point. But some properties like compressibility and the heat capacity are higher near the critical point than they are in liquids or gases. The properties change drastically with pressure near the critical point. This region where the changes are noticeable is commonly referred as 'near critical' region (often only referring to non-supercritical section). Density, viscosity and diffusivity of SCFs are shown in Table 1-1 together with typical values for gases and liquids. As can be seen from the table, the density of SCFs is two times that of a gas and less than half that of a liquid. It is this liquid like density of SCFs that allows many materials to be dissolved many times that predicted with ideal gas considerations. And so, temperature and pressure can be used for controlling the solubility and separation of a solute. Pressure and temperature are represented in terms of their reduced values which are the actual values divided by their critical values ($P_r=P/P_c$, $T_r=T/T_c$). The temperatures and pressures that is of most interest in SCF processes is between 1.0 and 1.2 for reduced temperatures and above 1 for reduced pressure.

Property	Gas	SCF	Liquid
Density [kg/m^3]	10^0	10^2	10^3
Viscosity [Pa·s]	10^{-5}	10^{-4}	10^{-3}
Diffusivity [m^2/s]	10^{-5}	10^{-7}	10^{-9}-10^{-10}

Table 1-1 Comparison of the physical properties of gases, liquids and SCFs (McCoy, 1999)

The mass diffusivity and viscosity are transport properties which influence rates of mass transfer. In general, these properties are at least an order of magnitude higher or lower than for liquids, respectively (see Table 1-1), meaning that the diffusion of a species through an SCF medium occurs at a faster rate than through a liquid solvent. Also, SCF are more efficient at penetrating a microporous solid structures, although mass transfer limitations do occur in SCF processes (Jessop and Leitner, 1999).

The diffusivity varies with both temperature and pressure and is strongly influenced by density and pressure (Liong et al., 1991). Density and viscosity both increase with pressure with a parallel decrease in the diffusion coefficient, however at high pressures this effect is less noticeable, as density will become less sensitive to pressure. The diffusion coefficient in general increases with temperature at constant pressure, however, when the density is constant, temperature has a minimal effect.

Supercritical fluids have a number of advantages over conventional liquid solvents. The distinct features of SCFs *viz*. adjustable solvent strength and favourable transport properties differentiate SCFs from liquid solvents. Another important advantage of SCFs is that after the release of pressure, components are left virtually free of residual supercritical solvent. Because of these advantages, i.e., high solubility of liquids and gases, and their tunability: adjusting the temperature and pressure to make alterations in physical properties making them from liquid-like to gas-like, SCFs are attractive as reaction and extraction media.

1.3.1 Supercritical fluids in Heterogeneous Catalysis

Heterogeneous catalysis has numerous industrial applications in chemical, pharmaceutical, automobile, petrochemical industries and emerging areas like fuel cells, green chemistry, and nanotechnology. About 90% of all chemical processes are heterogeneous catalytic in nature, according to some estimates. Principles of heterogeneous catalysis are typically formulated from studies of model catalysts in ideal reactor with simplified reactants.

Typically, a solid catalyst is used in a supercritical fluid as solvent. Catalytic heterogeneous reactions are very often controlled by the rate of diffusion to the catalyst surface. Because of the enhanced diffusion rates in SCFs (as discussed earlier), they are advantageous as reaction media in heterogeneous reactors over liquid solvents. Diffusion is enhanced in both the bulk phase and also within the pores of the catalyst particles (Jessop and Leitner, 1999)

As concluded by Baiker, (1999), SCFs can be used in many ways to control and improve heterogeneous catalytic reactions. As explained by Baiker, possibilities include:

(a) control of phase behaviour, elimination of gas/liquid and liquid/liquid mass transfer resistances, (b) enhanced diffusion rate in reactions controlled by external (fluid/particle) diffusion, (c) enhanced heat transfer, (d) easier product separation, (e) improved catalyst lifetime by dissolution of deactivating deposits, (f) tunability of solvent properties by pressure and cosolvents, (g) thermodynamic pressure effect on rate constants, and (h) control of selectivity by solvent-reactant (solute) interaction.

Continuous flow reactors are made possible because of the higher reaction rates and easy separation by the use of SCFs (Baiker, 1999). As Tundo, (1991) specifies, continuous processes reduce the needed size of the reactor. The reactions in SCF are characterized by reduced viscosity and improved mass transfer, when compared to liquid phase reactions With improved process control, enhanced productivity, easy separation of products from the catalyst and greater safety, packed bed continuous reactors are advantageous (Anderson, 2001). Continuous processes are also cost efficient compared to the batch processes on an industrial scale. When loading of reactants and recovery of products, depressurization can be circumvented in continuous operation, until the reaction is finished (Hyde et al., 2001). All these advantages cost and enhance operation, safety of the continuously operated high-pressure equipment.

Most of the SCFs study is focused on four fluids: CO_2, ethane, methane, and water. Among these, CO_2 is the most widely used, because it is non-toxic, non-flammable, relatively cheap, and inert. Some of the popular catalytic processes which can be implemented with supercritical fluids are, hydroformilation, hydrogenation of fats and oils, Fisher-Tropsch synthesis and transesterification.

1.4 COMPUTATIONAL FLUID DYNAMICS

Computational fluid dynamics (CFD) technique has become a standard in the modelling of flow systems in many areas of physical science and engineering. It can be used to build a mode for investigating flow, turbulence, heat and mass transfer characteristics of reactors and other

process equipment. For systems at high temperatures or pressure, or involving highly hazardous or corrosive materials, CFD models are may be the only good tools for studying the fluid dynamics.

CFD constitutes a third approach in studying the discipline of fluid dynamics after experimental and theoretical fluid dynamics. Until, say 1960, fluid dynamics was operating in two approaches of theory and experiments. And with the advent of high speed computers combined with accurate numerical algorithms has revolutionized the way we practice fluid dynamics. However, it should be noted that CFD only complements the theory and experiments and cannot replace either of them. Performing these CFD simulations using a program can be termed as numerical experiments, and they can be carried out in corresponding with physical experiments in a laboratory, and can sometimes be used to interpret the physical experiments.

With significant growth in computational capabilities over the last few decades, CFD has become one of the fast growing research area, with more and more applications as the capabilities become cheaper by day. In aerospace and automotive productions, CFD has taken a significant role, in which CFD has become an inexpensive alternative or supplement to the expensive tunnel testing resulting, thereby able to produce enhanced designs in lower periods of time. CFD has been used in for stress related calculations in construction applications, like flow in dams, canals etc, for a long time now. CFD has also been significantly used in the design of pumps, turbines and other related heavy mechanical equipment. Other major areas where CFD is used are manufacturing, environmental engineering applications, and naval architecture. The introduction of commercial CFD packages with specific fluid mixing programs and the option to solve chemical reactions has paved way for chemical engineering applications (Anderson, 1995; Harris et al., 1996; Ranade, 2003)

Numerical solutions for flow, mass and energy balances are obtained in complicated flow geometries using CFD software. Additional sets of equations are solved the are relevant to the specific problem at hand. These balance equations, the complete Navier-Stokes equations are solved by using a finite-difference numerical technique. The Navier-Stokes equations, along with other governing equations describing physical characteristics of fluid flow are presented and discussed in Chapter 2 of this thesis. The results show specific flow and heat transfer patterns that are hard to obtain experimentally or with conventional modelling methods.

CFD so can be used to have a detailed description of the flow in the packed bed. A detailed geometrical model resembling the flow field is necessary for a more accurate modelling. An unstructured grid can only be used for complex geometries like packed beds.

1.4.1 Development of CFD

The history of CFD is closely tied to the development of digital computer. Prior to the advent digital computers, most of the problems were solved analytically or empirically. In the 18th and 19th centuries, substantial work was done to mathematically describe the motion of fluids. In 18th Bernoulli's equation and Euler's equations which describe the conservation of momentum for an inviscid fluid, and conservation of mass were derived in the 18th century. Claud Navier and George Stokes introduced viscous transport into Euler's equations, resulting in the Navier-Stokes equations, which form basis for the modern day CFD, and include expression for the conservation of mass, momentum, pressure, species and turbulence.

Lewis Fry Richardson in 1922 developed numerical weather prediction system by dividing the physical space into mesh cells and used the finite difference approximations. It took six weeks to calculate weather for eight-hour period, ending up in failure. He proposed a solution to the massive calculation requirements, by proposing, what he called "forecast-factory". In which a large stadium is filled with thousands of people, each of them having a mechanical calculator performs a part of the flow calculation, while the leader in the centre uses signal lights to coordinate the calculations (Richardson, 1922). This would be an elementary form of CFD calculation. Thom, (1933) simulated flow past cylinder. Later Kawaguti, (1953) used mechanical desk calculator simulate and obtain solution for flow over cylinder. They took large periods of time, or huge human resources in obtaining the solutions.

Clough, (1960) the first comprehensive finite element method. Subsequently, it has been used for modelling fluid flow and heat transfer modelling. With ample ground work of numerical methods, numerical stability, iteration methods, by 1950, there was rapid growth in numerical simulations with the advent of electronic computing machines by the late 1950s.

Substantial breakthrough happened in the 1950s and 1960s towards solution of inviscid compressible flow equations. Lax, (1954) developed a technique which used the conservative form of governing equations. Particle-in-cell have been found to be intrinsically shock smearing (Evans and Harlow, 1957). A second order accurate finite difference scheme which reduces the shock smearing effect was proposed by Lax and Wendroff, (1960). This scheme later led to the development of the McCormack method (1969). Even today, some of these schemes are in extensive use. (Guardo, 2007)

Methods for handling flows in arbitrary shaped geometries have been significantly improved during 1980s. Techniques for converting complex geometries into simple ones have been

proposed. These methods were discussed by Thomson et al., (1985) and the assessments on this subject (Babuska et al., 1983; Pletcher et al., 1984) . Later, Baliga and co-workers (1983; 1983b;) have introduced a control volume based finite element method which can handle arbitrary geometries. Separately, weighted residual based FEM algorithms have been developed (Jackson and Cliffe, 1981; Peric, 1985; Taylor and Hughes, 1981). Majumdar et al., 1992; and Peric, 1985 have proposed the application of conservation laws to non-orthogonal control volumes. Research is still ongoing on these methods and several complex flow situations are being simulated using them. (Guardo, 2007).

While a large volumes of research publications have appeared in recent years on CFD, the potential for further research is expanding at an ever increasing rate. In future years, it appears that many more robust algorithms would be developed and several complex flow/heat/mass transfer problems would be successfully simulated.

1.4.2 CFD in chemical reaction equipment design

The wide variety of applications of CFD were extended to chemical engineering fields for reaction process equipment design and operation. The reaction equipment involves chemically reactive flows in single-phase or multiple-phases. Until the advent of CFD, this problem was typically solved with idealized and approximate solution strategies with experimental data wherever available. CFD techniques have effectively replaced these strategies.

The common step in all chemical process application is multiple chemical species come in contact with each other, involving mass transfer, heat transfer, or reaction. With the introduction of commercial packages in which chemical reactions can be readily defined, there has been rapid progress in the use of CFD for chemical reaction engineering applications. (Harris et al., 1996; Kuipers and van Swaaij, 1998; Ranade, 2002).

CFD models are used in the field of chemical reaction engineering for design, trouble shooting, and fundamental understanding. In designing models, quantitative relationship between the process equipment hardware and their performance is obtained. In trouble-shooting, various variables involved in the process are controlled in a statistical manner, in order to have an estimate of the possible cause of any issue in the equipment. Equipment designers would want CFD models which could predict what could happen as a result of a particular design, consequentially having a new design concept.

Catalytic reactors are characterized by the complex interaction of various physical and chemical processes. The transport of momentum, energy, and chemical species occurs not only in flow direction, but also in radial direction. Understanding the interaction of the catalyst with the

surrounding reactive flow is a significant challenge in catalysis. Sometimes, the exploration of these interactions can lead to the desired selectivity and yield. Hence, a better understanding these reactive flows in chemical reactors is necessary for the development of reliable simulation tools. CFD is able to predict complex flow fields, even combined with heat transport. Having detailed models for chemical reactions, especially for heterogeneous reactions is challenging because of many species conservation equations, their non-linear coupling.

The aim of CFD simulations of catalytic reactors is to comprehend the interactions of mass and heat transfer with the chemistry in the reactor, to support reactor design and engineering and to find optimal operational conditions for attaining maximum yield of wanted product and minimize the production of unwanted by-products.

1.4.3 CFD in packed beds

CFD has been widely used in heat and mass transfer and fluid flow behaviour in packed beds. CFD commercial software have become more sophisticated, allowing for more detailed simulations over complicated geometries. The factors effecting the operation of a packed beds are temperature, pressure, composition, flow rate, tube and particle dimensions. The design objective for a packed bed is to be having desired conversion or outlet temperature. This is achieved by adjusting the above parameters. For the case of a packed bed reactor the outlet concentration needs to be related to these parameters. Various mathematical models have been proposed and techniques were developed for solving these models.

Initially, packed bed CFD simulations used 2D models. Dalman et al., (1986) examined flow behaviour in an axisymmetric plane with 2 spheres; this limited strictly the packing arrangements but gave a first detailed understanding into fluid flow in packed beds.

As the commercial CFD software are expanding their possibilities and computer capabilities are increasing, the extent to which CFD can be applied to complicated systems has increased considerably. This enabled the use of three-dimensional models for the simulations in which the packing need not be symmetrical (an implied feature of two-dimensional models). Hence the true nature of the flow and transport effects can be shown, as they would be present in a packed bed.

1.5 OBJECTIVES AND SCOPE OF THE THESIS

Having realized the advantages of CFD in process equipment design, its ability to produce data that is comparable with experimental data, to produce information which otherwise cannot be

produced experimentally (due to equipment limitations), CFD can be used for study of packed bed design for heat and mass transfer along with reaction kinetics of transesterification reaction.

The general aim of the current work is to studying the modelling of a supercritical catalytic reactor using CFD by validating the simulation methodologies for solving fluid flow and heat and mass transfer, and reactive flow at supercritical conditions in packed bed of cylindrical catalysts packed randomly. To achieve this end, the following specific objectives are

- Attain familiarity with commercial CFD solver Ansys Fluent, by studying a flow validation case for flow over spherical/cylindrical particle in a rectangular duct.
- Estimation of physical properties at supercritical conditions for transesterification reaction components and comparing the properties with the CFD obtained properties.
- Develop a packed bed geometry with cylindrical particles resembling experimental model for use in simulations. Generation of mesh for the geometry and performing the mesh independence tests.
- Studying wall-to-fluid heat transfer in packed bed with higher temperature on the tube wall of the packed bed and comparing with standard correlations
- Studying particle-to-fluid heat transfer and mass transfer by having higher temperature on the cylindrical shaped catalyst particle surface or higher chemical species concentration on the particle surface respectively.
- Study one-step and three step kinetics of transesterification reaction in a catalytic reactor model with cylindrical particles under high pressure supercritical conditions using CFD with reaction activated on the particles surface.

1.6 THESIS STRUCTURE

And introduction is given to basic and state-of-the-art aspects of packed beds, supercritical fluids, and computational fluid dynamics, it's application for reaction equipment and in packed beds is presented in the Chapter 1. Chapter 2 deals with the important governing equations for fluid dynamics, which are mass, momentum, and energy conservation equations and their mathematical expressions for the CFD software uses, along with complementary models like species mixing, reactive flow models used for developing simulations in this thesis. The pre- and post-processing required for obtaining analysable data from the simulations is also presented. In Chapter 3, literature review for some of the aspects of study related to this thesis is presented. The literature review is presented for the packed bed reactor modelling, and its CFD applications, transesterification reaction and the use of supercritical fluids for the reaction.

In Chapter 4, physical properties estimation at supercritical conditions is explained. Density, viscosity, specific heat, thermal conductivities, are the primary properties for the reaction components (reactants and products) which are estimated as a function of temperature. Diffusivity of these components into carbon dioxide is estimated at different temperatures.

In Chapter 5, wall-to-fluid heat transfer in packed beds in supercritical conditions is analysed for a tertiary mixture of carbon dioxide, methanol and triolein. The temperature profiles obtained from CFD simulations are used to obtain wall Nusselt numbers. The velocity, concentration and temperature profiles are analysed. The CFD results were compared with empirical correlations for different flow rates. The results were compared for two different geometries: one-tenth model with periodical boundary conditions and a full length model were used.

In Chapter 6, particle-to-fluid heat transfer is studied with higher particles temperature than the inlet fluid (carbon dioxide, methanol and triolein). The comparison of the CFD obtained results with different empirical correlations is done and analysed.

In Chapter 7, particle-to-fluid mass transfer is studied with higher composition of triolein on the particles surface than in the inlet fluid, resembling extraction mass transfer process. Numerical results are presented and compared against experimental correlations.

In Chapter 8, the applicability of CFD for modelling and simulation of the transesterification reaction is investigated. The effect of two different kinetics, one step irreversible and three step reversible kinetics, in the conversion/yield is studied. The results were compared against experimental results obtained in our research group.

REFERENCES

Anderson, J.D., 1995. Computational Fluid Dynamics, The basics with applications, McGraw-Hill.

Anderson, N.G., 2001. Practical Use of Continuous Processing in Developing and Scaling Up Laboratory Processes. Org. Proc. Res. Dev. 5, 613.

Babuska, I., Chandra, J., Flaherty, J.E., 1983. Adaptive computational methods for partial differential equations, SIAM, Philadelphia.

Baiker, A., 1999. Supercritical fluids in heterogeneous catalysis. Chem. Rev. 99, 453–473. doi:10.1021/cr970090z

Baliga, B.., Pham, T.T., Patankar, S.V., 1983. Solution of some two-dimensional incompressible fluid flow and heat transfer problems, using a control volume finite-

element method. Numer. Heat Transf. 6, 263–283.

Baliga, B.R., 1978. A Control-Volume Based Finite Element Method for Convective Heat and Mass Transfer. Univ. Minnesota, Minneap.

Baliga, B.R., Patankar, S.V., 1983. A control volume finite element method for twodimensional fluid flow and heat transfer. Numer. Heat Transf. 6, 245–261.

Brunner, G., 1994. Gas Extraction. Springer -Verlag Berlin Heidelb. doi:10.1017/CBO9781107415324.004

Clough, R.W., 1960. The finite element method in plane stress analysis, in: Proceedings, 2nd Conference on Electronic Computation, A.S.C.E.Structural Division, Pittsburgh, Pennsylvania.

Dalman, M.T., Merkin, J.H., McGreavy, C., 1986. Fluid flow and heat transfer past two spheres in a cylindrical tube. Comput. Fluids 14, 267–281.

Evans, M.E., Harlow, F.H., 1957. The particle-in-cell method for hydrodynamic calculations. Los Alamos Sci. Lab. Rep. LA-2139.

Guardo, A., 2007. Computational Fluid Dynamics Studies in Heat and Mass Transfer Phenomena in Packed Bed Extraction and Reaction Equipment: Special Attention to Supercritical Fluids Technology. Univ. Politècnica Catalunya.

Harris, C.K.K., Doekaerts, D., Roekaerts, F.J.J., Buitendijk, F.G.J., Daskopoulos, P., Vreenegoor, A.J.N., Wang, H., 1996. Computational Fluid Dynamics for Chemical Reactor Engineering. Chem. Eng. Sci. 51, 1569–1594. doi:10.1016/0009-2509(96)00021-8

Hyde, J.R., Licence, P., Carter, D.N., Poliakoff, M., 2001. Continuous catalytic reactions in supercritical fluids. Appl, Catal, A-Gen. 222, 119.

Jackson, C.P., Cliffe, K.A., 1981. Mixed interpolation in primitive variable finite element formulations for incompressible flow. Int. J. Numer. Methods Eng. 1659–1688.

Jessop, P.G., Leitner, W., 1999. Chemical Synthesis Using Supercritical Fluids, Wiley-VCH, Weinheim.

Kawaguti, M., 1953. Numerical solution of the NS equations for the flow around a circular cylinder at Reynolds number 40. J. Phys. Soc. Japan 8, 747–757.

Kuipers, J. a. M., van Swaaij, W.P.M., 1998. Computational fluid dynamics applied to chemical reaction engineering. Adv. Chem. Eng. 24, 227–319. doi:10.1016/S0065-2377(08)60094-0

Lax, P.D., 1954. Weak solutions of nonlinear hyperbolic equations and their numerical computation. Commun. Pure Appl. Math. 7, 159–193.

Lax, P.D., Wendroff, G.F., 1960. Systems of conservation laws. Commun. Pure Appl. Math. 13, 217–237.

Liong, K.K., Wells, P. a., Foster, N.R., 1991. Diffusion in supercritical fluids. J. Supercrit. Fluids 4, 91–108. doi:10.1016/0896-8446(91)90037-7

Majumdar, S., Rodi, W., Zhu, J., 1992. Three-dimensional finite-volume method for incompressible flows with complex boundaries. J. Fluids Eng. Trans. ASME 496–503.

McCormack, R.W., 1969. The effect of viscosity in hypervelocity impact cratering. Am. Inst. Aeronaut. Astronaut. AIAA Pap. 354.

Moretti, G., Abbett, M., 1966. A time-dependent computational method for blunt body flows. AIAA J. 4 2136–2141.

Peric, M., 1985. Finite volume method for the prediction of three-dimensional fluid flow in complex ducts. Imp. Coll. London.

Pletcher, R.H., Tannehill, J.C., Anderson, D., 1984. Computational Fluid Mechanics and Heat Transfer, Third Edition. doi:10.1017/S0022112000003049

Ranade, V. V., 2003. Computational Fluid Dynamics for Designing Process Equipment : Expectations , Current Status , and Path Forward. Ind. Eng. Chem. Res. 42, 1115–1128.

Ranade, V. V., 2002. Computational Flow Modeling for Chemical Reactor Engineering, Academic Press. New York.

Richardson, L.F., 1922. Weather Prediction by Numerical Process, Cambridge University Press.

Taylor, C., Hughes, T.G., 1981. Finite element programming of the Navier-Stokes equations, Pineridge Press, Swansea.

Thom, A., 1933. The flow past circular cylinders at low speeds. Proc. R. Soc. A 141, 651–666.

Thomson, K.E., Warsi, Z.U.A., Mastin, C.W., 1985. Numerical grid generation, Elsevier, Amsterdam.

Tundo, P., 1991. Continuous Flow Methods in Organic Synthesis, Ellis Horwood, Great Britain.

CHAPTER II

2. MATHEMATICAL MODELLING OF FLOWS

2.1 FUNDAMENTAL ASPECTS OF CFD

Fluid flow is basically described by mathematical models (governing equations) which are based on physical principles of conservation of mass, and conservation of momentum. These are accurately described by transient three dimensional (3D) Navier-Stokes equations. These models coupled with energy and species models are summarized in this section. The standard numerical solution method for these model is finite differences, finite volumes, finite elements methods (continuum flow methods) For the FV (Finite volumes) code which is best for complex geometries, is employed for this study. The formulations of these models used in the FV code are presented. For all types of flow, the FV code solves the mass and momentum conservation equations. Energy conservation equation is solved for flows involving heat transfer. Species conservation equation is solved for flows involving multiple species mixing or reactions.

2.2 FINITE VOLUMES GOVERNING EQUATIONS

2.2.1 Mass Conservation Equation

If ρ is the density of fluid, then the balance of mass flow ρv_x entering and leaving an infinitesimal fluid element of volume dV (Figure 2-1) is the rate of change of density, expressed by the following relation.

$$\frac{\partial \rho}{\partial t} + \frac{\partial}{\partial x}(\rho v_x) \equiv \frac{\partial \rho}{\partial t} + \nabla \cdot (\rho \overline{v}) = S_m \tag{2-1}$$

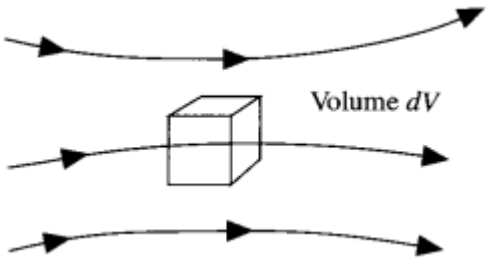

Figure 2-1 Infinitesimal fluid element fixed in space with the fluid moving through it.

Equation (2-1) shows the general form of the mass conservation equation which is applicable for both for incompressible and compressible flows. In Ansys Fluent software, the source S_m is

the mass added to the continuous phase from dispersed phase (e.g., due to particle-to-fluid mass transfer) and/or any user defined sources (ANSYS Inc, 2010)

2.2.2 Momentum Conservation Equation

The Equation (2-2) shows the conservation of momentum in an non-accelerating inertial reference frame (Batchelor, 1967) as used in the Fluent software.

$$\frac{\partial}{\partial t}(\rho\vec{v})\ \vec{v} + \nabla\cdot(\rho\,\overline{v}\,\overline{v}) = -\nabla p + \nabla\cdot(\bar{\bar{\tau}}) + \rho\overline{g} + \overline{F} \tag{2-2}$$

Where p is the static pressure, $\bar{\bar{\tau}}$ is the stress tensor (described below), and $\rho\overline{g}$ and $\overline{F}$ are the gravitational body force and external body forces (e.g., that arise from interaction with the dispersed phase), respectively. $\overline{F}$ can also contains other model-dependent source terms such as porous-media and user-defined sources. (ANSYS Inc, 2010)

The stress tensor ($\bar{\bar{\tau}}$) is given by

$$\bar{\bar{\tau}} = \mu\left[\left(\nabla\overline{v} + \nabla\overline{v}^{T}\right) - \frac{2}{3}\nabla\cdot\overline{v}\boldsymbol{I}\right] \tag{2-3}$$

Where μ is the molecular viscosity, $\boldsymbol{I}$ is the unit tensor, and the second term on the right hand side is effect of volume dilation.

2.2.3 Energy Conservation

The common forms of heat flow in a catalytic reactor system involves addition of heat via walls of the reactor for process requiring heat. For processes involving exothermic reactions, heat is released from the catalysts surface for catalytic reactions. These systems can be individually studied for their effects as wall-to-fluid heat transfer and particle-to fluid heat transfer. The energy transfer here occurs by conduction, convection and radiation. The models involving conduction and forced convection are simple, while models involving buoyancy driven flow, radiation are more complicated.

The FV code solves the energy equation in the following form

$$\frac{\partial}{\partial t}(\rho E) + \nabla \cdot \left(\vec{v}(\rho E + p)\right) = \nabla \cdot \left(k_{eff} \nabla T - \sum_j h_j \vec{J}_j + \left(\bar{\bar{\tau}}_{eff} \cdot \vec{v}\right) \right) + S_h \quad (2\text{-}4)$$

here, k_{eff} is the effective conductivity $(k + k_t)$,

k_t is the turbulent thermal conductivity, , and

$\vec{J}_j$is the diffusion flux of species j.

The first three terms on the right-hand side of Equation (2-4) denote energy transfer due to conduction, diffusion, and viscous dissipation, respectively.

S_h includes the heat of chemical reaction, and any other volumetric heat sources defined by user. (ANSYS Inc, 2010)

In Equation (2-4)

$$E = h - \frac{p}{\rho} + \frac{v^2}{2} \quad (2\text{-}5)$$

Where sensible enthalpy is defined for ideal gases as

$$h = \sum_j Y_j h_j \quad (2\text{-}6)$$

and for incompressible flows as

$$h = \sum_j Y_j h_j + \frac{p}{\rho} \quad (2\text{-}7)$$

In Equations (2-6), and (2-7), Y_j is the mass fraction of species *j*, and

$$h_j = \int_{T_{ref}}^{T} C_{p,j}\, dT \quad (2\text{-}8)$$

Where T_{ref} is 298.15 K.

2.2.4 Modelling Species Transport

For flows involving multiple-component mixtures, a species balance s for chemical species is solved in which the mass of each species m_i obeys the conservation law. When you chose to solve conservation equation for chemical species, the FV code predicts the local mass fraction

of each species, X_i, using the solution of a convection-diffusion equation for the i^{th} species. The conservation equation in its general form in shown below

$$\frac{\partial}{\partial t}(\rho Y_i) + \nabla \cdot (\rho \vec{v} Y_i) = -\nabla \cdot \vec{J}_i + R_i + S_i \quad (2\text{-}9)$$

R_i is the net rate of production of species *i* by chemical reaction and

S_i is the rate of creation by addition from the dispersed phase plus any user-defined sources.

This form of equation will be solved for *N – 1* species where *N* is the total number of fluid phase chemical species present in the system. As the mass fraction of the species must sum to unity, the N^{th} mass fraction is determined as one minus the sum of the *N – 1* solved mass fractions. In order to minimize numerical error, the N^{th} species should be selected as that species with the overall largest mass fraction. (ANSYS Inc, 2010) In our case, the solvent CO_2 has the highest mass fraction in the studied cases of extraction and reaction.

2.2.4.1 Mass Diffusion in Laminar Flows

In Equation (2-9) $\vec{J}_i$ is the diffusion flux of species *i*, which arises due to gradient of concentration and temperature. By default, the FV code uses the dilute approximation, under which the diffusion flux can be written as

$$\vec{J}_i = -\rho D_{i,m} \nabla Y_i - D_{T,i} \frac{\nabla T}{T} \quad (2\text{-}10)$$

Here $D_{i,m}$ is the diffusion coefficient for species *i* in the mixture. (ANSYS Inc, 2010)

2.3 SIMULATION MODEL SETUP

To conduct the CFD simulations, commercially available CFD codes have been used (ANSYS Fluent 13.2/14/16.2). These software, present common aspects in their operational. These commercial codes (like many other commercially-available CFD codes) consist of a number of different modules in which different parts of the process take place. Figure 2-2 below shows the operational flow of typical CFD software package.

Figure 2-2 Operational structure of commercial CFD software

2.3.1 Pre-processing

CFD is setup in three different steps

a. Geometry development or its import.

b. Mesh generation.

c. Physical problem set-up.

In the first step the geometry of the model is established, a computer aided design (CAD) program (DesignModeler of ANSYS Inc. in present case) is used to determine dimensions. The next step is the creation of the surface mesh, which is placed on the surfaces created in the CAD geometry modelling phase. And the final step is the interpolation of the surface mesh to the final fully 3D volume mesh. Mesh generation is a very important aspect in CFD setup. The mesh density, determines the accuracy of the simulation. The mesh consists of four major concepts, volumes, surfaces, edges and nodes. These concepts are hierarchical, a volume is bounded by surfaces, a surface is bounded by edges and an edge consists of nodes. The mesh creation consists of three major steps. (ANSYS Inc, 2010)

2.3.1.1 Geometry Design

In designing the geometry, a bottom-up sketching method was employed. This method necessitates planning on the creation of the model and its mesh. This method involves defining nodes and building up to edges, surfaces and volumes. *Figure 2-3* shows the nodes and edges in geometry from which the surface were generated through several operations. The topology of the simulation model is fixed in the initial geometry design phase. In this primary stage the main solid and fluid region interfaces are established.

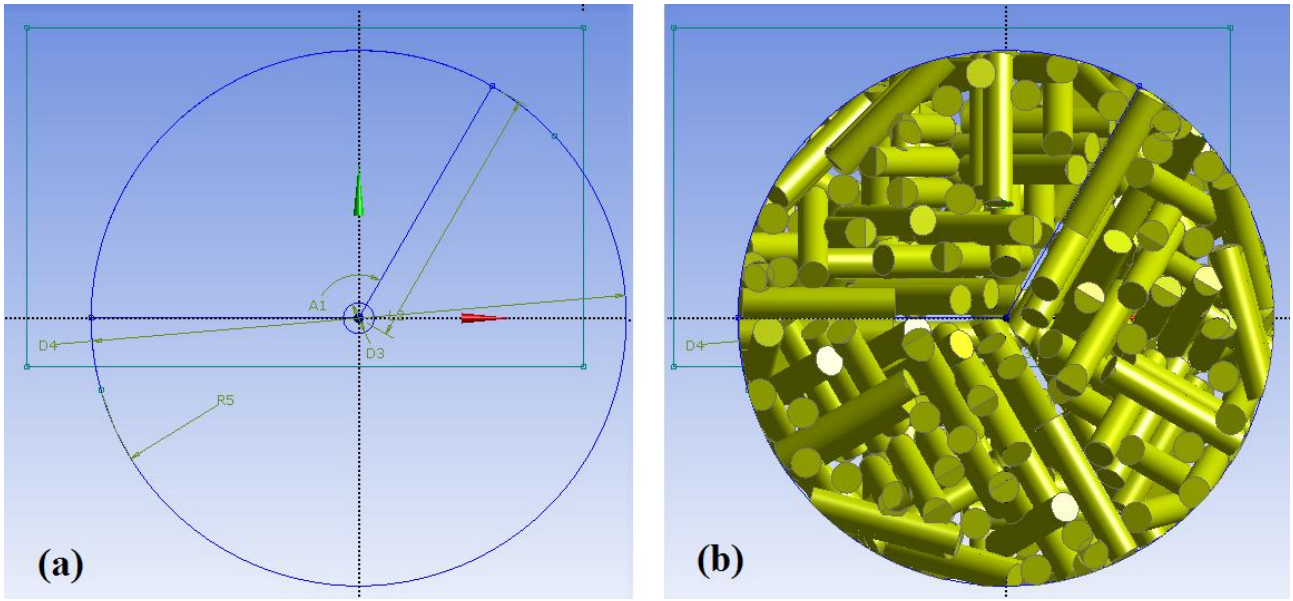

Figure 2-3 Bottom-up procedure for geometry design. (a) Node and edge generation; (b) Surfaces generation

Most importantly, the fluid region and solid regions are to be properly defined. Initially, an overall geometry is defined, for e.g. the tube comprising the catalyst. And then, the particles are positioned in the tube at their suitable sites by numerous operations. To form the proper fluid region, the particle volumes, need to be deducted from the tube volume. After forming the appropriate fluid and solid regions, the region interfaces need to be linked. When the fluid region is created it is a separate region from the solid particles, and the surfaces bounding the particles need to be connected to the surfaces bounding the fluid region. The connecting of these interface surfaces is critical in creating an appropriate energy solution in the model. When all regions and their interfaces have been properly defined by naming, the simulation model can be meshed. (ANSYS Inc, 2010)

2.3.1.2 Mesh design and generation

Based on mesh refinement needed the geometrical model can be meshed at three different stages, edges, surfaces and volumes. A mesh which is uniform throughout, volume mesh is generated. At this point one uniform control volume size is determined and the entire simulation geometry is meshed with this standard control volume size, creating a uniform mesh density.

In areas significant flow fluctuations can happen, local refinement is required, in sensitive regions of the geometry, different mesh densities can be defined to surfaces or edges specifically. For example, near contact point areas, between particles in the geometry, or between particles and the externally bounding column wall, the mesh needs to be finer than in larger void areas in the geometry to be able to get a converging flow solution. To be able to

adjust the mesh locally mesh densities have to be defined on edges along these contact points. *Figure 2-4* shows the particles surface whose mesh density is increased by refinement by surface meshing. (ANSYS Inc, 2010)

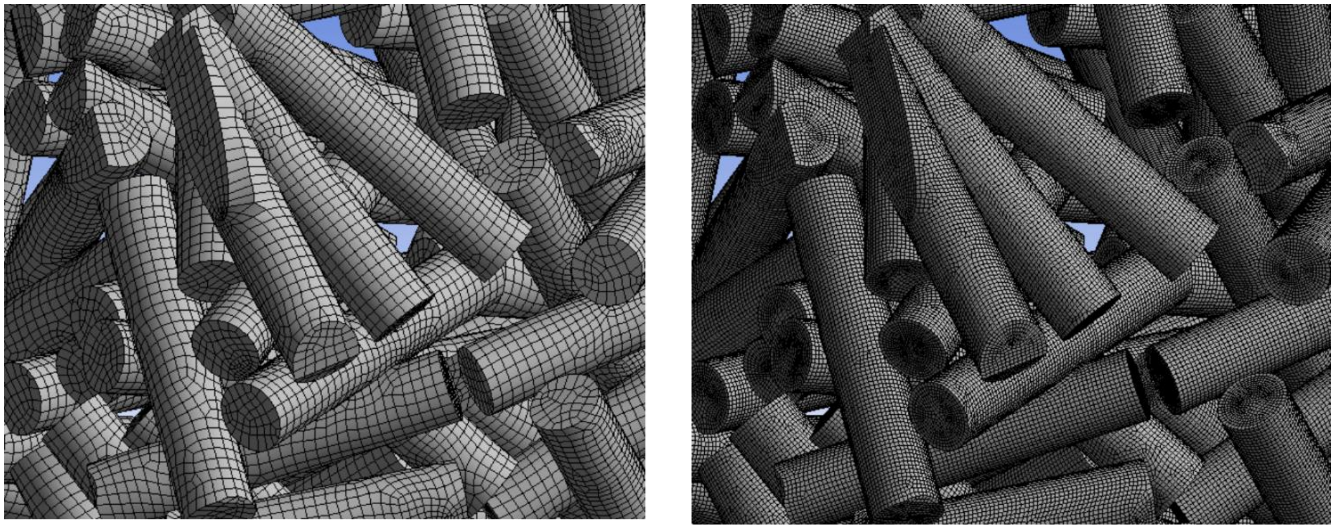

(a) (b)

Figure 2-4 Surface mesh refining detail over particles surface (a) Original mesh (b) Refined mesh on particles surface

For refining the mesh along a single edge several schemes are available. Node distribution on the edge can be uniform or graded with a higher node density in the appropriate areas.

After the mesh with proper densities in created, it is sent converted in the format that can be read by the CFD solver. The surface and zones are labelled, in order to identify them easily in the solver. The surfaces or volumes can also be grouped together under a common name to identify them as a single entity in the solver.

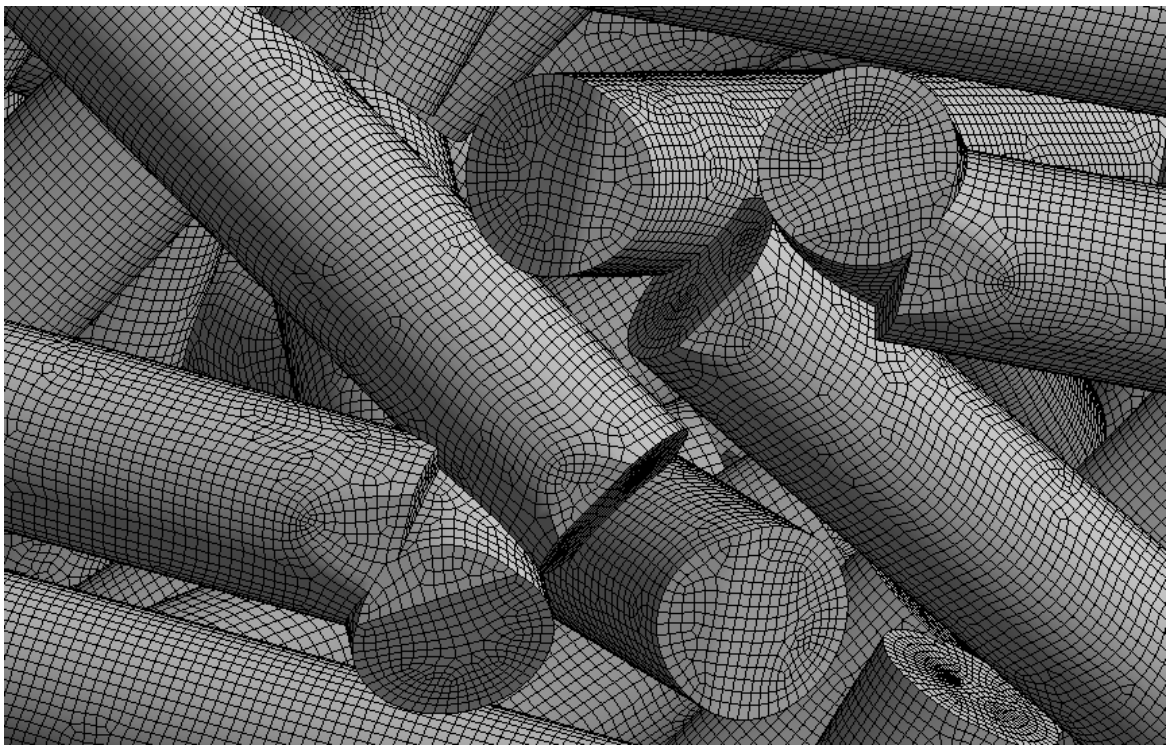

Figure 2-5 Overlapping particles with particle-to-particle contact points

Most of the previous reports have particles have no contact (Nijemeisland and Dixon, 2001), by leaving slight openings amid surfaces and assuming zero velocity in the opening to evade convergence glitches. The particles in this study were modelled overlapping about 1% of their volumes with adjacent particles in the geometry model. Convergence problems were not detected during runs. Figure 2-5 shows the particles overlapped with adjacent particles.

2.3.2 CFD solver setup

After the mesh is generated, with required mesh density at each location, and resolving any problems, the problem can be defined and computation can be initiated. The meshed geometry is imported into the CFD solvers, like Fluent, COMSOL, etc.

A sequence of steps is to be done; initially, the reactant or transport materials are to be defined at the operating conditions, and the boundary conditions for the system are set, based on the model to be simulated. The iteration parameters under-relaxation factors and residual cut off are set, which use the set reference values. The solver can be initiated and run for solutions. When the solution is sufficiently converged. The post processing (data retrieval and analysis) can be performed.

2.3.2.1 Materials definition

The materials involved in the simulation, fluid or solid has to be defined by setting its flow properties. The main properties of the material that are to be specified are the density and viscosity. And when the energy transport is taking place in the system, then additionally the thermal conductivity and specific heat are to be specified. The properties can be specified as a constant or as various functions of temperature.

A mixture material can also be defined, in order to specify the interaction between the chemical species. For non-reacting mixture species, it is needed to specify the mixture density, and mass diffusivity, additionally the mixture specific heat and thermal conductivity for flows with energy transport. For reactive flows, in addition to the mentioned properties, the details of reaction kinetics are to be specified.

2.3.2.2 Boundary conditions

The definition of the boundary at various locations in the simulation setup is necessary. These values determine the limits of the physical model. The major classification of the boundary conditions used are

- Flow inlet and exit boundaries: pressure inlet, velocity inlet, inlet vent, intake fan, pressure outlet, outflow, outlet fan, exhaust fan.
- Wall, repeating, and pole boundaries: wall, symmetry, periodic axis
- Internal cell zones: fluid, solid
- Internal face boundaries: fan, radiator, porous jump, interior

For the work done in this this in this thesis, velocity inlet, at the flow inlet of the packed bed, and a pressure outlet at the flow exit were used. The packed bed tube exterior and the surface of the particles are defined as wall boundary conditions. These wall boundary conditions separate the fluid zone and the solid zones. They also constrain the fluid to be within the packed bed tube. The inlet and outlet to the particles bed are defined as interfaces when its needed to use a periodic boundary condition for continuous packed beds in series.

After setting up the boundary condition, the initial guess for the solution can be specified. The closer the initial guess to the solution, the faster the solution can be achieved. For the current cases, we have used the upstream conditions as the initial guesses or the reference values, since the variation through the packed bed is steady and slight between consecutive steps.

2.3.2.3 Under relaxation and residual cut off

Under-relaxation factors and residual cut off values are to be set up before starting the simulation. In iterations for solution, the step change between consequent iteration, is multiplied with the under-relaxation factor before applying to the next iteration step. In iterations, the step change between consequent iterations is multiplied with under relation factor before applying to the next iteration step result. When the factor is greater than one, the process is said to be over-clocked. In this process the step-change is large and convergence is expected to be attained sooner. However, it is not recommended to over-clock a process unless it is very stable, otherwise it may lead to divergence of the calculation. When the under-relaxation factor is less than one, it is called under-relaxed. In under-relaxed calculations, the iterations take longer time and the likelihood of divergence is less. These factors are applied in Fluent to pressure, density, body forces, momentum, species and energy.

The difference between previous and current iterations is called the residual value. This determined. When the residual value is approaching zero, the solution is said to be converged. Upper limit for "cut off" value for the residual value is set to, such that it is low enough to give an accurate solution and not too high. High values of residual values speed up the attainment of convergence. Initial iteration is run based on reference values, there onwards, data from subsequent iterations is used. (ANSYS Inc, 2010)

2.3.3 Post -processing of the simulation data

When the simulation has converged, the data for final iteration is stored as solution. In which the data is recorded for each of the elements in the model. The data includes that of temperature, densities, and other similar physical properties, pressures, species concentrations and composition, velocities and other flow aspects etc. The data can be interpreted when reduced to comprehensible sizes, for example data from particular volume, or surface or lines in the simulation domain. The extraction, displaying and analysis of this legible data is called post-processing. This enables comparison of the simulations with each other and with external data. For the required data assessment, it is important to select how the data is presented. Some of the prevalent way the data is represented is through contour/vector plots over surfaces and XY plots on lines.

The contour plots are a graphical method in which a 3D surface is represented with constant z planes on 2D format. These give distinct assembly of control volumes. For a particular surface, various properties, like temperature, density can be shown. In these plots, a particular colour,

or lines, represent the region where the property is constant. Absolute velocities can also be plotted as contours, with areas of constant magnitude represented.

Velocity vector plots are needed to show the direction and (represented by a pointer) and magnitude (represented by the pointer). The vector plots are needed to examine the cross-flows/ back flows, eddies formation in the flow region. These velocity vectors can also be coloured by magnitude of different properties. This helps in checking the influence of a particular property on the flow direction and/or magnitude. Velocity vectors coloured by density are of particular interest as the show the can show the buoyancy effects in regions of very high densities or very low densities in the flow domain. While plotting the velocity vectors, the representation of the number of vectors and the reference size of the vectors has to be optimized, to make the vector plots more legible. Figure 2-6 shows velocity vectors coloured by density. Here the vectors direction is towards +x. The influence of the cylindrical obstacle on the vector can be observed around the cylinder.

The simulation data can also be exported in different forms (like ASCII), which can be read using other applications. And also, for using in the different case of the Fluent application, for further runs. Here, usually, profile data from the outlet surfaces is extracted which is used as the inlet profile for the subsequent geometry, forming a periodic boundary condition. This is particularly useful when running the whole geometry is computationally demanding, and so it can be divided to smaller parts.

This graphics data can also be viewed as animation video files with the contour or vector plots as frames along axis by sweeping surfaces or as plots with time for transient iteration simulations.

XY plots can also be used when analysing the numerical data. Two different properties in the simulation can be plotted against each other. Usually the length (or directional vector) is used to check the variation of a particular property along a line or curve (direction vector). This function is useful usually when checking the variation of for example temperature along the axis of a cylinder. Identical plots at different lines can be made for comparison of the numerical data.

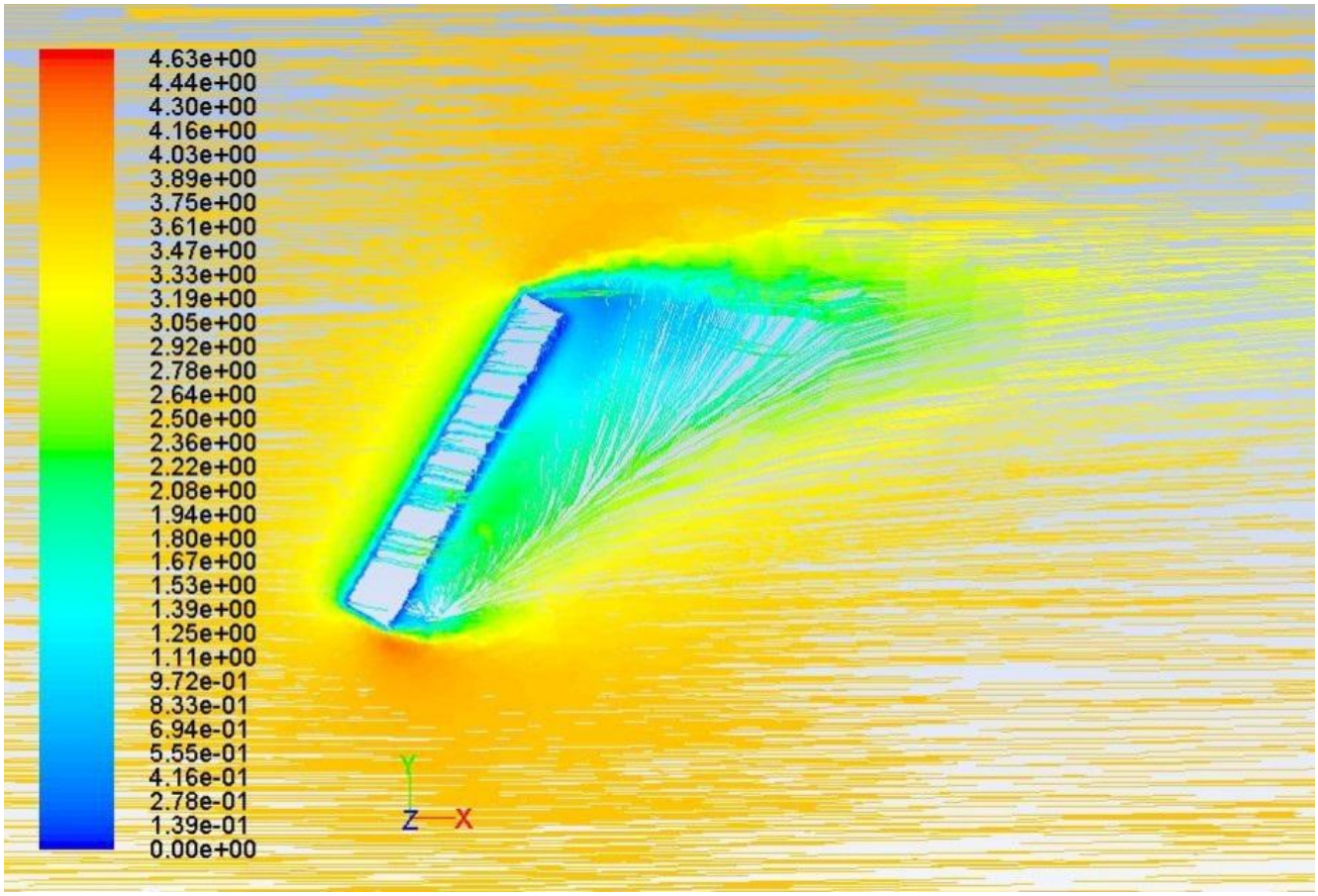

Figure 2-6 Velocity vector plot with vectors coloured by magnitude (m/s) as obtained from CFD solver for flow with Re 250 over a cylinder inclined at 60° angle of attack

2.3.4 Software used

For the development of the simulations presented in this work Ansys Fluent™ 13.0, 14.0, 16.2 finite volumes solver, Navier-Stokes based CFD code provided by Ansys Inc., has been used. This software is specific for solving PDEs of fluid dynamics i.e., CFD solver which employs Finite Volumes (FV) numerical method. This software has a built in CAD oriented geometrical design software DesignModeler™ suitable for complex geometries. The meshing capability features local mesh improvement/optimization. The continuity condition of the CFD solver is based on density and velocity gradients. The software has multiple complementary models, the models which are used in this thesis are Energy transfer, species transfer, chemical reaction models. The software has excellent graphics post processing capabilities. With its capacity for complex geometries and robust meshing capabilities, and high quality post-processing and with detailed models, the memory and computational effort are high and thereby delivering highly accurate results with robustness and numerical stability

REFERENCES

ANSYS Inc, 2010. ANSYS Fluent documentation, ANSYS Inc.

Batchelor, G.K., 1967. An Introduction to Fluid Dynamics, Oxford University Press. Oxford University Press.

Nijemeisland, M., Dixon, A.G., 2001. Comparison of CFD simulations to experiment for convective heat transfer in a gas–solid fixed bed. Chem. Eng. J. 82, 231–246. doi:10.1016/S1385-8947(00)00360-0

CHAPTER III

3. LITERATURE

3.1 PACKED BED REACTOR MODELLING

Knowledge of heat and mass transfer characteristics and their spatial distributions in packed beds is very important for the design and analysis of packed-bed catalytic or non-catalytic reactors. Packed beds have a wide range of applications in industry, either for separation processes, contacting or reaction equipment. The flexibility of packed beds in handling and their simplicity has caused many efforts by researchers in understanding their operation and control for better utilization in specific applications.

In estimating the overall steady-state temperature profiles, heterogeneous packed bed may be assumed to be a homogeneous single phase. The common parameters in packed bed heat transfer are the effective radial thermal conductivity and the wall heat transfer coefficient. The radial thermal conductivity, k_r, is a fluid conductivity for flow behaviour and solids conductivities so it can be applied as if the bed were uniform. The wall heat transfer coefficient, h_w, is a parameter that needs to be introduced to simulate the apparent temperature jump at the wall as is found in experiments because measurements can only be taken at a specific distance from the wall. Wakao and Kaguei, (1982) gave an extensive review and their development of experimental and theoretical works on packed bed heat and mass transfer

Modelling of packed beds involve proposing mathematical models for the description of mass transfer, or species transport, and for heat transfer characteristics. These theoretical models are usually developed with simplifying assumptions of the geometrical model. The experimental data is used for obtaining correlations that are used for description of some specific phenomena. The small size of the packing in the larger tube, allows for averaging of the flow packing, which are an essential part of the model, resulting in a successful use of empirical parameters, which use averaged flow and temperature profiles over the diameter of the bed.

3.1.1 Wall-to-fluid and particle-to-fluid heat transfer in packed beds

Data and understanding of heat transfer characteristics and spatial temperature distribution in packed beds is of foremost importance to design and analysis of packed bed catalytic reactors and packed bed heat exchangers. A packed bed model is usually composed of separate models

for fluid flow, heat transfer mass transfer or species transport. The heat transfer models are presented in terms of correlations based on a wide variety of experimental data.

Yagi and Wakao, (1959) carried out experiments of heat and mass transfer from the tube wall to the fluids flowing through the packed beds separately. Air was used as the fluid and several kinds of solid particles with low and high thermal conductivities were investigated to determine the effective thermal conductivities and wall heat transfer coefficients. The results were correlated in terms of Re and Pr.

Kunii and Suzuki, (1967) experimental data of Nusselt and Sherwood numbers of particle-to-fluid heat and mass transfer respectively, reported in previous literatures were theoretically interpreted. The authors observed that channelling or uneven contacting of fluids with solids decreased the apparent heat and mass transfer coefficients.

Li and Finlayson, (1976) have evaluated the available published experimental data for wall-to-fluid heat transfer, and excluding studies influenced by length effect. The data collected is correlated over a large range of Reynolds numbers (20-7000) for spherical packing and for cylindrical packing. The best correlations for the data are presented.

Wakao et al., (1979) have compiled published data from particle-to-fluid heat transfer measurements and corrected them for axial fluid thermal dispersion coefficient values. The authors presented the corrected data in the range of Reynolds number from 15 to 8500 in the form of correlation in terms of Re and Pr.

Dixon and Cresswell, (1979) developed a method for theoretically predicting effective heat transfer in packed beds from a two-phase continuum model, which takes into account the particle thermal conductivity. Effective radial conductivity, effective axial conductivity, and wall heat transfer coefficient can be predicted with the method.

Winterberg and Tsotsas, (2000a) presented correlations for effective heat transport coefficients in packed beds with cylindrical particles.

With the increase in the computational resources CFD studies were done to examine the wall-to-fluid heat transfer in packed beds by many authors. CFD has helped to test the applicability of various models and in improving them.

3.1.2 Packed bed mass transfer

Wakao, (1976) studied particle to fluid mass and heat transfer coefficients at low flow rates. Reporting that the assumption of concentration /temperature being centre-symmetric in solid particles in packed beds was found to be faulty at low flow rates.

Dwivedi and Upadhyay, (1977) have presented extensive review of previous reported literature of experimental data on mass transfer between particles and fluid in fixed and fluidized beds and correlating equations were developed for various situations.

Wakao and Funazkri, (1978) have compiled published data from particle-to-fluid mass transfer measurements and corrected them for axial fluid thermal dispersion coefficient values. The authors presented the corrected data in the range of Reynolds number from 3 to 10,000 in the form of correlation in terms of Re and Sc.

Stüber et al., (1996) conducted supercritical fluid extraction in packed bed, to study effects of flow direction of solvent on the particle-to-fluid mass transfer.

3.2 PACKED BED REACTORS MODELLING USING CFD

CFD studies of packed bed flow behaviour and their corresponding heat/mass transfer and reaction have been performed previously. CFD refers to the use of a numerical method to resolve a set of differential balances over a computational grid. Earliest CFD packages solved one or two dimensional models. Overtime CFD software packages have become more advanced allowing for detailed simulations. Numerical modelling is applied to fixed beds in many different aspects. The earliest packed bed CFD simulations used two-dimensional models, on the contrary Sørensen and Stewart, (1974a, 1974b, 1974c, 1974d) are one of the first groups to construct a numerical iteration method for solving flow and heat transfer in three-dimensional approach. They studied velocity profiles, convective boundary layers, heat and mass transfer in cubic array of spheres. The construction of the computational grid is also discussed; the calculated flow is limited to creeping flow. Later packed bed CFD simulations was applied by Dalman et al., (1986), using two-dimensional models, investigated flow behaviour in an axisymmetric radial plane with 2 spheres in a cylindrical long tube, for Reynolds number up to 200. This study gave the first high-detail insight into flow patterns in packed beds, showing that the eddies formed between the spheres led to a region of poor heat transfer. This problem was

seen to be increasing with the increase in Re. They also investigated the effects of Re and Pr on the process.

Parsons and Porter, (1992) proposed a general numerical technique for modelling three-dimensional, single phase gas flow patterns in packed beds. The general approach can be used to model flow patterns in adsorbers, catalytic reactors etc. Specifically, they represented a method for implementing a vectorial form of the Ergun equation in a CFD package. The approach was validated by comparison with independent experimental results.

Lloyd and Boehm (1994) studied a two-dimensional case; they used the commercial finite element package FIDAP and considered eight spheres in line as catalyst particles at Reynolds numbers of 40, 80 and 120 and Prandtl numbers from 0.73 to 7.3. In this study the influence of the sphere spacing on the drag coefficient was studied. The fully periodic drag coefficient was found to be inversely proportional to Re. The heat transfer from spheres was found to be decreasing with the decrease in sphere spacing.

With the increase in availability and robustness of CFD software and growing computer processing capabilities, the degree to which CFD can be applied to complex structures has improved significantly. 3-dimensional flow with heat transfer in packed beds were modelled using commercial Finite volumes software package *FLUENT UNS* and finite elements software ANSYS/FLOTRAN by Dixon and co-workers.

Derkx and Dixon developed a 3D model of three spheres arranged in a tube, for which they determined wall-heat transfer coefficient using ANSYS (version 5.0A) for model generation. This is one of the earliest 3D models. They used a finite element method in obtaining the numerical solution using FLOTRAN (Compuflo Inc). The obtained numerical results were in good agreement with those predicted by a theoretical model.

Logtenberg and Dixon, (1998a, 1998b) used commercial finite element software package ANSYS/FLOTRAN for solving 3d flow and energy equations. The geometrical model consisted of eight spheres arranged as two layers in a tube. The estimated effective heat transfer parameters with data from the CFD results. They compared well with theoretical model (Dixon and Cresswell, 1979) predictions. The fluid used was a hydrocarbon mixture, for which they studied the effect of density, viscosity and thermal conductivity variations with temperature. Although the 3D models were a significant step ahead of 2D models, they were deficient due to their simplicity

(Logtenberg et al., 1999) developed a model with 10 solid spheres in a tube with contact points incorporated. The 3D Navier-Stokes and energy equations were solved using ANSYS 5.3 which

is based on finite element method. Stagnant regions were observed near contact points, which were observed near contact points, which were due to high shear of the surfaces. The velocity gradients in the radial direction were observed to be high, indicating how heat transfer is increased within the bed. Back flow regions observed were in qualitative agreement with literature experimental findings.

Transversal dispersion in a structured packed bed was calculated using CFD by Gulijk, (1998). The CFD calculations were done using the parallel code CFX-4.1, which solved Navier-Stokes equations with a finite difference method. A simplifying model, the Toblerone model was developed which models the flow intersecting triangular channels. This model determined well the design properties for a reactor operation. The liquid flow field was solved using Ergun equation to account for porous flow through the pellets. By the Toblerone model it has been found that the transversal dispersion coefficient is a factor 40 higher compared to single phase packed bed flow. This result reminded the authors that, liquid transversal dispersion in this kind of packing would not be a limiting problem when designing a reactor.

McKenna et al., (1999) used a CFD software package to study heat transfer from spherical particles of different sizes and under different heat transfer conditions. They showed that Ransz-Marshall and similar other correlations are not valid for densely packed systems. They also demonstrated that convection is not the only means of removing heat from small, highly active particles. Conductive heat transfer between large and small particles present in the same reactor appears to help alleviate problems of overheating, explaining why earlier models of heat transfer in olefin polymerization over predict the temperature rise during early stages of polymerization.

Tobiś, (2000) studied the influence of bed geometry on its frictional resistance under turbulent flow conditions. The author presented both experimental and numerical investigations of air turbulent flow through six model packings composed of spheres in cubic arrangement. Theoretical study was done by FLUENT CFD code. The turbulence was modelled by the standard κ-ε model, Spalart and Allmaras, and the Reynolds Stress models to compare predictions of the frictional resistances. Although there is a large discrepancy of the values of Ergun constants, this comparison showed an acceptable agreement according to the author. It was noted that the bed porosity and the bed hydraulic diameter were not sufficient to describe hydrodynamic properties of an arbitrary designed packing. Tobis also mentioned that, the CFD approach appeared to be more general than any Ergun-like semi-empirical correlation. However, it was also stated that, more detailed experimental and theoretical studies of fluid flow through complex bed structures are required.

Zeiser et al., (2001) did CFD calculation of flow, dispersion and reaction in a catalyst filled tube by the lattice Boltzman method. The behaviour of a reacting viscous flow inside the complex geometry of a fixed-bed reactor has been studied. They have generated the geometrical structures of the fixed bed with a Monte-Carlo method. The results for local velocity distributions showed typical channelling effects close to walls. MC simulated packed beds were found to be in reasonable agreement with correlations gained from experimental investigations in terms of the void fraction distribution. The domain for the 3-D simulation of the flow field was discretized by 102 x 102 x 250 cells. Periodic boundary conditions were used perpendicular to the main flow direction. The results for the local velocity distributions obtained with the lattice Boltzman method show the channelling effects close to the walls that were observed in experiments. In addition to that, chemical reacting flow around a single catalytic particle was studied by the effect of molecular diffusivity and dispersion.

Nijemeisland and Dixon, (2001) created a 44-sphere model was created with N = 2. The compared radial temperature profiles of simulations with identical experimental setup. With proper considerations of limitations, it was shown that qualitative and quantitative similarities could be observed. It was also shown that, CFD produces the same data as is obtained experimentally, we can use the advantage of the CFD; where a lot more information is available than is used for the comparison of CFD data with experimental data, data that cannot be obtained through traditional experimental measurement.

Calis et al., (2001) studied CFD modelling of different types of packing and experimental validation. CFX-5.3 CFD software package was used for different bed structures. In each case 8-16 particles were used. An unstructured grid was applied in the form of tetrahedral cells, but 5 layers of prismatic cells were taken into consideration close to particle and wall surfaces for laminar flow. There were no prismatic cells for turbulent flow, and Re number up to 10000 was studied. Consequently, the grids prepared for laminar and turbulent flows were different. For turbulent flow, k-ϵ model and Reynolds-Stress Models were considered. Standard wall functions were used in case of turbulent flow. Experimental data, on the other hand, were obtained by a setup of $1 \leq N \leq 2$. Polyethylene spheres were supported by a wire mesh screen. Experimental Re's were varied from about 100 to about 6000. Pressure drops were measured across a bed length of about 500mm. Local velocity profiles were measured with laser-Dopler anemometry (LDA). After a comparison of modelling and experimental results, it was concluded by the authors that, CFD code predicts the pressure drop characteristics of the studied systems within an average error of about 10%. For the turbulent cases, both turbulence models

were found to be adequate. However, it was observed that, Ergun equation over predicts the experimental friction factors by an average of 80% in these cases.

Tobiś, (2002) modelled the pressure drop caused by a turbulent single fluid flow for a complex geometry. This model was compared and verified experimentally in the model systems of complex geometry. Experimental model packing consisted of 8000 spheres of 38mm diameter glued together in a cubic arrangement. Also, different complex structures were created by introducing different obstacles amid the spheres. Numerical modelling was carried out as interstitial flow modelling, superficial flow modelling, and structural macro correlations (SMC). Interstitial flow modelling was made by commercial CFD code FLUENT with the κ-ε turbulence model. It was discussed that, superficial flow model that is based on the empirical correlation, cannot be used alone to design a novel packing geometry. But the author pointed out that, if it coupled with an appropriate CFD code, it should enable flow prediction within large complex structures. It was also shown that, SMCs may facilitate the pressure drop prediction within the structures composed of different packing geometries.

Jiang et al., (2002) have done numerical simulations of multiphase flow using the k-fluid CFD model for packed beds at various operating conditions. The combined flow-reaction modelling scheme is proposed through the mixing cell network concept, in which the k-fluid CFD simulation can provide the information on sectional flow distribution. This model was shown to capture the longitudinally averaged radial profile of axial liquid velocity. The predictions of the model of the global liquid saturation and pressure gradient are comparable with the experimental data.

Hjertager et al., (2002) performed CFD simulations of fast chemical reactions in turbulent liquid flows. An in-house CFD code was used to simulate a single-phase acid–base neutralisation in a tubular reactor. The simulation results are compared to experimental data and the results have shown that the standard Eddy Dissipation concept (EDC)-model was not suitable for liquid phase reactions, a modified version of the model has shown good results. The most promising probability density function (PDF)-model is shown to be the beta-PDF-model.

Romkes et al., (2003) performed CFD modelling and experimental validation of particle-to-fluid heat and mass transfer in a packed bed. They used CFD software package CFX-5.3. The packed bed used has low N of $1 < N < 5$. Laminar simulations were done for 1.27 x 10-4< Re number < 127, and turbulent simulations for 127 < Re number < 1.27x 105. Authors wanted to find mass and heat transfer characteristics of a composite structured catalytic reactor packing (CSP) and they wanted to see whether CFD can be used to develop correlations. Turbulent

models; κ-ε, RNG κ-ε, and the Reynolds Stress were considered. The heat transfer rate was predicted within an error of maximum 10% depending on the correlation chosen for comparison. It was also found that RNG κ-ε model gave better heat transfer predictions with the available experimental data. For the mass transfer predictions, the model agreed well with the experimental values within an error of less than 15%.

CFD numerical simulations of single-phase reacting flows in randomly packed fixed-bed reactors and their corresponding experimental validations were done by Freund et al., (2003). They have also applied MC method to synthetically generate packings of spherical particles with N = 5. The simulations were done for Re number range was in between 0.1 and 100. The pressure drop of the packing was compared with measurements and well known correlations from literature, were found to be in good agreement with the pressure drop correlation and with the measurements.

Hydrodynamic and transport properties of packed beds were simulated by Magnico, (2003). They used Bennet method to generate random packings. For solving the Navier-Stokes equations the finite volume method was setup with a collocated grid. Periodic boundary conditions were specified at the ends of the reactor. The numerical results were found to be in good agreement with Ergun correlation in terms of normalized pressure drops for Re number in between 0.1 and 200. The validation of the Lagrangian method, that is used generally to characterize the mass transfer properties in the zones close to the wall, was found reasonable by comparing the results with the experimental ones available in literature.

Petre et al., (2003) have done a study of pressure drop through structured packings using CFD modelling. They developed a combined mesoscale and microscale predictive approach to apprehend the aerodynamic macroscale phenomena in structured packings. The method consists in identifying patterns by the representative elementary units (REU). An element of a structured packing was made up of an ensemble of Toblerone-like triangular flow channels. Non-structured tetrahedral meshing was applied for each REU by Gambit 1.2. For different structural type of REU's, flow field simulations were made by FLUENT version 5.5. The RNG κ-ε turbulence model was used, and simulations were done over a wide Re number range spanning up to 40000. The modelling study was validated by an experimental dry pressure drop data for five different packing types based on a thorough survey of the available pressure drop data published over the last two decades.

Dixon et al., (2003) carried out CFD simulation of steam reforming reaction. In this study, a 120-degree slice of the bed cross-sectional area which was called wall segment, WS, was

considered as model geometry. Simulations were done by FLUENT regarding spherical and cylindrical catalyst particles. Steam reforming kinetics was modelled considering the thermal effects of the reactions, which were represented by the inclusion of temperature dependent heat sinks in solid particles. It was concluded that, the results seemed to be physically reasonable, indicating that this approach can provide useful information about flow and energy in a catalyst tube under reaction conditions.

Nijemeisland et al., (2004) made a comparative study to investigate the influence of internal voids in cylindrical particles on heat transfer performance in the near wall region of a steam reforming packed bed reactor tube. They have shown that the interactions between heat transfer, fluid flow and reaction were complex. For the representative wall segment of full cylindrical particles, the thermal effects of the steam reforming reaction were represented with heat sinks approach.

Nijemeisland and Dixon, (2004) studied fluid flow and wall heat transfer in fixed bed of spheres using CFD. Detailed velocity and temperature fields were obtained. The results from wall segment are confirmed to reproduce those obtained from full bed of spheres. It was established a symmetrical portion of the bed could be used to reduce the computational load of the simulations, when the main focus is on near-wall phenomena.

Guardo et al., (2004) studied CFD flow and heat transfer in non-regular packings in a fixed bed. Pressure drop along the bed and wall-heat transfer parameters were estimated for the packed bed and validated with commonly used correlations. Laminar and turbulent flows were compared. Spalart-Allmaras turbulence model having damping functions, showed better agreement than those obtained using standard k-ε turbulence model for estimating pressure drop and heat transfer parameters.

Gunjal et al., (2005) studied fluid flow through an array of spheres using the unit-cell approach, in which instead of considering the entire packed bed or representative segment of the bed, only some part of the couple of particles are considered. The used Gambit 2.0 software for geometry generation, and solved by Fluent 6.1.18. Validation was done by comparing published experimental and computational results, which were in substantial agreement. The relative contributions of form drag and surface drag in overall resistance to flow was quantified using the simulation output.

Guardo et al., (2006) checked mesh sensitivity and compared CFD predictions with empirical correlations for particle-to-fluid heat transfer in packed beds. Nusselt numbers were calculated and compared to the predictions of Ranz and Marshall correlation. In order to include the

contact points between the particles the spheres were overlapped by 0.5% of their diameters. Simulations were carried out by Fluent 6.2 for very low Re values in investigate the mixed convection heat transfer at high pressure, obtaining modified correlations for free and forced convection Nusselt numbers. The authors found good agreement between numerical and experimental, and the predictions of the modified correlation. Later the authors (Coussirat et al., 2007) compared different turbulence models were with various mesh element densities. The results showed that the performance of eddy viscosity models is good given the complexity of the flow.

Dixon et al., (2007) studied intra-particle reaction and gradients for steam-reforming with porous spherical packing. The intra-particle effects such as conduction, species diffusion and reaction were coupled to 3D external flow and temperature fields. The authors noticed that, the assumption of symmetric species and temperature fields inside the pellets holds for particles away from the tube wall, hence particles positioned in the strong temperature gradient near the tube wall show substantial aberrations.

Taskin et al., (2007) made a comparative study of the wall segment (a 120° segment of the full bed) and full-bed models of fixed bed reactor with cylindrical packing. The WS model is not a realistic condition for cylindrical packing but suitable to for lowering computational effort. CFD simulations were done of heat transfer fields for industrial stream reformer. The radial velocity and temperature profiles of the two models were found to be in good agreement.

Augier et al., (2010) carried out numerical simulations of transport properties in packed bed of spherical particles. A very dense packing of spheres was built using Discrete Element Method. Heat or mass transfer has been well predicted by the model, in agreement with the Kunii-Levenspiel correlation. Longitudinal and transverse dispersion coefficients were determined and compared with theoretical and empirical dispersion expressions. CFD were found to be in acceptable agreement with literature. The near wall channelling effect was well predicted by the model.

Behnam et al., (2010) investigated catalyst deactivation for dehydrogenation of propane to propene. CFD has been used to couple the transport and reaction processes occurring inside the cylindrical pellet to the gas flow around the pellet. Due to the large imposed temperature gradient across wall particles

Wehinger et al., (2015) carried out detailed simulations of catalytic fixed-bed reactor with dry reforming of methane, showing the advantages of modelling heterogeneous catalytic fixed bed

reactors. The resolved simulations, according to the authors, can contribute a better understanding, so better choice of multiscale chemical reactors.

3.3 TRANSESTERIFICATION REACTION

The increasing demand for energy have placed a huge burden on the finite fossil fuels, which could trigger an energy crisis. Consequently, there has been increased interest in alternative, renewable and environmental friendly energy resources. Transesterification is the processes of producing biodiesel using renewable feed stock, in which plant oil reacts with alcohol to produced fatty acid methyl esters (biodiesel) and glycerol as the by-product. These esters have a good potential as an alternative or an emergency fuel to replace petroleum diesel. Biodiesel has a lower carbon footprint than petroleum diesel.

Chemically, biodiesel is a combination of fatty alkyl esters, or esters formed by fatty acids and an alcohol. Although transesterification has long been used in production of detergents, the resultant product was initally used as a diesel fuel by Austrian scientists during early 1980s (Mittelbach, 1983).

The feedstock oil, type of alcohol to be used, the catalyst type, and the method to produce are primary concerns in producing the esters. The reaction kinetics of the transesterification is to be understood for controlling the reaction temperature, reaction rates and energies of activation.

Plant oils and animal fats are potential feedstocks for the biodiesel production as they have similar composition. The chemical and physical properties of the oils and fats are mostly determined by the fatty acids they comprise and their location in triacylglycerol molecule.

Fats and oils are generally stated as glycerides as the glycerol molecule has three hydroxyl groups where a fatty acid can be attached. Glycerol, a component of vegetable oil and a by-product of biodiesel production, has structure as shown in Figure 3-1 (a). A triglyceride is a tri-ester of glycerol and three fatty acids. The fatty acids attached to it determine its properties.

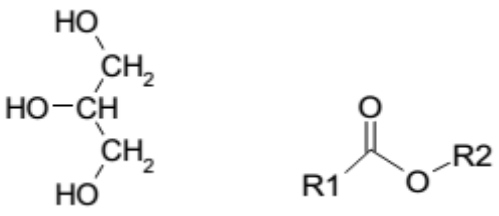

(a) (b)

Figure 3-1 (a) Glycerol molecular structure (b) Form of ester compound

Alcohols are carbon-based compounds of the form R-OH, where R is a hydrocarbon. Usual alcohols used in producing biodiesel are methanol, ethanol, propanol, and butanol. Among which, methanol is the most commonly used, which is commonly produced from natural gas. For ethanol and higher alcohols, it is harder to use because it forms emulsions easily, making the separation of end products more difficult, making methanol more preferred in which the chief products glycerol and fatty acid methyl esters are barely miscible and thus form distinct phases – the upper ester phase and the lower glycerol phase.

The biodiesel ester contains fatty acid chain on one side, replacing R1 in Figure 3-1 (b), and a hydrocarbon called an alkane on the other, replacing R2, hence biodiesel is called a fatty acid alkyl ester. Generally, the form of alkane is specified as 'methyl ester' or 'ethyl ester'. Typical, biodiesel molecule methyl ester is shown in Figure 3-2.

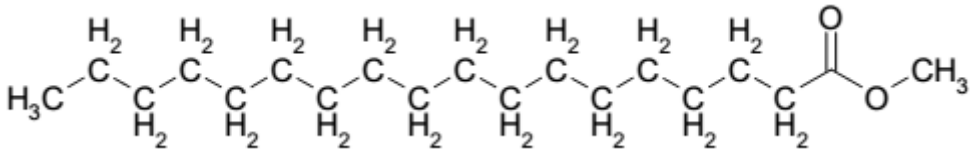

Figure 3-2 A typical biodiesel molecule, shown here is a fatty acid methyl ester.

Transesterification can be catalysed by both homogeneous (alkalis and acids) and heterogeneous catalysts. Homogeneous catalysts show greater performance when free acid content is <1%, however their separation from reaction mixture is expensive. Also, large amount of waste water is generated during separation and cleaning of catalyst and products and formation of unwanted by-product (soap) by reaction of free fatty acid. (Phan and Phan, 2008). Heterogeneous catalysts are advantageous when the free fatty acid content (FFA) is >1% and can be separated more easily from reaction products. Heterogeneous catalyst can be operated in continuous processes and can be reused and regenerated. They are also environmentally benign. (Ma and Hanna, 1999).

Acid-catalysed reactions are used to convert FFAs to esters, or soaps to esters as a pre-treatment step for high FFA feedstocks and are characterised by slow reaction rate and high ratio of alcohol. High conversion with acid-catalysed transesterification can be achieved by increasing molar ration of alcohol to oil, reaction temperature, catalyst loading and reaction time. (Gerpen and Canakci, 1999). Base catalysed process is fairly fast but is influenced by water content and FFAs of oils or fats. FFAs can react with base catalysts to form soap and water. Soap formation

not only decreases the yield of alkyl esters but also intensifies the effort in separation of biodiesel, glycerol.

The ratio of alcohol to triglyceride is an important variables effecting the yield of triglyceride. The stoichiometry for transesterification requires three moles of alcohol and one mole of glyceride to yield three moles of fatty acid ester and one mole of glycerol. The molar ratio is associated with the type of catalyst used. An acid catalysed reaction needed a 30:1 ratio of BuOH to soy oil, while alkali-catalysed reaction essential only a 6:1 ratio to achieve the same ester yield for a given time (Freedman et al., 1986). . Higher molar ratios result in greater ester conversion over a shorter time.

Kinetics

The chemical kinetics of transesterification remain controversial despite its importance. Most of the kinetic models are based on best fits for the empirical data. Some of the models are contradictory. (Komers et al., 2002)

Freedman and colleagues of USDA began the work on chemical kinetics specific to biodiesel production (Freedman et al., 1986, 1984). In Freedman's model, the overall stoichiometry of the transesterification reaction requires 1 mol of triglyceride (TG) for 3 mol of alcohol to give 3 mol of ester and 1 mol of glycerol (GL). This reaction is either acid or alkaline catalysed, comprises of stepwise conversions of TG to DG to MG to G producing 3 mol of ester in the process. In Figure 3-3, the reaction scheme for the production of mono alkyl esters from triacylglycerol is shown. Fatty acid methyl esters (FAMEs) are the most commonly used biodiesel species, while fatty acid ethyl esters are only produced in laboratory or pilot scale.

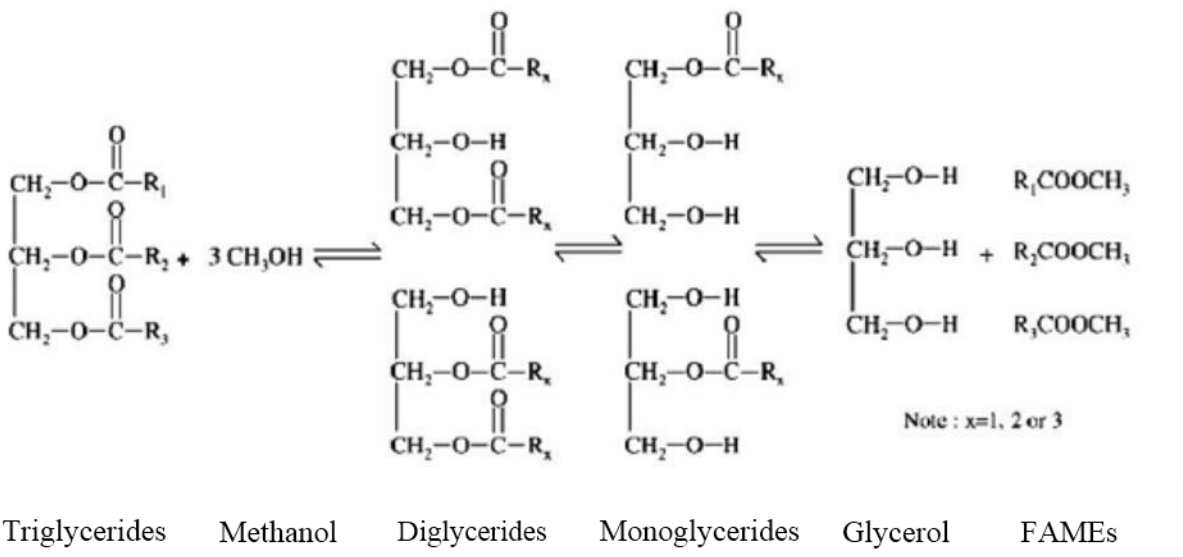

Figure 3-3 Reaction scheme for production of fatty acid methyl esters by transesterification (Pinnarat and Savage, 2008)

This reaction consists of three consecutive reversible reactions, where in each step, one mole of methyl ester is liberated and mono-glyceride and diglyceride are intermediate products (Freedman et al., 1986). When a reversible reaction takes place at the same rate in the forward and reverse directions, it is said to be in equilibrium. The overall reaction for transesterification can be represented by a single reaction as

$$TG + 3A \xrightarrow{k} G + 3E \tag{3-1}$$

This takes place in the following three steps

$$TG + A \underset{k_2}{\overset{k_1}{\rightleftharpoons}} DG + E \tag{3-2}$$

$$DG + A \underset{k_4}{\overset{k_3}{\rightleftharpoons}} MG + E \tag{3-3}$$

$$MG + A \underset{k_6}{\overset{k_5}{\rightleftharpoons}} GL + E \tag{3-4}$$

Where k_1, k_3, k_5 are rate constants for forward reactions and k_2, k_4 and k_6 are rate constants for backward reactions in reactions (3-2), (3-3), and (3-4) respectively.

Where,

TG = triglycerides,

DG = diglycerides,

MG = monoglycerides,

G = glycerol,

A = alcohol and

E = alkyl esters

When the molar ratio of alcohol to triglyceride is very high, then the concentration of alcohol to triglyceride is very high, then the concentration of alcohol can be assumed constant. The reaction rate then depends only on triglyceride concentration, a condition Freedman called ‘pseudo-first order (Freedman et al., 1986) . The rate equation for this reaction can be described as

$$-\frac{d[TG]}{dt} = k[TG] \tag{3-5}$$

3.3.1 Supercritical fluid technology for transesterification

In non-supercritical transesterification process high free fatty acids (FFA) and water cause soap formation, reduced catalyst efficiency and catalyst consumption, all these effects result in low conversion. Also, the reactants are not miscible at ambient temperature and form two layers. These difficulties can be lessened using supercritical methanol (alcohol) in the transesterification reaction The phase separation depends on the mixture composition, temperature and pressure. A supercritical single phase can be achieved by having sufficiently high temperature and pressure. As a result, good contact between the oil and alcohol greatly increase the rate of reaction. The low solubility of the alcohol in the triglyceride phase causes lag time in the reaction, which is overcome under supercritical conditions. The supercritical transesterification reaction is considerable fast completing in within minutes compared to non-supercritical reaction which takes several hours. So, supercritical process is a good method for having continuous operation. (He et al., 2007a)

Madras et al., (2004) have investigated for supercritical methanol and ethanol, determining the kinetics, getting high conversions at temperatures up to 400°C and 200bar. He et al., (2007b) have developed a continuous process with supercritical methanol using a tube reactor, and were able to get high conversions when side reactions are evaded by gradual heating,

However, due to severe temperature and pressure conditions causing high operational cost, synthesis of biodiesel by supercritical methanol is not a practical possibility on the large scale practice in industry. So, for past few years, research has been focused to decrease the severity

of the reaction conditions. The use of co-solvents, such as carbon dioxide, hexane, propane or subcritical condition with slight amount of catalyst, can reduce the operating conditions. Cao et al., (2005) used propane to decrease the operating temperature, and not using catalyst, found the purification to be much simpler. Demirbas, (2007) used co-solvents like hexane and carbon dioxide in supercritical methanol method to increase the product yield and 98% yield of methyl esters were observed in 20 min at the subcritical condition (160°C) with 0.1 wt.% KOH and methanol to oil ratio of 24:1. Maçaira et al., (2011) of our research group at the UPC have used carbon dioxide as supercritical co-solvent with methanol, making it possible to obtain high biodiesel yields at mild temperature conditions. A similar work was done at this group comparing with ethanol with yield of 80% in reaction time around 6 min. (Santana et al., 2012)

Below is the *Table 3-1* from literature (Borugadda and Goud, 2012) that shows various routes used to produce biodiesel under supercritical conditions.

Oil	Alcohol	Oil to alcohol	Temperature and pressure	Reaction time	Ester con	Reference
Sunflower	Methanol	1:40	350°C, 200 bar	40 min	96	(Madras et al., 2004)
Jatropha	Methanol	1:40	350°C, 200 bar	40 min	>90	(Rathore et al., 2007)
Rapeseed	Methanol	1:42	350°C, 45 MPa	250 s	95	(Saka et al., 2001)
Hazelnut	Methanol	1:42	350°C, NA	300s	95	(Demirbaş, 2002)
Jatropha	Methanol	1:40	350°C, 200 bar	40 min	90	(Rathore et al., 2007)
Soybean	Methanol	1:40	350°C, 35 MPa	25 min	-	(He et al., 2007b)
Coconut	Methanol	1:42	350°C, 19 MPa	400 s	95-96	(Kunchana et al., 2006)
Cottonseed	Methanol,	1:41	350°C, NA	8 min	98	(Demirbaş, 2008)
Sunflower	Methanol,	-	200°C - 400°C,	-	-	(Madras et al., 2004)
Soybean	Methanol	-	200 - 300°C	20 h	-	(Demirbaş, 2002)
Rapeseed	-	1:42	350 - 400°C, 45-65 MPa	10 min	-	(Rathore and Madras, 2007)
Jatropha	Methanol	-	8.4 MPa, 593 K	4 min	-	(Hawash et al., 2009)
Soybean	Methanol	1:24	280°C, 12.8 MPa	10 min	98	(Sawangkeaw et al., 2010)
Soybean	Methanol	1:24	280°C, 14.3 MPa	10 min	98	(Sawangkeaw et al., 2010)
Soybean	Methanol	1:6	400°C, 2 MPa	1.6 min	98	(Sawangkeaw et al., 2010)
Rapeseed	Methanol	1:24	250°C, 6 MPa	10 min	97	(Sawangkeaw et al., 2010)
Soybean	Methanol	1:24	160°C, 10 MPa	10 min	98	(Sawangkeaw et al., 2010)

Soybean	Methanol	1:40	310°C, 13 MPa	12 min	96	(Sawangkeaw et al., 2010)
Sunflower	Methanol	1:41	252°C, -	6 min	98	(Sawangkeaw et al., 2010)
Soybean	Methanol	1:36	250°C, 24 MPa	10 min	96	(Sawangkeaw et al., 2010)
Rapeseed	Methanol	1:24	20 MPa, 280 °C	30	95	(Sawangkeaw et al., 2010)
Soybean	Ethanol	1:40	20 MPa, 350°C	15	80	(Raman et al., 2008)
Soybean	Ethanol	1:40	20 MPa, 350°C	15 min	77.	(Raman et al., 2008)
Rapeseed	Ethanol	1:42	25 MPa, 350°C	12 min	10	(Raman et al., 2008)
Rapeseed	Ethanol	1:42	40 MPa, 300°C	20 min	80	(Raman et al., 2008)
Cottonseed	Ethanol	1:41	–, 250°C	8 min	85	(Raman et al., 2008)
Linseed	Ethanol	1:41	–, 250°C	8 min	>8	(Raman et al., 2008)
Sesame	Ethanol	1:40	20 MPa, 325°C	40 min	10	(Raman et al., 2008)
Mustard	Ethanol	1:40	20 MPa, 325°C	25 min	10	(Raman et al., 2008)
Sunflower	Ethanol	1:40	20 MPa,400°C	40 min	10	(Raman et al., 2008)
Castor	Ethanol	1:40	20 MPa, 350°C	30 min	10	(Raman et al., 2008)
Linseed	Ethanol	1:40	20 MPa, 350°C	40 min	10	(Raman et al., 2008)
Palm	Ethanol	1:50	20 MPa, 400°C	30 min	95	(Raman et al., 2008)
Groundnut	Ethanol	1:50	20 MPa, 400°C	30 min	95	(Raman et al., 2008)
Pongamia	Ethanol	1:50	20 MPa, 400°C	30 min	90	(Raman et al., 2008)
Jatropha	Ethanol	1:50	20 MPa, 400°C	30 min	90	(Raman et al., 2008)

Table 3-1 Transesterification reaction under supercritical condition. (Borugadda and Goud, 2012)

REFERENCES

Augier, F., Idoux, F., Delenne, J.Y., 2010. Numerical simulations of transfer and transport properties inside packed beds of spherical particles. Chem. Eng. Sci. 65, 1055–1064. doi:10.1016/j.ces.2009.09.059

Behnam, M., Dixon, A.G., Nijemeisland, M., Stitt, E.H., 2010. Catalyst Deactivation in 3D CFD Resolved Particle Simulations of Propane Dehydrogenation. Ind. Eng. Chem. Res. 49, 10641–10650. doi:10.1021/ie100456k

Borugadda, V.B., Goud, V. V., 2012. Biodiesel production from renewable feedstocks: Status and opportunities. Renew. Sustain. Energy Rev. 16, 4763–4784. doi:10.1016/j.rser.2012.04.010

Calis, H.P.A., Nijenhuis, J., Paikert, B.C., Dautzenberg, F.M., Bleek, C.M. Van Den, 2001. CFD modelling and experimental validation of pressure drop and # ow pro " le in a novel

structured catalytic reactor packing. Chem. Eng. Sci. 56, 1713–1720.

Cao, W., Han, H., Zhang, J., 2005. Preparation of biodiesel from soybean oil using supercritical methanol and co-solvent. Fuel 84, 347–351. doi:10.1016/j.fuel.2004.10.001

Coussirat, M., Guardo, A., Mateos, B., Egusquiza, E., 2007. Performance of stress-transport models in the prediction of particle-to-fluid heat transfer in packed beds. Chem. Eng. Sci. 62, 6897–6907. doi:10.1016/j.ces.2007.08.071

Dalman, M.T., Merkin, J.H., McGreavy, C., 1986. Fluid flow and heat transfer past two spheres in a cylindrical tube. Comput. Fluids 14, 267–281.

Debus, K., Nirschl, H., Delgado, A., Denk, V., 1998. Numerische simulation des lokalen impulsaustausches in kugelschüttungen. Chemie Ing. Tech. 415–418.

Demirbaş, A., 2008. Studies on cottonseed oil biodiesel prepared in non-catalytic SCF conditions. Bioresour. Technol. 9, 1125.

Demirbaş, A., 2007. Biodiesel from sunflower oil in supercritical methanol with calcium oxide. Energy Convers. Manag. 48, 937–941. doi:10.1016/j.enconman.2006.08.004

Demirbaş, A., 2002. Biodiesel from vegetable oils via transesterification in supercritical methanol. Energy Convers. Manag. 43, 2349–2356. doi:10.1016/S0196-8904(01)00170-4

Derkx, O.R., Dixon, A.G., 1996. Determination of the Fixed Bed Wall Heat Transfer Coefficient Using Computational Fluid Dynamics. Numer. Heat Transf. Part A Appl. 29, 777–794. doi:10.1080/10407789608913819

Dixon, A.G., Arias, J., Willey, J., 2003. Wall-to-liquid mass transfer in fixed beds at low flow rates. Chem. Eng. Sci. 58, 1847–1857. doi:10.1016/S0009-2509(02)00685-1

Dixon, A.G., Cresswell, D.L., 1979. Theoretical Prediction of Effective Heat Transfer Parameters in Packed Beds. AIChE J. 25, 663–676.

Dixon, A.G., Taskin, M.E., Hugh Stitt, E., Nijemeisland, M., 2007. 3D CFD simulations of steam reforming with resolved intraparticle reaction and gradients. Chem. Eng. Sci. 62, 4963–4966. doi:10.1016/j.ces.2006.11.052

Dwivedi, P.N., Upadhyay, S.N., 1977. Particle-Fluid Mass Transfer in Fixed and Fluidized Beds. Ind. Eng. Chem. Process Des. Dev. 16, 157–165.

Freedman, B., Butterfield, R.O., Pryde, E.H., 1986. Transesterification Kinetics of Soybean Oil. J. Am. Oil Chem. Soc. 63.

Freedman, B., Pryde, E.H., Mounts, T.L., 1984. Variables affecting the yields of fatty esters from transesterified vegetable oils. J. Am. Oil Chem. Soc. 61, 1638–1643. doi:10.1007/BF02541649

Freund, H., Zeiser, T., Huber, F., Klemm, E., Brenner, G., Durst, F., Emig, G., 2003. Numerical simulations of single phase reacting flows in randomly packed fixed-bed reactors and experimental validation. Chem. Eng. Sci. 58, 903–910. doi:10.1016/S0009-2509(02)00622-X

Gerpen, J. Van, Canakci, M., 1999. Biodiesel production via acid catalysts. Trans. ASAE 42, 1203–10.

Guardo, A., Coussirat, M., Larrayoz, M.A., Recasens, F., Egusquiza, E., 2004. CFD Flow and Heat Transfer in Nonregular Packings for Fixed Bed Equipment Design. Ind. Eng.

Chem. Res. 43, 7049–7056. doi:10.1021/ie034229+

Guardo, A., Coussirat, M., Recasens, F., Larrayoz, M.A., Escaler, X., 2006. CFD study on particle-to-fluid heat transfer in fixed bed reactors: Convective heat transfer at low and high pressure. Chem. Eng. Sci. 61, 4341–4353. doi:10.1016/j.ces.2006.02.011

Gulijk, C. van, van Gulijk, C., 1998. Using computational fluid dynamics to calculate transversal dispersion in a structured packed bed. Comput. Chem. Eng. 22, S767–S770. doi:Doi 10.1016/S0098-1354(98)00144-6

Gunjal, P.R., Ranade, V. V., Chaudhari, R. V., 2005. Computational study of a single-phase flow in packed beds of spheres. AIChE J. 51, 365–378. doi:10.1002/aic.10314

Hawash, S., Kamal, N., Zaher, F., Kenawi, G., 2009. Biodiesel fuel from Jatropha oil via non-catalytic supercritical methanol transesterification. Fuel 88, 579–82.

He, H., Sun, S., Wang, T., Zhu, S., Sun, Æ.S., Wang, Æ.T., 2007a. Transesterification kinetics of soybean oil for production of biodiesel in supercritical methanol. JAOCS, J. Am. Oil Chem. Soc. 84, 399–404. doi:10.1007/s11746-007-1042-8

He, H., Wang, T., Zhu, S., 2007b. Continuous production of biodiesel fuel from vegetable oil using supercritical methanol process. Fuel 86, 442–447. doi:10.1016/j.fuel.2006.07.035

Hjertager, L.K., Hjertager, B.H., Solberg, T., 2002. CFD modelling of fast chemical reactions in turbulent liquid flows. Comput. Chem. Eng. 26, 507–515. doi:10.1016/S0098-1354(01)00799-2

Jiang, Y., Khadilkar, M.R., Al-Dahhan, M.H., Dudukovic, M.P., 2002. CFD of multiphase flow in packed-bed reactors: II. Results and applications. AIChE J. 48, 716–730. doi:10.1002/aic.690480407

Komers, K., Skopal, F., Stloukal, R., Machek, J., 2002. Kinetics and mechanism of the KOH - Catalyzed methanolysis of rapeseed oil for biodiesel production. Eur. J. Lipid Sci. Technol. 104, 728–737. doi:10.1002/1438-9312(200211)104:11<728::AID-EJLT728>3.0.CO;2-J

Kunchana, B., Sukunya, M., Ruengwit, S., Somkiat, N., 2006. Continuous production of biodiesel via transesterification from vegetable oils in supercritical methanol. Energy and Fuels 20, 812.

Kunii, D., Suzuki, M., 1967. Particle-to-fluid heat and mass transfer in packed beds of fine particles. Int. J. Heat Mass Transf. 10, 845–852. doi:10.1016/0017-9310(67)90064-6

Li, C.-H., Finlayson, B.A., 1976. Heat Transfer in Packed Beds - A Reevaluation. Chem. Eng. Sci. 32, 1055–1066.

Logtenberg, S.A., Dixon, A.G., 1998a. Computational Fluid Dynamics Studies of the Effects of Temperature-Dependent Physical Properties on Fixed-Bed Heat Transfer. Ind. Eng. Chem. Res. 37, 739–747.

Logtenberg, S.A., Dixon, A.G., 1998b. Computational fluid dynamics studies of fixed bed heat transfer. Chem. Eng. Process. Process Intensif. 37, 7–21. doi:10.1016/S0255-2701(97)00032-9

Logtenberg, S.A., Nijemeisland, M., Dixon, A.G., 1999. Computational fluid dynamics simulations of fluid flow and heat transfer at the wall-particle contact points in a fixed-bed reactor. Chem. Eng. Sci. 54, 2433–2439. doi:10.1016/S0009-2509(98)00445-X

Ma, F., Hanna, M.A., 1999. Biodiesel production : a review. Bioresour. Technol. 70, 1–15.

Maçaira, J., Santana, A., Recasens, F., Larrayoz, M.A., 2011. Biodiesel production using supercritical methanol/carbon dioxide mixtures in a continuous reactor. Fuel 90, 2280–2288. doi:10.1016/j.fuel.2011.02.017

Madras, G., Kolluru, C., Kumar, R., 2004. Synthesis of biodiesel in supercritical fluids. Fuel 83, 2029–2033. doi:10.1016/j.fuel.2004.03.014

Magnico, P., 2003. Hydrodynamic and transport properties of packed beds in small tube-to-sphere diameter ratio: Pore scale simulation using an Eulerian and a Lagrangian approach. Chem. Eng. Sci. 58, 5005–5024. doi:10.1016/S0009-2509(03)00282-3

McKenna, T.F., Spitz, R., Cokljat, D., 1999. Heat transfer from catalysts with computational fluid dynamics. AIChE J. 45, 2392–2410. doi:10.1002/aic.690451113

Mittelbach, M., 1983. Diesel fuel derived from vegetable-oils: preparation and use of rape oil methyl-ester. Energy Agric. 2, 369–384.

Nijemeisland, M., Dixon, A.G., 2004. CFD study of fluid flow and wall heat transfer in a fixed bed of spheres. AIChE J. 50, 906–921. doi:10.1002/aic.10089

Nijemeisland, M., Dixon, A.G., 2001. Comparison of CFD simulations to experiment for convective heat transfer in a gas–solid fixed bed. Chem. Eng. J. 82, 231–246. doi:10.1016/S1385-8947(00)00360-0

Nijemeisland, M., Dixon, A.G., Stitt, E.H., 2004. Catalyst design by CFD for heat transfer and reaction in steam reforming. Chem. Eng. Sci. 59, 5185–5191. doi:10.1016/j.ces.2004.07.088

Nirschl, H., Dwyer, H.A., Denk, V., 1995. Three-dimensional calculations of the simple shear flow around a single particle between two moving walls. J. Fluid Mech. 283, 273–285. doi:10.1016/S0301-9322(97)88402-9

O'Brien, R.D., 2004. Fats and Oils: Formulating and Processing for Applications. CRC Press. Florida.

Parsons, I.M., Porter, K.E., 1992. Gas flow patterns in packed beds: A computational fluid dynamics model for wholly packed domains. Gas Sep. Purif. 6, 221–227. doi:10.1016/0950-4214(92)80026-F

Petre, C.F., Larachi, F., Iliuta, I., Grandjean, P.A., Grandjean, B.P.A., 2003. Pressure drop through structured packings: Breakdown into the contributing mechanisms by CFD modeling 58, 163–177. doi:10.1613/jair.301

Phan, A., Phan, T., 2008. Biodiesel production from waste cooking oils. Fuel 87, 3490.

Pinnarat, T., Savage, P., 2008. Assessment of noncatalytic biodiesel synthesis using supercritical reaction conditions. Ind. Eng. Chem. Res. 47, 6801.

Raman, J., Sariah, A., Denis, P., Seng, C., Pogaku, R., 2008. Production of biodiesel using immobilized lipase—a critical review. Crit. Rev. Biotechnol. 28, 253.

Rathore, V., Madras, G., 2007. Synthesis of biodiesel from edible and non-edible oils in supercritical alcohols and enzymatic synthesis in supercritical carbon dioxide. Fuel 86, 2650–2659. doi:10.1016/j.fuel.2007.03.014

Romkes, S.J.., Dautzenberg, F.M., van den Bleek, C.., Calis, H.P.A., 2003. CFD modelling and experimental validation of particle-to-fluid mass and heat transfer in a packed bed at very low channel to particle diameter ratio. Chem. Eng. J. 96, 3–13. doi:10.1016/j.cej.2003.08.026

Saka, S., Kusdiana, D., 2001. Biodiesel fuel from rapeseed oil as prepared in supercritical methanol. Fuel 80, 225–231.

Santana, A., MaçAira, J., Larrayoz, M.A., 2012. Continuous production of biodiesel using supercritical fluids: A comparative study between methanol and ethanol. Fuel Process. Technol. 102, 110–115. doi:10.1016/j.fuproc.2012.04.014

Sawangkeaw, R., Bunyakiat, K., Ngamprasertsith, S., 2010. A review of laboratoryscale research on lipid conversion to biodiesel with supercritical methanol (2001-2009). J. Supercrit. Fluids 55, 1–13.

Sørensen, J.P., Stewart, W.E., 1974a. Computation of forced convection in slow flow through ducts and packed beds—I extensions of the graetz problem. Chem. Eng. Sci. 29, 811–817. doi:10.1016/0009-2509(74)80199-5

Sørensen, J.P., Stewart, W.E., 1974b. Computation of forced convection in slow flow through ducts and packed beds—II velocity profile in a simple cubic array of spheres. Chem. Eng. Sci. 29, 819–825. doi:10.1016/0009-2509(74)80200-9

Sørensen, J.P., Stewart, W.E., 1974c. Computation of forced convection in slow flow through ducts and packed beds—III. Heat and mass transfer in a simple cubic array of spheres. Chem. Eng. Sci. 29, 827–832. doi:10.1016/0009-2509(74)80201-0

Sørensen, J.P., Stewart, W.E., 1974d. Computation of forced convection in slow flow through ducts and packed beds—IV. Convective boundary layers in cubic arrays of spheres. Chem. Eng. Sci. 29, 833–837. doi:10.1016/0009-2509(74)80202-2

Stüber, F., Vazquez, A.M., Larrayoz, M.A., Recasens, F., 1996. Supercritical Fluid Extraction of Packed Beds : External Mass Transfer in Upflow and Downflow Operation. Ind. Eng. Chem. Res. 35, 3618–3628.

Taskin, M.E., Dixon, A.G., Stitt, E.H., 2007. CFD Study of Fluid Flow and Heat Transfer in a Fixed Bed of Cylinders. Numer. Heat Transf. Part A Appl. 52, 203–218. doi:10.1080/10407780601149896

Tobiś, J., 2002. Modeling of the Pressure Drop in the Packing of Complex Geometry. Ind. Eng. Chem. Res. 41, 2552–2559.

Tobiś, J., 2000. Influence of bed geometry on its frictional resistance under turbulent flow conditions. Chem. Eng. Sci. 55, 5359–5366. doi:10.1016/S0009-2509(00)00155-X

Wakao, N., 1976. Particle-to-fluid transfer coefficients and fluid diffusivities at low flow rate in packed beds. Chem. Eng. Sci. 31, 1115–1122. doi:10.1016/0009-2509(76)85021-X

Wakao, N., Funazkri, T., 1978. Effect of fluid dispersion coefficients on particle-to-fluid mass transfer coefficients in packed beds. Correlation of Sherwood Numbers. Chem. Eng. Sci. 33, 1375–1384. doi:10.1016/0009-2509(78)85120-3

Wakao, N., Kaguei, S., 1982. Heat and Mass Transfer in Packed Beds, Gordon and Breach, Science Publishers, Inc. Gordon and Breach.

Wakao, N., Kaguei, S., Funazkri, T., 1979. Effect of fluid dispersion coefficients on particle-to-fluid heat transfer coefficients in packed beds. Correlation of Nusselt Numbers. Chem. Eng. Sci. 34, 325–336.

Wehinger, G.D., Eppinger, T., Kraume, M., 2015. Detailed numerical simulations of catalytic fixed-bed reactors : Heterogeneous dry reforming of methane. Chem. Eng. Sci. 122, 197–209. doi:10.1016/j.ces.2014.09.007

Winterberg, M., Tsotsas, E., 2000. Correlations for effective heat transport coefficients in beds packed with cylindrical particles. Chem. Eng. Sci. 55, 5937–5943.

Yagi, S., Wakao, N., 1959. Heat and Mass Transfer from Wall to Fluid in Packed Beds. AIChE J. 5, 79–85.

Zeiser, T., Lammers, P., Klemm, E., Li, Y.W., Bernsdorf, J., Brenner, G., 2001. CDF-calculartion of flow, dispersion and reaction in a catalyst filled tube by the lattice Boltzmann method. Chem. Eng. Sci. 56, 1697–1704. doi:10.1016/S0009-2509(00)00398-5

CHAPTER IV

4. WALL-TO-FLUID HEAT TRANSFER

4.1 INTRODUCTION

4.1.1 Packed bed wall-to-fluid heat transfer

Packed beds are widely used in chemical industries due to their simplicity in structure and effectiveness in terms of providing abundant contact area for surface reaction or for heat or mass transfer area. The study of heat transfer rate in packed beds is important not only important for design of heat exchangers but also for catalytic reactors. In shell-and-tube heat exchanger type packed bed reactor, heat is added (or removed) through the packed tube wall from a surrounding heat exchange fluid. To attain optimal performance, it is necessary to have good model for heat transfer.

Mathematical Models for heat transfer in packed beds

A simple one dimensional model was developed (Wasch and Froment, 1972), which considers the temperature of the fluid to be uniform in section perpendicular to flow, not taking into account the radial gradients. This model fails significantly in estimating the conditions, as there is significant cross flow, and heat effects in catalytic reactors. This led to the use of a two-dimensional model, in which heat transfer in radial direction is superimposed upon the heat transfer by convection in the flow direction.

There are several mechanisms in radial heat flow, so to limit the complexity, the packing material and the fluid are taken as a continuum, neglecting the temperature differences between the fluid and solid phases, through which heat transfer is considered to occur by 'effective conduction'. This 'conduction' is characterized by 'effective conductivity' k_{er}. This conductivity, when calculated at various locations perpendicular to the flow, is found to be decreasing strongly near the wall. This extra resistance near the wall causing the temperature jump, is described by as wall heat transfer coefficient h_w, which described the heat rate as:

$$q_A = h_w(T_w - T_i) \tag{4-1}$$

A two-dimensional model which has been a standard model, was presented by of Coberly and Marshall, (1951), Hatta and Maeda, (1948) which is described as pseudo-homogeneous model,

is a classic heat balance equation given by Equation (4-2) for a cylindrical packed bed operated as a steady-state heat exchanger, assuming phase continuum. The steady state temperature profiles can be described by this equation solution. The solution of the two-dimensional model is used for determining effective radial thermal conductivity k_e, and wall heat transfer coefficient h_w from axial temperature profiles. This model is preferred over the heterogeneous model which is more complicated and requires more transport parameters.

$$GC_{p,f}\frac{\partial T}{\partial z}=k_r\frac{1}{r}\frac{\partial}{\partial r}\left(r\frac{\partial T}{\partial r}\right)+k_{ax}\left(\frac{\partial^2 T}{\partial x^2}\right) \tag{4-2}$$

With the following boundary conditions, applicable to the situation simulated:

(4-3)

$$T=T_0 \qquad z=0$$
$$\frac{\partial T}{\partial r}=0 \qquad r=0$$
$$k_r\frac{\partial T}{\partial r}=h_w\left(T_w-T\right) \qquad r=R$$

Some other models

The parameters h_w and k_r are also found to be influenced by the solid thermal conductivity and tube-to-particle diameter ratio (N). Dixon and Cresswell, (1979) derived a theoretical model that has taken into account these influences. A two-phase model was developed which relates the effective wall heat transfer coefficient and the solid thermal conductivity of the particle.

A model with the axial velocity component v_z which varies radially, was developed to account for the channelling near the walls was introduced. This model was in better agreement with the experimental data. (Daszkowski and Eigenberger, 1992). This model represents a modification of earlier models, which assume plug-flow.

Empirical correlations proposed for packed bed heat transfer

Various researchers have proposed empirical correlations using their experimental data of temperatures in packed beds. Experimental data has been expressed in terms of h_w and k_r (or in terms of dimensionless parameters Nu_w and k_r/k_f), obtained from models with temperature profiles from experiments. Considerable amount of discrepancy exists with these literature data. Some of the correlations are mentioned below.

Hanrattry, (1954) developed a correlation for their experimental data, for cylindrical packings. The correlation, given by Equation (4-4).

$$\frac{h_w\, d_p}{k_f} = 1.1 \sqrt{\frac{d_p U_0 \rho}{\mu}}\ \sqrt{\frac{C_p \mu}{k}} \tag{4-4}$$

The wall heat transfer coefficient and effective thermal conductivity are found to be influenced by the length of the packed bed. Li and Finlayson, (1976) have compiled experimental data and correlated which reduced effect of length. The correlation (for $20 \leq Re \leq 800$; $3.3 < N < 20$) they presented for cylindrical packing is:

$$\frac{h_w\, d_p}{k_f} = 0.16 \left(\frac{G d_p}{\mu}\right)^{0.93} \tag{4-5}$$

A correlation was presented for wall-to-fluid heat transfer data for various particles of different thermal conductivities.by Yagi & Wakao, (1959), is given by Equation (4-6).

$$\frac{h_w\, d_p}{k_f} = 3 + 0.054\, \mathrm{Pr}\, Re_p \tag{4-6}$$

Experimental Techniques to study the heat transfer in packed beds

Heat exchanger studies in packed beds are commonly carried out in wall-heated cylindrical beds with steam jackets (Gunn and Khalid, 1975; Wasch and Froment, 1972). Many difficulties are encountered in accurately measuring temperature profiles inside packed beds. Direct intrusive measurement would mean obstructing the flow and disturbing the geometry of the bed. This poses as an influential issue especially at low Re when temperature profiles very flat, making measurement errors very significant. This questions the accuracy of experimental data and their corresponding correlation predictions (Freiwald and Paterson, 1992). Another way would be to obtain temperatures at the outlet of the bed. This method only adds to the discrepancy. A non-disturbing experimental methods that could be used to obtain flow patterns in packed beds is magnetic resonance imaging (MRI). However, this is restricted to low flow rates, up-to *Re* = 100, and for fluid that can produce suitable signal for measurement, like water. Gas flow has not been investigated using MRI. CFD studies can be of significant use in estimating the flow profiles (Harris et al., 1996).

4.1.2 Use of CFD in packed bed heat transfer simulation

The use of computational fluid dynamics to simulate the fluid flow and heat transfer phenomena is becoming a standard approach. It was found to be useful in wide areas of applications including reaction engineering. This method is advantageous in obtaining temperature profiles without disturbing the geometry, avoiding the consequence of building expensive pilot-plants. (Harris et al., 1996; Ranade, 2002)

Actual temperatures and velocities in the bed are required for determining the effective heat transfer parameters. Derkx and Dixon, (1996) have used CFD in a packed bed by solving 3D Navier-Stokes equations using FEM, reporting Nu_w values. They studied fluid and heat flow around three spheres. The wall heat transfer coefficient was obtained using the temperature profiles data, and compared with empirical correlations. Logtenberg and Dixon, (1998) studied wall-to-fluid heat transfer to a small number of spherical particles of a packed bed. They studied the heat transfer parameters from CFD, experiments and correlations for plug flow models and axial axially dispersed plug flow model at different temperatures. Particles with no internal voids showed better performance in heat transfer. The above studies were some of the earliest CFD studies in packed bed geometries. They used a very basic packed bed geometry with small number of particles as an approximation of packed bed. These studies were done for laminar flow. Guardo et al., (2005) done simulations of wall-to-fluid heat transfer in a packed bed 44 randomly-packed spheres studying the influence of various turbulence models. With the increasing computational power full bed packed columns are used for CFD work. Behnam et al., (2013) used a validated full bed 3D CFD model temperature profiles to test the 2D pseudo-continuum model, given by Equation (4-2).

Spherical catalysts have often been employed for packed bed heat transfer studies. CFD has been used for designing the catalyst shape in packed bed (Taskin et al., 2008). Dixon et al., (2008) studied wall-to-particle heat transfer for cylindrical multi-holed catalysts.

Guardo et al., (2006) have performed simulations for heat transfer from particle-to-fluid which occurs during an endothermic reaction. The simulations were performed for low and supercritical high pressure conditions. Only some studies are available for CFD studies for packed beds at supercritical conditions are available. The properties of supercritical fluids vary generally between those of liquids and gases. This is due to the fact that gaseous phase and liquid phases merge together and become indistinguishable at critical point. These properties, especially density, are highly sensitive to small changes in temperature and pressure near the

critical point. (Baiker, 1999). Experiments at high Reynolds were performed by Dixon et al., (2012), validating CFD simulations.

4.2 SIMULATION STRATEGY

When modelling packed beds, there has to be good qualitative understanding and accurate quantitative description of fluid flow and heat transfer. The platform used to construct the geometry has to be one which allows for the feasibility of generating good mesh and able to capture all the phenomena of the problem.

4.2.1 Packed bed geometry

The packed bed is based on the geometry of a packed bed catalytic reactor which is of length 152mm and diameter 17.5mm (shown in *Figure 4-1* (a)). This reactor is filled with cylindrical particles of diameter 1mm and length of 5mm, resulting in tube-to-equivalent spherical particle diameter ratio of 9. Packed bed models have been usually developed for high tube-to-particle diameter ration (N) beds, in which temperature gradients are less and could be averaged (Winterberg and Tsotsas, 2000b).

A wall-segment (WS) model geometry shown in *Figure 4-1* (c, d) is used, which takes less computational effort. WS model is a 120º segment of the packed bed as opposed to a complete wall (CW) full bed model shown in *Figure 4-1* (b). The WS model geometry was found to have overall axial velocities and temperatures only slightly different as compared to a full bed (CW) model (Taskin et al., 2007). By taking the cut parts as symmetrical, one third of the tube is run for simulations decreasing the computational effort.

The arrangement of the cylindrical particles is random, as shown in *Figure 4-1 (e).* The particles are arranged at random with angle of cylindrical particle axis varying from 0º to 90º to the axis of the tube. Arranging particle at random to avoid bad flow distribution and channelling. Each particle is arranged by sequential operations in the software for moving the particle around in the tube. The cylindrical particles are arranged such that their axis is at angle 0º, 15º, 30º, 45º, 60º, 75º, 90º with the axis of the tube. *Table 4-1* shows the number of particles by their orientation and geometric model. The overall voidage of the bed is about 0.6. Because of slight overlapping (about 1 to 2% of the volume) as shown in *Figure 4-1(e)* the bed void is not exactly the volume deducted due to the particles volume. The whole bed consists of 3780 cylindrical particles. The geometric models are given extensions before and after the bed of

cylinders, in order to minimize the end effects, and the back flow temperature condition at the outlet.

Particles angle with the tube axis	Number of Particles in Half-length WS model	Number of Particles in Full length WS models	Number of Particles in Full packed bed (CW model)
0º	90	180	540
15º	105	210	630
30º	105	210	630
45º	90	180	540
60º	75	150	450
75º	90	180	540
90º	75	150	450

Table 4-1 Particles in half-length and full length wall-segment (WS) model and in full packed bed (CW model) geometry with inclination angles with tube axis

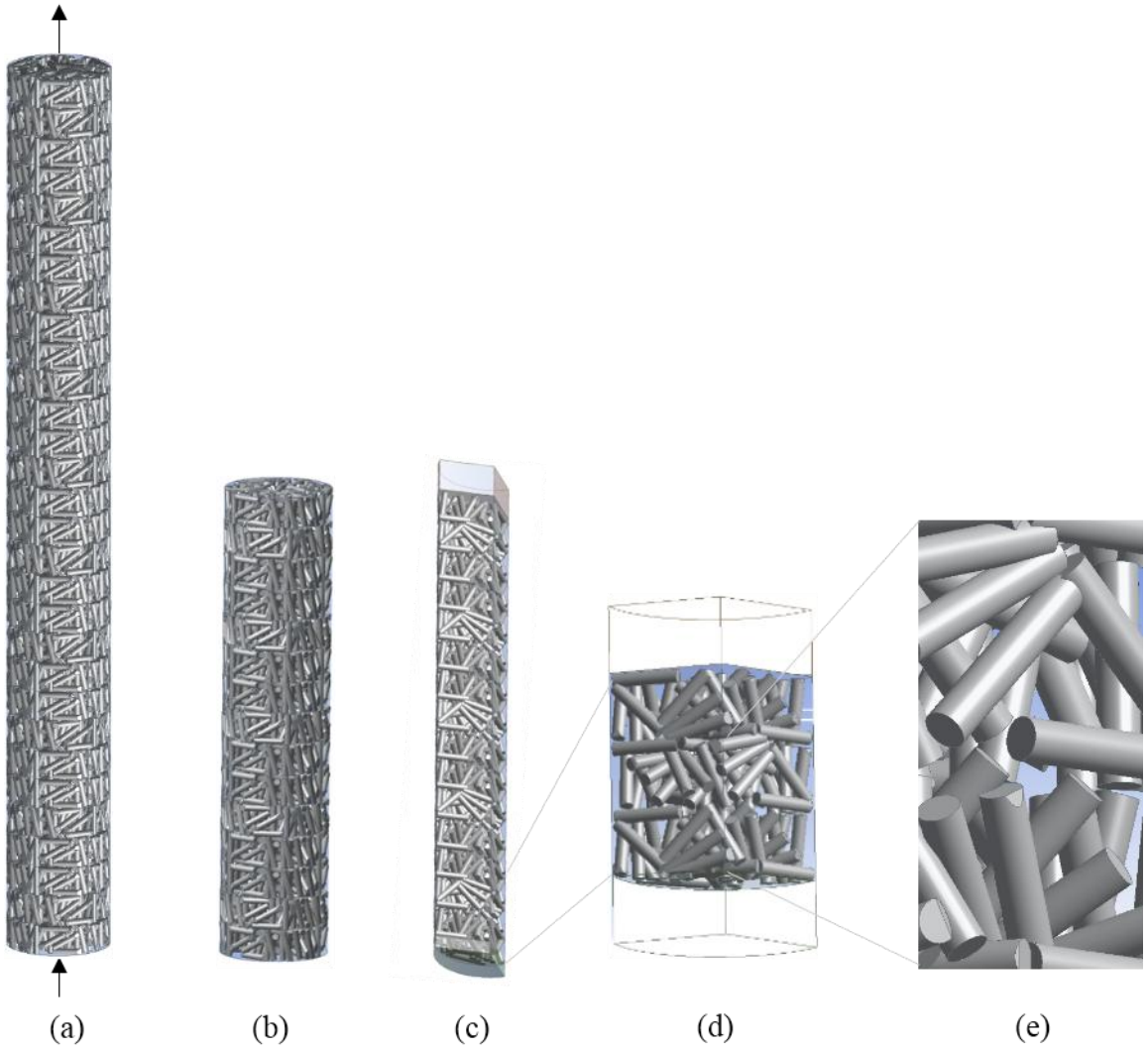

Figure 4-1 Packed bed geometry: (a) Full packed bed CW model; (b) Half-length CW model; (c) A 120° half-length WS model, with inlet and outlet extensions; (d) One-tenth length WS model; and (e) Randomly arranged overlapping cylindrical particles

In the geometries previously reported (called near-miss model) by Dixon group, the particles have small gaps (and assumed zero velocity) between each other to avoid convergence problems, (Nijemeisland and Dixon, 2001). But Guardo et al., (2006) has the particles overlap about 1% at the contact points and found no convergence problem. For the model used current work, particle-to-particle contact areas were overlapped about 1 to 2% of the particle volume with adjacent particles as shown in *Figure 4-1* (e). Some particles were chipped near the wall of the tube, and within the segment sides. This helps in treating the whole particles as a single volume so having ease of mobility of particles and avoiding meshing errors causing convergence problems. The particles are however avoided contact with the tube wall by having a very small gap at the wall contact points. This was done to avoid errors during meshing. No convergence problems were detected during simulation runs.

Packing structure for spherical particles has been well documented. Various packing forms have been studied by Yang et al., (2010), which showed significant influence on flow, pressure drop and heat transfer. Experiments at high Reynolds were performed by Dixon et al., (2012), validating CFD simulations.

4.2.2 Mesh generation and independence tests

The Finite volumes mesh is based on 3D tetrahedral elements. The wall surfaces are meshed using an unstructured triangular mesh as shown in Figure 4-2 (a) and this surface mesh is used to construct the volume mesh. And the particles surfaces are refined by unstructured quadrilateral mesh. The generated mesh was further refined on the surface of the particles (surface mesh by rectangular face sizing), and other sensitive regions of the geometry like the tube-particle contact regions where the particles are cut, although the tube and particles are not in direct contact.

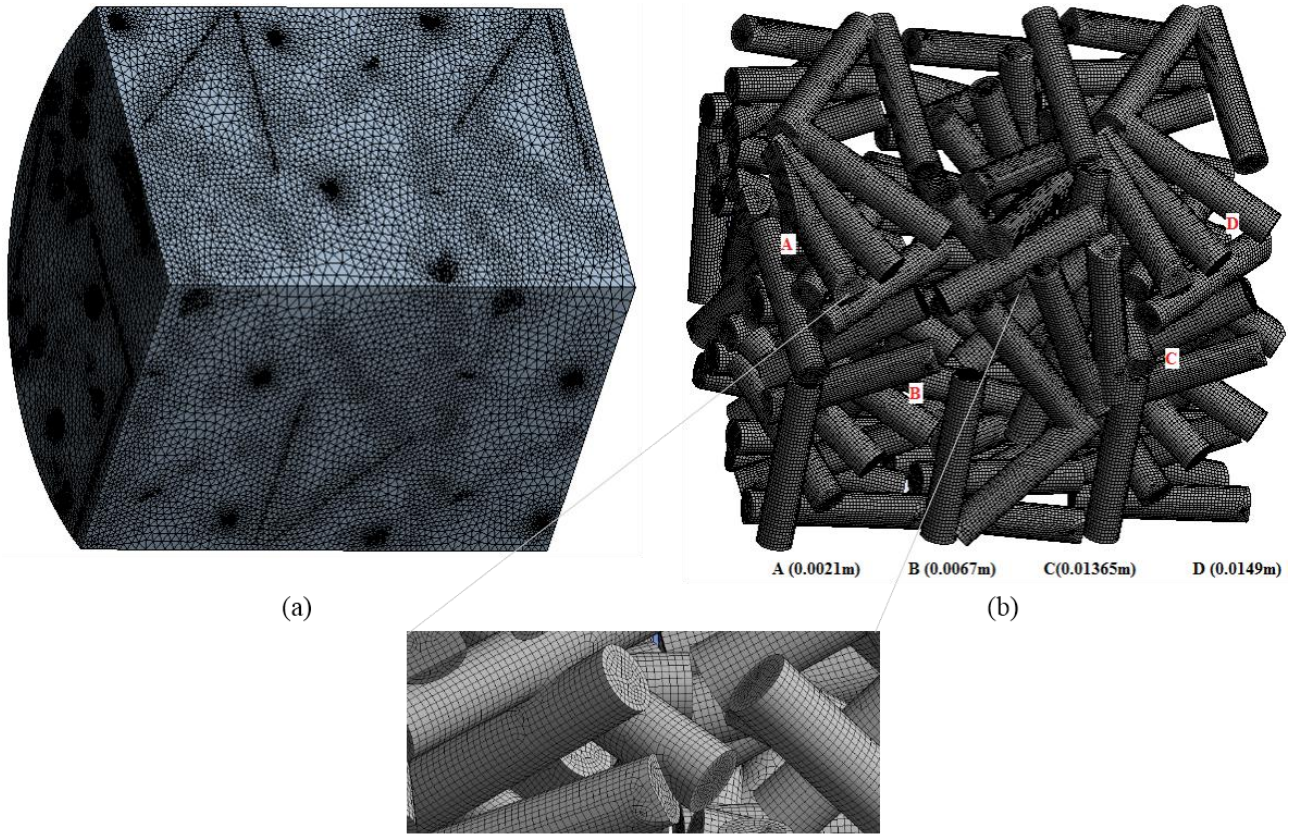

Figure 4-2 Packed bed geometry, shown with mesh of one tenth WS model used for testing the mesh independence (a) the packed bed tube which is bulk meshed. (b) face mesh with element size of 1*10^-4m on the particles surface, with locations A, B, C, D for monitored (c) magnified image of face meshing

Meshing is done with meshes of different degrees of refinement. The number of elements for the different meshes of one-tenth WS model are 1.77, 1.83, 1.94 and 2.18 million as mentioned in Figure 4-3. The *Figure 4-2 (a)* shows a mesh that is checked for independence with face sizing of 1E-4m with meshed tube and the particles with face-sized mesh. Face mesh shown in *Figure 4-2 (b).* This geometry of one-tenth length WS model is meshed with various levels of refinement by checking velocity for flow through the packed bed geometry. And optimum mesh refinement is selected for the heat transfer study. The *Figure 4-3* shows the unchanged velocity for different element refinement levels, given by the number of elements. The velocity remained changed from 0.288583m/s to 0.288571m/s for halving of the element size on the particles surface from 1.2E-4m to 6.0E-5m or for number of elements in the mesh from 1776959 to 2188770. This was tested for four different locations A, B, C, D in the geometry as shown in *Figure 4-3* (b).

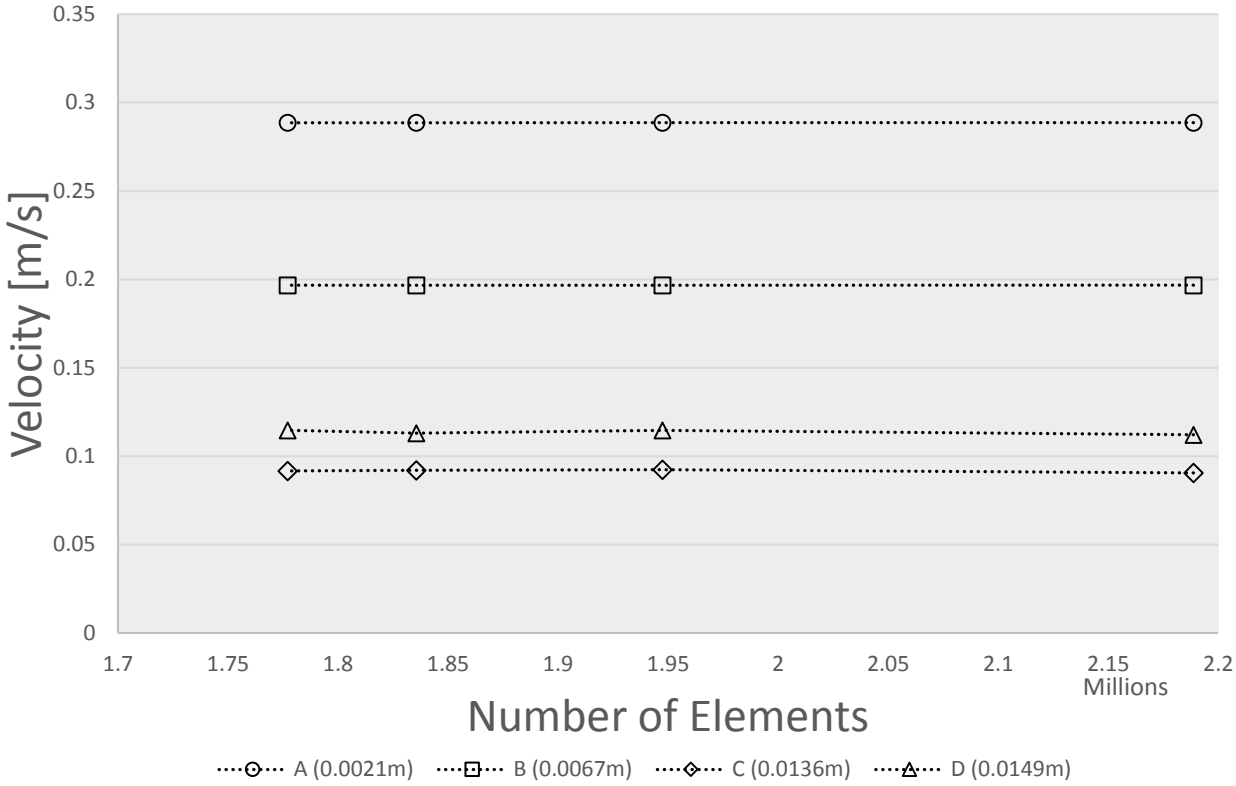

Figure 4-3 Velocity monitored at four locations A, B, C, D, as shown in previous Figure 5-2 (b) in the geometry for four meshes of different refinements for one tenth WS model given by the number of elements

4.2.3 Model Setup

The fluid, mixture of carbon dioxide (CO_2), methanol (CH_3OH) and triolein ($C_{57}H_{104}O_6$), (reactants for transesterification reaction with supercritical solvent CO_2) is flown into the packed bed at 250 bar pressure and 473.15K temperature, is taken to be Newtonian, in laminar flow. The tube wall is maintained at temperature 483.15K. At the inlet, the methanol to triolein molar ratio is 25:1. And carbon dioxide to methanol ratio is 75/25 wt.%. This system is analysed for different inlet velocities, to study the effect of flow rates. The initial Reynolds number (*Re*) is calculated with assumption of average temperature of 478.15K, and the characteristic length for Re is the equivalent spherical diameter of the cylindrical particle volume. Boundary conditions for each analysed case are shown in *Table 4-2*.

Pure component properties are taken at this pressure as a function of temperature. Density, viscosity, thermal conductivity and specific heat of the fluid components are estimated as a function of temperature. Dilute approximation mass diffusivity coefficients are estimated for methanol-carbon dioxide and triolein-carbon dioxide. Methanol and triolein are taken to be dilute species for the diffusivity estimations. The mixture properties are based volume

weighted for density and specific heat, and mass weighted average for thermal conductivity and viscosity. The components form a single phase by the presence of supercritical CO_2. Further discussion on the properties estimation and modelling is given in Appendix A1.

Boundary conditions, methods	Value
Fluid mixture	$CO_2 + CH_3OH + C_{57}H_{104}O_6$
Mass fraction ratio methanol: oil (Case 1)	0.19589: 0.21685
Mass fraction ratio methanol: oil (Case 2)	0.22998: 0.0801
Methanol to oil molar ratio (Case 1)	7.89
Methanol to oil molar ratio (Case 2)	25
Fluid temperature at inlet	473.15 K
Wall temperature	483.15 K
Pressure	25000000 Pa
Fluid velocity at the inlet	0.000249 to 0.25134 m/s
Shear condition on wall, particle surface	No slip
Discretization	First order
Models solved	Flow, energy, species
Flow model	Laminar

Table 4-2 Boundary conditions and methods for the analysed cases

4.2.4 Model Equations and numerical solution

Fluid flow is described by mathematical models (governing equations) which are based on physical principles of conservation of mass, and conservation of momentum. These are accurately described by three-dimensional (3D) Navier-Stokes equations. A Finite Volume (FV) code solves the conservation equations for mass and momentum. These models coupled with energy for flows involving heat transfer and species conservation models are solved for flows involving species mixing or reactions by the FV codes. Further details of the governing equations are given in Chapter II.

The standard numerical solution methods for these models are three spatial discretization methods, finite differences (FD), finite volumes (FV), finite elements methods (FE) (continuum flow methods). A Finite volume (FV) code is employed for this study. For all types of flow, the FV code solves the mass and momentum conservation equations.

The solution to the model is said to be reached when the convergence monitors are no longer decreasing monotonically. The convergence is also checked by examining variables like velocity or temperature at various localities in the geometry. It should be noted that that in complex geometries there exists no single exact solution. The final trend could be oscillatory in nature as there could exist multiple solutions or acceptable limit set is reached. For unstable fluid flow like in packed beds, there exists such flow. The solutions which are within acceptable limits are taken as final.

4.3 RESULTS AND DISCUSSION

In this section the influence of different flow rates on the heat transfer coefficients is examined. The capability of the CFD implemented laminar model is tested for packed bed reactor design for a tertiary mixture of CO_2, methanol and triolein. Simulations were run as shown in Table 4-3, for several flow rates, for the two geometrical models. The heat transfer parameters were estimated for CFD results using a theory based model with axial data from CFD. The numerical results were compared with standard correlations as reference values for heat transfer parameters. Velocity, temperature and density profiles are presented.

Velocity (m/s)	Re obtained	Methanol to oil mass ratio	Methanol to oil mole ratio	Solvent(CO_2 +CH_3OH) flow rate (g/min)	Simulation model used	Case ID
0.00025	0.37	0.905	7.89	0.7239	One-tenth WS	OT.WFHT0.4
0.00174	2.61	0.905	7.89	5.0678	One-tenth WS	OT.WFHT.3
0.00261	3.91	0.905	7.89	7.6018	One-tenth WS	OT.WFHT.4
0.00348	5.21	0.905	7.89	10.135	One-tenth WS	OT.WFHT.5
0.00436	6.52	0.905	7.89	12.669	One-tenth WS	OT.WFHT.7
0.00523	7.82	0.905	7.89	15.203	One-tenth WS	OT.WFHT.8
0.00411	12.28	2.871	25	13.213	Full length WS	F.WFHT.12
0.00661	19.74	2.871	25	21.247	Full length WS	F.WFHT.20
0.00864	25.83	2.871	25	27.792	Full length WS	F.WFHT.26
0.01341	40.06	2.871	25	43.102	Full length WS	F.WFHT.40
0.01750	52.30	2.871	25	56.274	Full length WS	F.WFHT.52
0.02513	75.11	2.871	25	80.817	Full length WS	F.WFHT.75

Table 4-3 Velocity boundary conditions applied to CFD at inlet, obtained Re and the methanol to oil mass and molar ratio, geometrical model used for each case simulated

4.3.1 Velocity and density profiles

Axial and radial cuts were made along the packed bed to generate velocity vector/contour plots for studying velocity distribution in the packed bed The velocity profiles are plotted as velocity vectors coloured by density, magnitude and velocity magnitude contours. These profiles are used, in order to assess the effect of density on the flow magnitude and direction, to check for any buoyancy effects. The profiles were presented for axial and radial cuts.

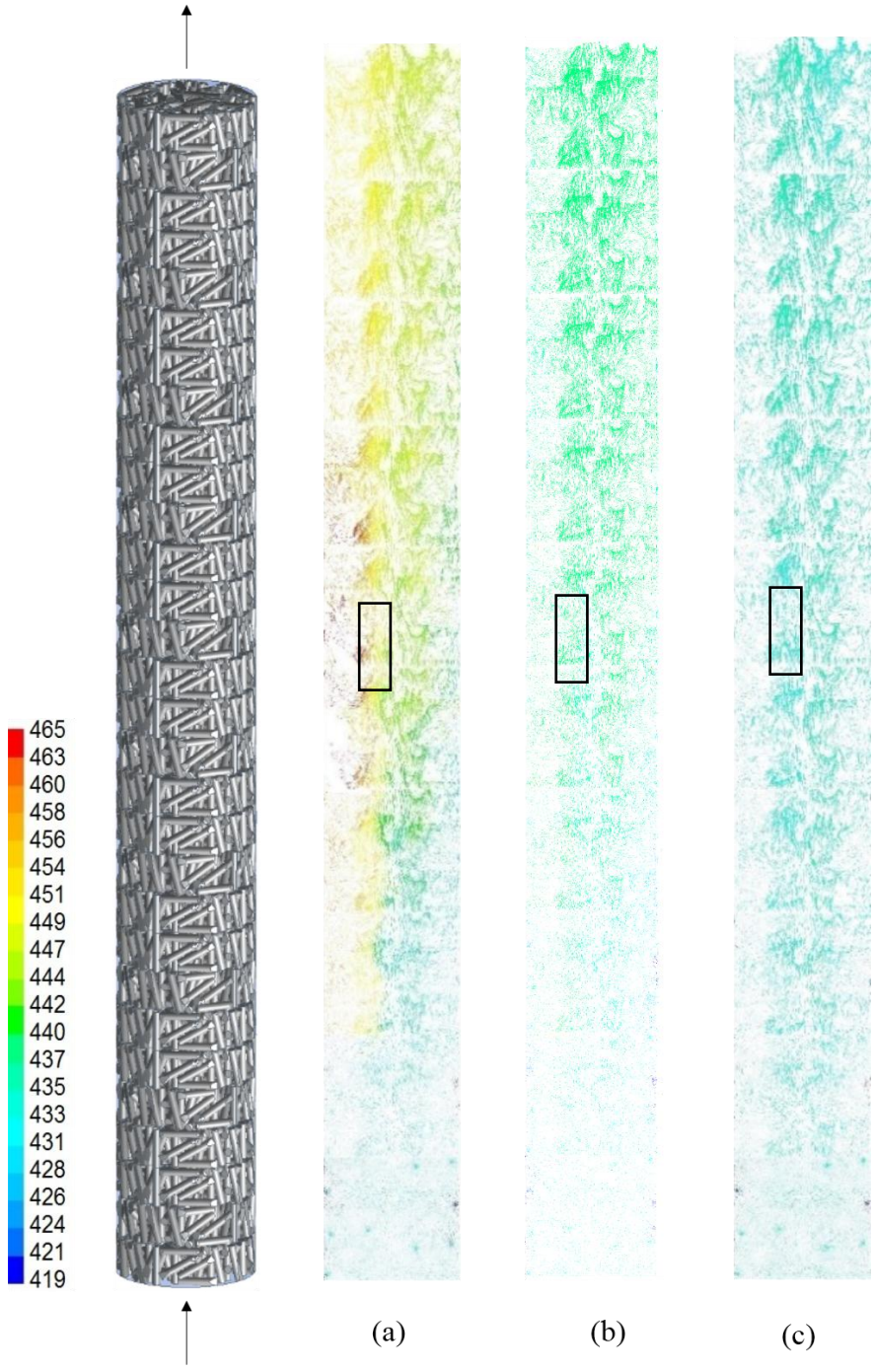

Figure 4-4 Packed bed geometry with velocity vectors coloured by density (kg/m^3) for (a) Re 0.37 (b) Re = 2.6 and (c) Re = 7.8 for one-tenth length wall-segment model with periodic boundary conditions, taken from symmetric planes passing through the axis of the bed, the area in rectangle is shown in Figure 4-5

Velocity vectors on axial cuts for Re = 0.37, 2.6 and 7.8 are shown in *Figure 4-4*. The simulations for these cases were run in a one-tenth length wall-segment model with periodic boundary conditions. The length of the pointers indicates the velocity magnitude and the velocity vectors are coloured by density. At the entrances of the packed bed it can be seen that the vectors are uniform throughout the bed at all the Re. In this area, the pointers are of almost uniform size and are coloured by such that the densities are low. The densities are low here as the fluid is still at low temperature, as wall temperature has less effect at the inlet region.

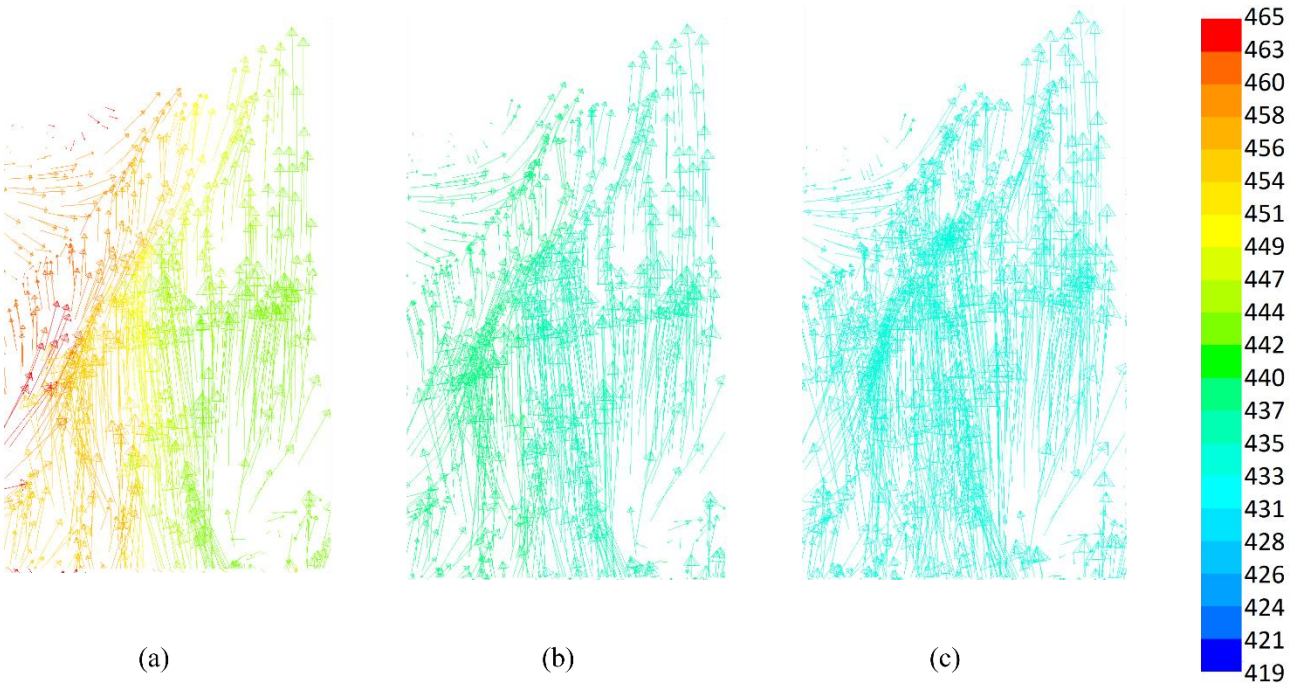

Figure 4-5 Magnified velocity vectors coloured by density (kg/m^3) on axial planes in the middle area of bed shown in rectangle in Figure 4-4, for (a) Re 0.37 (b) Re = 2.6 and (c) Re = 7.8 for one-tenth length wall-segment model with periodic boundary conditions

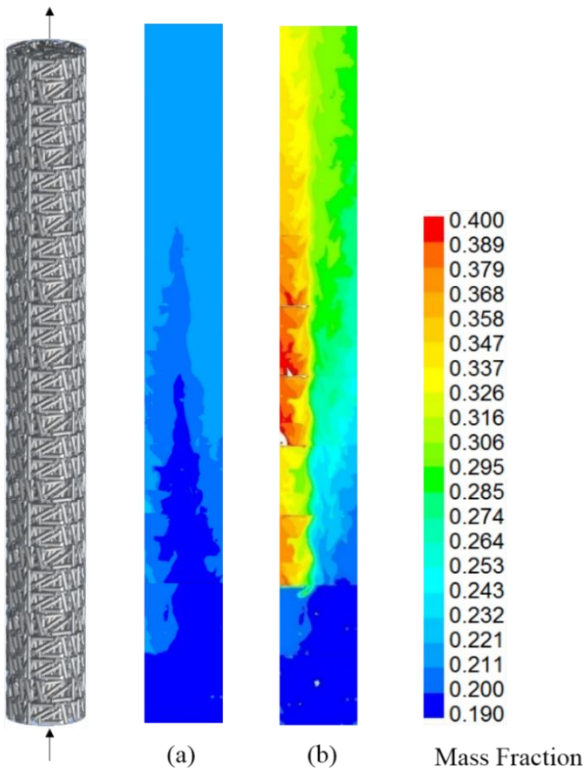

Figure 4-6 Packed bed geometry with methanol mass fraction contours for (a) Re = 7.8 (b) Re = 0.37 for one-tenth length wall-segment model with periodic boundary conditions

Channelling can be seen occurring near the axis of the bed, resulting in strong axial flow and reduced radial flow (lengthy vector pointers in axial region are noticeable). The channelling is seen to be increased with the length of the bed. The velocity has increased about five times the inlet velocity in some constrained areas in these regions. In the magnified images of velocity vectors shown in *Figure 4-5* the channelling and crossflow regions can be observed.

High densities can be observed for very low Re of 0.37 in *Figure 4-4*. For the very low Re, there is accumulation of higher density species methanol and triolein (see *Figure 4-6*) this effect is augmented due to the use of higher oil ratio for the case of Re 7.8 to Re 0.37 (methanol to oil mole ratio is 7.89, while for full-length WS model cases of Re 75 to Re 12, it is 25). Though it is expected that the density to be decreasing for lower Re, due to higher temperature for lower Re, as it is observed for the cases of Re 75 to Re 12 as shown *Figure 4-8*.

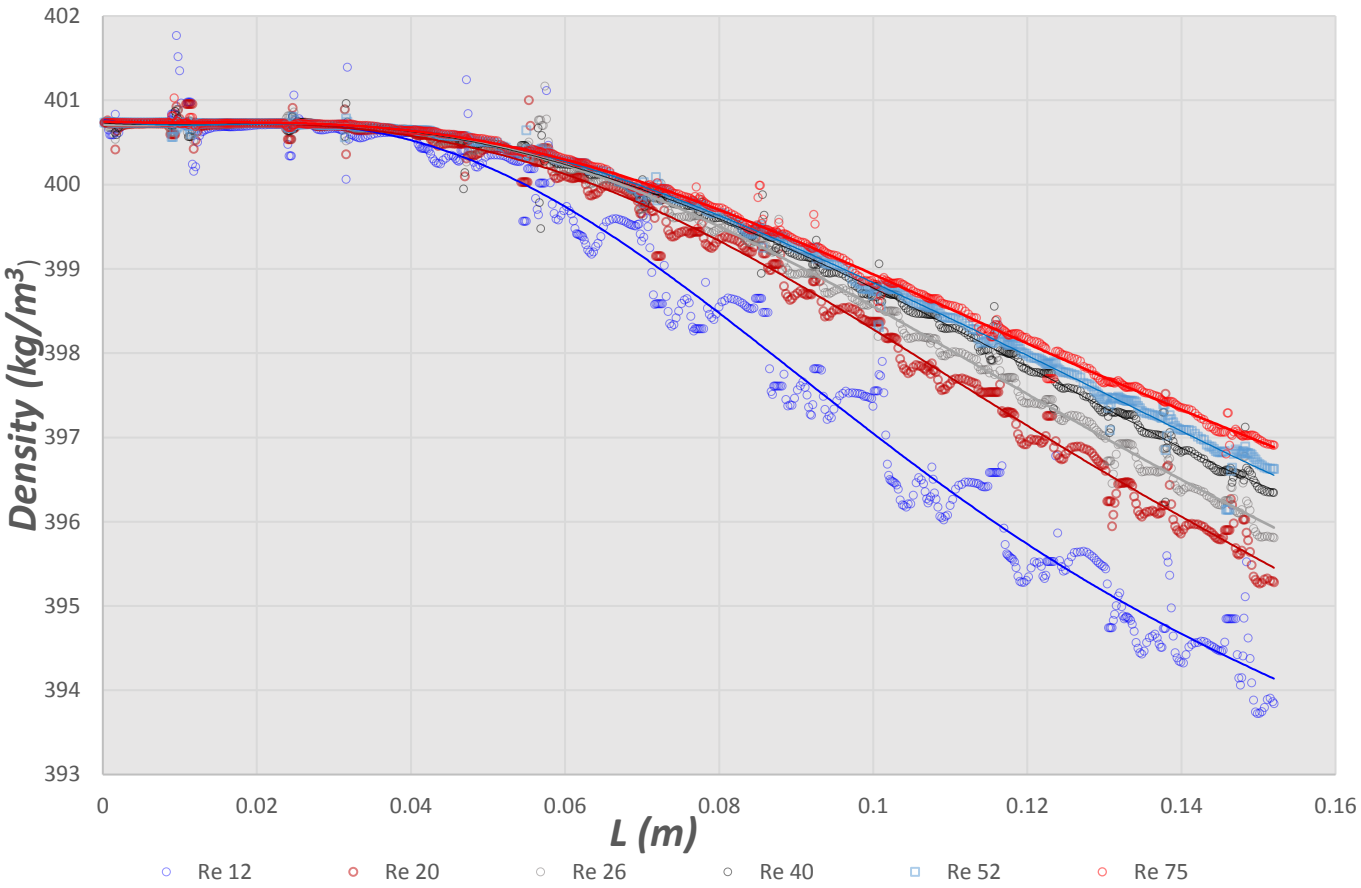

Figure 4-7 Densities along the axial line for full-length WS model with methanol to oil ratio of 25.

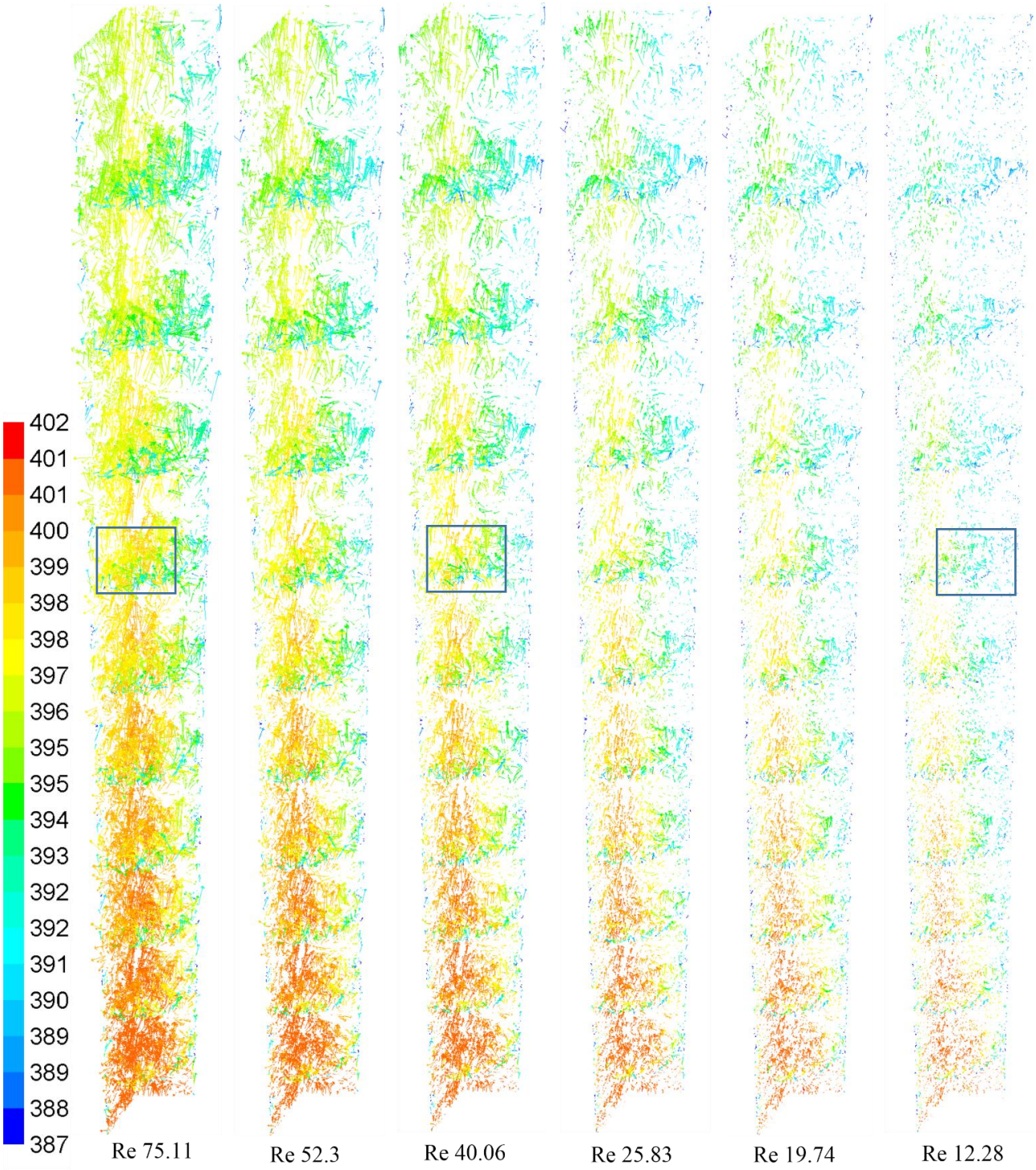

Figure 4-8 Radial and axial velocity vectors coloured by density (kg/m^3) for full length wall segment model, the section in rectangle is shown in Figure 4-9

For Re 75 to Re 12 velocity vectors coloured by density are shown in *Figure 4-8.* Magnified images of the radial plane section in square of *Figure 4-8* are shown in *Figure 4-9*. Velocity vectors coloured by magnitude for Re 75 to Re 12 are shown in *Figure 4-10*.

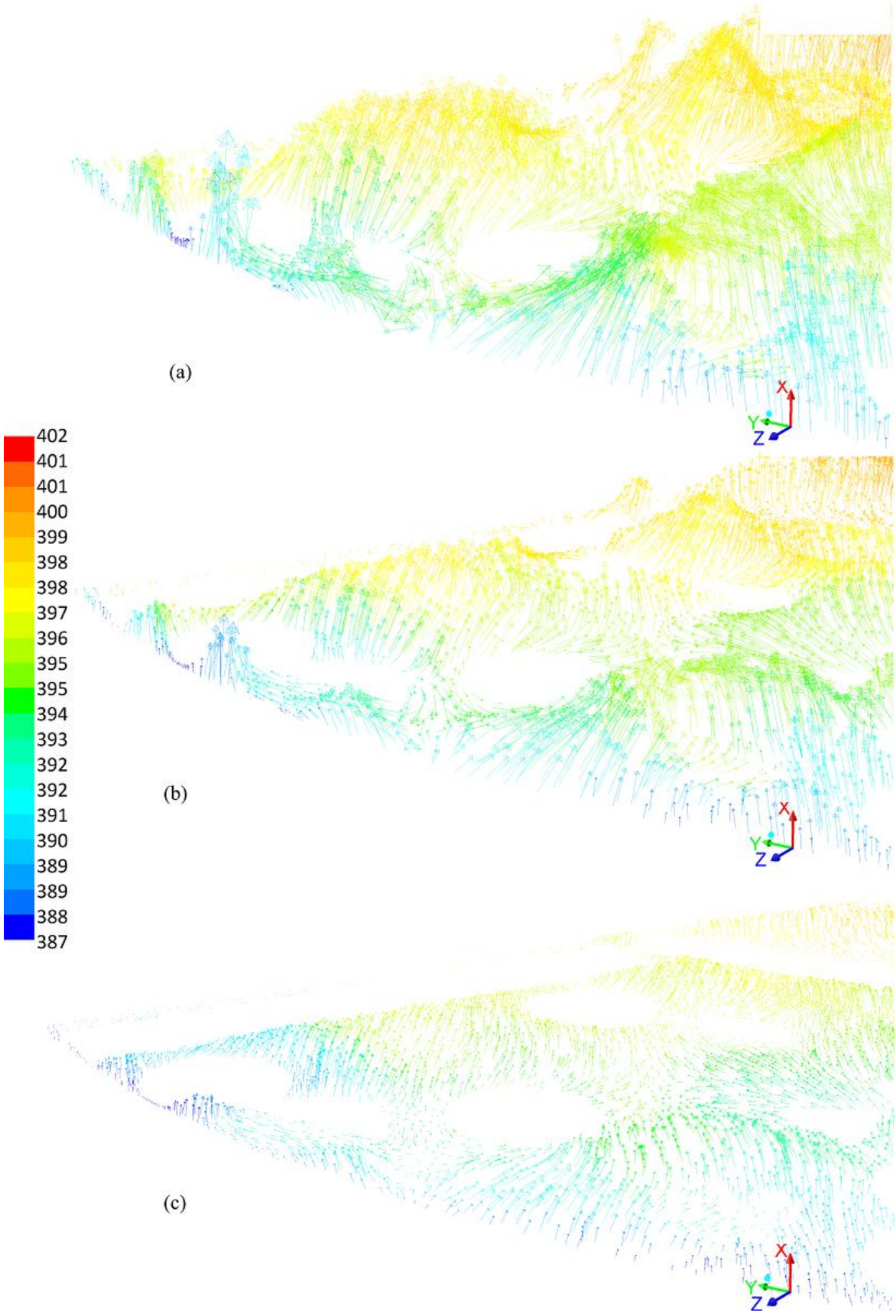

Figure 4-9 Velocity vectors coloured by density (kg/m^3) on radial plane 0.914m into the packed bed for (a) Re 75 (b) Re 40 and (c) Re 12

Stagnation points were noticed near the contact points of the particles (*Figure 4-8* to *Figure 4-10*). Crossflows / secondary flows can be seen where the fluid flows over particles resulting

in cross/back flows. For the low Re, the wall effects and particle surface effects are at a minimum. However, at the ending of the bed crossflows can be seen. The wall effects can be seen in this region of the bed, where the flow is developed. These features mentioned above were observed by Suekane et al., (2003) who used magnetic resonance imaging technique to measure velocity of flow in pore space.

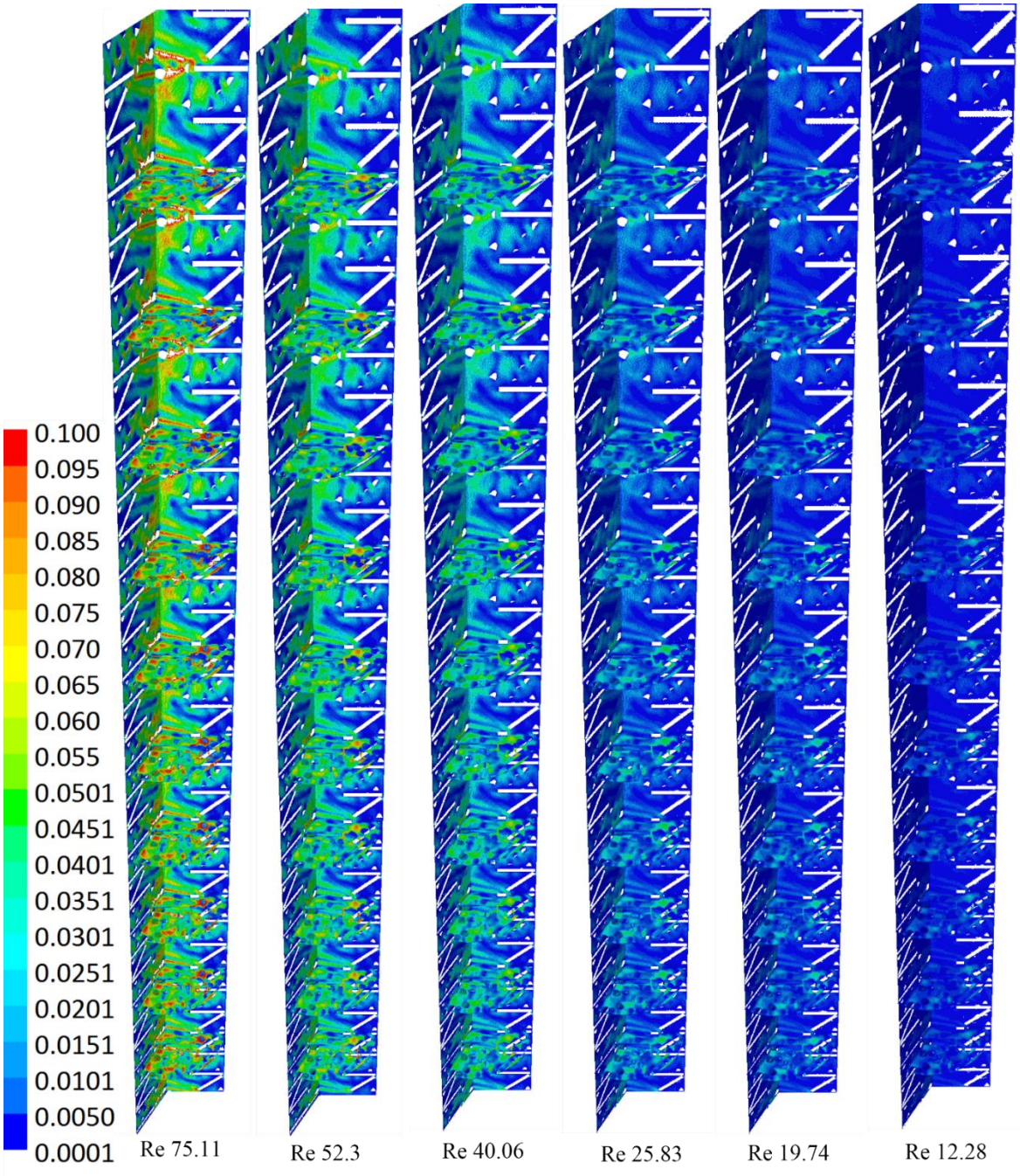

Figure 4-10 Radial and axial velocity contours (m/s) for full length wall segment model

As it can be seen from the velocity contours (*Figure 4-10*) and velocity vectors (*Figure 4-8*), for higher Re, higher velocities were observed away from the walls, whereas for lower

velocities, the velocities were uniform throughout the bed as can be seen in Figure 4-10 (Re 12). Also it can be seen form the density plots along the axial line in *Figure 4-7* that the axial densities are same for up to certain length where the influence of wall temperature is minimum, but as the length is increasing, the densities decreased at a higher rate for lower Re where higher temperature is observed.

4.3.2 Mixed convection

For high pressure flows, mixed convection heat transfer is likely to occur. So the effects of density and flow velocities were studied. With gravitational acceleration opposite to the direction of flow (upward flow), there is greater amount of free/natural convection heat transfer due to presence of large density gradients, resulting in the formation of hydrodynamic instabilities (viz., counter current flow, recirculation, stream differentiation) which are caused by buoyancy effects. (Benneker et al., 1998).

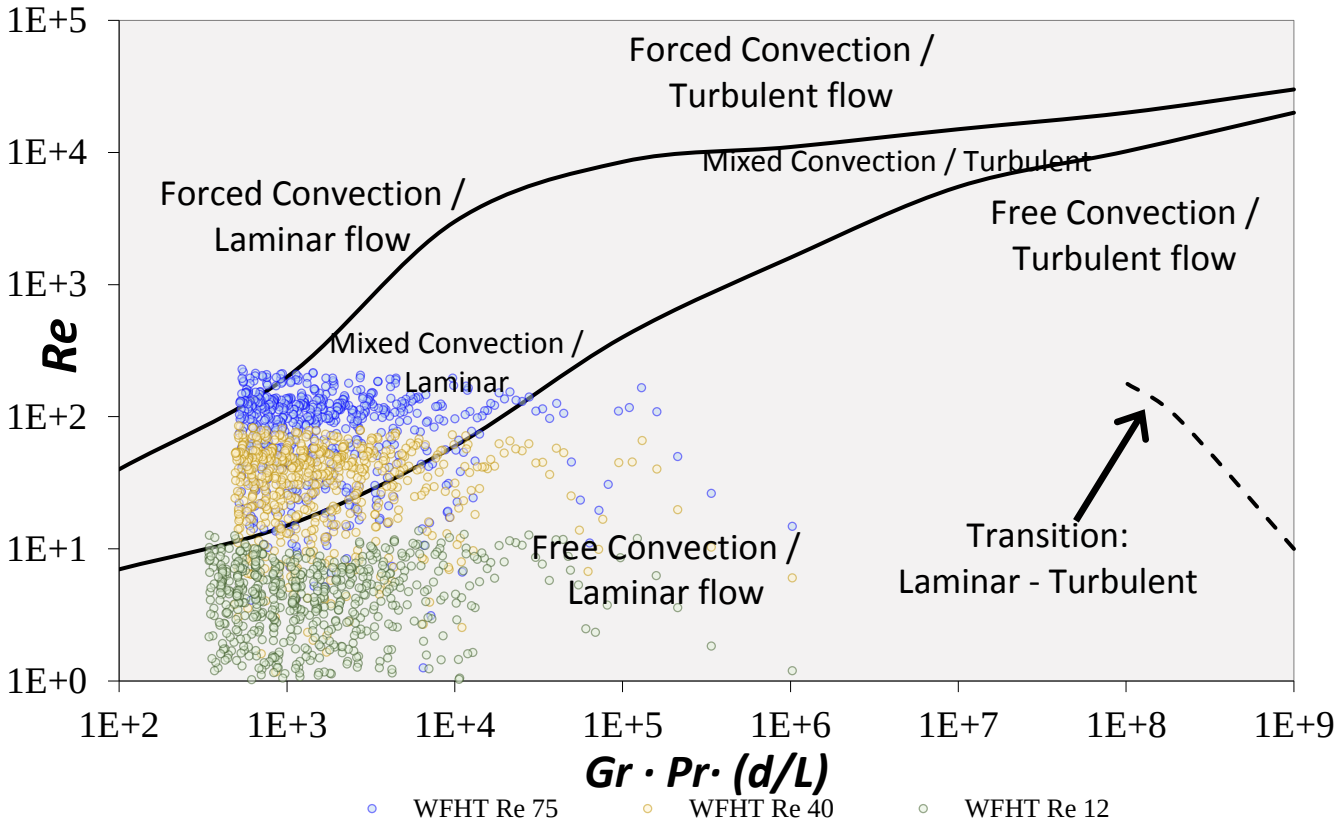

Figure 4-11 Simulation data compared with Metais-Eckert maps for Re 75, Re 40 and Re 12 with data from corresponding axial lines

The data points on axial lines for Re 75 and 40 lie mostly in the mixed convection, laminar area. And for Re 12 the data points lie in the natural convection, laminar area. Showing that the in the axial region for low Re, the heat convection is mostly due to natural convection. So, for higher Re, the heat transfer takes place both by forced convection, and natural convection, as a result of higher velocity of the fluid molecules in the fluid.

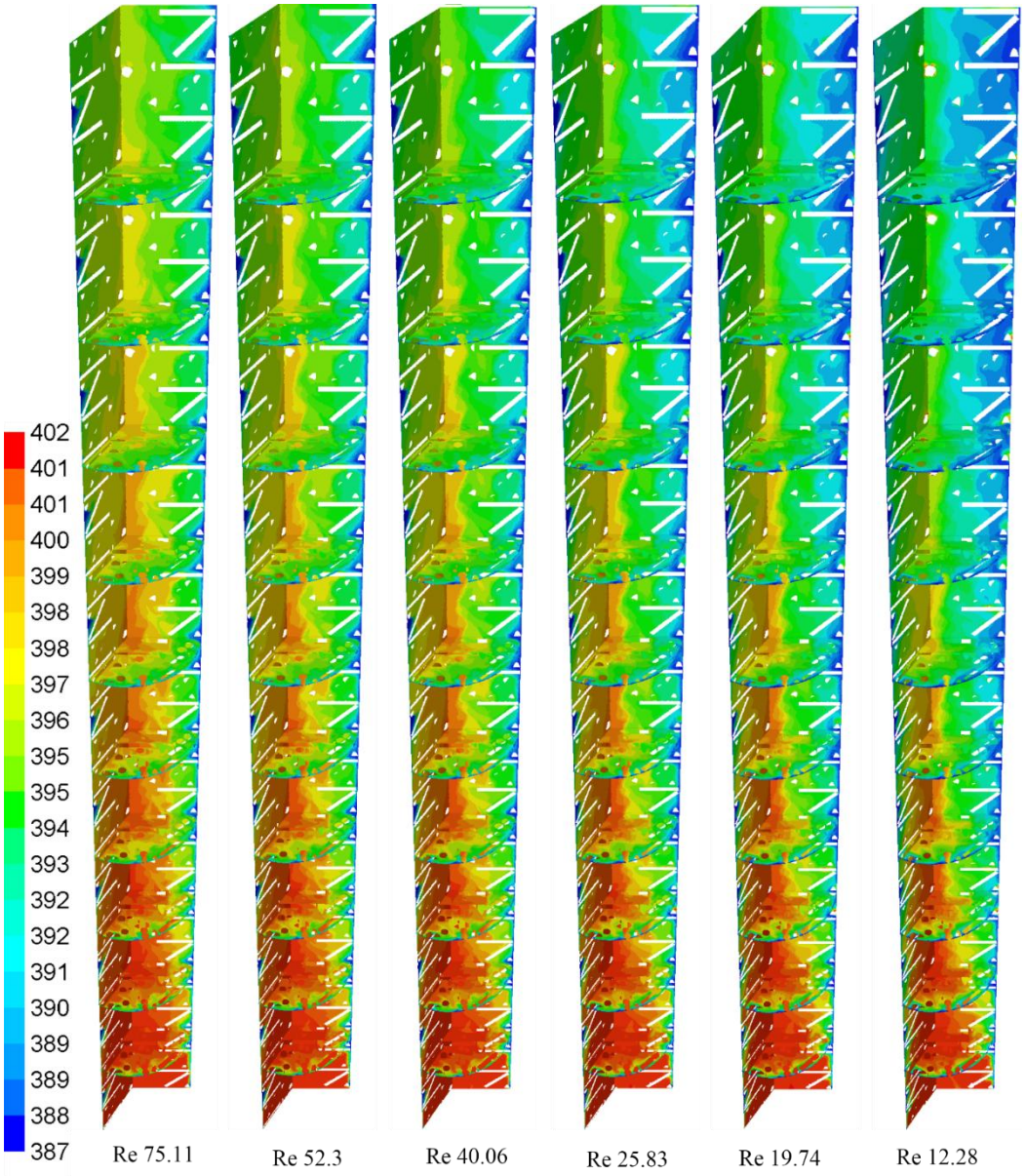

Figure 4-12 Radial and axial density contours (kg/m^3) for full length wall segment model

Figure 4-7 shows higher density fluctuations for Re 12 on the axial line, which causes the natural convection. Figure 5-10 shows density contour plots. The density is decreasing from Re 75 to Re 12, as the overall temperature increased from Re 75 to Re 12.

To test the convection at different areas in bed for Re 12. Data points from axial line, mid-section line, and a line near the wall are plotted on the Metais-Eclert maps. The map in *Figure 4-13* shows that the convection took place mostly by natural convection on the axial line, whereas the convection took place by mixed convection near the wall area of the bed. Indicating higher density gradient in the axial region. This is expected as the temperature is more uniformly high near the wall alongside the density is more uniformly low near the wall resulting in lesser gradients.

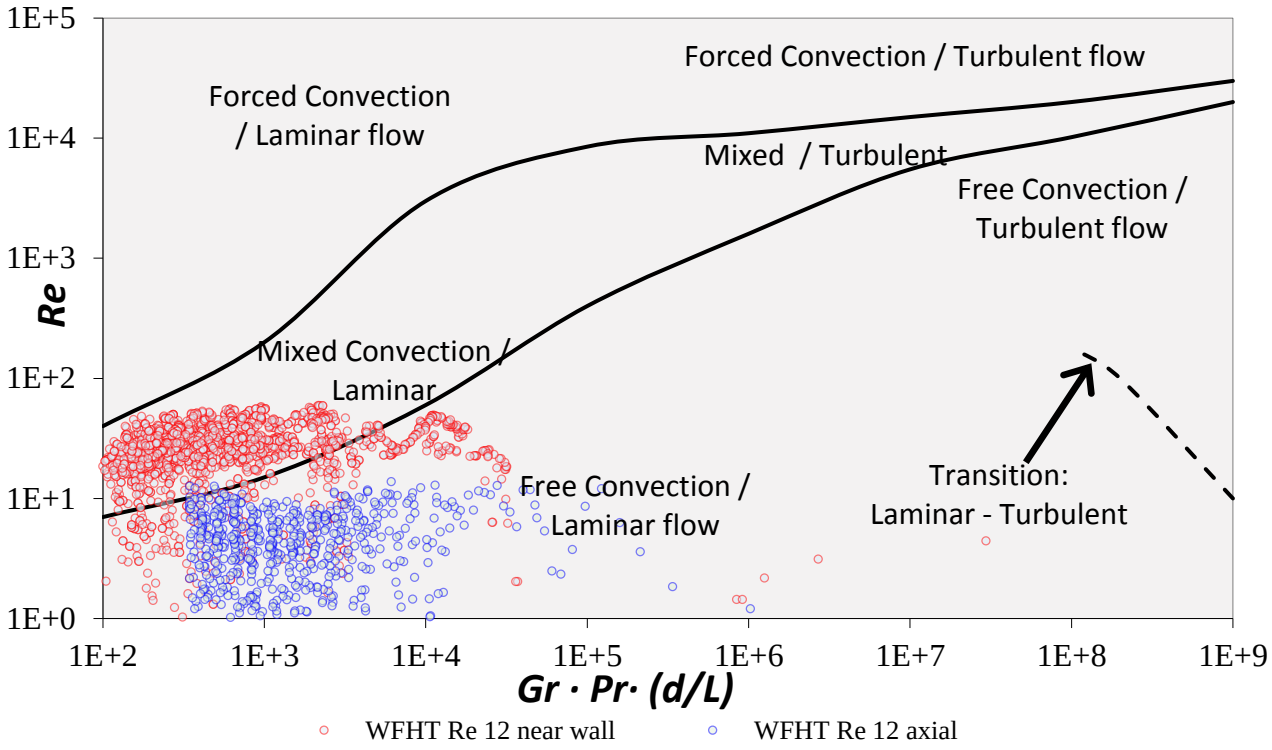

Figure 4-13 Simulation data compared with Metais-Eckert maps for Re 12 with data from lines at axis, and near wall

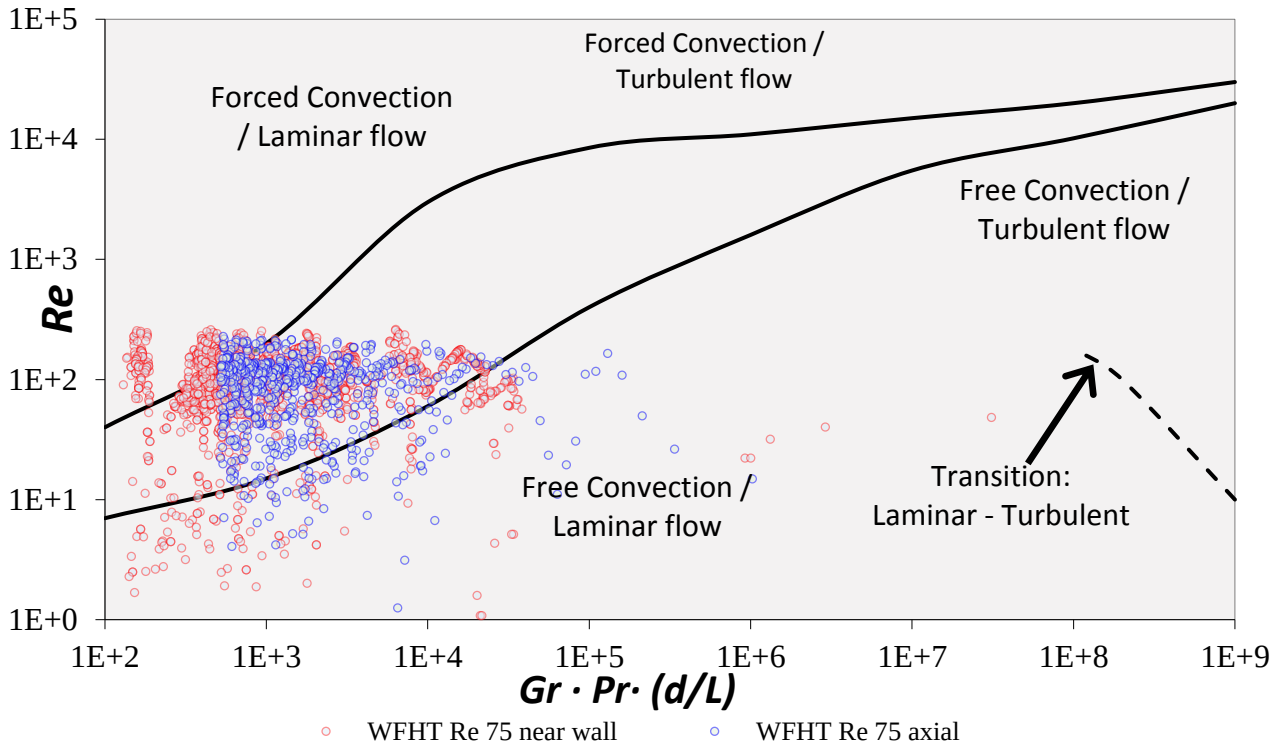

Figure 4-14 Simulation data compared with Metais-Eckert maps for Re 75 with data from lines at axis, and near wall

4.3.3 Temperature contours

As mentioned earlier, the fluid mixture of CO_2, methanol and triolein enters the packed bed at temperature 473.15K and the tube wall is heated at temperature 483.15K. Temperature contours were obtained for radial and axial planes along the packed bed. *Figure 4-15* shows axial and radial profiles for Re 0.37, 2.6 and 7.8 for one-tenth length WS model. *Figure 4-16* and *Figure 4-18* show radial and axial temperature profiles respectively for Re 12 to Re 75 for full-length WS model.

As expected, the temperatures decreased with the increase in flow rates for both cases of methanol to oil ratio of 7.89 (*Figure 4-15*) and the ratio of 25 (*Figure 4-16* and *Figure 4-18*). The temperature spread more at lower flow rate (*Re*=0.37) than at higher flow rate (*Re*=7.82), similarly for Re 12 and Re 75 respectively. For the higher *Re* there is mixing near the wall because of higher kinetic energy. And because of higher temperature gradient due to more fluid molecules at lower temperature entering, the heat transfer rate is higher. The fluid with flow *Re*=0.37, is nearer to an equilibrium temperature because of more residence time of fluid molecules. This effect is more visible for Re 12 in *Figure 4-18*.

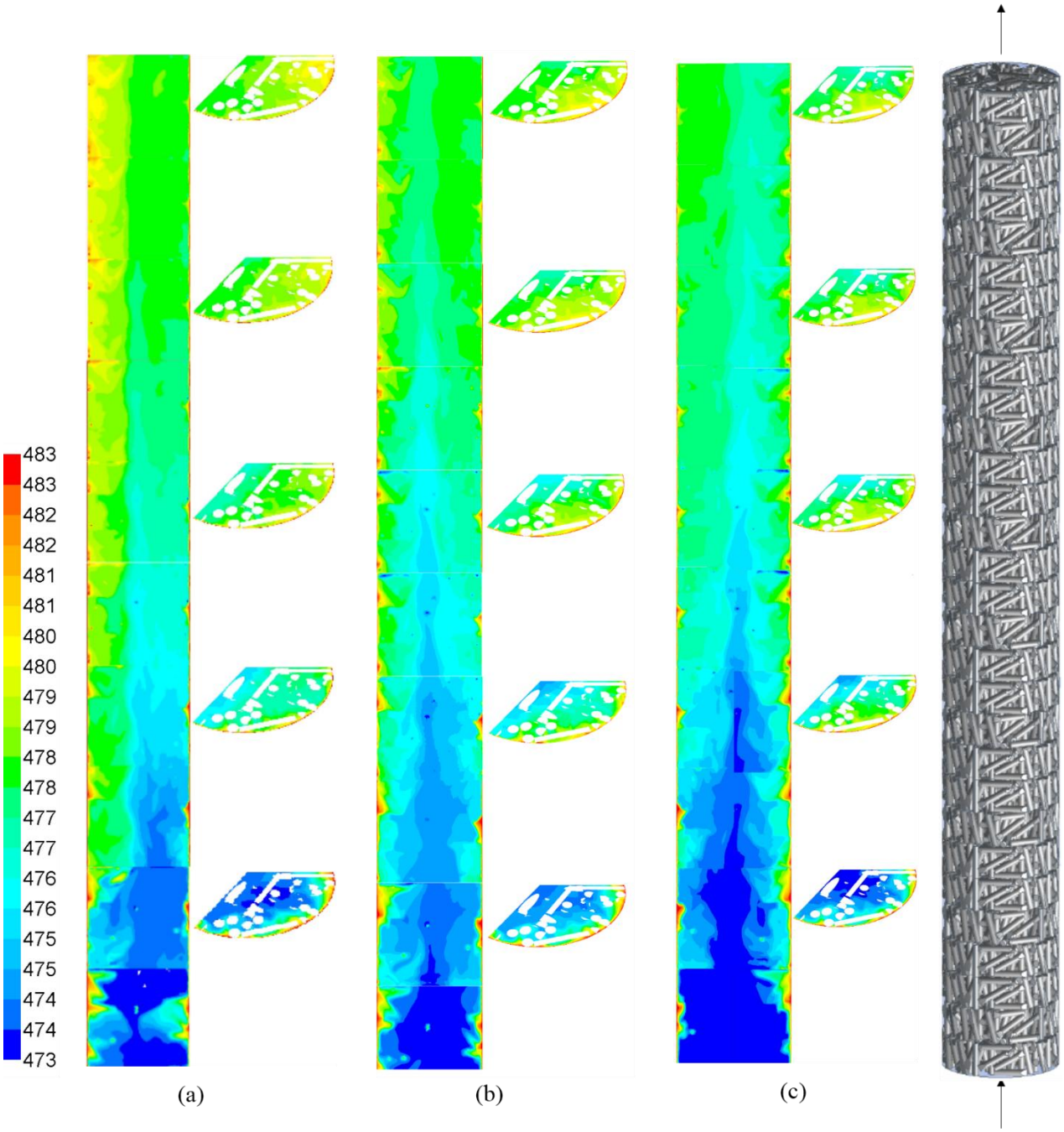

Figure 4-15 Packed bed geometry with temperature contours for radial and axial directions for (a) Re 0.37 (b) Re = 2.6 and (c) Re = 7.8 for one-tenth length wall-segment model with periodic boundary conditions

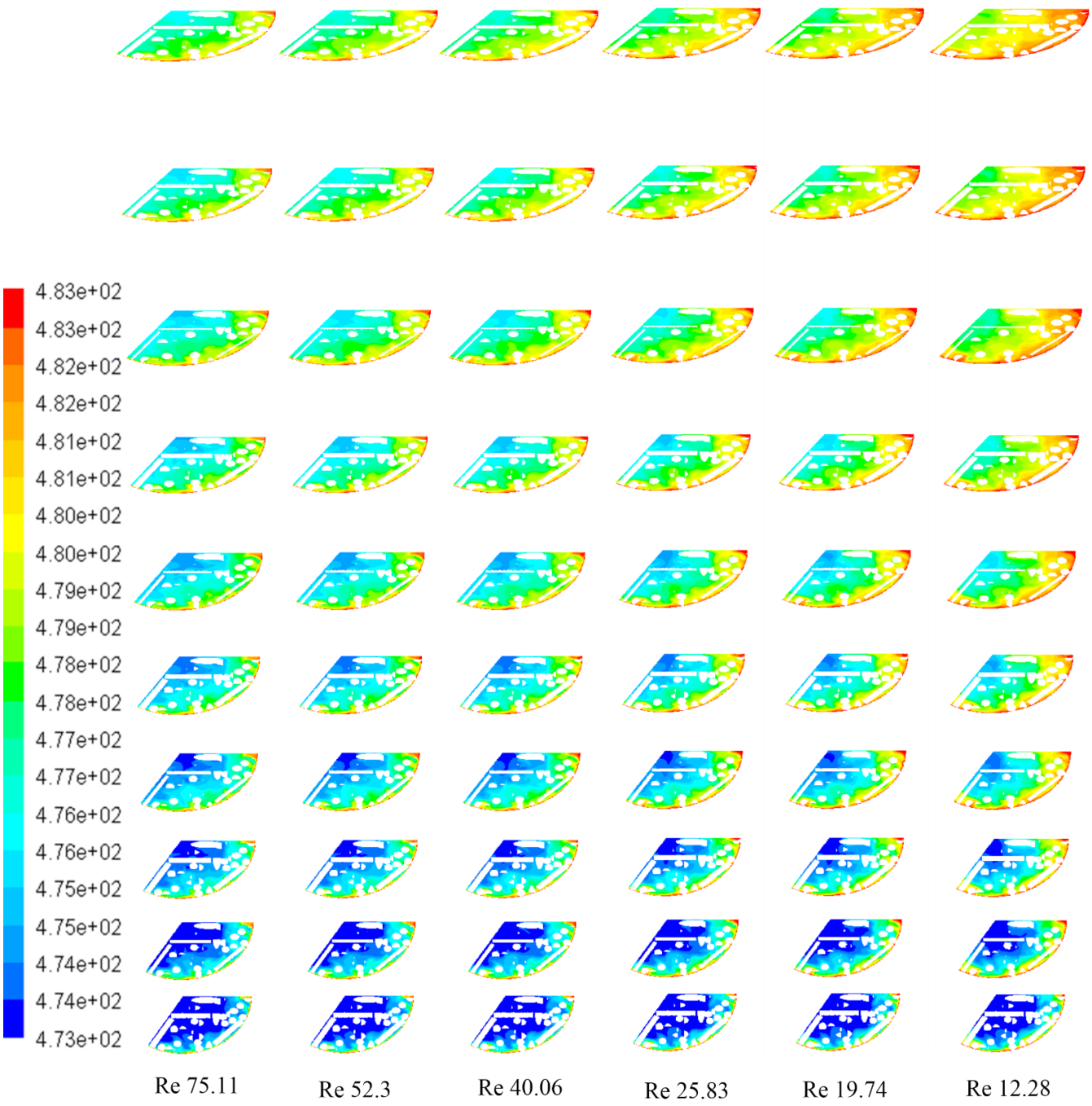

Figure 4-16 Radial temperature contours for full length wall segment model

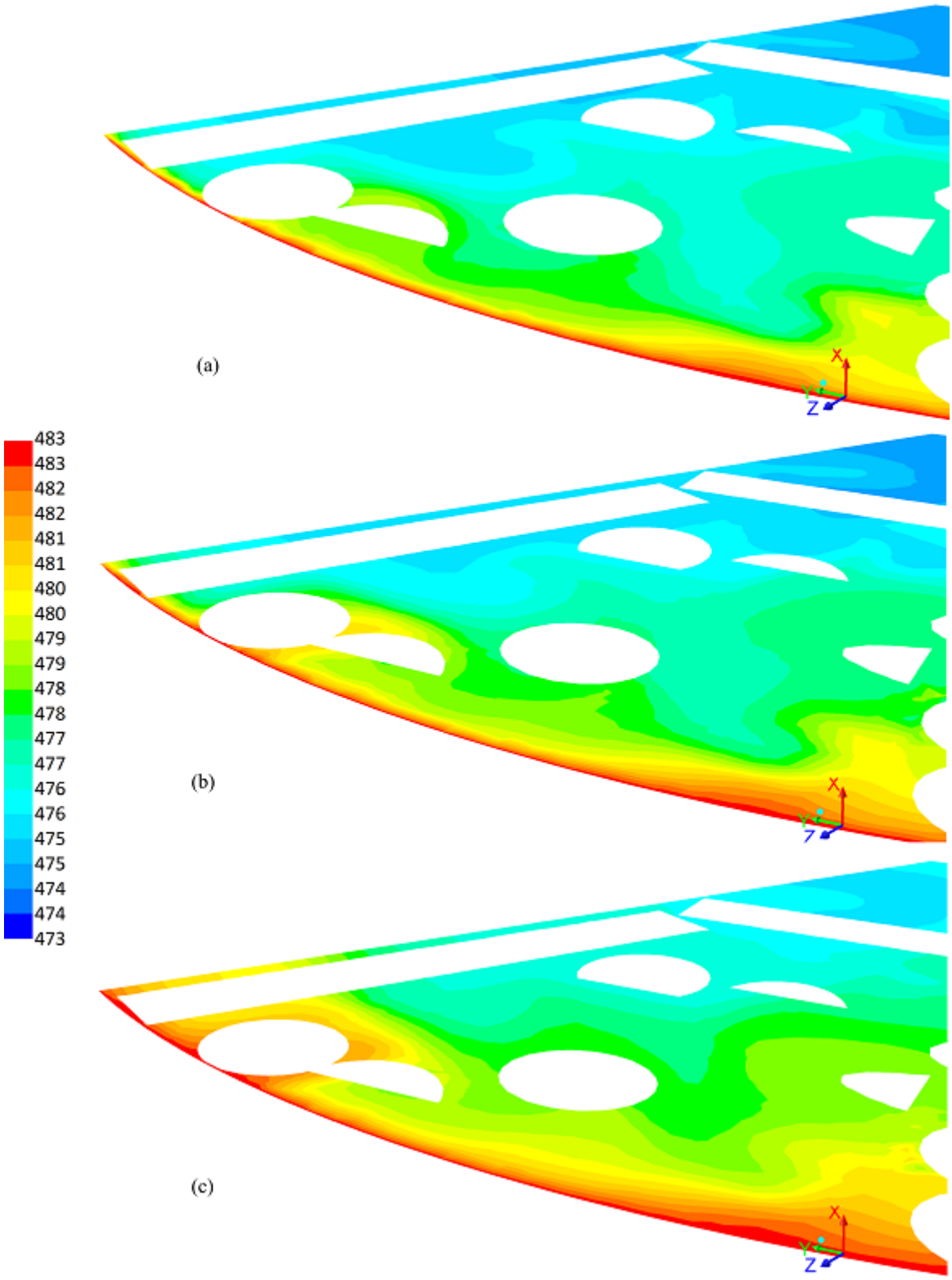

Figure 4-17 Temperature contours on radial plane 0.0914m into the packed bed for (a)Re 75 (b)Re 40 and (c)Re 12

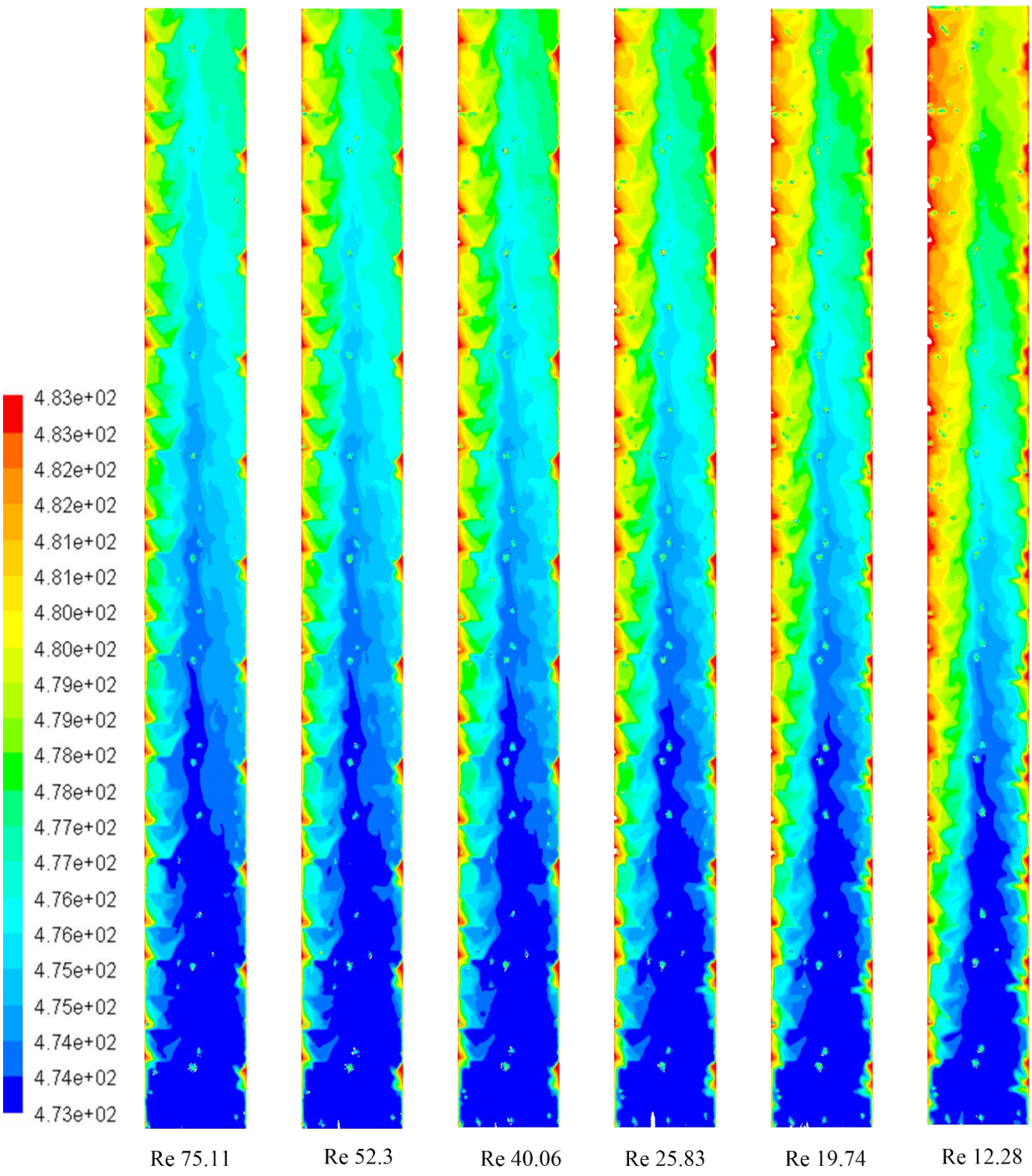

Figure 4-18 Axial temperature contours for full length wall segment model

4.3.4 Effective radial thermal conductivities and wall heat transfer coefficients

The model in Equation (4-2) is used to evaluate the heat transfer coefficients and radial thermal conductivities in Figures 4.21 to 4.24 from CFD temperature profiles. Unlike the previous sections where the CFD results are presented directly.

The solution to the model in Equation (4-2) is presented below to explain how the heat transfer coefficient and radial thermal conductivities are estimated. As mentioned in previous section, this model is a standard energy balance equation, approximated for packed bed, tested in literature published (Wakao and Kaguei, 1982). The solution without the axial second derivative, which is very small compared to the other terms, with boundary conditions given by Equation (4-3) is given by Hatta and Maeda, (1948) and later, by Coberly and Marshall, (1951), (Wakao and Kaguei, 1982)

$$\frac{T_w - T}{T_w - T_0} = 2\sum_{n=1}^{\infty} \frac{J_0(a_n r/R) e^{-a_n^2 y}}{a_n \left(1 + (a_n/Bi)^2\right) J_1(a_n)} \tag{4-7}$$

Where

$$y = \frac{k_r z}{G C_{p,f} R^2} \tag{4-8}$$

Bi is the Biot number and an is an n-th root of the following equation of Bessel functions (J_0 is a Bessel function of first kind and zeroth-order and J_1 is that of first kind and first-order):

$$BiJ_0(a_n) = a_n J_1(a_n) \tag{4-9}$$

When *y*, as defined by Equation (4-8), is greater than about 0.2, the series in Equation (4-7) converges so rapidly such that only the first term of the series is significant. Therefore,

$$\frac{T_w - T}{T_w - T_0} = \frac{2J_0(a_1 r/R) e^{-a_1^2 y}}{a_1 \left(1 + (a_n/Bi)^2\right) J_1(a_1)} \tag{4-10}$$

Where

$$BiJ_0(a_1) = a_1 J_1(a_1) \tag{4-11}$$

Equation (4-10) gives the temperature profile deep in the bed. At $r = 0$, $(T = T_c)$, This equation reduces to

$$\frac{T_w - T_c}{T_w - T_0} = \frac{2e^{-a_1^2 y}}{a_1 \left(1 + (a_n/Bi)^2\right) J_1(a_1)} \tag{4-12}$$

which gives the temperature profile along the central axis of the bed under the conditions specified.

The two heat transfer parameters, k_r and h_w, are straightforwardly obtained from measurements of axial temperature profiles. The temperature profiles at any radial position will do, but the temperature measurements along the central axis of the bed, where radial temperatures level off, are most preferable.

If the measured temperatures at the centre of the bed, T_c, are plotted as $ln\ [(T_w - T_c)/(T_w - T_0)]$ versus z for a particular flow rate. A straight line will be produced at sufficiently large values of z. This straight line means that this is the region where Equation (4-12) holds. *Figure 4-19* and *Figure 4-20* shows examples of the aforementioned for a simulation case.

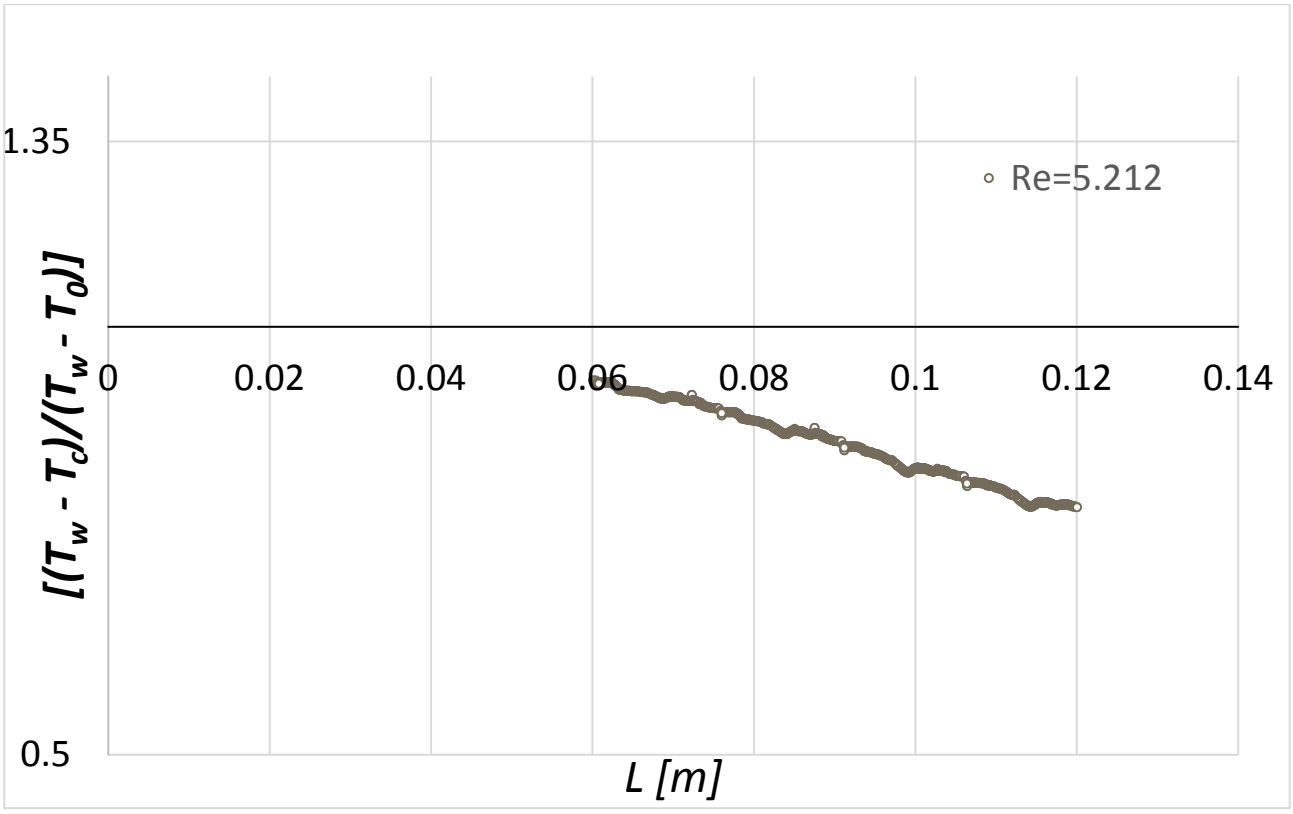

Figure 4-19 $ln\ [(T_w - T_c) / (T_w - T_0)]$ versus L for Re = 5.212 of for one-tenth length WS model with periodic boundary conditions

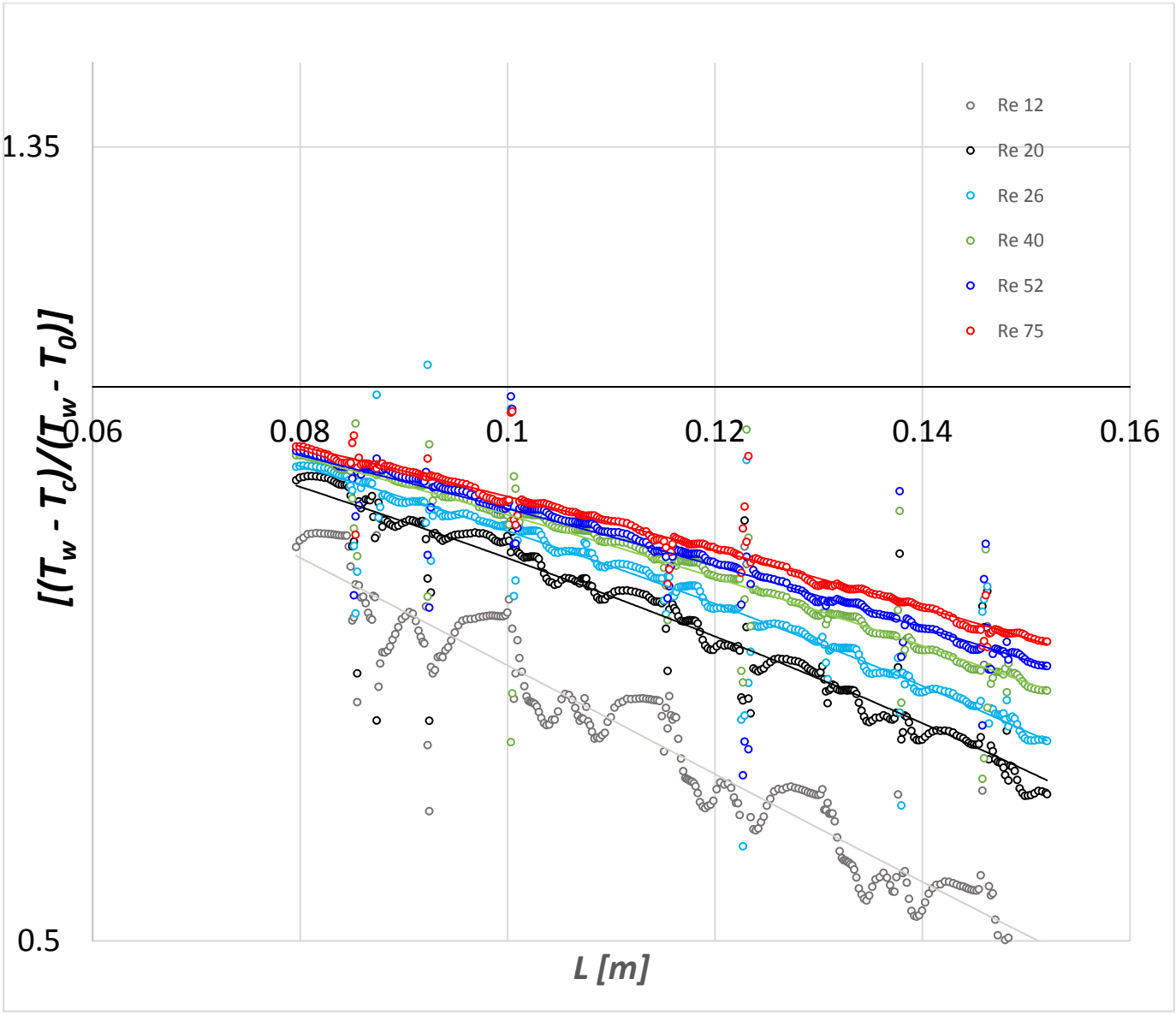

Figure 4-20 *ln [(*T_w *–* T_c*) / (*T_w *–* T_0*)]* versus axial length *L* from length 0.08m to 0.152m for Re 75, 52, 40, 26, 20 and 12 for full length WS model

The slope and the intercept, (obtained from *Figure 4-19* for Re 5.212 or *Figure 4-20*) of the straight line are

$$\textbf{\textit{Slope}} = -a_1^2\left(\frac{k_{er}}{GC_{p,f}R^2}\right) \tag{4-13}$$

And

$$\textbf{\textit{Intercept}} = \ln\frac{2}{a_1\left(1+\left(a_1/Bi\right)^2\right)J_1\left(a_1\right)} \tag{4-14}$$

Also, Equation (4-12) shows that, when x is large, the mixed mean temperature of the effluent fluid, T_m, is related to T_c by:

$$\frac{T_w - T_m}{T_w - T_0} = \frac{2J_1(a_1)}{a_1} \tag{4-15}$$

Therefore, the parameters, k_{er} and h_w, can be determined by either (a) Equations (4-13) and (4-15), or (b) Equations (4-13) and (4-14), both in conjunction with Equation (4-11). In method (b), the value of a_1, based on Equations (4-13) and (4-14), is easily affected by a slight change in the value of the intercept obtained from the extrapolation of the linear relationship between $ln\ [(T_w - T_c) / (T_w - T_0)]$ and x. On the other hand, a_1 is more safely determined from equation 0). Therefore, k_{er} and h_w may, in general, be more accurately evaluated from method (a) than method (b).

Conclusively, equation (4-12) gives the temperature profile in the packed bed. The heat transfer wall heat transfer coefficient h_w, is determined from measurements of axial temperature profiles i.e. $T = T_c$ at $r = 0$. The temperature profiles at any radial position will do, but the temperature measurements along the central axis of the bed, where radial temperatures level off, are most preferable.

4.3.5 Numerical response to flow

It is necessary to control the reaction temperature of the fluid as the reaction components' properties are very much dependent on the temperature. Hence the knowledge of the effective thermal conductivity and the wall heat transfer coefficient for the reactants flowing through the packed beds is very important.

For the calculations of Nu_w, fluid thermal conductivity k_f was kept a constant reference value. Re was calculated at the average values of viscosity in the bed and mass flux $G=\dot{m}/S=\rho u_0$. In *Figure 4-21* and *Figure 4-22* are shown the values for Nu_w for different values of Re for methanol to oil mole ratio of 7.89 and 25 respectively. The wall heat transfer coefficient was obtained from the calculated heat flux and the temperature profiles. The heat transfer coefficient is correlated in terms of Nusselt number. The Nu vs. Re plots show increase of heat transfer with Re as predicted by the correlations. This effect can also be seen in the temperature contour plots of *Figure 4-15* to *Figure 4-18*. The empirical models by Hanrattry (1954) correlated for cylinders for Re~20 are shown for reference. There is agreement with the correlation at Re~8 however for lower Re it predicts higher heat transfer. Yagi and Wakao, (1959) predicted much lower heat transfer for both the mole ratios (*Figure 4-21* and *Figure 4-22*). This is expected as

the correlations were prepared from experiments with air and is for spherical packings while the simulations are for supercritical flows and cylindrical particles. The high rate of heat transfer in supercritical fluids is due to high density as shown in *Figure 4-12* and low viscosities under the high pressure supercritical conditions.

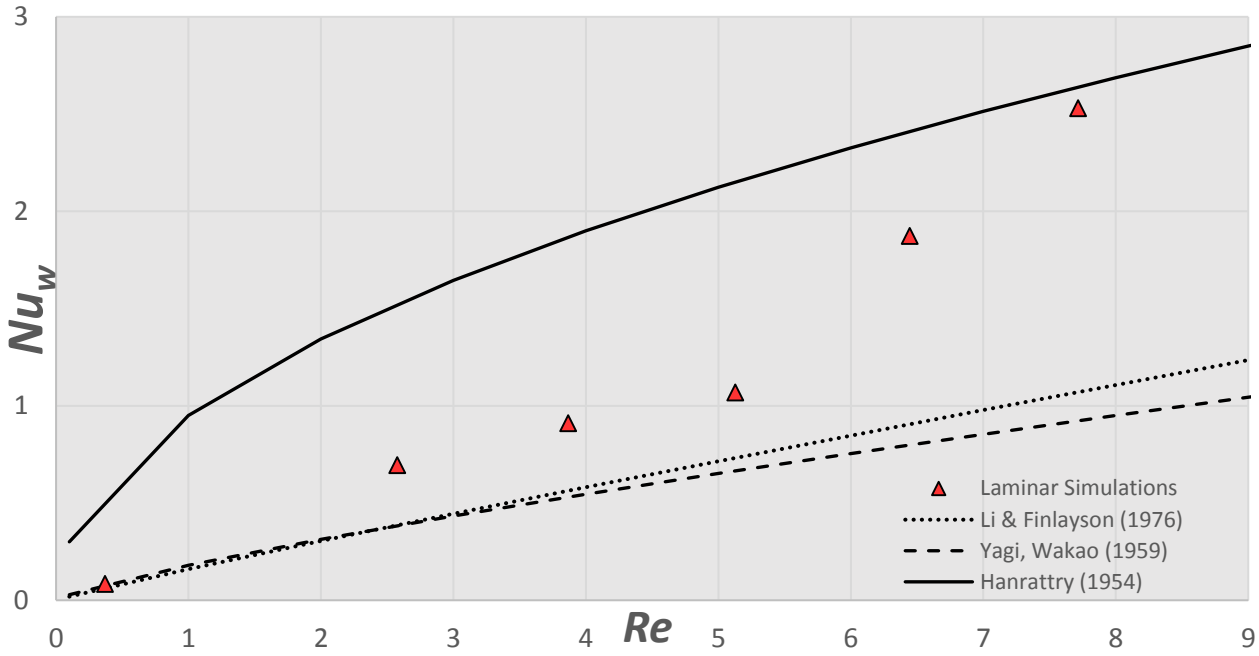

Figure 4-21 Wall Nusselt number vs Reynolds number for CFD simulations (laminar) compared with various correlations based on experiments for Re 2 to 8 for one-tenth length wall-segment model with methanol to oil ratio molar of 7.89

But the Li and Finlayson, (1976) correlation is based on wide range of experiments involving chemically reactive flows from various researchers which is applicable for Re ranging from 20 to 800. As, the *Figure 4-22* shows the data agreed well, but as expected for *Figure 4-21* which is for below Re 8, the data is not predicted. The data of these correlations are modelled for non-supercritical conditions, which also contributes to their variation with the simulations. The Nu_w predicted for Re 7.71 in *Figure 4-21* is higher due to higher fluid thermal conductivity (which is due to less methanol to oil mole ratio) as compared to Re 12.29 in *Figure 4-22*.

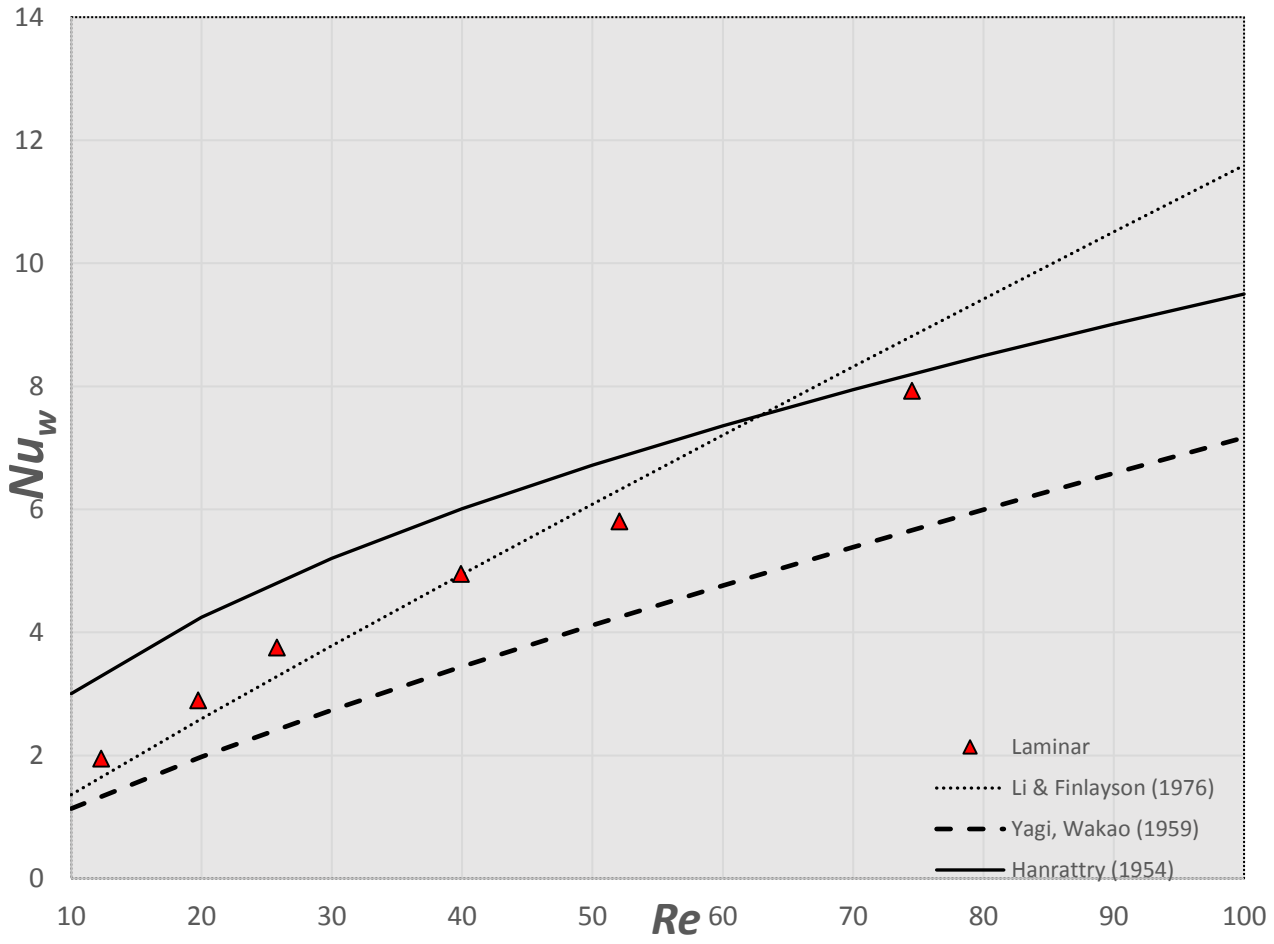

Figure 4-22 Wall Nusselt number vs Reynolds number for CFD simulations (laminar) compared with various correlations based on experiments for Re 12 to 75 for full-length wall segment model with methanol to oil molar ratio of 25

Figure 4-23 and *Figure 4-24* show effective radial thermal conductivities for the cross section of the bed in radial direction. Which are determined from Equation (4-13) as explained in that section. The condition required is that the measurements should be made at high flow rates under which axial heat conduction may be ignored. The figures show a good agreement with the correlations proposed (Yagi and Kunii, 1960; Yagi and Wakao, 1959). For the Re of 0.37 the effective radial thermal conductivities are predicted much higher. This could be due to axial heat conduction due to back flows which are prevalent in gravitational opposing flows at this very low Re.

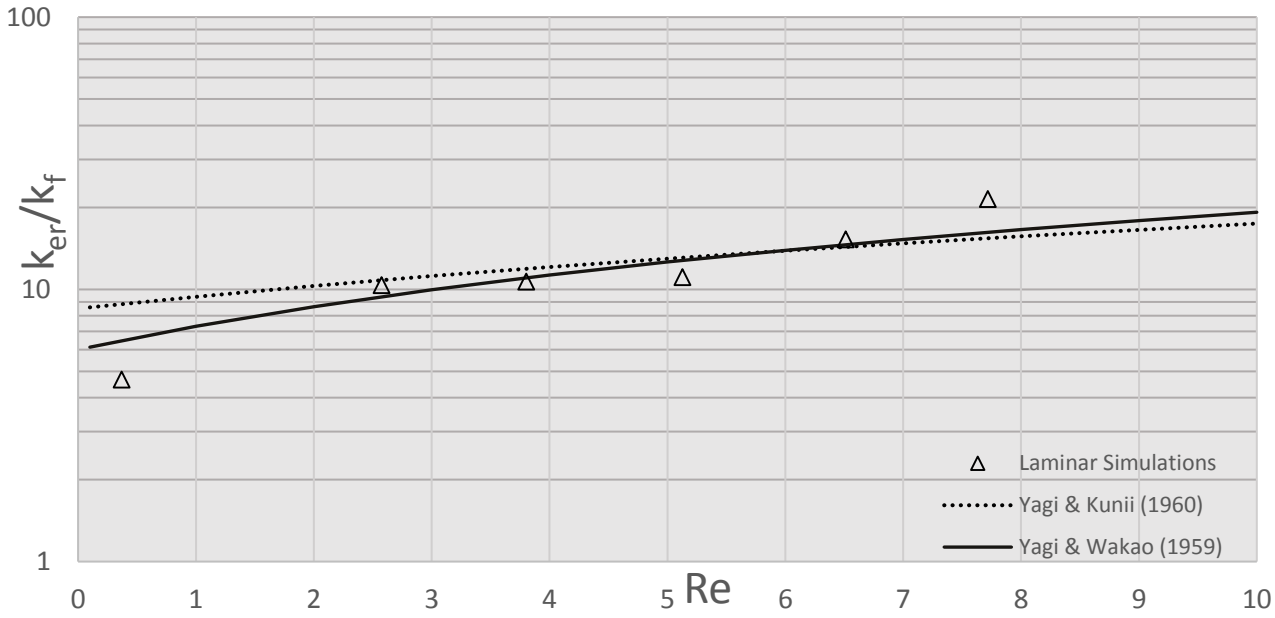

Figure 4-23 Effective radial thermal conductivity vs Reynolds number for CFD simulations (laminar) compared with various correlations based on experiments for Re 2 to 8 for one-tenth length wall-segment model

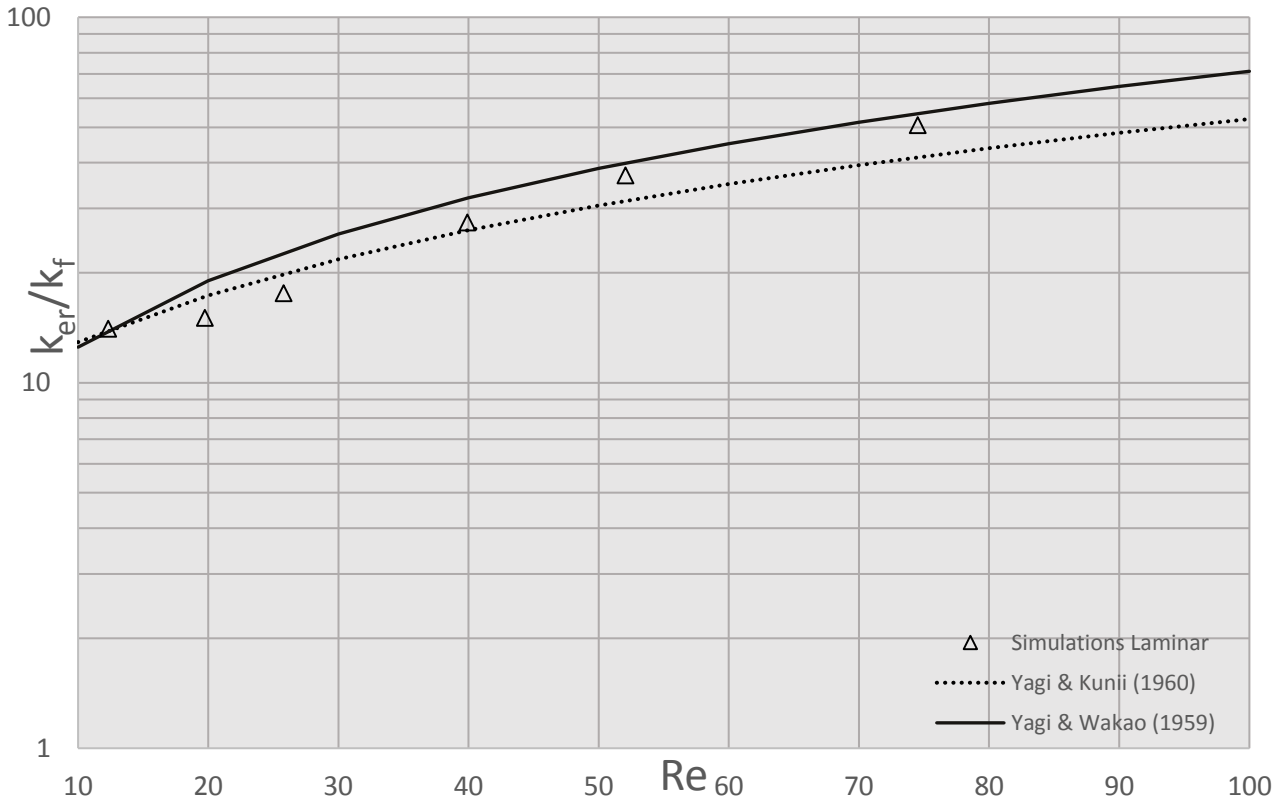

Figure 4-24 Effective radial thermal conductivity vs Reynolds number for CFD simulations (laminar) compared with various correlations based on experiments for Re 12 to 75 full length wall-segment model

4.4 CONCLUSIONS

Heating of reactor walls is necessary to maintain the reactor under specified reaction conditions. A wall-segment packed bed model is created with randomly packed cylindrical particles. It is possible to model a realistic case of packed bed of cylinders including the contact point within the surfaces involved in the geometry. Computational grids of different mesh densities and element size are generated for the geometric model and checked for their independence. The simulation model is set up for high pressure supercritical conditions with tertiary mixture fluid. The use of CFD for studying the wall-to-fluid heat transfer in packed bed assessed. Flow, energy and species mathematical models have been solved for the setup.

CFD simulations were done for two cases of methanol to oil molar ratios in two different packed bed geometries of one-tenth WS model and full-length WS model. Velocity, density and temperature profiles are obtained on radial, axial planes and axis of the packed bed. The temperature profiles showed higher temperature for lower *Re.* Velocity vector fields show higher velocities near the exit end of the bed. Higher density at lower *Re* can be observed, which is due to accumulation of methanol in the bed at this *Re*, although there is higher temperature at lower Re. However, for full-length bed (oil to alcohol ratio of 25), the density is as expected. Large density gradients are observed for lower Re and near to the outlet of the packed bed, resulting in free convection in these regions.

Mixed convection at high pressure in a packed bed was also analysed. For a supercritical fluid in laminar flow regime, it was possible to study the effects of density gradient, velocity over mass transfer. The density gradients observed neat the outlet of the packed bed and for lower Re number, generated hydrodynamic instabilities leading to convection due to natural convection as observed in the Metais-Eckert maps.

Values of wall Nusselt number and effective radial thermal conductivity are estimated for different Re are obtained with data of temperature profiles along the axis of the bed. The results show a trend of increase with Reynolds number for wall Nusselt number. Higher heat transfer is observed than what is predicted by some empirical correlations, which signifies the higher heat transfer for supercritical fluids. The Nu_w almost increases linearly with Re number for full length packed bed, along with some empirical correlation, validating the numerical results for higher Re. But for Re<10, the simulation results are not linear.

Hence, CFD proves to be a reliable tool for modelling convective wall-to-fluid heat transfer in high pressure supercritical conditions for species mixtures in complex geometries. Free/Forced convection situations in the packed bed can be analysed.

REFERENCES

Baiker, A. (1999). Supercritical fluids in heterogeneous catalysis. *Chemical Reviews*, *99*, 453–473. http://doi.org/10.1021/cr970090z

Behnam, M., Dixon, A. G., Nijemeisland, M., & Stitt, E. H. (2013). A New Approach to Fixed Bed Radial Heat Transfer Modeling Using Velocity Fields from Computational Fluid Dynamics Simulations. *Industrial & Engineering Chemistry Research*, *52*, 15244–15261. Retrieved from http://pubs.acs.org/doi/abs/10.1021/ie4000568\nhttp://pubs.acs.org/doi/pdf/10.1021/ie4000568\nhttp://dx.doi.org/10.1021/ie4000568

Benneker, a. H., Kronberg, a. E., & Westerterp, K. R. (1998). Influence of buoyancy forces on the flow of gases through packed beds at elevated pressures. *AIChE Journal*, *44*(2), 263–270. http://doi.org/10.1002/aic.690440205

Coberly, C. A., & Marshall, W. R. (1951). Temperature gradients in gas streams flowing through fixed granular bed. *Chemical Engineering Progress*, *47*(3), 141–150.

Derkx, O. R., & Dixon, A. G. (1996). Determination of the Fixed Bed Wall Heat Transfer Coefficient Using Computational Fluid Dynamics. *Numerical Heat Transfer, Part A: Applications*, *29*(8), 777–794. JOUR. http://doi.org/10.1080/10407789608913819

Dixon, A. G., & Cresswell, D. L. (1979). Theoretical Prediction of Effective Heat Transfer Parameters in Packed Beds. *AIChE Journal*, *25*(4), 663–676.

Dixon, A. G., Taskin, M. E., Nijemeisland, M., & Stitt, E. H. (2008). Wall-to-particle heat transfer in steam reformer tubes: CFD comparison of catalyst particles. *Chemical Engineering Science*, *63*(8), 2219–2224. http://doi.org/10.1016/j.ces.2008.01.017

Freiwald, M. G., & Paterson, W. R. (1992). Accuracy of model predictions and reliability of experimental data for heat transfer in packed beds. *Chemical Engineering Science*, *47*(7), 1545–1560. http://doi.org/10.1016/0009-2509(92)85003-T

Guardo, A., Coussirat, M., Larrayoz, M. A., Recasens, F., & Egusquiza, E. (2005). Influence of the turbulence model in CFD modeling of wall-to-fluid heat transfer in packed beds. *Chemical Engineering Science*, *60*(6), 1733–1742. http://doi.org/10.1016/j.ces.2004.10.034

Guardo, A., Coussirat, M., Recasens, F., Larrayoz, M. A., & Escaler, X. (2006). CFD study on particle-to-fluid heat transfer in fixed bed reactors: Convective heat transfer at low and high pressure. *Chemical Engineering Science*, *61*(13), 4341–4353. http://doi.org/10.1016/j.ces.2006.02.011

Gunn, D. J., & Khalid, M. (1975). Thermal Dispersion and Wall Heat Transfer in Packed Beds. *Chemical Engineering Science*, *30*, 261–267.

Hanrattry, T. J. (1954). Nature of wall heat transfer coefficient in packed beds. *Chemical Engineering Science*, *3*, 209–214.

Harris, C. K., Roekaerts, D., Rosendal, F. J. J., Buitendijk, F. G. J., Daskopoulos, P., Vreenegoor, A. J. N., & Wang, H. (1996). Computational Fluid Dynamics for Chemical Reactor Engineering. *Chemical Engineering Science*, *51*(10), 1569–1594. http://doi.org/10.1016/0009-2509(96)00021-8

Hatta, S., & Maeda, S. (1948). Heat transfer in beds of granular catalyst I. *Kagaku Kogaku*, *12*, 56.

Li, C.-H., & Finlayson, B. A. (1976). Heat Transfer in Packed Beds - A Reevaluation. *Chemical Engineering Science*, *32*, 1055–1066.

Logtenberg, S. A., & Dixon, A. G. (1998). Computational fluid dynamics studies of fixed bed heat transfer. *Chemical Engineering and Processing: Process Intensification*, *37*(June 1997), 7–21. http://doi.org/10.1016/S0255-2701(97)00032-9

Nijemeisland, M., & Dixon, A. G. (2001). Comparison of CFD simulations to experiment for convective heat transfer in a gas–solid fixed bed. *Chemical Engineering Journal*, *82*(1–3), 231–246. http://doi.org/10.1016/S1385-8947(00)00360-0

Ranade, V. V. (2002). *Computational Flow Modeling for Chemical Reactor Engineering*. *Academic Press*. New York.

Suekane, T., Yokouchi, Y., & Hirai, S. (2003). Inertial flow structures in simple-packed bed of spheres. *AIChE Journal*, *49*, 10–17.

Taskin, M. E., Dixon, A. G., Nijemeisland, M., & Stitt, E. H. (2008). CFD Study of the Influence of Catalyst Particle Design on Steam Reforming Reaction Heat Effects in Narrow Packed Tubes. *Industrial & Engineering Chemistry Research*, *47*(16), 5966–5975. http://doi.org/10.1021/ie800315d

Taskin, M. E., Dixon, A. G., & Stitt, E. H. (2007). CFD Study of Fluid Flow and Heat Transfer in a Fixed Bed of Cylinders. *Numerical Heat Transfer, Part A: Applications*, *52*(3), 203–218. http://doi.org/10.1080/10407780601149896

Wasch, A. P. De, & Froment, G. F. (1972). Heat transfer in packed beds. *Chemical Engineering Science*, *27*, 567–576.

Winterberg, M., & Tsotsas, E. (2000). Impact of tube-to-particle-diameter ratio on pressure drop in packed beds. *AIChE Journal*, *46*(5), 1084.

Yagi, S., & Kunii, D. (1960). Studies on Heat Transfer Near Wall Surface in Packed Beds. *AIChE Journal*, *6*(1), 97–104.

Yagi, S., & Wakao, N. (1959). Heat and Mass Transfer from Wall to Fluid in Packed Beds. *AIChE Journal*, *5*(1), 79–85.

CHAPTER V

5. PARTICLE-TO-FLUID HEAT TRANSFER

5.1 INTRODUCTION

Heat transfer between solids and flowing fluids in an often occurring mechanism carrying various purposes in a packed bed especially a catalytic packed bed reactor. Knowledge of temperatures of flowing fluid and of particles is necessary in rationally designing a catalytic packed bed reactor. Determining the particle/solid surface temperature in a packed bed is especially difficult. The prediction of heat transfer coefficients using the temperature profiles is important for estimation of local and overall conversions.

Particle-to-fluid heat transfer coefficients in one of the most important parameters for design of packed bed systems. Considerable amount of work has been done in determining the heat transfer parameters considering its importance (Wakao et al., 1979). A number of experimental correlations have been reported for the determination of the particle-to-fluid heat transfer parameters, but these data does not agree much especially in the low Reynolds number region. (Wakao and Kaguei, 1982)

Spatial temperature distribution data in the bed and in the catalyst particles is very important for design and analysis. While the temperature of the fluid can be obtained with little difficulty, the measurement of temperature on and near the particle surfaces is not easy. The temperature drop at the particle surface is estimated in terms of particle-to-fluid heat transfer coefficient, a significant effort has been made in evaluating this parameter. An extensive review has been made on the work on particle-to-fluid heat transfer can be found in Wakao and Kaguei, (1982)

Most of the data available is for low pressures. Very less data is available for high-pressure situations or supercritical pressures. Most research for high pressure situations is focussed on catalytic reactions using supercritical fluids as a solvent (Ramìrez, 2005; Santana et al., 2007), with main interest in kinetics of chemical reactions under supercritical conditions. And other researchers studied mass transfer in packed beds at supercritical conditions, for applications like supercritical fluid extraction. (Debenedetti and Reid, 1986; Stüber et al., 1996)

In the following sections, models for particle-to fluid heat transfer will be discussed, and their analytical solutions for steady-state temperature profiles are presented. The CFD simulation strategy for the estimation of particle-to-fluid heat transfer coefficients is presented, with the

geometrical model, mesh development and simulation setup. The obtained numerical results are analysed and compared against experimental correlations.

5.2 THEORITICAL WORK DEVELOPMENT

Free-Surface Model:

This model was introduced by Happel, (1958) The energy equation based on free surface model was solved. They obtained solutions for Péclet (Pe) numbers between 0.1 and 100, and void fractions of 0.4 to 1.0, and showing that average Nusselt (Nu) number is a function of both void fraction and the Pe number. Pfeffer, (1964) combined the free surface model with 'thin boundary large solution'. This model is found to be valid for sufficiently high Pe numbers.

Channelling Model:

Analogous to the particle-to-fluid mass transfer, channelling model is applicable to the heat transfer. When some groups of particles are packed closely forming aggregates, while others are packed loosely, then it leads to selective flow of fluids in volumes in which packing are loose. Such flow is called channelling. By assuming that in aggregated particles, concentration of the fluid is in equilibrium with interspersed solids, two-dimensional plug flow, and that heat transfer is restricted to fluid thermal conductivity in the direction perpendicular to flow, channelling model was introduced by Kunii and Suzuki, (1967)The anomaly of the previous experimental data for low Peclet numbers were interpreted by taking into consideration channelling, using the model. The Nusselt number derived assuming the model,

$$Nu_p = \frac{h_p D_p}{k_f} = \frac{\Phi_s(1-\Psi_1)}{6(1-\varepsilon)\xi} . \frac{D_p C_p G_0}{k_f} \tag{5-1}$$

The above models are based on theories for a single sphere and hence have failed for packed beds at low Re, because of incorrect boundary conditions.

Schumann Model

Schumann, (1929) developed the energy balance equation for the particle-to fluid heat transfer system with the assumptions of plug flow with no dispersion and neglecting the temperature gradient inside the particle.

Continuous Solid-Phase (C-S) Model

This is a model which assumes that heat transfer takes place axially through a continuous solid phase by conduction. Also, has dispersed plug flow assumption. (Littman et al., 1968)

Dispersion Concentric (D-C) Model

This model is based on assumption of concentric temperature profile in the particle, and that the fluid is in dispersed plug flow, a modified version of this model called modified dispersion concentric model, (Wakao, 1976) also with the same assumptions that of the original D-C model, but the axial thermal diffusion coefficient is replaced by an effective axial diffusion term. The modified D-C model is shown to have advantage over the C-S and D-C models (Kaguei et al., 1977).

This model, the steady-state energy balance equation for the dispersion concentric model (D-C) is given by:

$$u\frac{dT_f}{dx}+\frac{6h\cdot(1-\varepsilon)}{d_p\cdot\varepsilon\cdot C_p\cdot\rho}\left(T_f-T_p\right)=\alpha_{ax}\frac{d^2T_f}{dx^2} \tag{5-2}$$

The analytical solution to this equation is based on the Danckwerts boundary conditions (Danckwerts, 1953), given by

$$u\left(T_f-T_0\right)=\alpha_{ax}\frac{dT_f}{dx} \qquad \text{At } x=0 \text{ (inlet),} \tag{5-3}$$

$$\frac{dT_f}{dx}=0 \qquad \text{at } x=x_L \text{ (outlet)}$$

The Dankwerts solution was arrived analytically for reactor,

$$\frac{T_{ps}-T_{exit}}{T_{ps}-T_{in}}=\frac{4Aexp\left(\frac{LU}{2\alpha_{ax}}\right)}{(1+A)^2exp\left(A\frac{LU}{2\alpha_{ax}}\right)-(1-A)^2exp\left(-A\frac{LU}{2\alpha_{ax}}\right)} \tag{5-4}$$

Where,

$$A=\left(1+\frac{4ah\alpha_{ax}}{\varepsilon_b U^2}\right)^{1/2} \tag{5-5}$$

The axial fluid thermal dispersion coefficient α_{ax} under laminar flow range is given by,

$$\alpha_{ax} = (0.7)\alpha_F \tag{5-6}$$

Wakao, (1976) proposed a modification for the axial fluid dispersion coefficient for and effective term given by

$$\alpha_{ax}^{*} = \frac{k_{eax}}{\varepsilon_b C_F \rho_F} \tag{5-7}$$

5.3 SIMULATION MODEL SETUP

The packed bed of cylindrical catalyst particles geometrical model is based on the dimensions of a catalytic reactor used for supercritical transesterification experiments. A wall-segment model of packed bed is developed in DesignModeler software. The cylindrical particles are arranged randomly in the packed bed tube. The tube-to-particle diameter ratio (N) is about 9. This geometry model development and description is discussed in the earlier chapters. For the current study, two different geometries of were used: a full-length WS model and a half-length WS model. The models have extensions in the inlet and the outlet of the bed as shown in *Figure 5-1*. More details of the geometry are given in *CHAPTER IV*, section *4.2.1*. The geometry is assembly level meshed as finite volumes mesh based on 3D tetrahedral element. The wall surfaces are meshed using unstructured triangular mesh and this surface extended to construct the volume mesh. The particle surfaces are refined by unstructured quadrilateral mesh. The mesh independence tests with different quality meshes are done and optimal mesh size is used. More details of the mesh are reported in earlier *Chapter IV*, section *4.2.2* of this thesis.

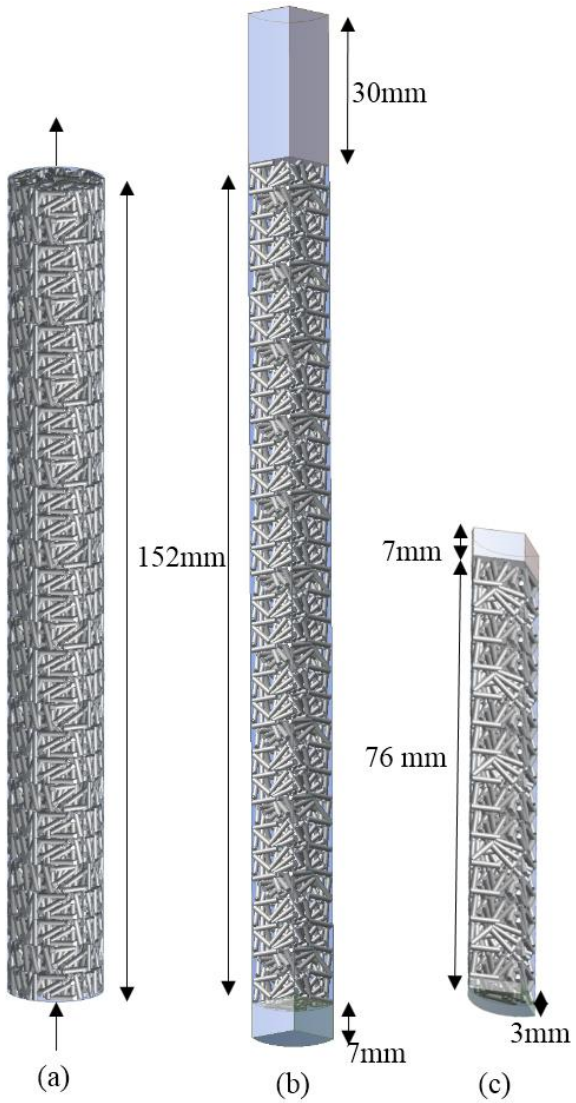

Figure 5-1 Packed bed geometries (a)Full segment model (b)Full-length wall segment (WS) model (c) Half-length wall-segment model

The fluid, mixture of carbon dioxide (CO_2), methanol (CH_3OH) and triolein ($C_{57}H_{104}O_6$), (reactants for transesterification reaction with supercritical solvent CO_2) is flown into the packed bed at 250 bar pressure and 473.15K temperature, is taken to be Newtonian, in laminar flow. Pure component properties are taken at this pressure as a function of temperature. Density, viscosity, thermal conductivity and specific heat of the fluid components are estimated as a function of temperature. Dilute approximation mass diffusivity coefficients are estimated for methanol-carbon dioxide and triolein-carbon dioxide. Methanol and triolein are taken to be dilute species for the diffusivity estimations. The particles surface is maintained at temperature 483.15K. The mixture properties are based volume weighted for density and specific heat, and mass weighted average for thermal conductivity and viscosity. The components form a single phase by the presence of supercritical CO_2. The fluid is flown in at a flow inlet velocities of

0.0008 to 0.005 m/s. The governing equations corresponding to the mass, momentum and energy are detailed in the chapter two.

Boundary conditions, methods	Value
Fluid mixture	CO_2 + CH_3OH + $C_{57}H_{104}O_6$
Mass fraction ratio methanol: oil inlet	0.22998: 0.0801
Methanol to oil molar ratio inlet	25:1
Fluid temperature at inlet	473.15 K
Wall temperature	483.15 K
Pressure	25000000 Pa
Fluid velocity at the inlet	0.000822 to 0.025134 m/s
Shear condition on wall, particle surface	No slip
Discretization	First order
Models solved	Flow, energy, species
Flow model	Laminar

Table 5-1 Boundary conditions and methods for the analysed cases

Navier-Stokes equations together with energy balance were solved using commercially available finite volume code software Ansys Fluent. The fluid is taken to be Newtonian and in laminar flow regime and with varying density, specific heat, thermal conductivity and viscosity with temperature.

5.4 RESULTS AND DISCUSSION

In this section the capabilities of CFD for studying the influence of different flow rates on the particle to-to fluid heat transfer is examined. The CFD implemented laminar model is tested for particle-to-fluid heat transfer for packed bed reactor design for tertiary mixture of CO_2, methanol and triolein. The simulations run are tabulated in *Table 5-2*

Velocity (m/s)	Re obtained	Methanol to oil mole ratio	Solvent(CO_2+CH_3OH) flow rate (g/min)	Simulation model used	Case ID
0.0101	30.04	25	32.327	Half-length WS	PFHTH.30
0.0050	15.02	25	16.163	Half-length WS	PFHTH.15
0.0027	8.01	25	8.620	Half-length WS	PFHTH.8
0.0013	3.94	25	4.249	Half-length WS	PFHTH.4
0.00082	2.46	25	2.642	Half-length WS	PFHTH.2
0.025134	75.11	25	80.817	Full length WS	PFHT.80
0.013405	40.06	25	43.102	Full length WS	PFHT.40
0.006608	19.74	25	21.247	Full length WS	PFHT.20
0.004109	12.28	25	13.213	Full length WS	PFHT.12

Table 5-2 Velocity boundary conditions applied to CFD inlet, obtained Re and methanol to oil molar ratio, geometrical model used for each simulated case

5.4.1 Velocity and Density Profiles / Mixed convection effects

Velocity and density required for studying their influence on the effectiveness of heat transfer with the bed. Axial and radial surface cuts were defined in the bed to study in which the profiles were plotted.

The velocity magnitude contours are shown in *Figure 5-2*. For higher Re in *Figure 5-2* (a) and (b), higher velocities can be seen in the bed with low velocities near the particle surface (can be seen from the radial profiles) and the wall surface. However, for lower Re, the velocities are almost uniform throughout the bed, due to lesser wall resistance at lower Re. This gradual increase in the uniformity of flow velocity can be observed for half-length WS model as well. This regions of high velocities for higher Re indicate the formation of eddies. It can also be observed the velocity is uniform in the axial direction of the bed indicating a developed flow in axial direction with little end effects due to the presence of extensions in the bed (shown in the geometry *Figure 7-1*). For higher Re, channelling can be seen occurring near the axis of the bed, resulting in strong axial flow. The velocity has increased about five times the inlet velocity in some constrained areas in these regions. Stagnation points can be observed near the contact points of the particles in *Figure 5-2* (a).

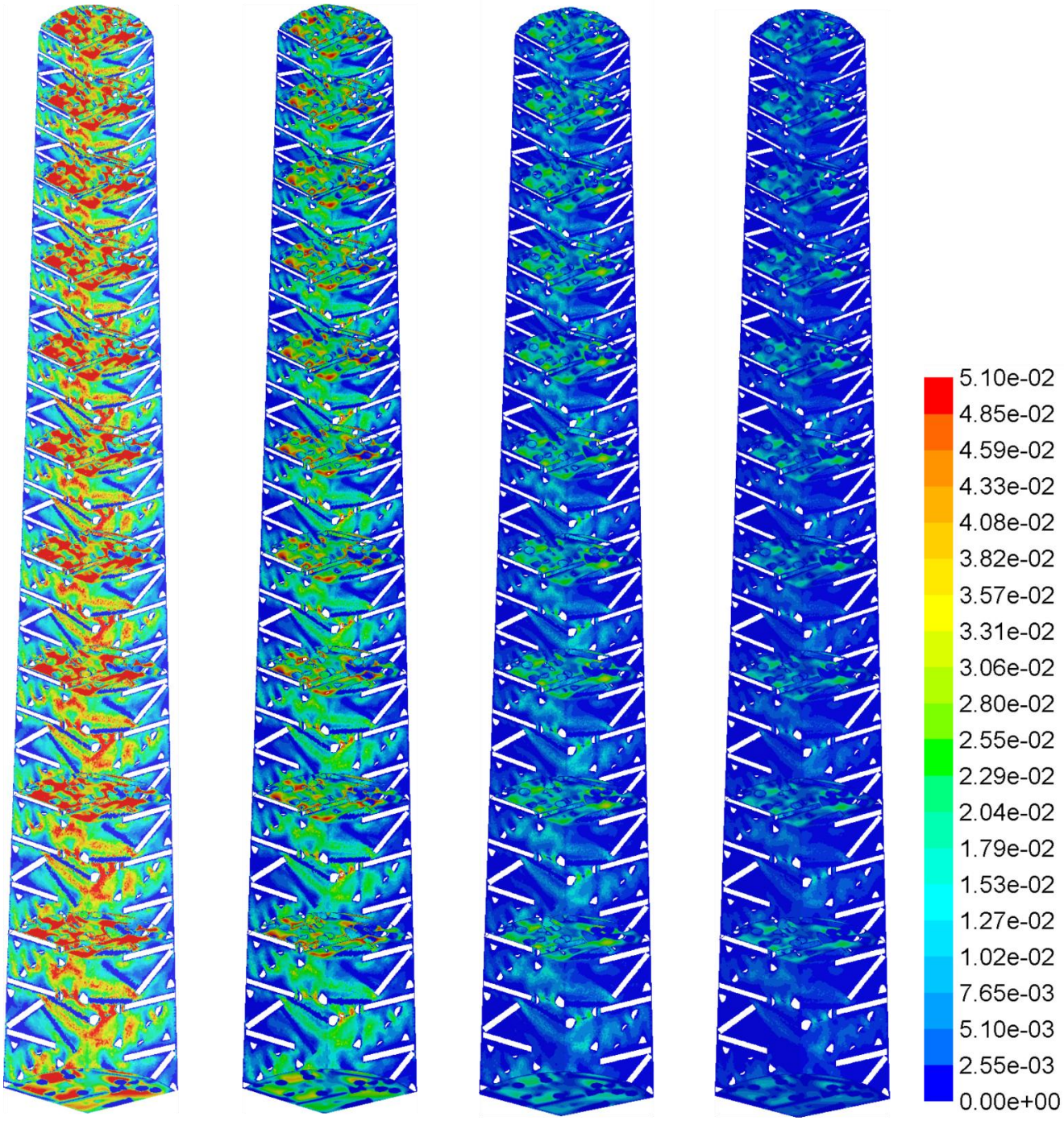

Figure 5-2 Velocity magnitude (m/s) contours isometric view on axial and radial surfaces for full length WS model for (a) Re 75.1 (b) Re 40 (c) Re 19.7 and (d) Re 12.2

In order to assess the type of convection taking place at different locations in the bed and for different flow rates, data from the simulations is plotted on Metais-Eckert maps (Metais and Eckert, 1964) as shown in *Figure 5-3*. As the flow proceeded from length 0.0153 m to 0.0609

m, the type of convection has changed from predominantly being mixed convection to being predominantly forced convection. Except for very low Re of 2.45 and 3.95 where the heat transfer was by mixed convection even at length of 0.0609 m into the packed bed.

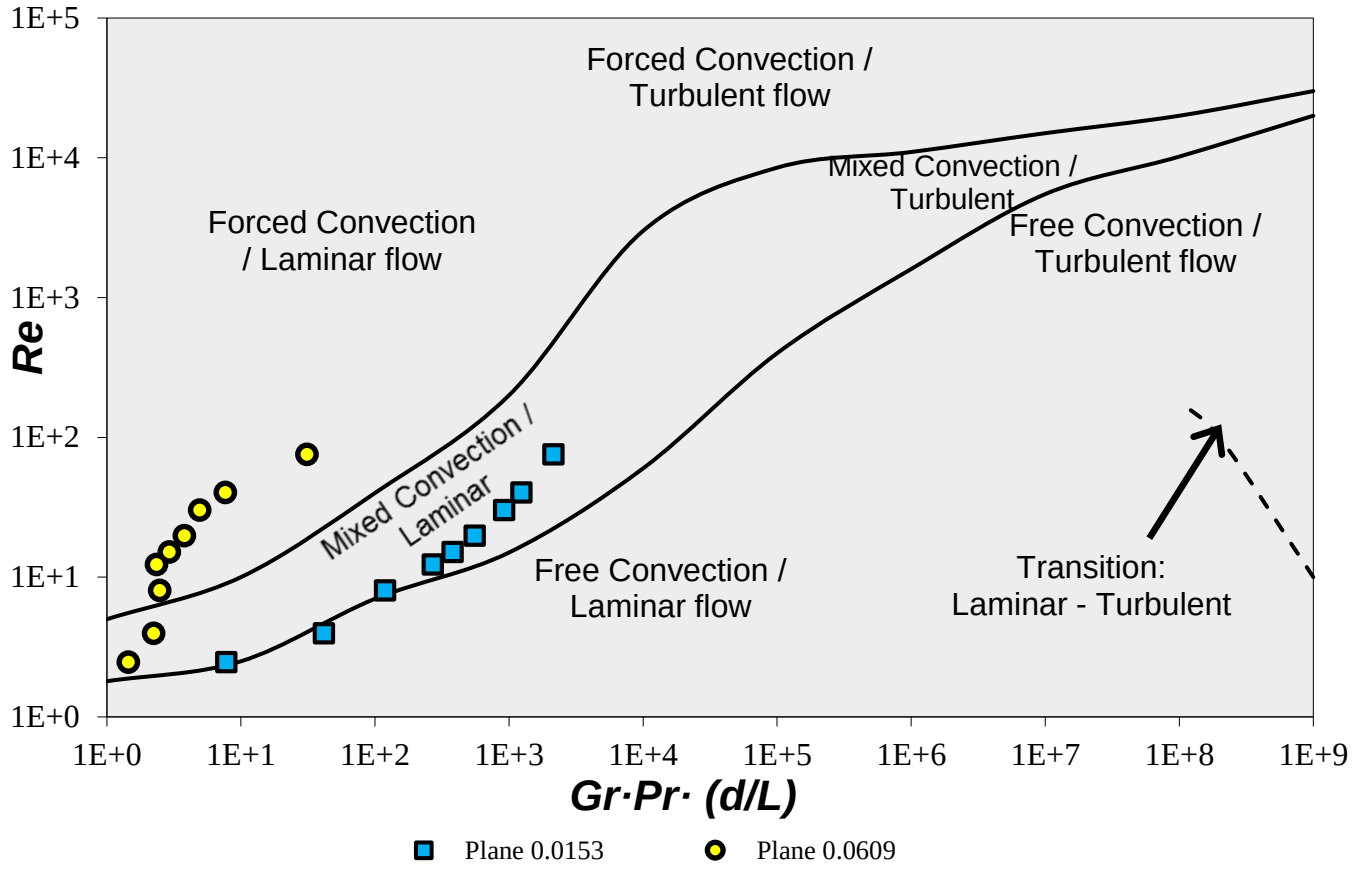

Figure 5-3 Simulation data compared with Metais-Eckert maps for different flow rates with data from radial planes at two different locations into the packed bed

Density contours are shown in *Figure 5-4* and *Figure 5-5* on radial and axial surfaces for half-length WS model and full length WS model respectivel y. The density is uniform in the radial direction on all the radial cuts as seen from the figures. But as expected the density is higher for higher Re along the axial direction. This is due to lower temperature in the inlet region and the temperatures reach a maximum along the axis concurrently the density reaches minimum along the axis. As seen in *Figure 5-4(e) Figure 5-5(d)* the density reaches its minimum nearest to the inlet for lowest Reynolds numbers. This is due to higher temperatures for lower Reynolds numbers. Large density gradients are observed near the inlet of the bed.

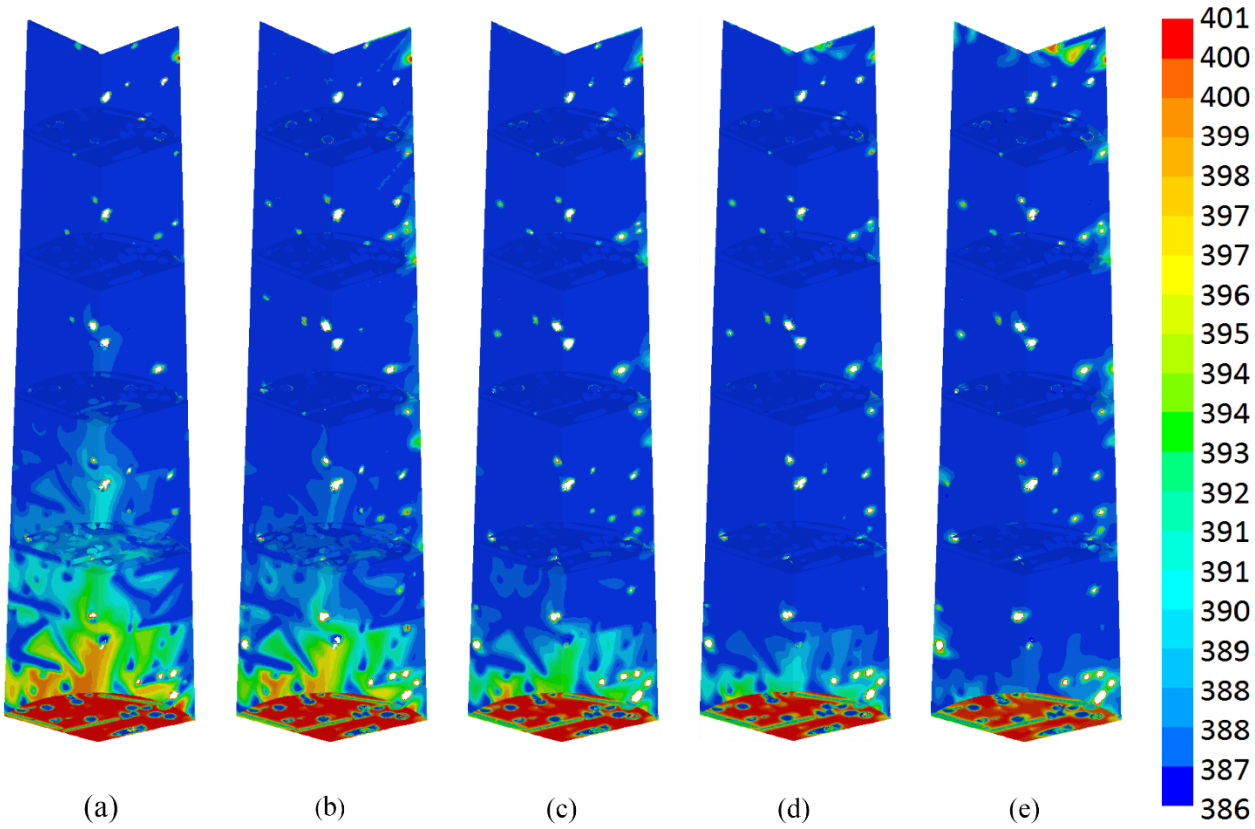

Figure 5-4 Density (kg/m3) contours isometric view on axial and radial surfaces for half-length WS model for (a) Re 30 (b) Re 15 (c) Re 8 (d) Re 3.9 and (e) Re 2.4

For very low Re, as a result of back flow due to the high density gradients for gravity opposing flow mixed convection is observed even at length 0.0609 m into the bed. Density gradients appear near particles surfaces can be seen, which are due to high temperature on particles. As noted by various researchers, buoyancy effect caused by density differences lead to significant increase in the axial dispersion (Benneker et al., 1998). As the solvent density under supercritical condition processes is high, the effect of high density of solute on the flow stability due to buoyancy effects is lower as compared to non-supercritical processes. Density gradients are predominant near the inlet length of the packed bed as seen in *Figure 5-4* and *Figure 5-5*, which verifies the cause for the mixed convection on plane, x = 0.0153 m shown in *Figure 5-3*.

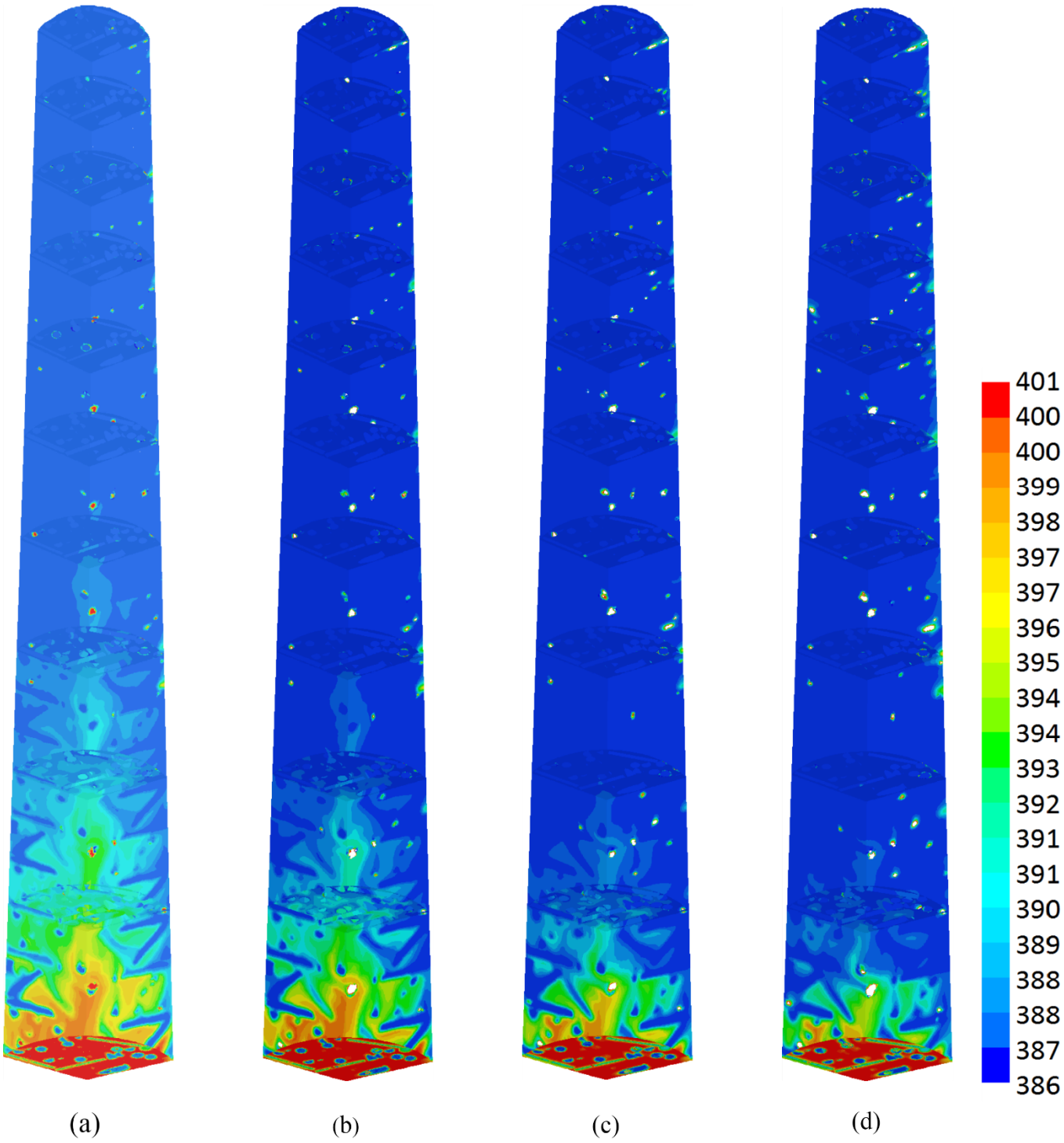

Figure 5-5 Density (kg/m^3) contours isometric view on axial and radial surfaces for full length WS model for (a) Re 75.1 (b) Re 40 (c) Re 19.7 and (d) Re 12.2

Flow velocity is directly proportional to heat transfer when forced convection is taking place. With the increase in velocity, there is better mixing and higher heat transfer coefficients. In *Figure 5-6* forced convection and natural convection are plotted for changing flow rate (Re). The forced convection component is directly proportional to Re, following the behaviour, while natural convection component is almost constant for all the cases indicating its independence

of flow velocity and intrinsically related to density and temperature fields. Hence while describing natural convection, the main dimensionless group used is Gr and not Re.

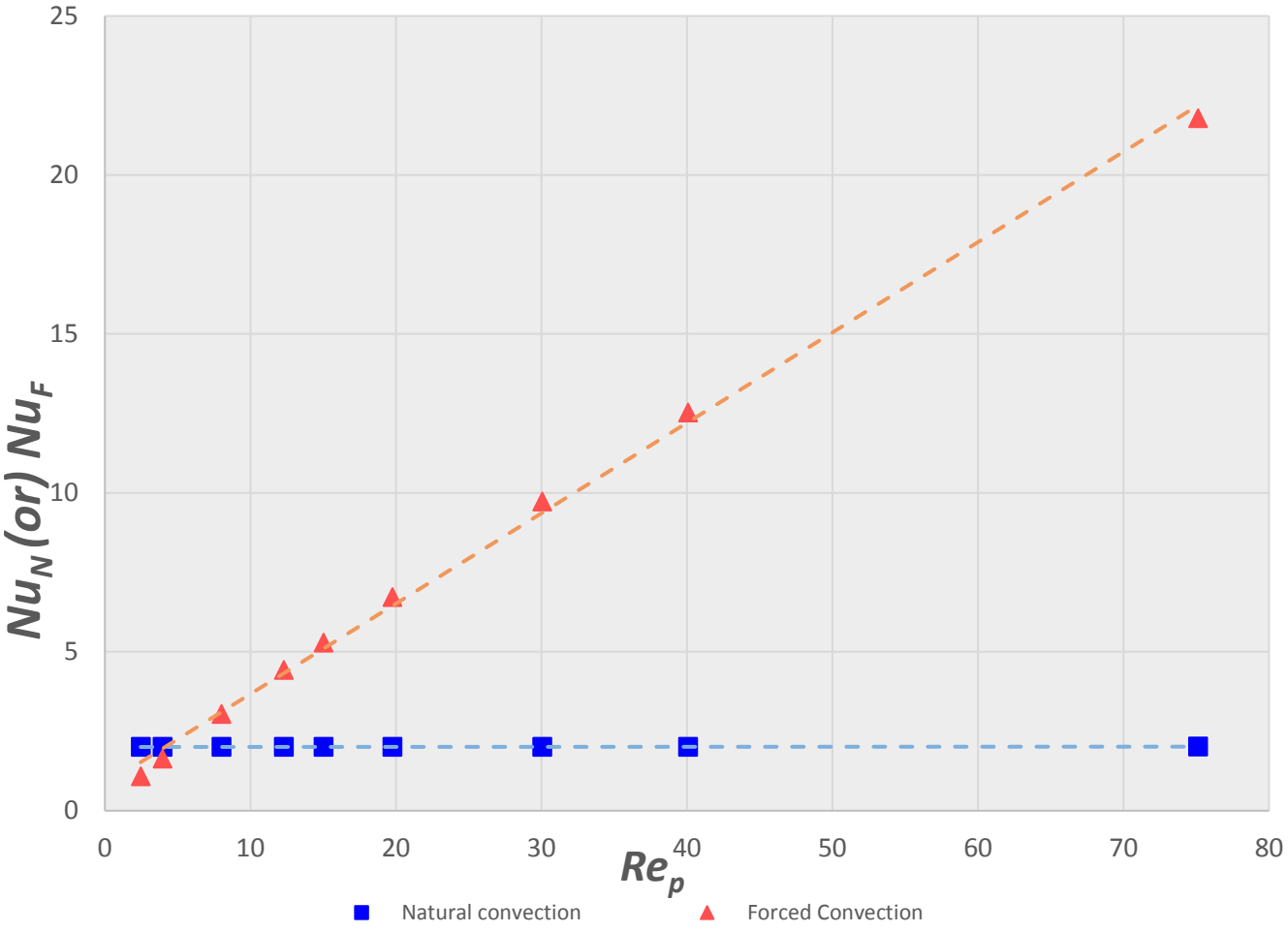

Figure 5-6 Nusselt number vs Reynolds number for free and forced convection

The contribution of natural convection to the total heat transfer with Re is shown in *Figure 5-7*. It can be seen that the contribution of natural convection to the total convection decreases with increase in Re. For very lower Re, the contribution of natural convection is higher than forced convection to the overall heat transfer. For Re points 2.45 and 3.94, heat transfer due to natural convection is higher than forced convection. In *Figure 5-8* the contribution of forced convection to the total convection is plotted, which increased with Re as expected. The numerical results are also in concordance with the experimental analogous mass transfer results presented by Stüber et al., (1996).

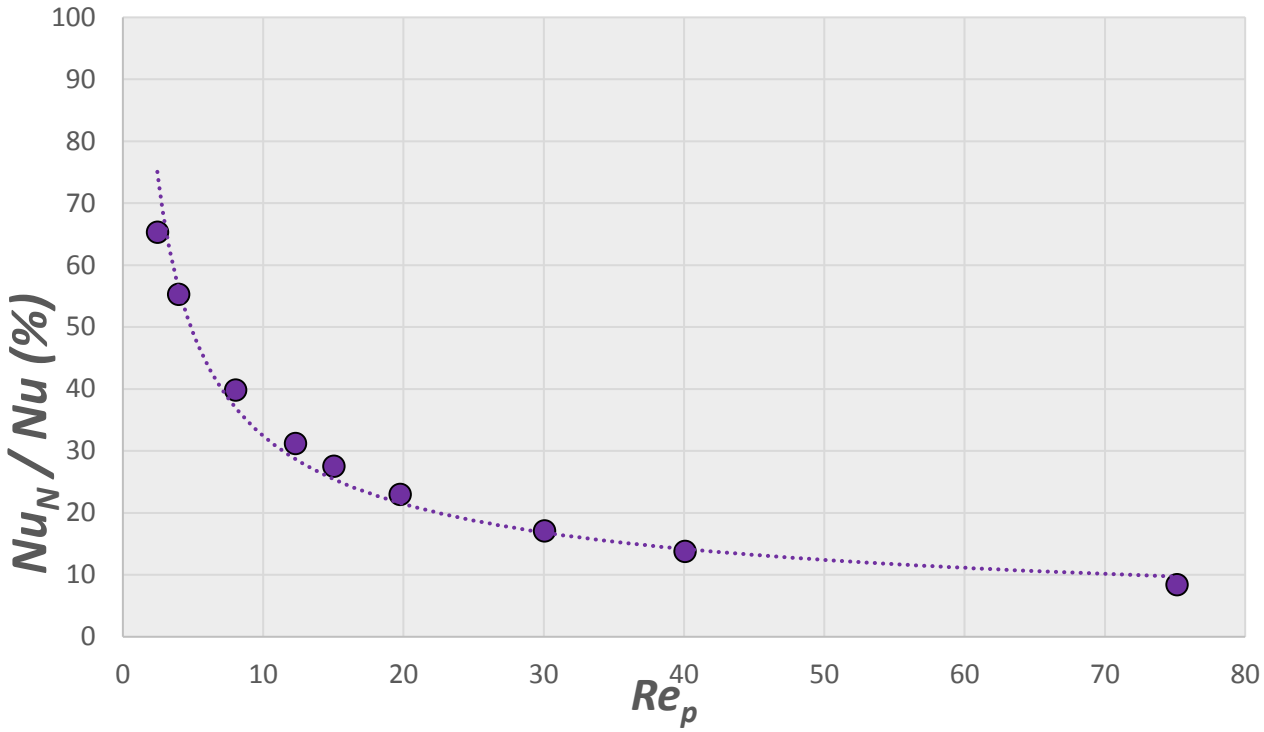

Figure 5-7 Contribution of natural convection to total heat transfer vs. Reynolds number

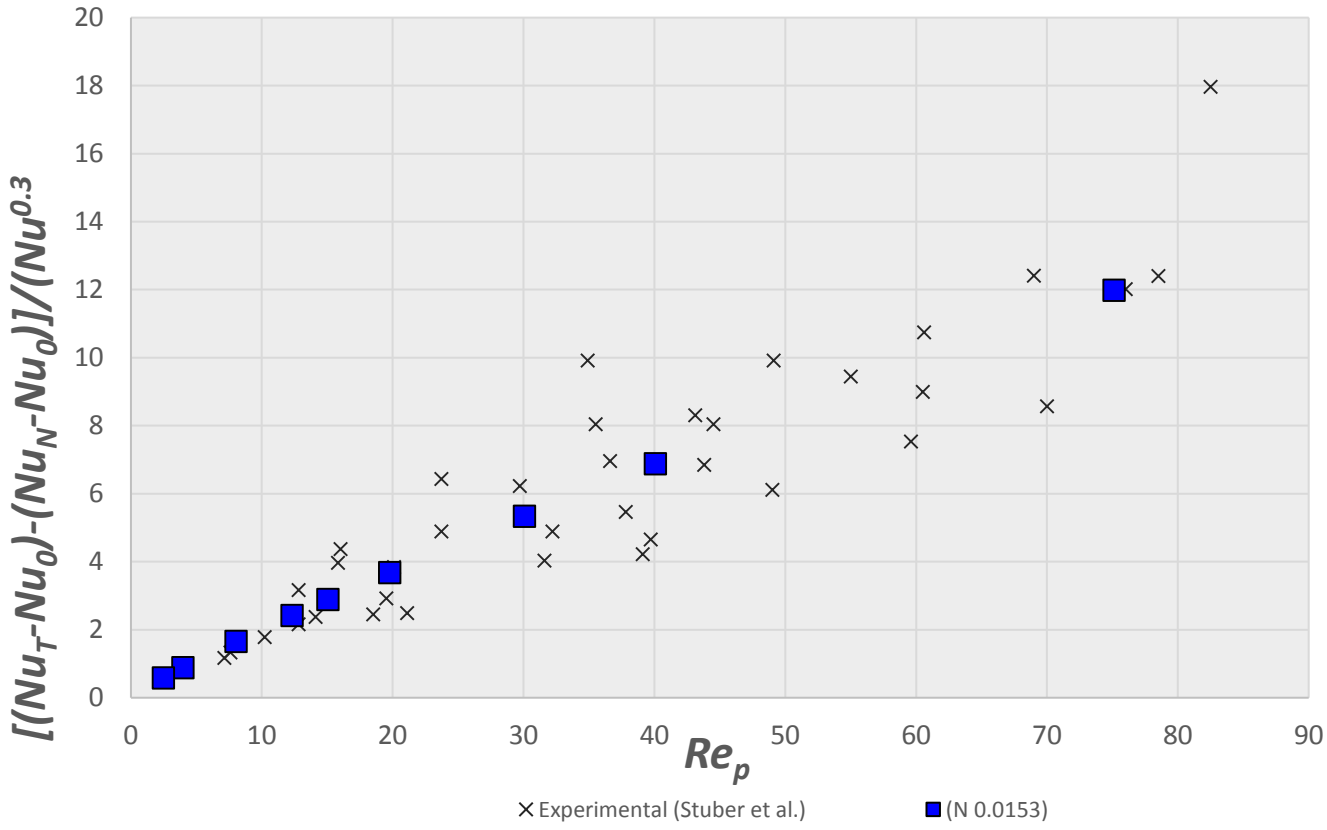

Figure 5-8 CFD obtained contribution of forced convection to total heat transfer vs. Reynolds number and comparison against mass transfer analogous experimental data presented by Stüber et al., (1996)

5.4.2 Temperature Profiles

Temperature contours are presented for axial surfaces along the length of the packed bed. and *Figure 5-9* and *Figure 5-10* show the temperature contours for half-length WS model and full-length WS model respectively. It can be seen from the contour profiles, the temperature reached its highest, nearest to the inlet for lower Reynolds numbers. The exit temperatures decrease with the increase in Re for a particular length of the bed.

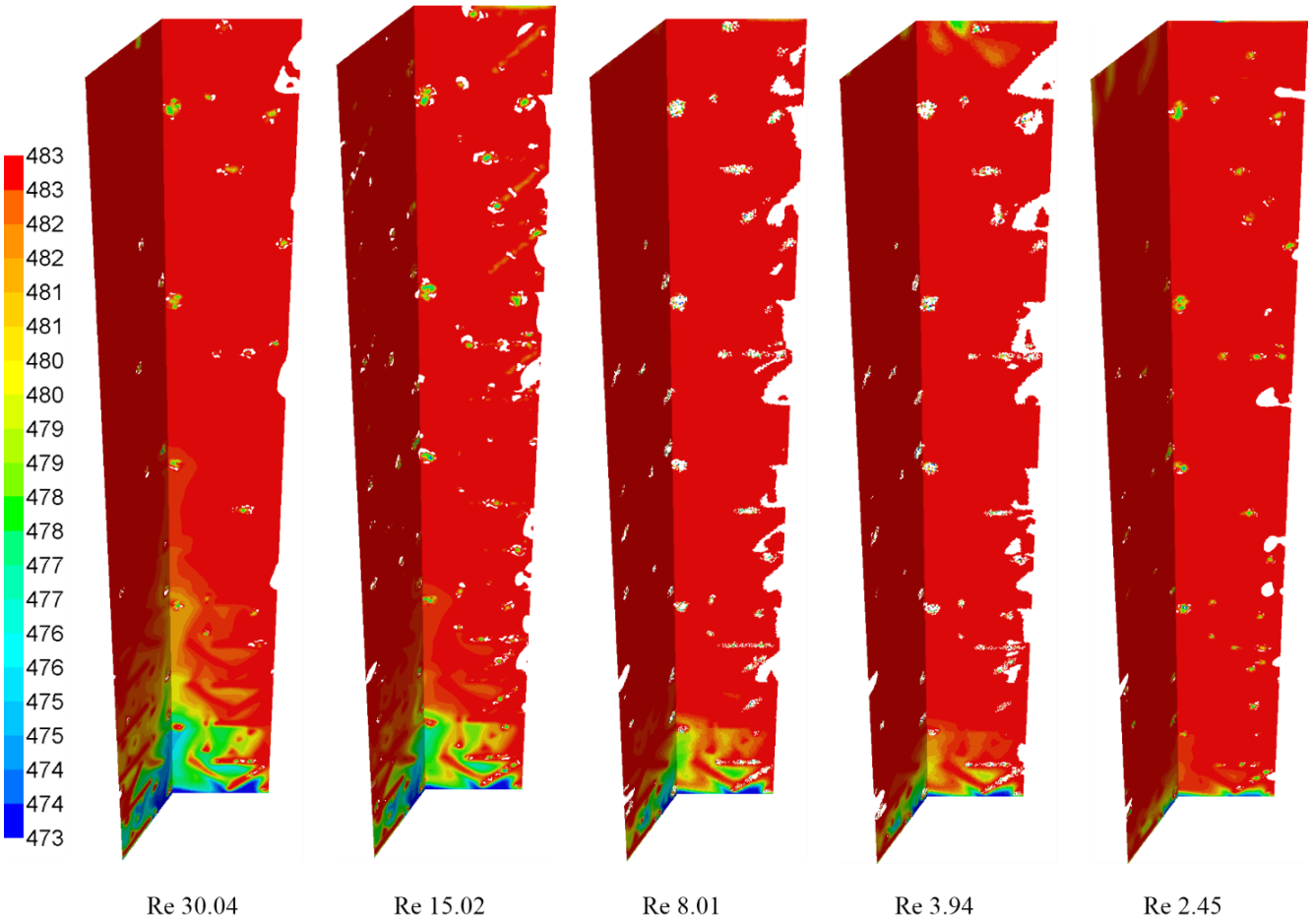

Figure 5-9 Temperature contours on axial planes for half-length WS model with particle temperature at 473.15 K and particle surface temperature at 483.15 K.

High temperature gradients are observed near the inlet of the packed bed with high temperature on the particles surface and low temperatures in the fluid in vicinity of the particles. These temperature gradients give rise to density gradients causing heat transfer by natural convection as observed in previous section.

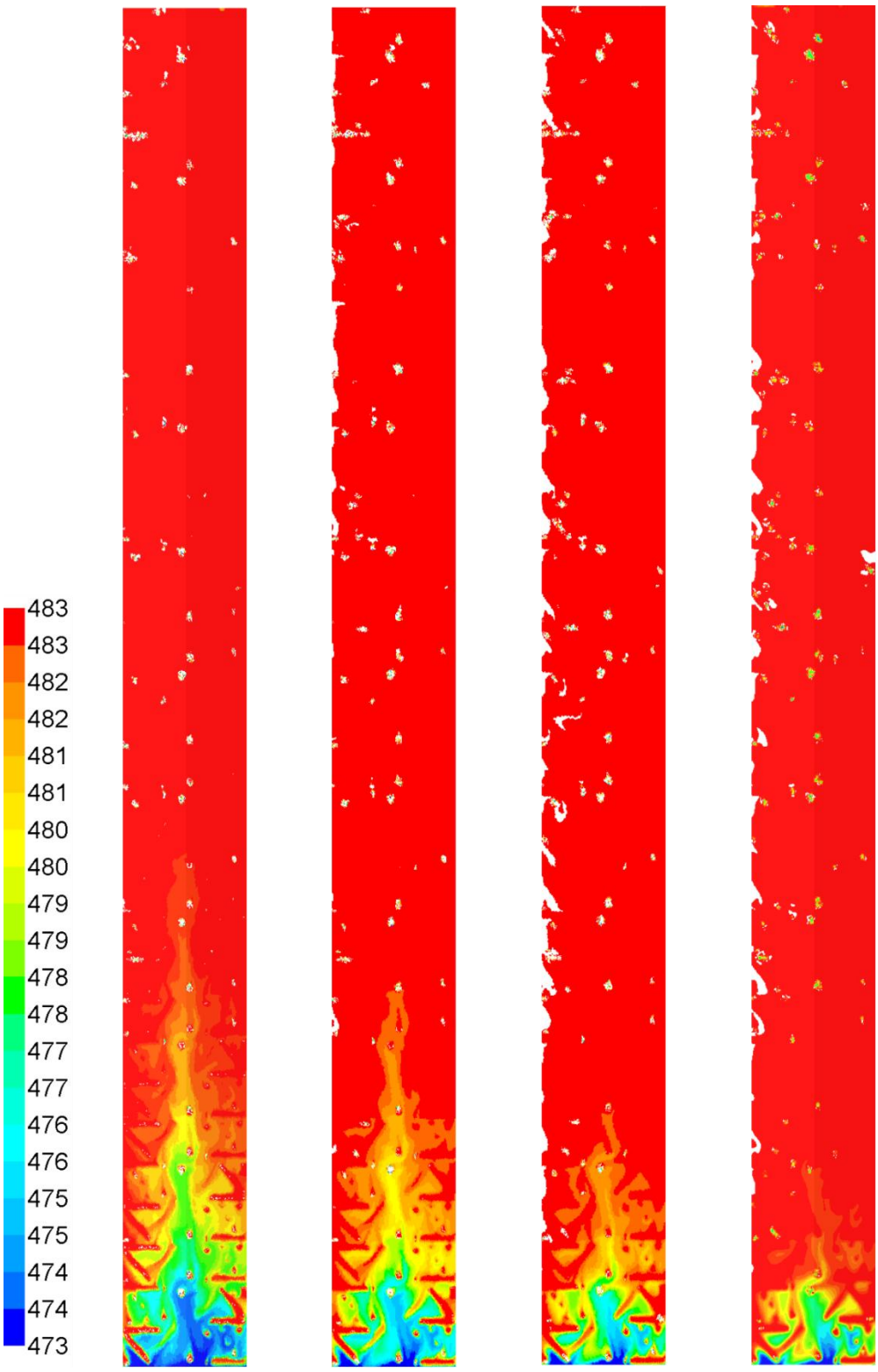

Figure 5-10 Temperature contours on axial surfaces for full length WS model with particle temperature at 473.15 K and particle surface temperature at 483.15 K.

Temperatures along the axial line in the packed bed are plotted in *Figure 5-11* for different flow rates. The data in plots like these, can be plotted in dimensionless coordinates with reference to

the full length of the bed and/or applied temperature, however, actual values are used to present the real condition. Large temperature gradient can be observed near the inlet to the bed. The equilibrium temperature is arrived nearer to the inlet for lower Re, due to longer time fluid particles spend in the packed bed.

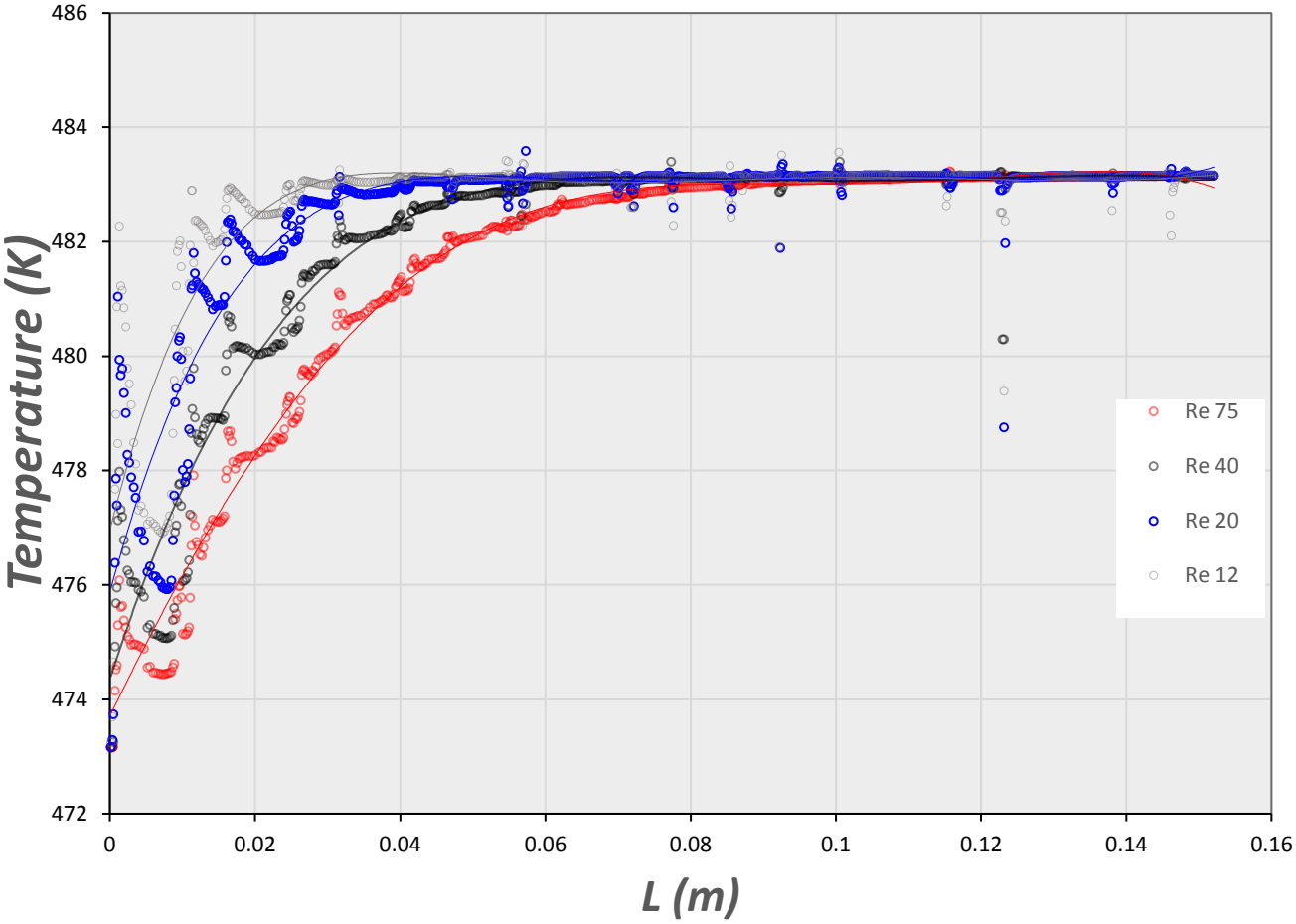

Figure 5-11 Temperature (K) along axial-line for different flow rates for full length WS model packed bed

As compared to wall-to-fluid heat transfer, in particle-to-fluid heat transfer the surface area of heated surface (particles) is much higher than for heated surface (wall) in wall-to-fluid heat transfer, as a result the temperature reaches highest temperature in much shorter lengths of the bed compared to wall-to-fluid heat transfer. This can be observed in temperature profiles in Figure 4-18 and Figure 5-10. As a result of this high temperatures, forced convection is predominant in flows of particle-to-fluid heat transfer compared to wall-to-fluid heat transfer. Also in wall-to heat transfer, free convection is higher in the areas distant from the wall (axial).

5.4.3 Concentration Profiles

Concentration profiles are added to check the effect of flow rates on the distribution of species in the reactor. In order to assess possible influence of species densities (triolein is highest density component) on the flow effects. As seen below, triolein, higher density species is accumulated more near to the inlet for lower flow rates, as would be expected in gravity opposing flows.

Figure 5-12 shows the triolein concentration plots along the axis of the bed. For higher Re, it can be seen from the plot the higher concentration of the triolein up until about one-fourth of the length of the bed. The change in the concentration profiles is due to the same reason as that the density is higher (due to lower temperatures) in the inlet regions. And that for the lower Re the densities reach equilibrium (concurrently the concentrations reach equilibrium), nearer to the inlet.

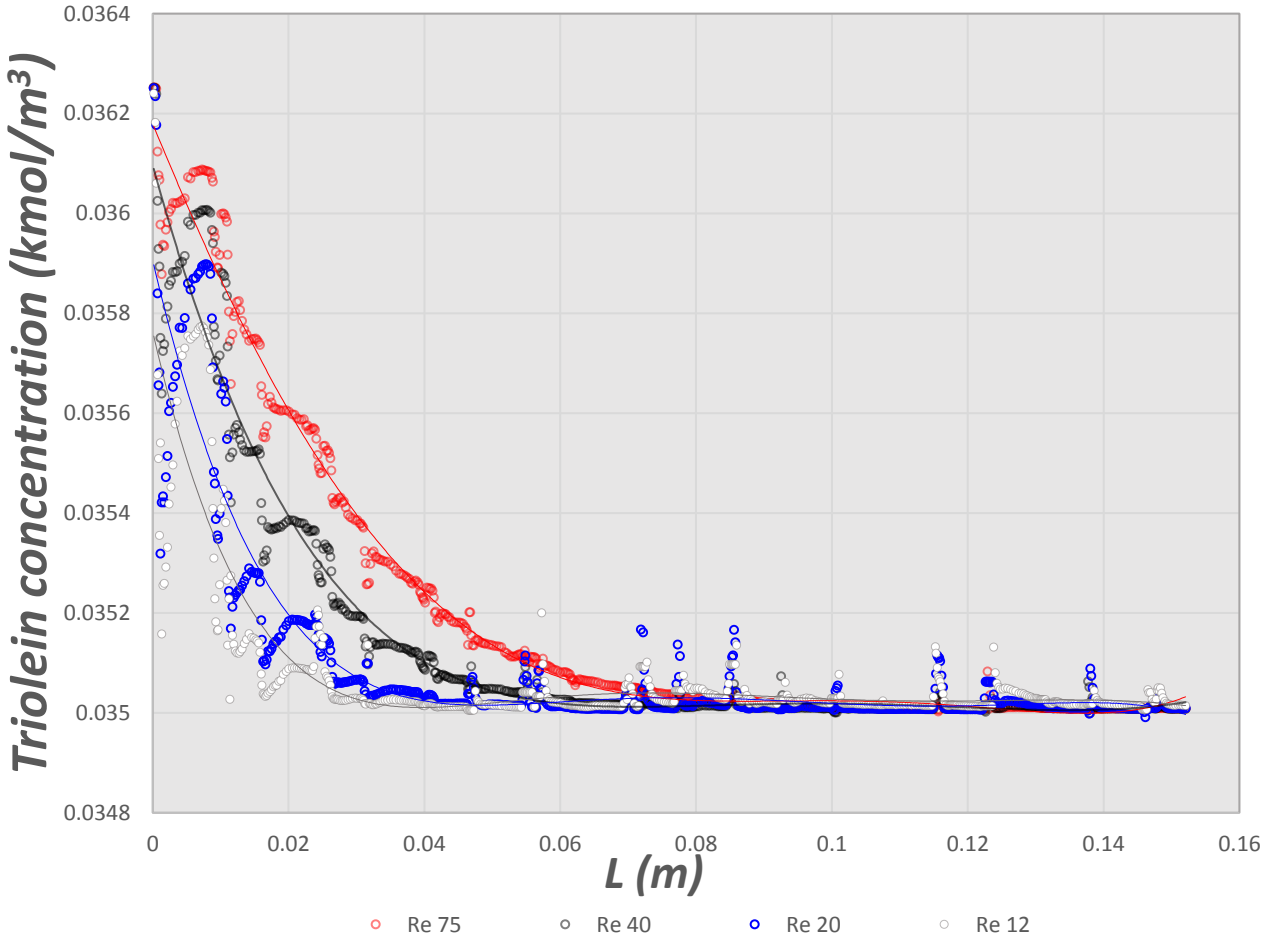

Figure 5-12 Triolein concentration (kmol/m^3) along axial-line for different flow rates for full length WS model packed bed

5.4.4 Effects of flow rate

The objective of this set of simulations was to test the capabilities of CFD in particle-to-fluid heat transfer packed bed model. For each simulation the velocity is varied as shown in Table 5-2 and laminar model is solved in FV code with energy and species equations. The temperature profiles in the bed and at the exit, and other variables were recorded and analysed. For and heat transfer coefficient is obtained from solution of the energy balance equation (5-2) which takes into consideration the axial dispersion, and the boundary conditions in equation (5-3) using temperature data from simulations. The heat transfer coefficients obtained were presented in the form of *Nu*.

The obtained values of heat transfer coefficient (h) in dimensionless form Nu were compared against broadly accepted empirical correlations (Cybulski et al., 1975; Evans and Harlow, 1957; Gunn, 1978; Kunii and Levenspiel, 1969; Lim et al., 1990; Wakao et al., 1979)

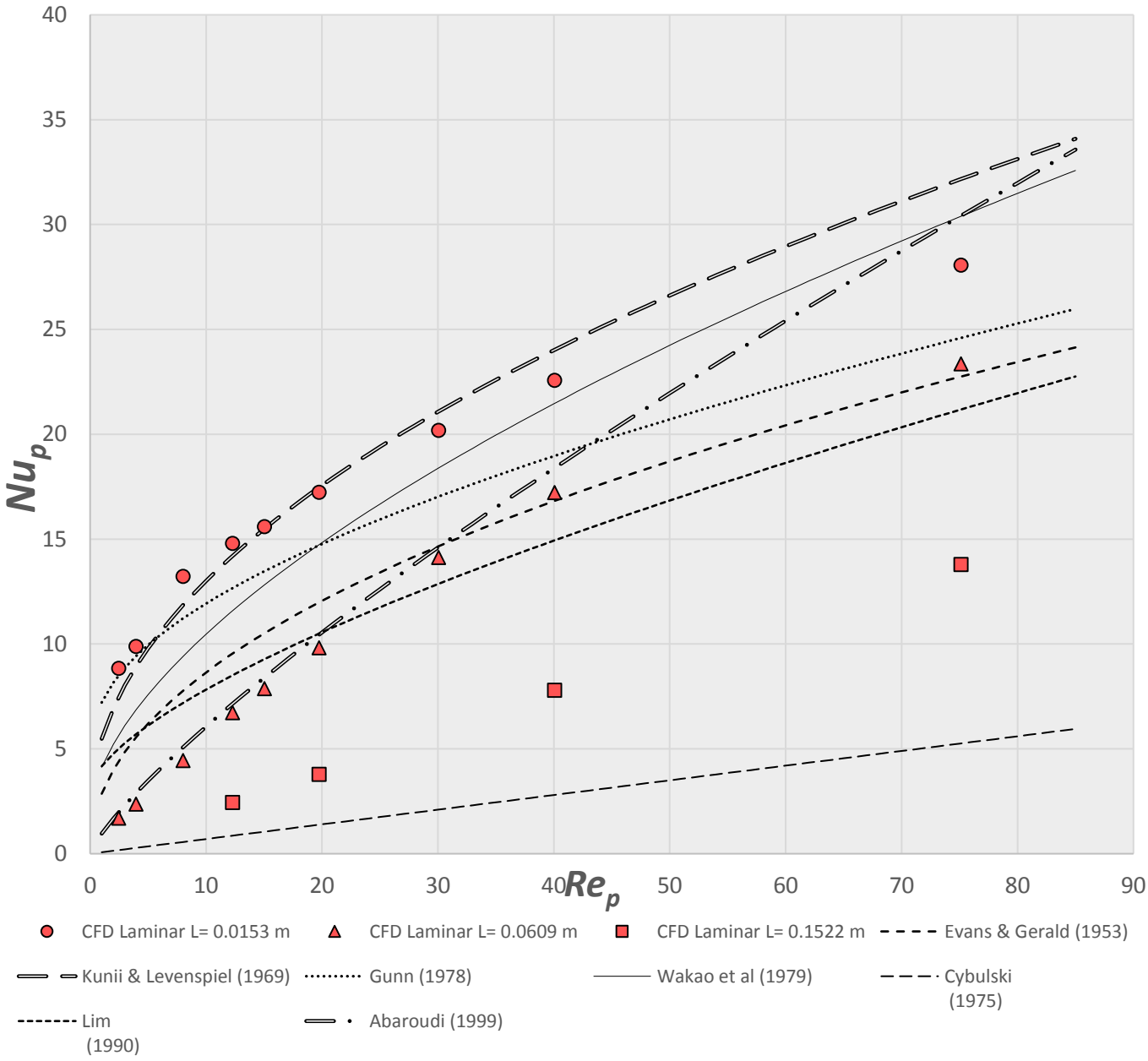

Figure 5-13 Nusselt number vs. Reynolds number for particle to fluid heat transfer for Re 2.5 to 75 estimated for exit temperatures at locations 0.0153m, 0.0609m and 0.1522m compared with some empirical correlations

The obtained Nusselt numbers were computed and plotted against Reynolds numbers. *Figure 5-13* shows the Nusselt number for all the cases (from Re 2.5 to 75) simulated for "hot" particles heat-transfer in packed bed. The simulations of Re 12.2, 19.7, 40.06 and 75.11 were performed for full-length WS model, for which data is available for length 0.1522 m. The Prandtl number for all the cases is Pr = 7.24. The temperature data at three lengths (which are one-tenth, four by tenth, and full-length of the packed bed located at 0.0153 m, 0.0609 m and 0.1522 m respectively from the inlet) were recorded for analysing the heat transfer coefficients at these lengths.

The Nu (as heat transfer coefficient, h) decreases with the increase in bed length (L) is as required in equation (5-4). This is since the temperature reaches equilibrium with the increase in length into the packed bed. And the decrease in the effective temperature driving force (the difference between local exit temperature and inlet temperature) is not proportional to the increase in the length of the packed bed.

Some of the correlations agreed well with the CFD results. For the data from length 0.0153 m, the correlation by Kunii and Levenspiel, (1969) and the data from length 0.0609 m agrees well with the Abaroudi et al., (1999) With further away from the inlet the Nu has decreased much lower for the same Re, such that only the Cybulski et al., (1975) correlation estimates lower.

5.5 CONCLUSIONS

Heat transfer from particle to bulk fluid in a packed bed is studied. A geometric model of packed bed is created with cylindrical packing particles with tube-to particle diameter ratio of about 9. Full-length and half-length wall segment models have been used. The simulations model was set up for high-pressure and temperature supercritical conditions with tertiary mixture. Flow, energy and species mathematical models have been solved for the setup.

Mixed convection at high pressure in a packed bed was also analysed. For a supercritical fluid in laminar flow regime, it was possible to study the effects of density gradient, velocity over heat transfer. Large density gradients were observed near the inlet of the packed bed. These density gradients generated hydrodynamic instabilities leading to convection due to natural convection as observed in the Metais-Eckert maps.

For very low Re, the equilibrium temperature is achieved at shorter lengths of the packed bed. Hence for a given requirement, low Re conditions, shorted packed bed is sufficient.

Heat balance equation, which takes into consideration the axial dispersion is used for estimating heat transfer coefficients. The influence of velocity over the heat transfer is analysed and plotted. The value of Nu increases almost linearly with the increase in velocity. The simulation data agrees with many empirical correlations for predicting particle-to-fluid heat transfer. The heat transfer coefficients decreased with increase in length into the packed bed.

Computational fluid dynamics proved to be a reliable tool for modelling convective heat transfer in high pressure supercritical conditions for species mixtures in complex geometries. Free/Forced convection situations in the packed bed can be analysed at different locations in

the packed bed. The obtained results can be compared qualitatively and quantitatively with previously published data.

REFERENCES

Abaroudi, K., Trabelsi, F., Calloud-gabriel, B., Recasens, F., 1999. Mass Transport Enhancement in Modified Supercritical Fluid. Ind. Eng. Chem. Res. 38, 3505–3518. doi:10.1021/ie990105e

Benneker, a. H., Kronberg, a. E., Westerterp, K.R., 1998. Influence of buoyancy forces on the flow of gases through packed beds at elevated pressures. AIChE J. 44, 263–270. doi:10.1002/aic.690440205

Cybulski, A., Van Dalen, M.J., Verkerk, J.W., Van Den Berg, P.J., 1975. Gas-particle heat transfer coefficients in packed beds at low Reynolds number. Chem. Eng. Sci. 30, 1015–1018.

Danckwerts, P.V., 1953. Continuos flow systems. Distribution of residense times. Chem. Eng. Sci. 2, 1–13.

Debenedetti, P.G., Reid, R.C., 1986. Diffusion and mass transfer in supercritical fluids. AIChE J. 32, 2034–2046. doi:10.1002/aic.690321214

Evans, M.E., Harlow, F.H., 1957. The particle-in-cell method for hydrodynamic calculations. Los Alamos Sci. Lab. Rep. LA-2139.

Gunn, D.J., 1978. Transfer of heat or mass to particles in fixed and fluidised beds. Int. J. Heat Mass Transf. 21, 467–476.

Happel, J., 1958. Viscous flow in multiparticle systems; slow motion of fluids relative to beds of spherical particles. AIChE J. 4, 197–201.

Kaguei, S., Shiozawa, B., Wakao, N., 1977. Dispersion-Concentric Model for packed bed heat transfer. Chem. Eng. Sci. 32, 507–513. doi:10.1016/0009-2509(77)87007-3

Kunii, D., Levenspiel, O., 1969. Fluidization Engineering, Wiley, New York.

Kunii, D., Suzuki, M., 1967. Particle-to-fluid heat and mass transfer in packed beds of fine particles. Int. J. Heat Mass Transf. 10, 845–852. doi:10.1016/0017-9310(67)90064-6

Lim, G.-B., Holder, G.D., Shah, Y.T., 1990. Mass transfer in gas-solid systems at supercritical conditions. J. Supercrit. Fluids 3, 186–197. doi:10.1016/0896-8446(90)90022-E

Littman, H., Barile, G., Pulsifer, A.H., 1968. Gas-Particle Heat Transfer Coefficients in Packed Beds at Low Reynolds Number. Ind. Eng. Chem. Fundam. 7, 554.

Metais, B., Eckert, E.R.G., 1964. Forced, Mixed, and Free Convection Regimes. J. Heat Transfer 86, 295.

Pfeffer, R., 1964. Heat and mass transport in multiparticle systems. Ind. Eng. Chem. Fundam. 380–383. doi:10.1021/i160012a018

Ramìrez, E., 2005. Contribution to the Study of Heterogeneous Catalytic Reactions in SCFs :

Hydrogenation of Sunflower Oil in Pd Catalysts at Single - Phase Conditions . Barcelona Tech.

Santana, A., Larrayoz, M.A., Ramìrez, E., Nistal, J., Recasens, F., 2007. Sunflower oil hydrogenation on Pd in supercritical solvents: Kinetics and selectivities. J. Supercrit. Fluids 41, 391–403. doi:10.1016/j.supflu.2006.12.009

Schumann, T.E.W., 1929. Heat transfer: A liquid flowing through a porous prism. J Franklin Inst 208, 405–416.

Stüber, F., Vazquez, A.M., Larrayoz, M.A., Recasens, F., 1996. Supercritical Fluid Extraction of Packed Beds : External Mass Transfer in Upflow and Downflow Operation. Ind. Eng. Chem. Res. 35, 3618–3628.

Wakao, N., 1976. Particle-to-fluid transfer coefficients and fluid diffusivities at low flow rate in packed beds. Chem. Eng. Sci. 31, 1115–1122. doi:10.1016/0009-2509(76)85021-X

Wakao, N., Kaguei, S., 1982. Heat and Mass Transfer in Packed Beds, Gordon and Breach, Science Publishers, Inc. Gordon and Breach.

Wakao, N., Kaguei, S., Funazkri, T., 1979. Effect of fluid dispersion coefficients on particle-to-fluid heat transfer coefficients in packed beds. Correlation of Nusselt Numbers. Chem. Eng. Sci. 34, 325–336.

CHAPTER VI

6. PARTICLE-TO-FLUID MASS TRANSFER

6.1 INTRODUCTION

The problem of mass transfer between a fluid and exposed surface in a packed bed through which it flow is encountered in operations like leaching, chromatography, drying, ion exchange, extraction, combustion of fuel, and petroleum reservoir engineering. These operations have a variety of applications in chemical processes. The prediction of particle to fluid mass transfer is especially important for the design of catalytic reactor, since it is used for the determination of conversions.

The steep decrease of viscosity resulting in increased mass transfer makes solvents at supercritical conditions more advantageous to subcritical conditions. From these, a large number of experimental correlations are reported. Relatively few data on liquids are available. But the correlations are not very much in agreement, especially at low Reynolds number where the buoyancy forces may play a significant role.

For a packed bed, at the interface between a soluble solid and a fluid, a saturated solution is formed and the concentration gradient between the interface and bulk fluid is the driving force for the mass transfer. Mass transfer of the solute into the bulk fluid takes place in three ways, based on the system conditions. If the fluid is stagnant, then for an infinitely small solid particle, mass transfer occurs by molecular diffusion alone. As the particle size is increased, due to the density differences at the interfaces and bulk fluid, natural convection occurs. And when there is flow, forced convection is also a form of mass transfer. The decrease in kinematic viscosities as the fluid goes from dilute gas to dense fluid state (high density fluid) in supercritical region, results in increased natural conviction in supercritical fluids.

6.2 THEORITICAL BACKGROUND

Frossling developed the basic theory for particle-to-fluid mass transfer. Ranz and Marshall, (1952) studied for evaporation of pure liquid. Frossling presented ideas for accounting for the local behaviour and derived the overall surface average transport.

Free surface model:

This model was introduced by Happel, (1958). Pfeffer, (1964) combined the 'free surface model' with 'thin boundary layer solution'. This model is valid only at sufficiently high Peclet numbers.

Channelling Model:

When some groups of particles are packed closely forming aggregates, while others are packed loosely, then it leads to selective flow of fluids in volumes in which packing are loose. Such flow is called channelling. By assuming that in aggregated particles, concentration of the fluid is in equilibrium with interspersed solids, two-dimensional plug flow, and that mass transfer is restricted to molecular diffusion in the direction perpendicular to flow, channelling model was introduced by Kunii and Suzuki, (1967). The anomaly of the previous experimental data for low Peclet numbers were interpreted by taking into consideration channelling, using the model. The Sherwood number derived assuming the model,

$$Sh_p = \frac{k_p D_p}{D_v} = \frac{\Phi_s(1-\Psi_1)}{6(1-\varepsilon)\xi}.\frac{D_p C_p G_0}{D_v} \tag{6-1}$$

The above models are based on theories for a single sphere and hence have failed for packed beds at low Re, because of incorrect boundary conditions.

Nelson & Galloway model and solution

A model was developed by Nelson and Galloway, (1975) in which a boundary condition is applied at the position where the concentration gradient becomes zero symmetrically between particles. The resulting unsteady state diffusion problem is solved, the equations:

$$D\frac{1}{r^2}\frac{\partial}{\partial r}\left(r^2\frac{\partial c}{\partial r}\right) = \frac{\partial c}{\partial r} \tag{6-2}$$

$$c(r,0) = c_0 \tag{6-3}$$

$$c(r_0,t) = c_0' \tag{6-4}$$

$$\frac{\partial c(R,t)}{\partial r} = 0. \tag{6-5}$$

Solving the above Equation (6-2) and rearranging,

$$Sh = \frac{2\xi + \left\{\frac{2\xi^2(1-\varepsilon)^{1/3}}{[1-(1-\varepsilon)^{1/3}]^2} - 2\right\} tanh\,\xi}{\frac{\xi}{1-(1-\varepsilon)^{1/3}} - tanh\,\xi} \tag{6-6}$$

Where

$$\xi = \left[\frac{1}{(1-\varepsilon)^{1/3}} - 1\right]\frac{\alpha}{2} Re^{1/2} Sc^{1/3} \tag{6-7}$$

This model is applicable for range of Reynolds numbers from 0.01 to 1000, but best for 0.08 to 100.

Dispersion model solved based on Danckwerts boundary conditions:

For a system in which the concentration on particle surface is constant, the resistance to mass transfer is considered to exist only in fluid phase. Then the unsteady state mass balance equation of transferring species, the dispersion model for the system is:

$$\frac{\partial C}{\partial t} = D_{ax}\frac{\partial^2 C}{\partial x^2} - U\frac{\partial C}{\partial x} - \frac{a}{\varepsilon_b} k_f (C - C_{ps}) \tag{6-8}$$

Determination transfer coefficients under unsteady state involves additional parameters like intraparticle diffusivity and intraparticle void making the solution much more complicated. Under steady-state conditions, the above equation becomes:

$$U\frac{\partial C}{\partial x} = D_{ax}\frac{\partial^2 C}{\partial x^2} - \frac{a}{\varepsilon_b} k_f (C - C_{ps}) \tag{6-9}$$

For the packed bed with empty column before mass transferring packed bed (0 < x < L), with Danckwerts, (1953) boundary conditions:

$$U(C - C_{in}) = D_{ax}\frac{\partial C}{\partial x} \qquad \text{at } x = 0 \tag{6-10}$$

$$\frac{dC}{dx} = 0 \qquad \text{at } x = L \tag{6-11}$$

The Dankwerts solution was arrived analytically for reactor,

$$\frac{C_{ps} - C_{exit}}{C_{ps} - C_{in}} = \frac{4A exp\left(\frac{LU}{2D_{ax}}\right)}{(1+A)^2 exp\left(A\frac{LU}{2D_{ax}}\right) - (1-A)^2 exp\left(-A\frac{LU}{2D_{ax}}\right)} \tag{6-12}$$

Where

$$A = \left(1 + \frac{4k_f a D_{ax}}{\varepsilon_b U^2}\right)^{1/2} \quad (6\text{-}13)$$

The dispersion coefficient D_{ax} under the condition where a diffusion controlled reaction is taking place at the particle surface, and the inside of the particle is not involved in the, mass transfer of chemical reaction,

$$\frac{\varepsilon_b D_{ax}}{D_v} = 20 + 0.5\, Sc\, Re \quad (6\text{-}14)$$

Models for high pressure supercritical conditions

In supercritical conditions, kinematic viscosities become very low, and density differences are increased across boundary layer, resulting in increased mass transfer. Mass transfer between beds of solid particles and SCFs is important in many operations such as catalysis, chromatography, and adsorption. The design of supercritical extractor, or reactor requires data of solubility of in solvent, equilibrium distribution between the solvent and the oil phase, in case of two phase system.

Lee et al., (1986) presented a one-dimensional unsteady state model of a fixed bed extractor, which is solved by method of characteristics.

Neglecting axial and radial dispersion effects and with equilibrium concentration on the particle surface, assuming mass transfer coefficient is independent of concentration, Tan et al., (1988) have presented a model

$$u\frac{\partial C}{\partial z} = k_{fs} a_{fs} (C_p - C) \quad (6\text{-}15)$$

From the data of initial rates of extraction, for a differential bed (assuming equal sized non-porous pellets) of impregnated with solute to be extracted, at constant pressure, temperature and flow rate, the conservation equation of the solute at t = 0 is given by Stuber et al. (1996),

$$-\frac{dm}{dt} = K_G a (C_G^* - C_G) V M_{solute} \quad (6\text{-}16)$$

The mass transfer coefficient can be evaluated using the above equation above, where $-\frac{dm}{dt}$ is the initial slope of the extraction curve, V is the total bed volume, M_{solute} is the molar weight of solute and C^*_G is the concentration of solute in the fluid at saturation, or its solubility at the selected operating conditions.

Puiggene et al., (1997) solved the solute conservation equations in fluid phase assuming plug flow, and the fluid-holdup ε_g is approximated by dry-bed void fraction ε_b.

6.3 SIMULATION STRATEGY

CFD codes make it possible to numerically solve flow, species and energy balances in complicated flow geometries like packed bed. These differential equations are applied to large number of finite control volumes, together giving a numerical solution. The balance equations solved in the CFD codes are mentioned in the earlier chapter.

Geometric model

The base model of packed bed reactor is a cylinder of length 0.152 m, filled with cylindrical catalysts of length 0.005 m and diameter of 0.001 m, equivalent spherical diameter of 0.00196 m. In this work irregular particle configurations are studied. The configuration of particles was such that each particle is aligned at a different angle with the axis of the reactor in a random fashion. The random is useful to avoid bad flow distribution and channelling.

A wall-segment (WS) 120º segment of the geometry is used for the current analysis. By taking the cut sides of the bed as symmetrical, one third of the tube is run for simulations reducing the computational effort.

The particle-to-particle contact points were included by overlapping about 1 to 2% of the particle volume with adjacent particles. This helps in treating the particles as a single volume so having ease of mobility of particles and avoiding meshing errors causing convergence problems. No convergence problems were detected during runs.

The transesterification reaction was carried out in continuous mode in a fixed bed titanium reactor with length 152 mm and 17.5mm internal diameter. This model was created in a 3D geometry generation software DesignModeler^{TM}. The length of the bed is divided in to parts of 76 mm length beds which is one half of the total length (see). The data of flow conditions, properties and species data from the interface at exit of a bed is input to the inlet of the subsequent other half comprising the total length of the reactor of 152mm. Particles of length 5mm and diameter of 1mm are arranged in the tube segment. Each particle is arranged by sequential operations in the software for moving the particle around in the tube. The cylindrical particles are arranged such that their axis is at angle 0º, 15º, 30º, 45º, 60º, 75º, 90º with the axis of the tube. The particles are arranged such way to have a random arrangement to avoid channelling. Some particles were chipped near the wall of the tube, and within the segment

sides. Table shows the number of particles and their orientation with respect to the tube. The overall void of the bed is about 0.6. Because of slight overlapping (about 1 to 2% of the volume) the bed void is not exactly the volume deducted due to the particles volume. The bed void is measured by treating all the particles as a lump volume. The model is constructed following the bottom-up technique (generating surfaces and volume from nodes and edges) in order to control mesh size at critical points as particle-to-particle and particle-to-wall contact points

A particle packing can be built by different methods like deposition algorithms or by dynamic prototype

The tube has extensions before and after the bed of cylinders, in order to minimize the end effects, and the back flow temperature condition at the outlet. The bed is not in contact with the tube wall, to be treated as a separate volume from the tube.

Mesh Design

The packed bed region is meshed with unstructured tetrahedral volume grid for appropriate discretisation of the computational domain because of their complicated geometry. While the extensions are structured meshed. The generated mesh was further refined on the surface of the particles with element size of 0.00006 m, with structured rectangular surface meshing (refer section 4.2.2 of Chapter 4 for general aspects). The extension walls are also face meshed with element size of 0.0001 m. The velocity is checked for different mesh refinement and the results are consistent for different mesh refinement (see *Figure 4-3* of Chapter 4). To make maximum use of computational resources, the optimal mesh is used for the study.

Model Setup

In particle-to-fluid (e.g., catalysis, extraction) mass transfer, supercritical conditions are preferable for its gas like viscosity and liquid like density resulting in high mass transfer rates. CO_2 is most preferred as supercritical solvent because of its relatively low critical temperature of 31ºC.

In the case of transesterification reaction, CO_2 along with alcohol CH_3OH are used as co-solvents. For the study of mass transfer, solute triolein ($C_{57}H_{104}O_6$, a component representing oil), is concentrated on the particle surface. And to maintain a supercritical single phase experimental condition based on critical properties of the mixture, a case with temperature of 205ºC and pressure of 250 bar was studied for mass transfer. Most theoretical models for mass transfer in packed beds are available for low pressure conditions only a few authors have

modelled for supercritical conditions. (Abaroudi et al., 1999; Lee et al., 1986; Puiggene et al., 1997; Stüber et al., 1996; Tan et al., 1988).

The circulating fluid, solvent methanol/carbon dioxide (25/75 wt.%) is in the inlet. The concentration of solute (at equilibrium), triolein on the particle surface is 0.2164 (molar ratio methanol:oil as 25:1), with rest being solvent. With the pressure of 250 bar, different the cases of inlet velocities are solved.

Triolein is diffused into the bulk solvent CO_2-CH_3OH under laminar flow conditions. For laminar flow, dilute approximation for diffusion coefficient is applicable. For supercritical conditions, the method proposed by He and Yu, (1998), using the critical properties of bulk fluid (CO_2). The diffusion of triolein into is CO_2, calculated at using the method and compared with experimental diffusion (Owen J Catchpole and King, 1994) of triolein into supercritical CO_2 at 251 bar, and the error is 1.9718%. So the method is used for further calculations.

The viscosities, densities of carbon dioxide, methanol and triolein are estimated at the operating conditions of 250 bar, and 205ºC. The mixture properties are calculated by volume weighted mixing law for density and mass weighted mixing law for viscosity.

Boundary conditions, methods	**Value**
Fluid mixture inlet	CO_2 + CH_3OH
Particle surface species	$C_{57}H_{104}O_6$
Mass fraction ratio methanol: carbon dioxide: triolein	0.25: 0.75: 0
Fluid temperature at inlet	473.15 K
Wall temperature	Zero Diffusive flux
Particle surface mass fractions methonol: triolein	0.22995: 0.080099
Pressure	25000000 Pa
Fluid velocity at the inlet	0.0007 – 0.0048 m/s
Shear condition on wall, particle surface	No slip
Discretization	First order
Models solved	Flow, energy, species
Flow model	Laminar

Table 6-1 Boundary conditions for the analysed cases

The flow through the particles is described by momentum, material and chemical component balance equations. Flow is considered to be incompressible and at steady state

Mass Transfer Coefficients

Most advanced models for packed bed mass transfer use the data of fully developed exit concentration for calculation of mass transfer coefficients. Such model by Wakao and Funazkri, (1978), which is based on Danckwerts, (1953) boundary conditions, considering the axial dispersion coefficient D_{ax}. This approach has been used.

For high pressure, supercritical conditions, a simple model was developed (Tan et al., 1988) with assumption of negligible axial dispersion. This assumption is only valid for sufficiently long packed beds. The exit concentration data is used to calculate mass transfer coefficients, with boundary condition, $z = 0$ at $C = 0$, the solution to Equation (6-15) is

$$\frac{C_e}{C_s} = 1.0 - \exp\left(-k_{fs} a_{fs} \frac{L}{u}\right) \tag{6-17}$$

The use of the initial rates of mass transfer for the determination of mass transfer coefficients was given by Stüber et al., (1996), by solving the Equation (6-16)

$$K'_G = \frac{-(-dm/dt)_{t=0}}{a C''_G V M_{solute}} \tag{6-18}$$

6.4 RESULTS AND DISCUSSION

CFD as a design tool for extraction mass transfer in packed bed is studied in this section. Velocity, density and concentration profiles are examined for their influence on the mass transfer effectiveness. The simulations executed are shown in *Table 6-2*

Velocity (m/s)	Re obtained	Oil mole ratio at inlet	Solvent(CO_2+CH_3OH) flow rate (g/min)	Simulation model used	Case ID
0.00789	6.62	0	2.642	Half-length WS	PFMTH.7
0.00127	10.65	0	4.249	Half-length WS	PFMTH.11
0.00257	21.606	0	8.620	Half-length WS	PFMTH.22
0.004829	40.511	0	16.163	Half-length WS	PFMTH.40
0.007726	64.818	0	25.861	Half-length WS	PFMTH.65
0.009658	81.023	0	32.327	Half-length WS	PFMTH.81

Table 6-2 Simulations performed with velocity boundary conditions applied to CFD inlet, geometrical model used for each simulated case

6.4.1 Velocity and Density Profiles

Density contours are shown in *Figure 6-2* on radial and axial surfaces for half-length WS model for Re 6 to Re 81. The density is uniform in the radial direction on all the radial cuts as seen from the figures. It can be seen that the density is decreasing with the increase in Re. This is due to decrease in the concentration of triolein (the high density fluid) in the bed with increased flow rates. For lower Re, density reaches the high of 393-394 kg/m^3 (red area in contour plots), nearer to the inlet. This is due to more extraction at lower Re flows.

The plots of density along the axis of the bed show the presence of large density gradients (see *Figure 6-1*). The density points are much scattered for lower Re, indicating larger density gradients for small flow rates. These density gradients would cause free convection mass transfer which is discussed in later section.

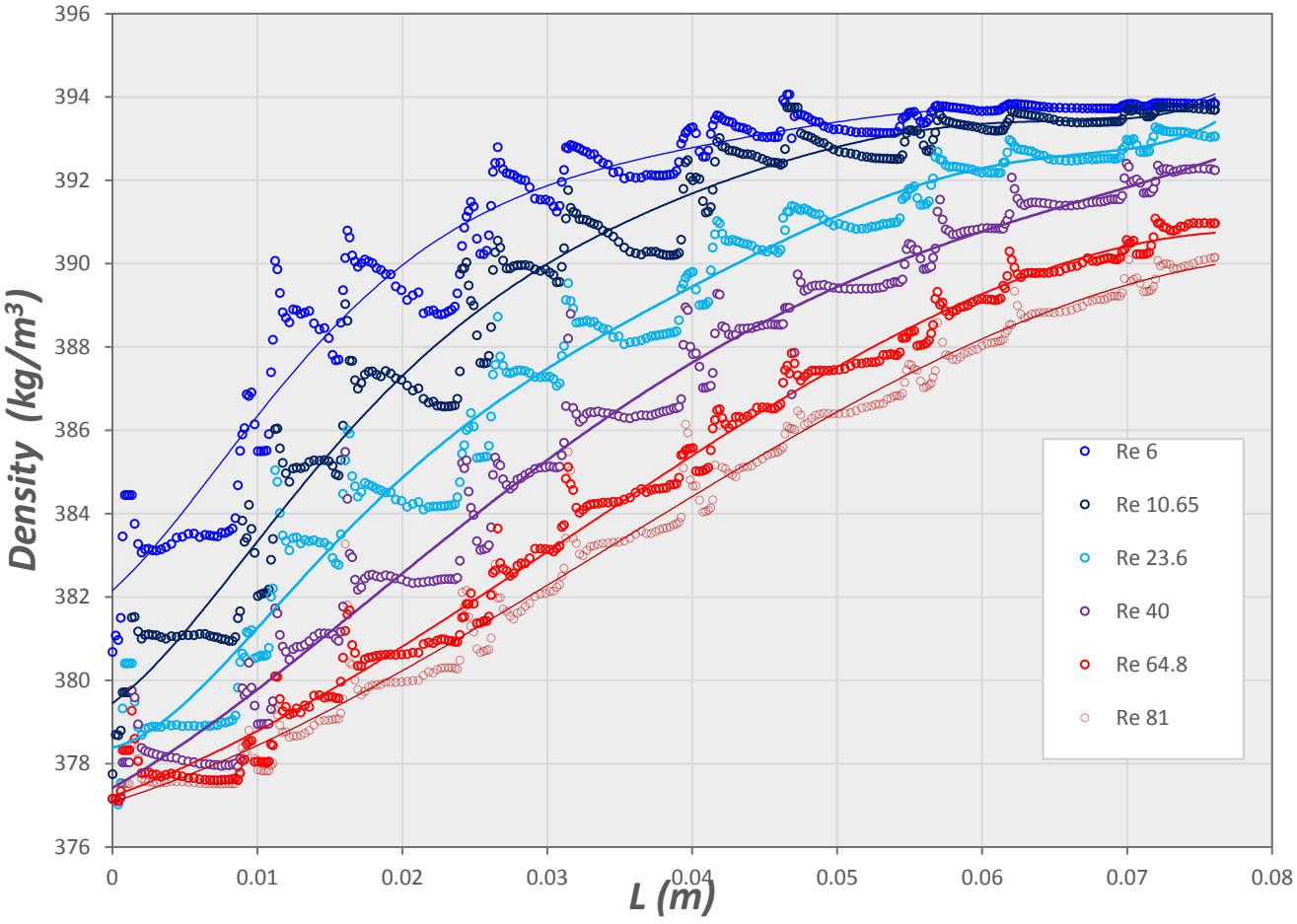

Figure 6-1 Density along axis plotted for different flow rates.

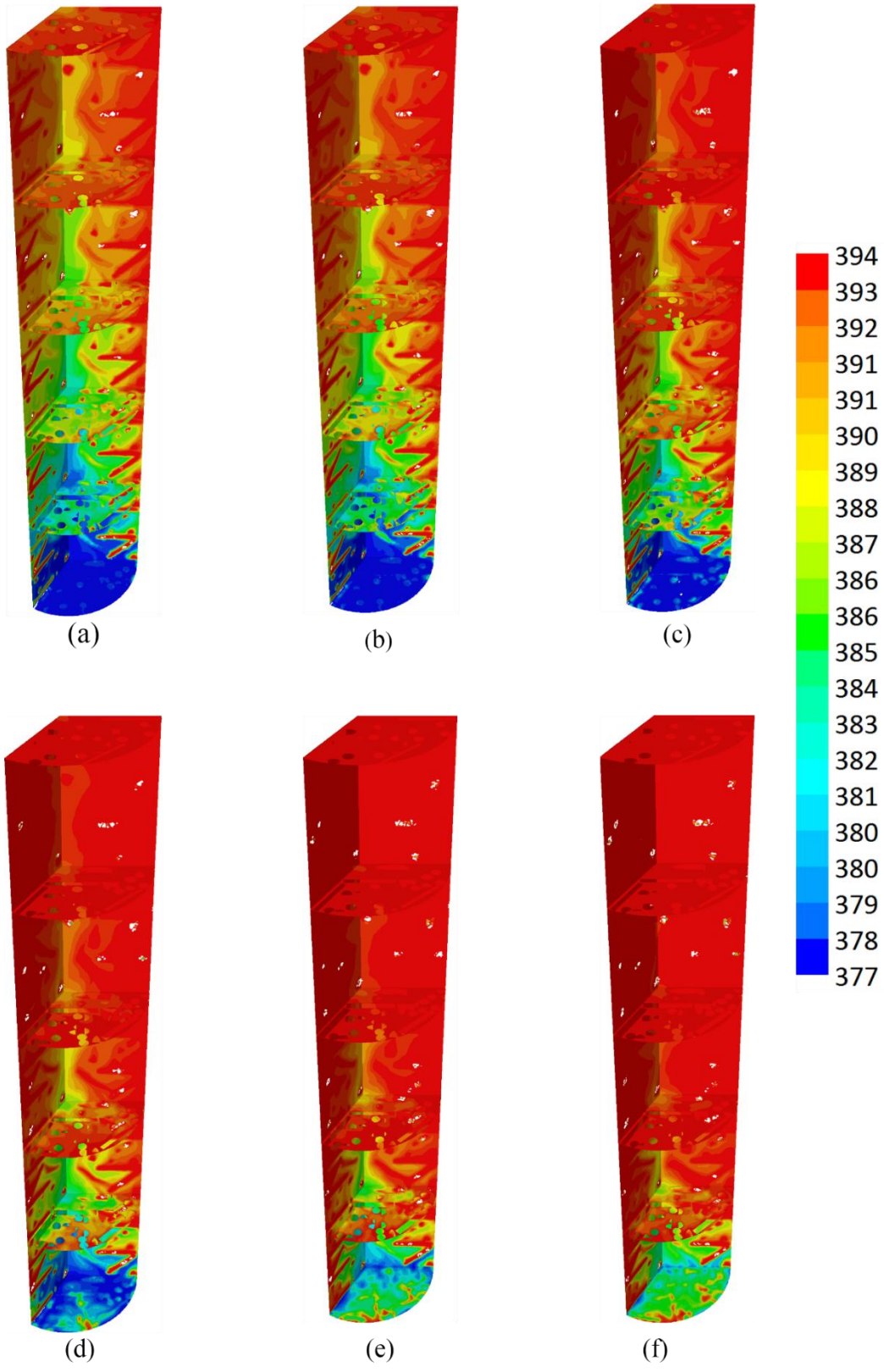

Figure 6-2 Density (kg/m^3) contours on axial and radial planes for half-length WS model for (a) Re = 81 (b) Re = 64 (c) Re = 40 (d) Re = 21 (e) Re = 10 and (f) Re = 6.

The velocity magnitude contours are shown in Figure 6-3. For lower Re the velocities are uniform throughout the bed due to lesser wall-resistance. However, for higher Re, higher

velocities can be seen in the bed. Low velocities are (dark blue regions) near the particle surface (can be seen from the radial profiles) and the wall surface. It can also be observed the velocity is uniform in the axial direction of the bed indicating a developed flow in axial direction with little end effects due to the presence of extensions in the bed (shown in the geometry *Figure 5-1*). The velocities are have not changed in the radial and axial directions for all the Re.

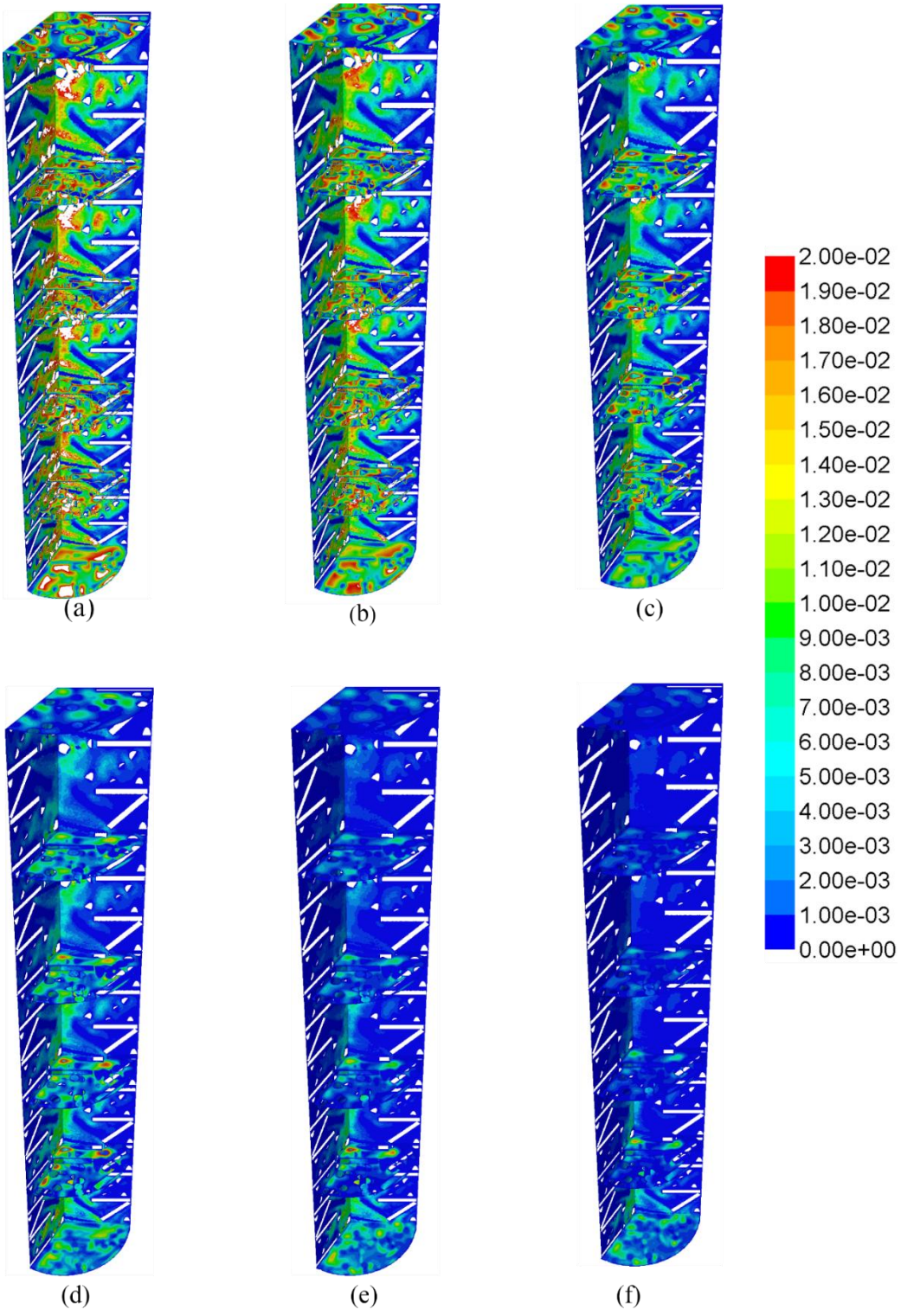

Figure 6-3 Velocity (m/s) contours on axial and radial planes for half-length WS model for (a) Re = 81 (b) Re = 64 (c) Re = 40 (d) Re = 21 (e) Re = 10 and (f) Re = 6

Density gradients exist in particle to fluid heat or mass transfer. As noted by various researchers (Benneker et al., 1998), buoyance effect caused by density differences lead to significant increase in the axial dispersion. As the solvent density under supercritical condition processes is high, the effect of high density of solute on the flow stability due to buoyancy effects is lower as compared to non-supercritical processes.

6.4.2 Natural and forced convection effects

For high pressure flows, mixed convection mass transfer is likely to occur. Hence the effects of density and flow velocities were studied. The simulations were performed with gravitational acceleration activated in opposite direction to the flow (i.e., the flow is in upward direction). So the flow is called opposing flow in which greater amount of free/natural convection mass transfer is found due to the presence of high density gradients, resulting in the formation of hydrodynamic instabilities (viz., counter current flow, recirculation, stream differentiation) which are caused by buoyancy effects. (Benneker et al., 1998).

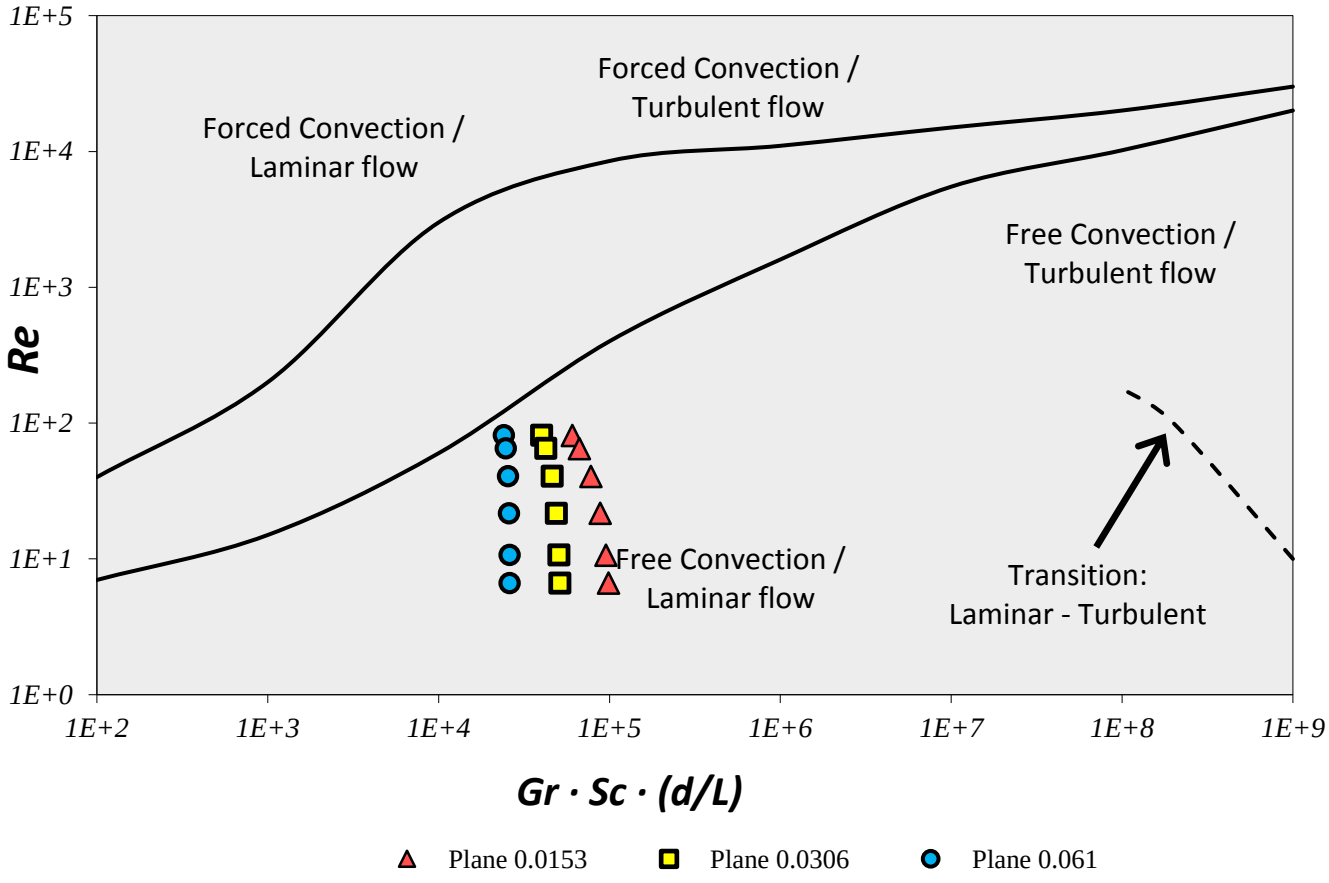

Figure 6-4 Simulation data compared with Metais-Eckert maps for different flow rates with data from radial planes at three different locations into the packed bed

The local values of Gr, Sc and Re values on radial planes were estimated and plotted on Metais-Eckert maps (Metais and Eckert, 1964) in order to verify the transport mechanism inside the packed bed at different locations. *Figure 6-4* shows the plotted values estimated for different Re on three radial planes at different lengths into the packed bed in axial direction. All the points lie in the free-convection laminar region, indicating the presence of hydrostatic instabilities mentioned earlier.

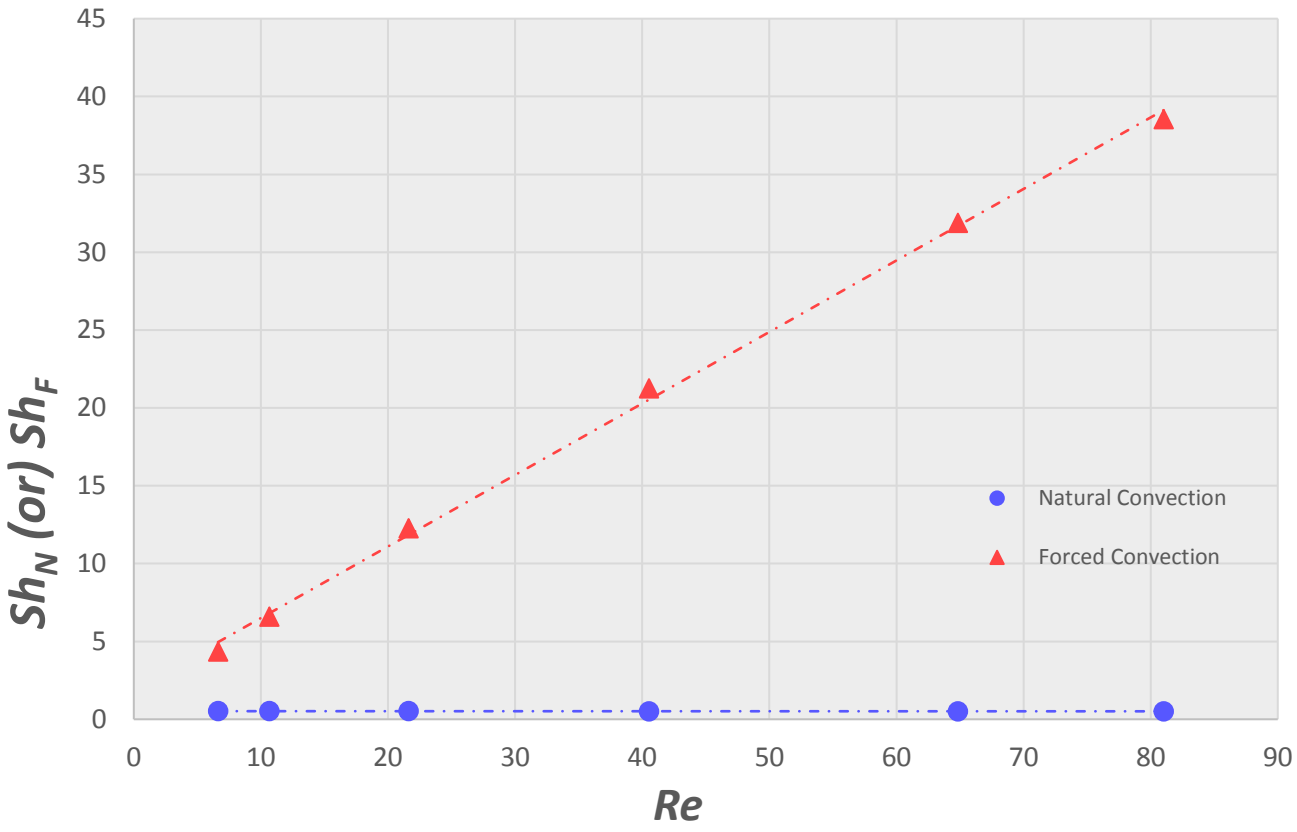

Figure 6-5 Sherwood number vs Reynolds number for free and forced convection

Flow velocity is directly proportional to forced convection mass transfer (Guardo et al., 2007b; Stüber et al., 1996). With the increased there is better mixing resulting in higher mass transfer coefficients. Analysing the mixed convection the results indicate the although the forced convection component is seen increasing with flow velocity, the natural convection component is almost constant for all the cases (see *Figure 6-5*). Indicating that the free convection is intrinsically related to density and temperature fields and not effected by velocity.

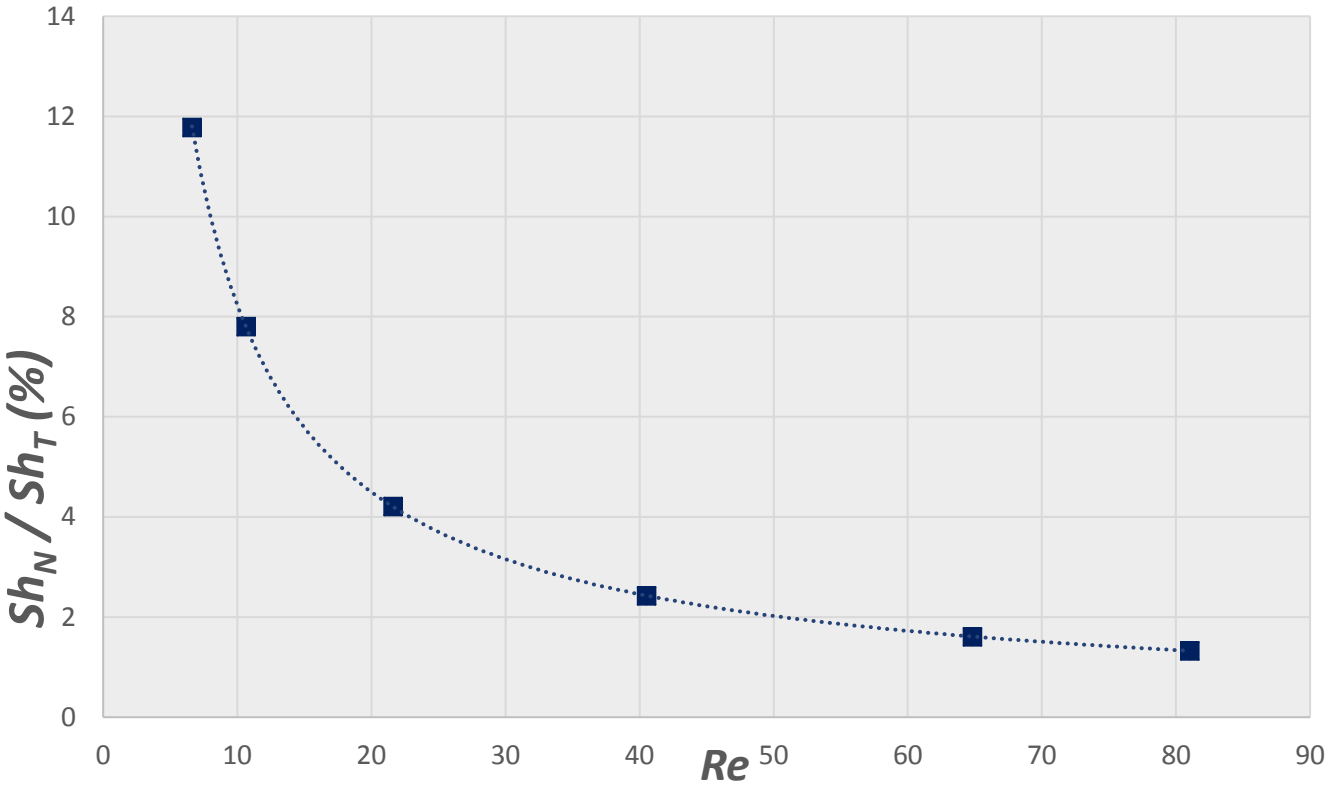

Figure 6-6 Contribution of natural convection to total mass transfer vs. Reynolds number

The contributions of free and forced convections to mass transfer could be assessed following the suggestions of (Stüber et al., 1996). *Figure 6-6* shows the contribution of natural convection to the mass transfer with Re, which is decreasing with the increase in Re. contribution of forced convection to the total convection is plotted which increased with Re as expected. The numerical results are also in concordance with the experimental results by Stüber et al., (1996) reported in that paper as shown in *Figure 6-7*.

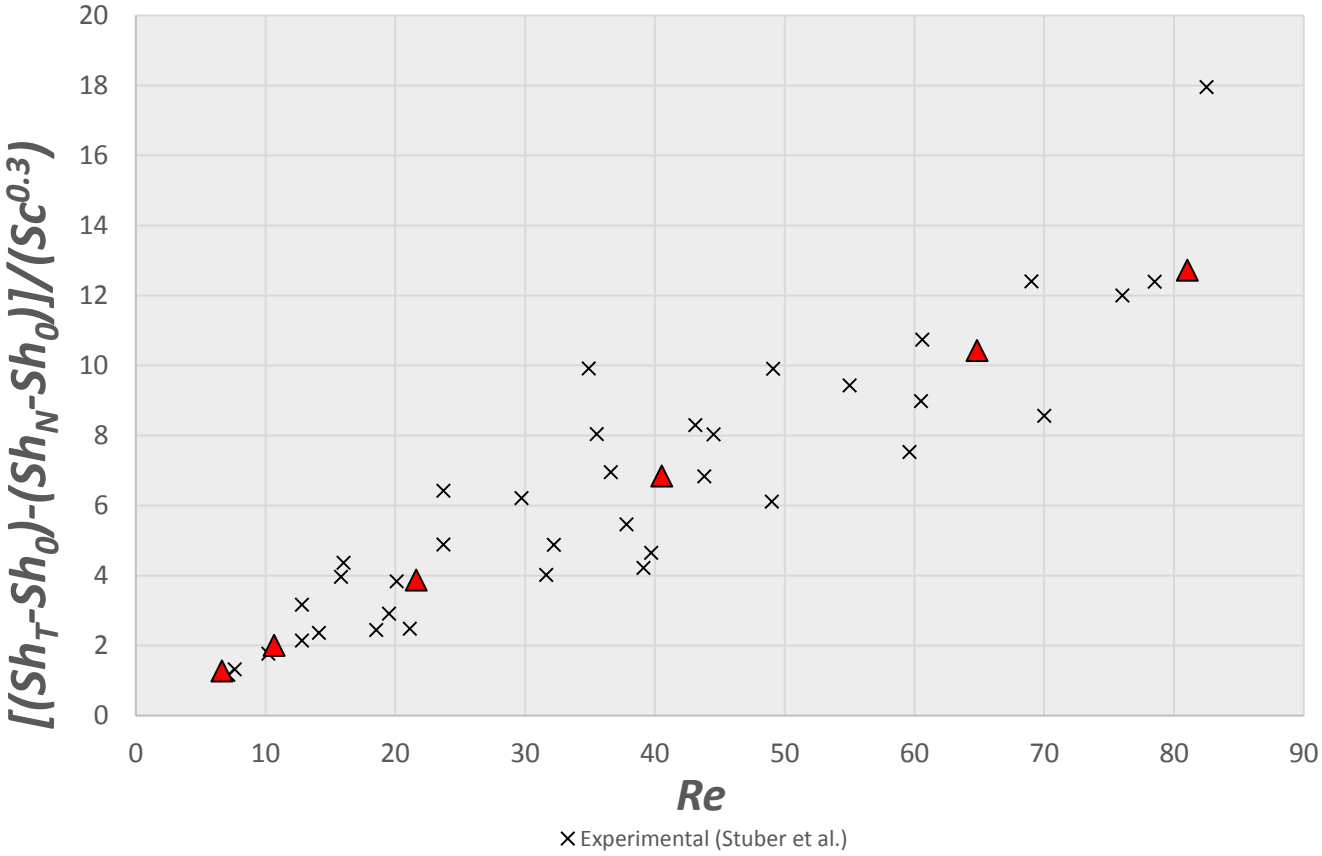

Figure 6-7 CFD obtained contribution of forced convection to total mass transfer vs. Reynolds number and comparison against experimental data presented by Stüber et al., (1996)

6.4.3 Concentration Profiles

Figure 6-9 shows concentration contours on axial and radial planes and *Figure 6-8* shows the triolein concentration plots along the axis of the bed. For higher Re, it can be seen from the plot the lower concentration of the triolein, as the amount of triolein extracted from the particle surface is low with the increase inflow rate. For the required amount of triolein to be extracted, the length of the packed bed or the flow rate has to be adjusted appropriately. As can be seen from the plot in *Figure 6-8* at length 0.076 m, the concentrations of triolein have not reached the maximum concentration (i.e., the concentration on particles). So, for higher Re flows, it is recommended to have longer packed bed for the current case.

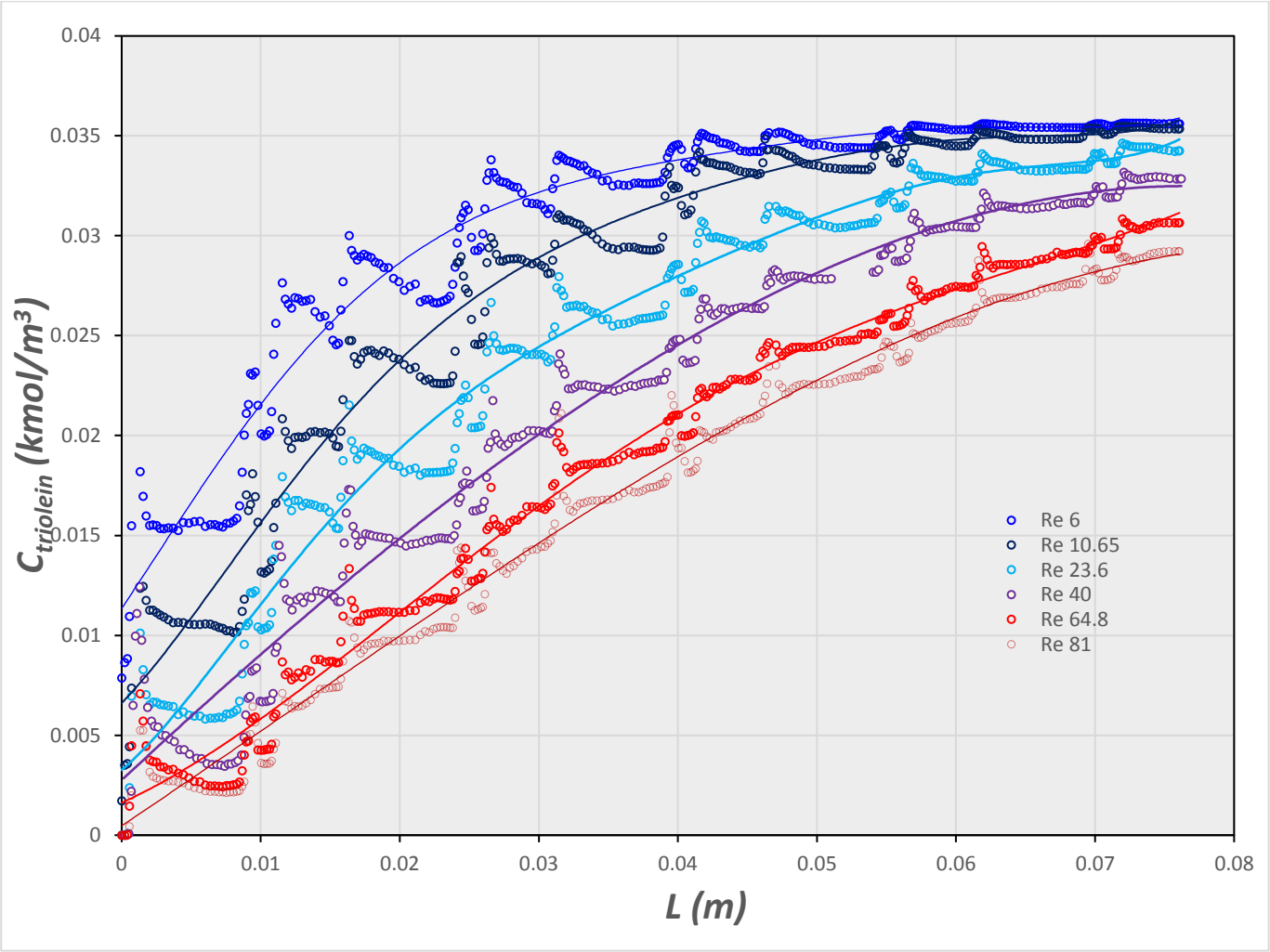

Figure 6-8 Triolein concentration along axis for different flow rates.

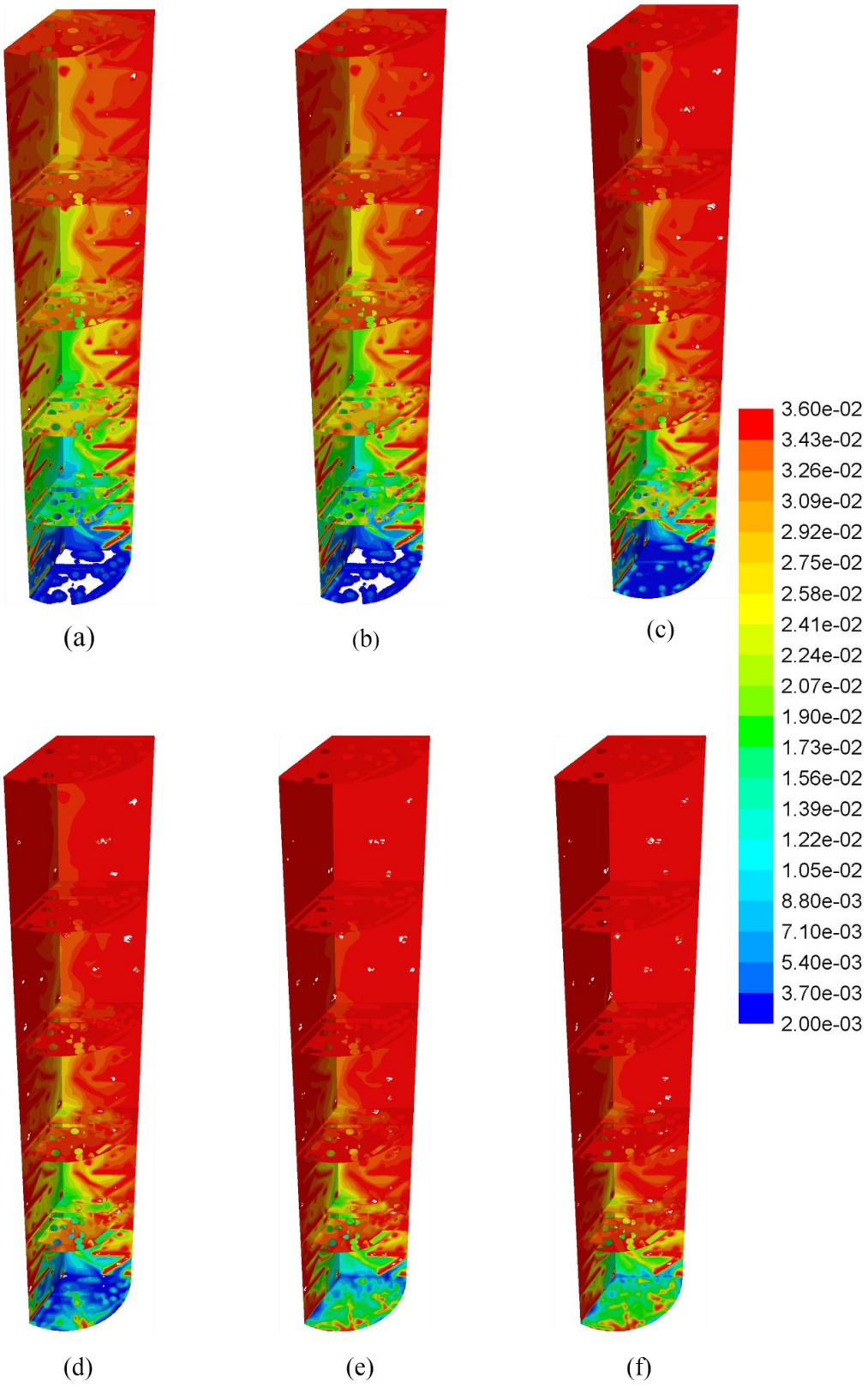

Figure 6-9 Concentration (kmol/m^3) contours of triolein on axial and radial planes for half-length WS model for (a) Re = 81 (b) Re = 64 (c) Re = 40 (d) Re = 21 (e) Re = 10 and (f) Re = 6.

6.4.4 Effect of solvent flow rate and validation of numerical results

The objective of this section is to present mass transfer coefficients in terms of Sherwood number with CFD results and compare them against some empirical correlations, validating the numerical results and comment on the how the different correlations behave compared to the CFD results. The mass transfer coefficient (k_f) values were evaluated at from the solution of the mass balance equation obtained with Danckwerts boundary conditions by Wakao and Funazkri, (1978) from the concentration and property data from numerical simulations. It is obtained from solution of the mass balance equation (6-9) which takes into consideration the axial dispersion, and the boundary conditions in equation (6-10) and (6-11) using temperature data from simulations. The mass transfer coefficients obtained are presented in the dimensionless form Sh. The obtained Sh for $6<Re<80$, and Prandtl number 14.85 were compared against broadly accepted empirical correlations for predicting mass transfer coefficients (Abaroudi et al., 1999; Evans and Gerald, 1953; Lim et al., 1989; Tan et al., 1988; Wakao and Funazkri, 1978)

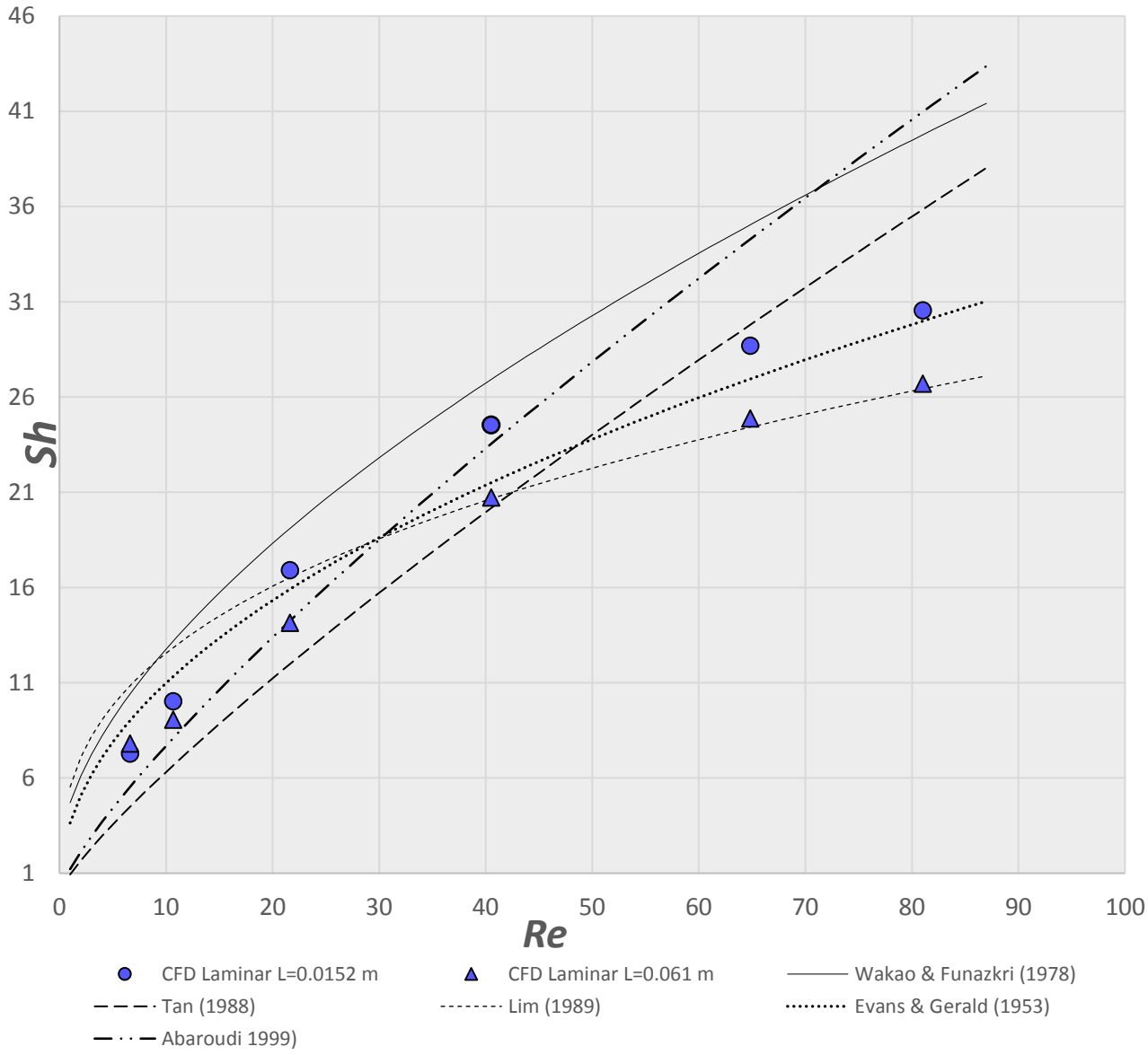

Figure 6-10 Sherwood number vs Reynolds number for particle to fluid mass transfer in packed bed for exit concentration data from 0.0152 m and 0.061 m into the bed

The results are presented in *Figure 6-10*. The simulation data is plotted for concentration data from two exits of the packed bed at 0.0152 m and 0.061 m into the bed. The Sh for 0.0152 m are obtained higher than for 0.061 m. This is due to the higher concentration gradients near the inlet of the packed bed compared to the gradients near the exit of the bed, for a given length. This effect can be observed in *Figure 6-9* and *Figure 6-8*. Mass transfer coefficient from (6-12) quantifies this effect. From the *Figure 6-10* it can be seen that there is increased difference in Sh for 0.0152 m and 0.0609 with the increase in Re, but however for lower Re, the difference between the Sh value is narrowed. This is because for lower Re the concentration reaches equilibrium nearer to the inlet of the packed bed.

The simulation data agrees well with the empirical correlations. All the CFD results fall within the range of the correlations. A good agreement between the numerical results and the correlation predictions of Lim et al., (1989) which is for supercritical conditions at Re~20 with natural convection considerations. Abaroudi et al., (1999) also correlated with supercritical empirical data, which gave good estimate at lower Re but much higher estimate for higher Re. Wakao and Funazkri, (1978) also give high estimates. Tan et al., (1988) predicts much lower mass transfer coefficient for lower Re as the radial and axial dispersion effects are not considered, but much higher for higher Re.

6.5 CONCLUSIONS

CFD proves to be a reliable tool for modelling convective mass transfer in high pressure supercritical conditions for species mixtures in complex geometries. Free/Forced convection situations in the packed bed can be analysed at different locations into the packed bed. The obtained results can be compared qualitatively and quantitatively with previously published data.

Mass transfer from particle surface to bulk fluid in a packed bed is studied. Diffusion of triolein from particle (oil extraction) to bulk fluid mixture of methanol and carbon dioxide is simulated. A geometric model of packed bed is created with randomly packed cylindrical packing particles. A half-length wall segment models have been used. The simulations model was set up for high-pressure and temperature supercritical conditions with tertiary mixture. Flow, and species mathematical models have been solved for the setup.

Mixed convection at high pressure in a packed bed was also analysed. For a supercritical fluid in laminar flow regime, it was possible to study the effects of density gradient, velocity over mass transfer. Large density gradients were observed near the inlet of the packed bed. These density gradients generated hydrodynamic instabilities leading to convection due to natural convection as observed in the Metais-Eckert maps.

Mass balance equation, which takes into consideration the axial dispersion is used for estimating heat transfer coefficients. The influence of velocity over the mass transfer is analysed and plotted. The value of Sh increases almost linearly with the increase in velocity. The simulation data agrees with many empirical correlations for predicting particle-to-fluid heat transfer. The mass transfer coefficients decreased with increase in length into the packed bed.

REFERENCES

Abaroudi, K., Trabelsi, F., Calloud-gabriel, B., Recasens, F., 1999. Mass Transport Enhancement in Modified Supercritical Fluid. Ind. Eng. Chem. Res. 38, 3505–3518. doi:10.1021/ie990105e

Benneker, a. H., Kronberg, a. E., Westerterp, K.R., 1998. Influence of buoyancy forces on the flow of gases through packed beds at elevated pressures. AIChE J. 44, 263–270. doi:10.1002/aic.690440205

Catchpole, O.J., King, M.B., 1994. Measurement and Correlation of Binary Diffusion Coefficient in Near Critical Fluids. Ind. Eng. Chem. Res. 33, 1828–1837. doi:10.1039/C2CP90196J

Danckwerts, P.V., 1953a. Continuous flow systems. Chem. Eng. Sci. 2, 1–13. doi:10.1016/0009-2509(53)80001-1

Danckwerts, P.V., 1953b. Continuos flow systems. Distribution of residense times. Chem. Eng. Sci. 2, 1–13.

Evans, G.C., Gerald, C.F., 1953. Mass transfer from benzoic acid granules to water in fixed and fluidized beds at low Reynolds numbers. Chem. Eng. Prog. 49, 135.

Guardo, A., Coussirat, M., Recasens, F., Larrayoz, M.A., Escaler, X., 2007. CFD studies on particle-to-fluid mass and heat transfer in packed beds: Free convection effects in supercritical fluids. Chem. Eng. Sci. 62, 5503–5511. doi:10.1016/j.ces.2007.02.040

Happel, J., 1958. Viscous flow in multiparticle systems; slow motion of fluids relative to beds of spherical particles. AIChE J. 4, 197–201.

He, C.-H., Yu, Y.-S., 1998. New Equation for Infinite-dilution diffusion coefficients in supercritical and high-temperature liquid solvents. Ind. Eng. Chem Res. 37, 3793–3798. doi:10.1016/S0378-3812(98)00239-8

Kunii, D., Suzuki, M., 1967. Particle-to-fluid heat and mass transfer in packed beds of fine particles. Int. J. Heat Mass Transf. 10, 845–852. doi:10.1016/0017-9310(67)90064-6

Lee, A.K.K., Bulley, N.R., Fattori, M., Meisen, A., 1986. Modelling of supercritical carbon dioxide extraction of canola oilseed in fixed beds. J. Am. Oil Chem. Soc. 63, 921–925. doi:10.1007/BF02540928

Lim, G.-B., Holder, G.D., Shah, Y.T., 1989. Solid-fluid mass transfer in a packed bed under supercritical conditions, in: Supercritical Fluid Science and Technology. ACS Symposium Ser. 406, Washington USA.

Metais, B., Eckert, E.R.G., 1964. Forced, Mixed, and Free Convection Regimes. J. Heat Transfer 86, 295.

Nelson, A., Galloway, R., 1975. Particle-to-Fluid Heat and Mass Transfer in Dense Systems of Fine Particles. Chem. Eng. Sci. 30, 1–6.

Pfeffer, R., 1964. Heat and mass transport in multiparticle systems. Ind. Eng. Chem. Fundam. 380–383. doi:10.1021/i160012a018

Puiggene, J., Larrayoz, M.A., Recasens, F., 1997. Free liquid-to-supercritical fluid mass transfer in packed beds. Chem. Eng. Sci. 52, 195–212.

Ranz, W.E., Marshall, J., 1952. Evaporation from drops PArt II. Chem. Eng. Prog. 48, 173–

180.

Stüber, F., Vazquez, A.M., Larrayoz, M.A., Recasens, F., 1996. Supercritical Fluid Extraction of Packed Beds : External Mass Transfer in Upflow and Downflow Operation. Ind. Eng. Chem. Res. 35, 3618–3628.

Tan, C.-S., Liang, S.-K., Liou, D.-C., 1988. Fluid—solid mass transfer in a supercritical fluid extractor. Chem. Eng. J. 38, 17–22. doi:10.1016/0300-9467(88)80049-2

Wakao, N., Funazkri, T., 1978. Effect of fluid dispersion coefficients on particle-to-fluid mass transfer coefficients in packed beds. Correlation of Sherwood Numbers. Chem. Eng. Sci. 33, 1375–1384. doi:10.1016/0009-2509(78)85120-3

CHAPTER VII

7. REACTIVE FLOW MODELLING OF TRANSESTERIFICATION REACTION

7.1 INTRODUCTION

Alternative to petroleum diesel are being explored because of the limited resources of crude oil, its increasing price and environmental concerns. Transesterification with methanol, ethanol or butanol is found to be a viable option. The diesel produced by this method called biodiesel is attractive because of the renewable nature of the primary source. It is produced by transesterification of triglycerides commonly in plant oils with alcohol producing mono-alkyl esters of long-chain fatty acids (the molecules of biodiesel) and glycerol. This method has been a standard method to produce biodiesel for a long time (Ma and Hanna, 1999; Schwab et al., 1987). The transesterification reaction is typically done with the help of a catalyst. The use of solid catalyst over liquid alkali or acid catalyst is advantageous for the reusability of the solid catalysts. This process has long been in development and the fuel produced is marketed in many countries, however it is relatively time consuming and needs purification of the product.

Because of the two phase nature of the oil/alcohol mixture, vigorous stirring is needed for the reaction to proceed, and also has the disadvantages of soap formation and reduces catalyst effectiveness. The use of methanol and CO_2 in supercritical state solves the two phase state methanol/oil mixture, due to decrease in dielectric constant of methanol in supercritical state (Kusdiana and Saka, 2001). And are able to catalyse both transesterification and esterification reactions.

However, the use of supercritical alcohols has the disadvantage of high cost of the apparatus due to the use of high temperature and pressure. The addition of co-solvent has been effective in reducing the required operating conditions for the reaction. Supercritical CO_2 has been found to be an effective as co-solvent with methanol in the transesterification reaction.

Packed beds have diverse applications in reaction, separation and purification units. A randomly packed bed is advantageous over structured packing as it reduces the occurrence of channelling. The aspect ratios (tube-particle diameter ratios) above 10 plug flow assumption can be made.

Computational fluid dynamics is a well-developed tool for simulating fluid flow. It is able to simulate even complex flow fields. With increase in the capabilities of computer hardware and their availability, detailed simulations of flow operations is increasingly becoming viable. Computational fluid dynamics of reactive flow is done by coupling the chemical reactions with

species conservation equations and solved with boundary conditions. However, the development of detailed models for multiple chemical reactions is challenging due to their non-linear coupling, large number of species conservation equations, and various reaction timescales due to complicated reaction networks. Heterogeneity, multi-phase reactions add to the challenge of defining detailed models.

7.1.1 Reactive Flow Modelling

Computational fluid dynamics has been widely applied model reactive flow in packed beds. A simpler approach is to model at isothermal conditions. This has shown good agreement with experimental results. (Yuen et al., 2003, Freund et al., 2003. Zimmermann and Taghipour, 2005) modelled reaction kinetics for fluidized bed reactor and compared with experimental data. Dixon et al., (2007) has presented simulations for steam reforming, including effects of temperature, species diffusion and reaction within the particle, and in flow. Guardo et al., (2007) has modelled diffusional effects for supercritical hydrogenation reaction. (Portha et al., 2012) have modelled the transesterification reaction in a modular reactor. (Wehinger et al., 2015) have modelled with detailed reaction mechanism of methane reforming in a packed bed reactor.

The objective of the current work is to perform a detailed modelling with temperature, species diffusion and reaction kinetics of a supercritical transesterification reaction. The problem was setup with model of experiments done in this research group (Maçaira et al., 2011). Simulations with varying temperature, and space-time have been investigated for the reaction modelling. The kinetics of the reaction were also determined for the single step reaction kinetics. The CFD results are compared with the experimental results obtained.

7.1.2 Transesterification Kinetics

Biodiesel has become attractive because of its renewable feedstock and its environmental benefits. It has lower carbon footprint than petroleum derived diesel. As a renewable fuel, biodiesel has the potential of becoming an alternative to petroleum diesel.

The most common method to produce biodiesel is through catalysed transesterification reaction. This reaction occurs with tri-glycerides which are main components of vegetable oils or animal fats, react with methanol producing fatty acid methyl esters (biodiesel) and glycerol as the bi-product.

Freedman et al., (1986) studied transesterification with different alcohols, molar ratio of alcohol to oil, catalyst type and reaction temperature. Their objective was to determine their effect on kinetic order, reaction rates, and energies of activation. Hence optimizing these parameters is important for required yield. Methanol was often used because of its economic advantage over ethanol. (Ma and Hanna, 1999).

The stoichiometry requires three moles of alcohol for one mole of oil (triolein). Higher molar ratios result in greater ester conversion in a shorter time. High alcohol to oil molar ratio (20 to 30) is advantageous as the reaction follows a (pseudo) first order kinetics. Hence the kinetics is dependent only on the concentration of oil (triolein). Freedman et al., (1986) calls this pseudo first order.

Transesterification can be catalysed by both homogeneous and heterogeneous catalysts, Alkali catalysts have several problems in transesterification: it is energy intensive, recovery of glycerol is difficult, alkaline waste water retains fatty acids and this water interfering with reaction (Noureddini et al., 2005). Acid catalysed transesterification is advantageous over alkali catalysts when raw material oil has relatively high free fatty acid content. Heterogeneous (generally solid) acid catalysts are helpful as they are able to catalyse both transesterification and esterification, which becomes necessary when feedstock quality is low (Lotero et al., 2005). The solid catalysts can also be reused and are easier to separate. They also avoid undesired saponification reactions and are less corrosive. (Ma and Hanna, 1999)

The use of methanol in supercritical state solves the two phase state methanol/oil mixture, due to decrease in dielectric constant of methanol in supercritical state. Having the system in supercritical conditions, makes it single phase accelerating the reaction rate as there is no interphase mass transfer limiting the reaction rate. (Pinnarat and Savage, 2008).

Due to the severe reaction conditions, the operating costs are high making this process less suitable for industrial production. To overcome this disadvantage, the use of supercritical co-solvents is found useful in lowering the high operating conditions required for supercritical methanol. Co-solvents such as carbon dioxide, hexane, and propane, ionic liquids are used (Demirbaş, 2009; Varma et al., 2010). The addition of co-solvent CO_2 increased the rate of the supercritical alcohols transesterification, making it possible to obtain higher biodiesel yields at mild temperature conditions.

Transesterification of triglyceride with methanol, in the presence of acid catalyst, yields esters of fatty acids and glycerol.

Freedman et al.,(1986) presented a reaction model for transesterification: The overall reaction,

$$TG + 3ROH \xrightarrow{k} G + 3E \quad (7\text{-}1)$$

The reverse reaction in the overall reaction scheme can be ignored and a pseudo-first-order reaction mechanism can be used with high methanol to oil molar ratio. Effectively ignoring the reverse reaction, the rate equation for the first-order reaction can be modelled as:

$$-\frac{d[TG]}{dt} = k[TG] \quad (7\text{-}2)$$

The consecutive reversible reaction steps are in equation below with rate constants k_1 to k_6. The triglyceride is converted stepwise to diglyceride, then monoglyceride, and finally glycerol. A mole of ester is released in each step. Although the reactions are reversible, equilibrium is towards the production of fatty acid esters and glycerol at the maintained conditions. For transesterification of soybean oil studied by Freedman et al., (1986) for acid or alkali catalysis, the forward reaction followed pseudo-first-order kinetics when alcohol to oil molar ratio was 30:1. However forward reaction followed consecutive second-order kinetics for the ratio 6:1. The rate constants increased with increase in the amount of catalyst used.

$$TG + A \underset{k_2}{\overset{k_1}{\rightleftharpoons}} DG + E \quad (7\text{-}3)$$

$$DG + A \underset{k_4}{\overset{k_3}{\rightleftharpoons}} MG + E \quad (7\text{-}4)$$

$$MG + A \underset{k_6}{\overset{k_5}{\rightleftharpoons}} GL + E \quad (7\text{-}5)$$

When the three-step reversible reactions scheme is considered, the transesterification follows a second-order kinetics. The species balance equations (rate equations) characterizing the second order kinetics of the three step reversible reactions are as follows: (Maçaira et al., 2011).

$$\frac{d[TG]}{dt} = -k_1[TG][A] + k_2[DG][E] \quad (7\text{-}6)$$

$$\frac{d[DG]}{dt} = k_1[TG][A] - k_2[DG][E] - k_3[DG][A] + k_4[MG][E] \quad (7\text{-}7)$$

$$\frac{d[MG]}{dt} = k_3[DG][A] - k_4[MG][E] - k_5[MG][A] + k_6[GL][E] \quad (7\text{-}8)$$

$$\frac{d[GL]}{dt} = k_5[MG][A] - k_6[GL][E] \quad (7\text{-}9)$$

$$\frac{d[E]}{dt} = k_1[TG][A] - k_2[DG][E] + k_3[DG][A] + k_4[MG][E] + k_5[MG][A] - k_6[GL][E] \quad (7\text{-}10)$$

$$\frac{d[A]}{dt} = \frac{-d[E]}{dt} \quad (7\text{-}11)$$

Where k_1 to k_6 are reaction rate constants; [*TG*], [*DG*]. [*MG*], [*A*], and [*E*] are molar concentrations (mol/L) of TG, DG, MG, methanol, and esters respectively. The concentration change data for each component can be obtained from experiments or corresponding simulations, and the equations can be fitted to obtain the rate constants.

From the rate constants obtained at different temperatures, for each transesterification step, activation energies for the corresponding reactions can be estimated from Arrhenius equation

$$k = Ae^{-E_a/RT} \tag{7-12}$$

where *A* is the Arrhenius pre factor,

E_a is the activation energy and

R is gas constant.

Taking logarithm on both sides of the Equation (7-12),

$$\ln(k) = -\frac{E_a}{RT} + \ln(a) \tag{7-13}$$

This equation is linear with respect to *1/T*, and the plot of *ln(k)* vs. *1/T* produces a straight line of slope $-E_a/R$.

The reaction rate for the packed bed reactor, mole balance (with respect to catalyst weight) is derived as

$$F_{A0}\frac{dX}{dW} = -r'_A \tag{7-14}$$

where, F_{A0} is rate of flow of A into the system

X is conversion

W is weight of catalyst

This equation is used for the calculation of rate constant with conversion and catalyst weight data.

7.1.2.1 Supercritical single phase

In a transesterification process, the reactants are not miscible at ambient temperature and form two layers. The phase separation depends on the mixture composition, temperature and pressure. Hence, supercritical single phase can be achieved by having sufficiently high

temperature and pressure. The critical component data for estimating temperature and pressure required for maintaining supercritical single phase mixture are available in literature.

Components	**Molecular weight (kg/k.mol)**	**Critical temperature T_c (K)**	**Critical pressure P_c (bar)**
Methanol	32	513	80
CO_2	44	31	74
Triolein	884	705	3.3

Table 7-1 Critical data for pure components (Maçaira et al., 2011; Poling and Prausnitz, 2001)

The critical point for the system (CO_2/ methanol) + triolein was determined by Maçaira et al., (2011) at different temperatures, estimating the k_{ij} values from the ratio of fugacity coefficients obtained with PR-EOS. Based on the estimation, the mixture (CO_2/methanol) + triolein exhibits a convergence pressure around 200 bar and temperature 150°C. Based on these estimations, the pressure was kept constant at 250 bar, to ensure supercritical single phase condition.

7.2 SIMULATION MODEL SETUP

A full length wall-segment geometrical model (WS) was developed and used for study of reactive flow, which is based on the reactor used for high pressure transesterification reaction experiments. The reactor is a titanium fixed bed reactor, with length 152mm and diameter of 17.5 mm. The geometry is shown in

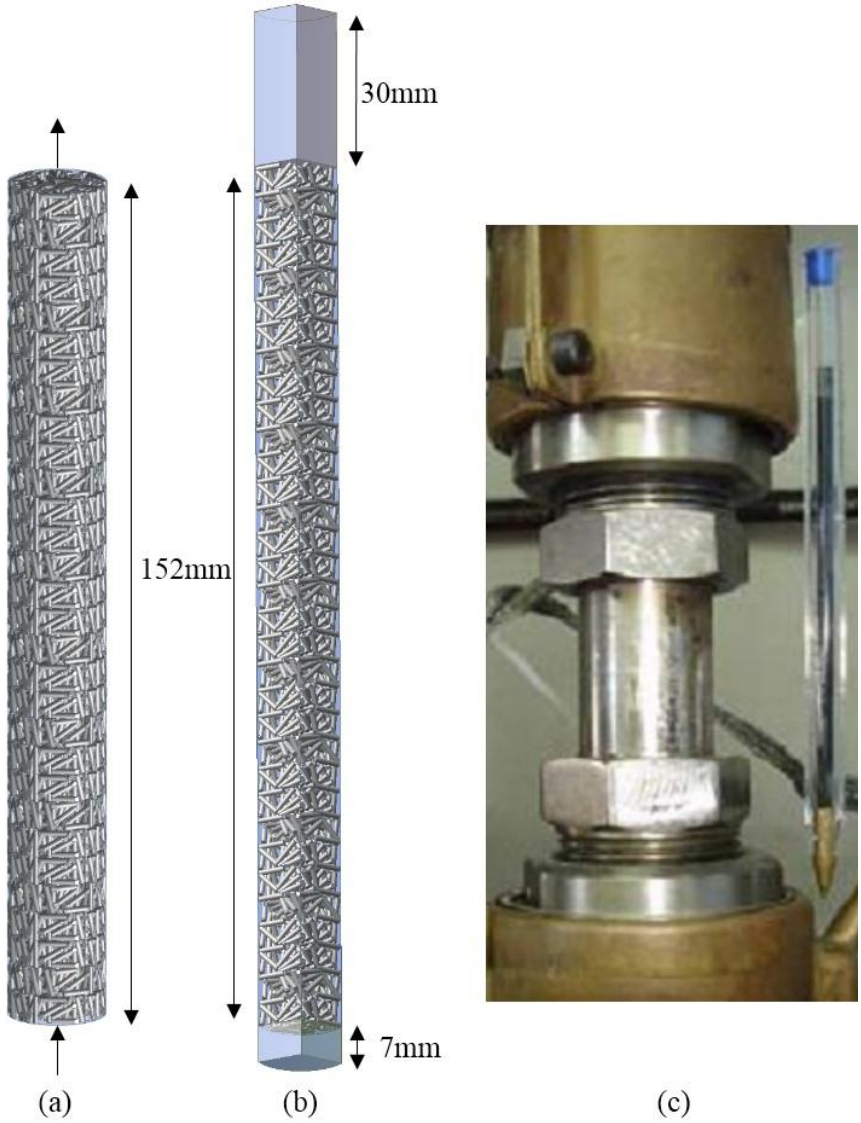

Figure 7-1 Geometrical model of packed bed reactor (a) Packed bed model with inlet from below, gravity opposing flow (b) Full length 120-degree wall-segment (WS) model with extensions. (c) Titanium packed bed reactor used for high pressure experiments.

The simulations were done for cases corresponding to the experiments run in our supercritical fluid research group, which were based on phase equilibrium consideration, the temperature was varied 180° and 205°C and the space time from 0.5 to 4 min. The total system pressure was kept constant at 250 bar. The pressure of 250 bar was chosen as the estimated critical pressure for 99% methanol/CO_2 (25 wt.% methanol in CO_2) and 1% triolein for temperatures up to 205° was found to be up to 245 bar. The maximum biodiesel yield was found to be achieved at temperature of 205°C but not at a maximum value of space time.

Boundary conditions, methods	Value
Fluids in	CO_2 + CH_3OH + $C_{57}H_{104}O_6$
Mass fraction ratio methanol: oil	0.19589: 0.21685 (molar ratio 25:1)
Fluid temperature at inlet	478.15, 453.15 K
Wall temperature	Zero heat flux
	For 453 K for three step kinetics, 120 and 210s
Pressure	25000000 Pa
Fluid velocity at the inlet	0.0006 – 0.004 m/s (Of space-time 30s to 210s)
Shear condition on wall, particle surface	No slip
Discretization	First order
Models solved	Flow, energy, species
Flow model	Laminar

Table 7-2 Boundary conditions for the analysed cases.

The methanol to oil molar ratio was 25:1 and catalyst mass was 9g for the experiments where as for the simulations tube geometry was filled randomly with cylindrical catalysts of length 5mm and diameter 1mm with void fraction of about 0.6.

Simulation Run	Temperature (°C)	Space time (min)
1	205	0.5
2	205	1.0
3	205	2.0
4	205	3.8
5	180	0.5
6	180	1.0
7	180	2.0
8	180	3.8

Table 7-3 Simulation runs for transesterification reaction. These were run for both one-step irreversible and three-step reversible reaction kinetics

For the one-step irreversible reaction scheme, first order kinetics were assumed as given by the Arrhenius Equation (7-2). The kinetic data used in the simulations is obtained from published experimental data (Maçaira et al., 2011) of the work done at our research group lab is given Table 7-4.

Temperature (K)	Space time (min)	Activation Energy	Rate constant (1/s)
478	0.5	1.28E+08	0.4392
478	1.0	1.28E+08	0.3289
478	2.0	1.28E+08	0.2245
478	3.9	1.28E+08	0.0332
453	0.5	1.28E+08	0.0447
453	1.0	1.28E+08	0.0181
453	2.0	1.28E+08	0.0257
453	3.9	1.28E+08	0.0332

Table 7-4 Kinetic data for one-step reaction kinetics data (Maçaira et al., 2011)

7.3 RESULTS AND DISCUSSION

7.3.1 Effect of inlet flow rate, temperature and axial length

The simulations mentioned in Table 7-3 were run using one-step kinetics and three step kinetics. To evaluate use of CFD in studying the influence of operating conditions for transesterification reaction, the simulations were run with varying inlet flow rates and for two different temperatures. The methanol to oil ratio is maintained constant for all the simulation runs. The operating pressure is also kept constant at 250 bar.

The FAME yield for varying inlet flow rates is shown in *Figure 7-2*. This data is for the full length of the packed bed model. The data is compared against experiments conducted in our research group. With high conversion rates for the simulations, a jump in yield for 30s can be seen, while for experiment at 453 K, the data shows, high yield only for space-time of 60s and above. The yield reached maximum for about 60 sec space time flow rate for 478 K for the simulations and the experiments, but for 453 K experiments the yield reached maximum for above 60 sec space time The trend of higher yield for lower temperature is followed in simulation data.

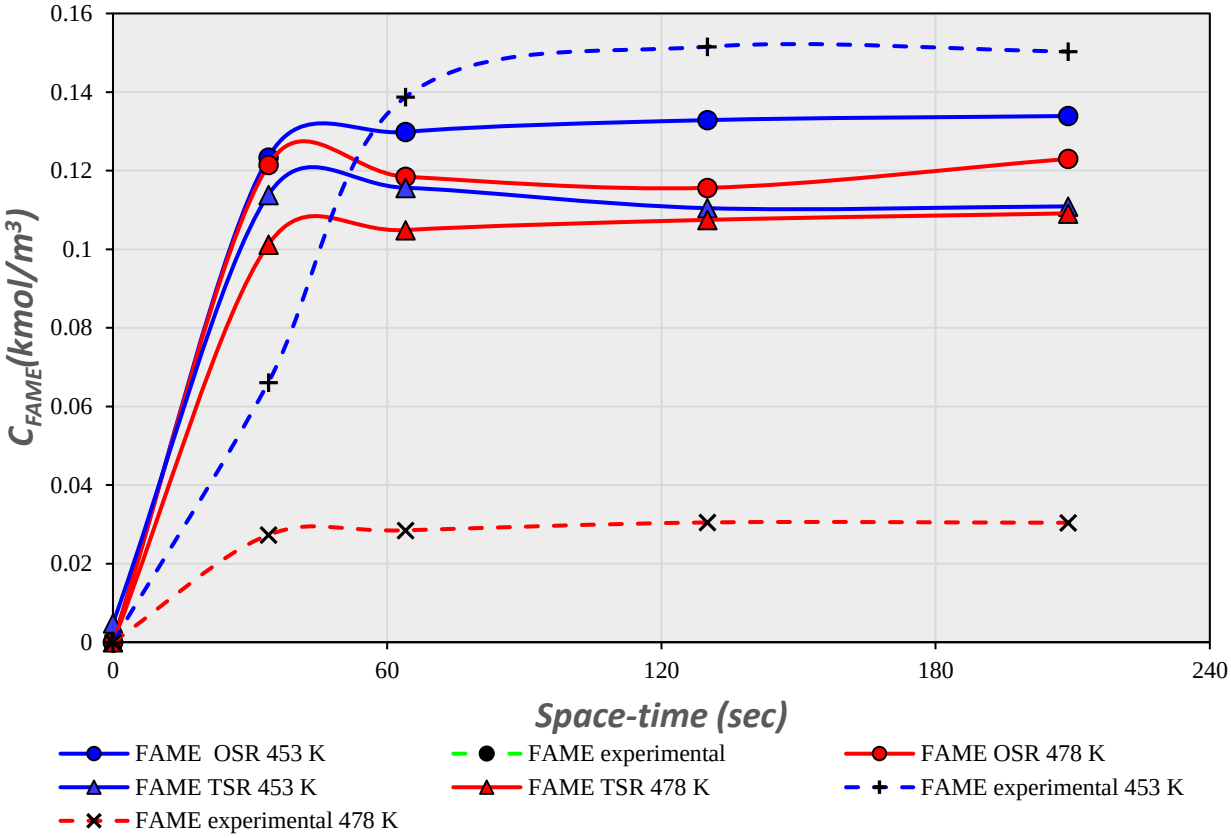

Figure 7-2 FAME yield for with varying flow rates

The exit concentration data for reaction species triolein, FAMEs, and glycerol for full-length bed is shown in *Figure 7-3*. Higher yield is observed for experiments for higher triolein inlet concentration, except for the higher flow rate, 30sec space-time, as the conversion is obtained for less space -time in simulations.

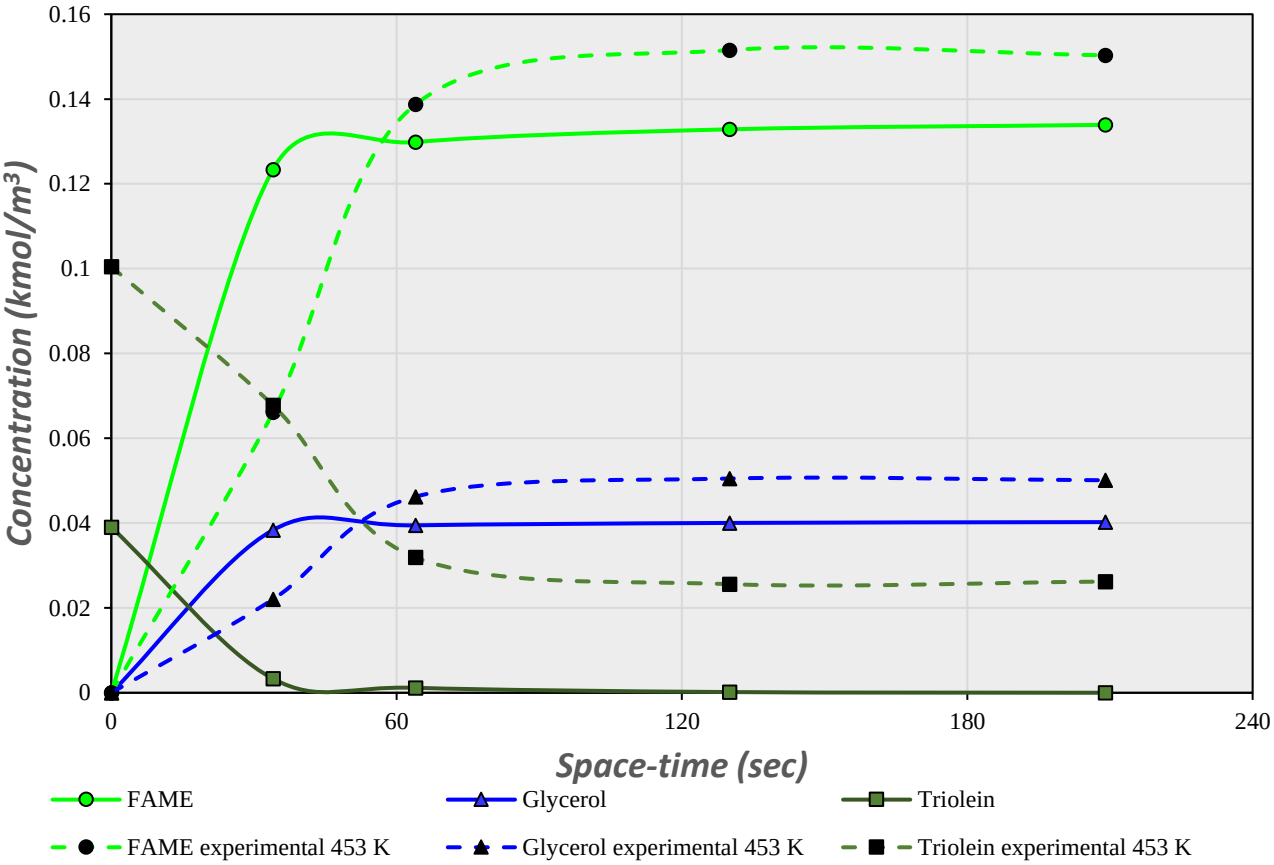

Figure 7-3 Reaction species concentration for one-step kinetics simulations at 453 K

The FAME concentration contours for the 453K temperature and one-step kinetics are shown in Figure 7-4. As can be seen from figure the FAME yield is high for low flow rates (or high space-times). The figure also illustrates the effect of packed bed length or the amount of catalyst on the FAME yield. The increase yield with the increase in the length. High amounts of FAME on the catalyst surface can be noticed.

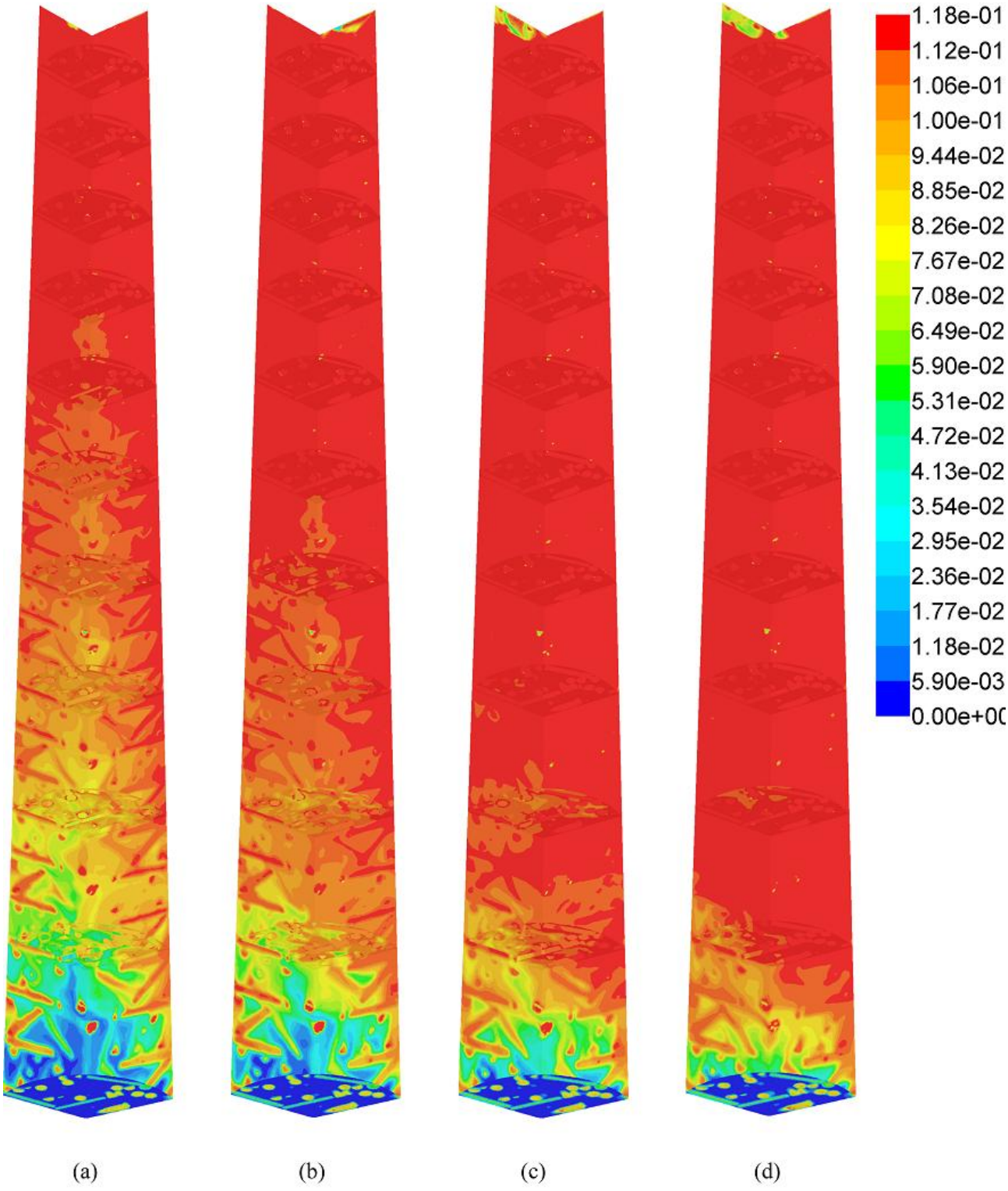

Figure 7-4 Concentration contours of fatty acid methyl esters on radial and axial planes in packed bed for one-step reaction kinetics at 453K for space-times (a)30sec (b)60sec (c)130sec and (d)210 sec

The concentration of the FAME formation with flow rate or in this case space-time is shown in Figure 7-5 for one-step kinetics simulations and for three-step kinetics simulations. The simulation data is for one-tenth length reactor model. The concentration of FAMEs for one-step

kinetics can be seen to be slightly higher than that of three-step kinetics. This agrees with that fact that transesterification of oils into methyl esters is a three step series of reversible reactions with intermediates monoglyceride and diglyceride formation. With further into the rector model length, the concentration of FAME reaches maximum and the triolein concentration to a minimum and both the kinetic models arrive at steady concentrations as observed in Figure 7-3 which is for full length model.

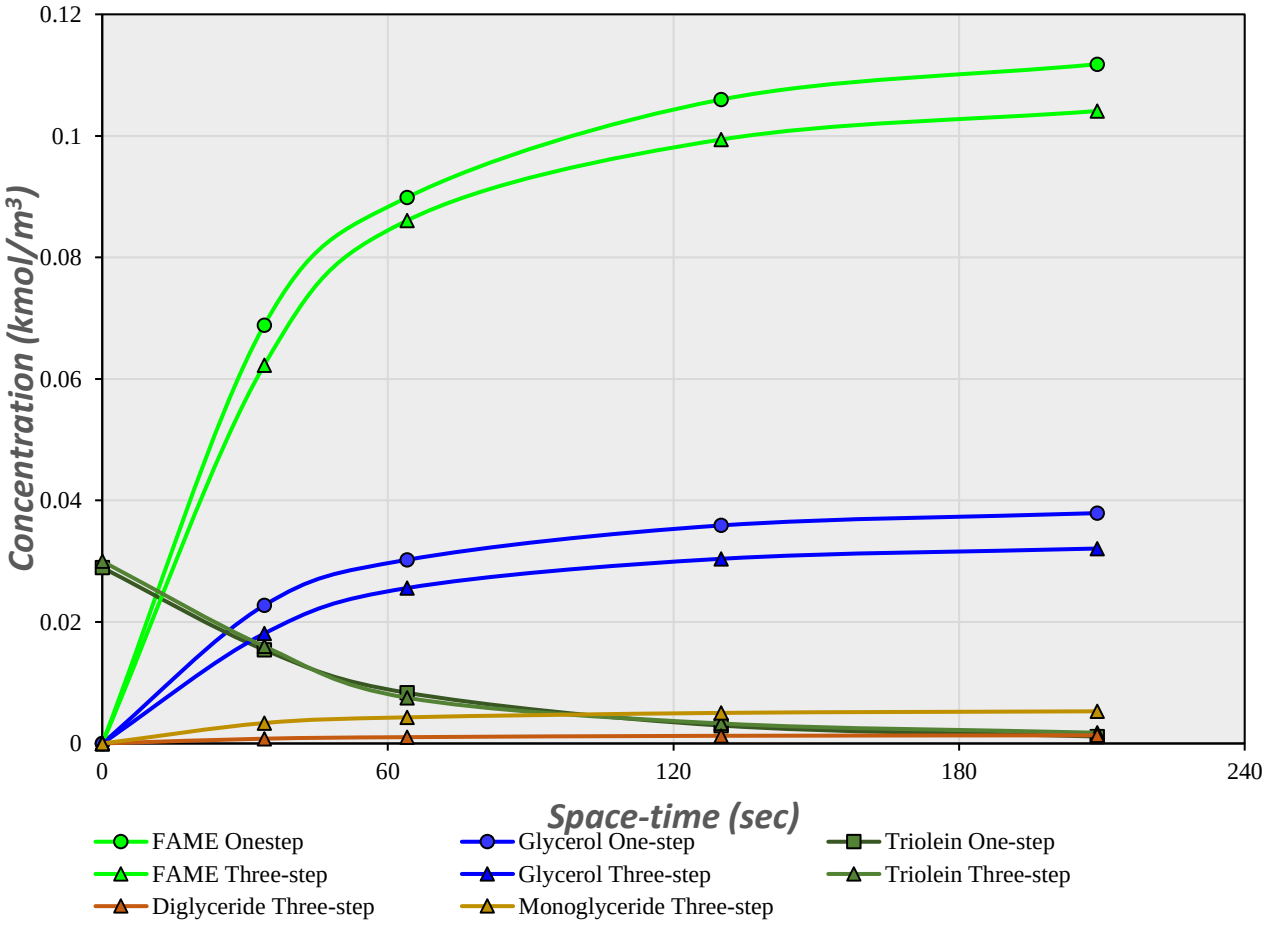

Figure 7-5 Concentration of reaction species with space-time for three-step kinetics

Concentration profiles of reaction species are shown in Figure 7-6. The concentration of FAMEs reaches its maximum at about 0.06m into the packed bed. The concentration gradients are highest near the bed inlet.

In points for the concentration of FAME in Figure 7-6, the data points are from axial plane, markers are added to see the actual points. The actual profile of FAME concentration for this case can be seen in Figure 7-9(b). As the concentrations near the inlet to the bed are not developed, the trends in this regions may not be as smooth compared to further into the bed.

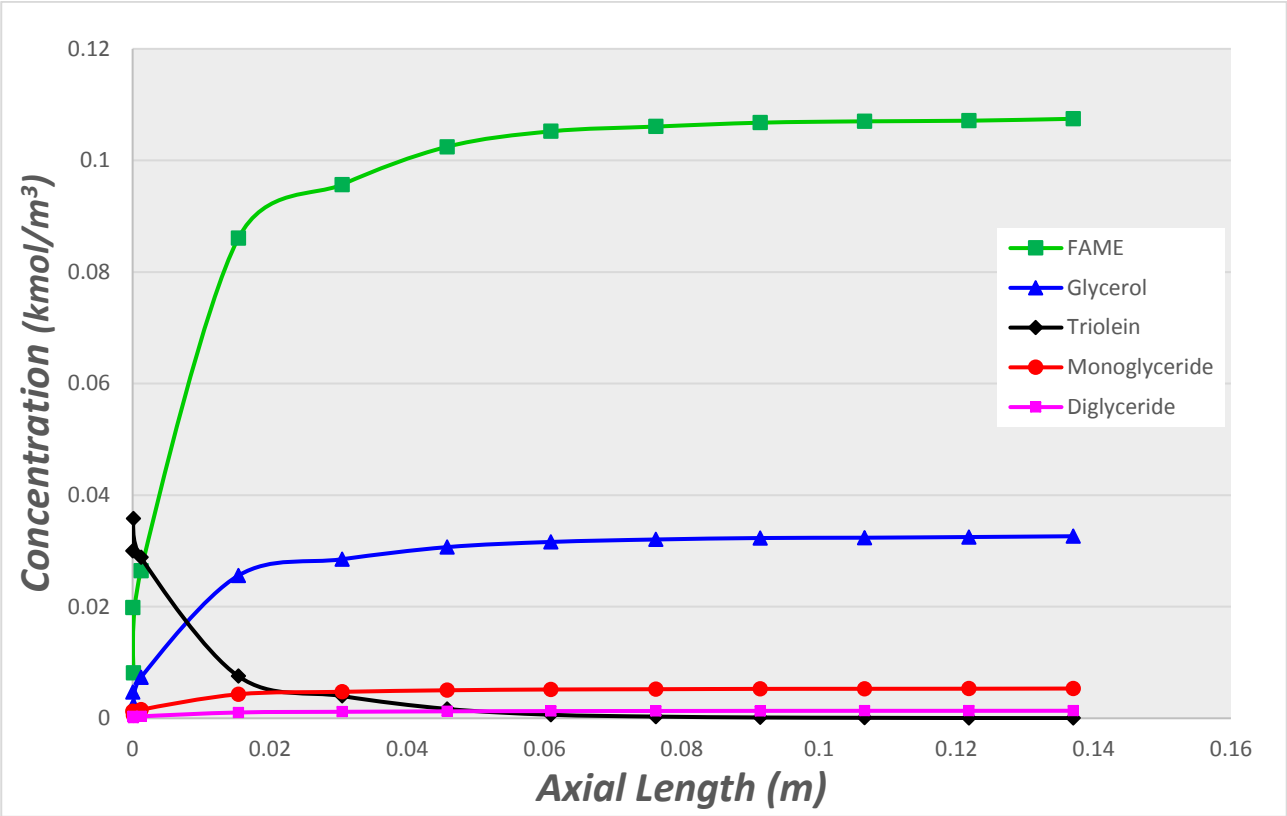

Figure 7-6 Concentrations of reaction species on radial planes in axial direction for three step kinetics and 60sec space-time at 453 K

The effect of radial length on triolein concentration for different space-times is shown in *Figure 7-7* for 478 K and one-step kinetics. The triolein concentration is decreasing at a higher rate with the increase in space-time for the initial length of the reactor.

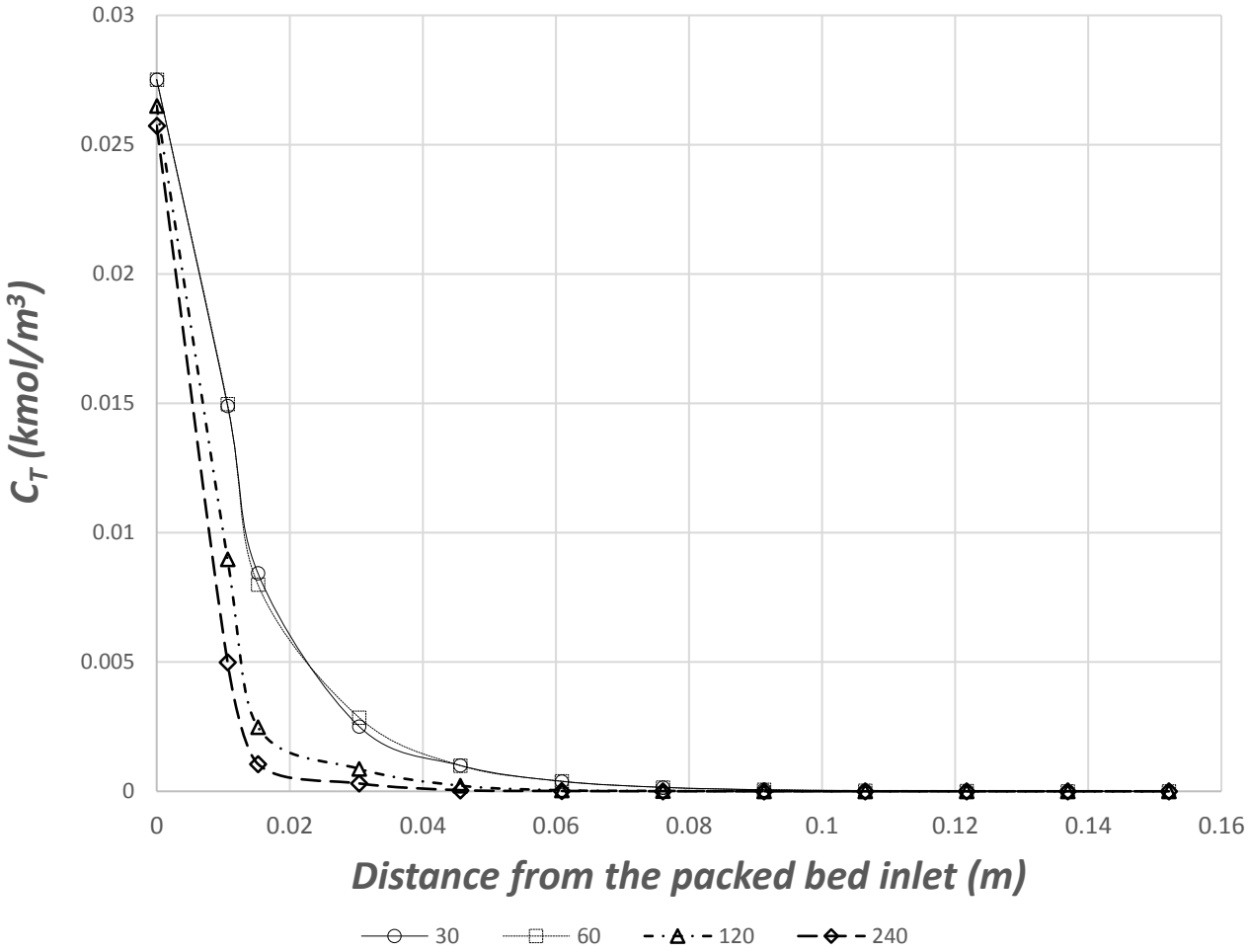

Figure 7-7 Triolein concentration for different space times along axial length for one-step kinetic

The corresponding concentration contours of triolein for 453 K and three-step kinetics are shown in *Figure 7-8*. The concentration contours of FAME are shown in *Figure 7-9*. It can be seen that the higher flow rates require longer reactor length to achieve maximum FAME yields. The very concentration of triolein on catalysts surface can be seen in figure.

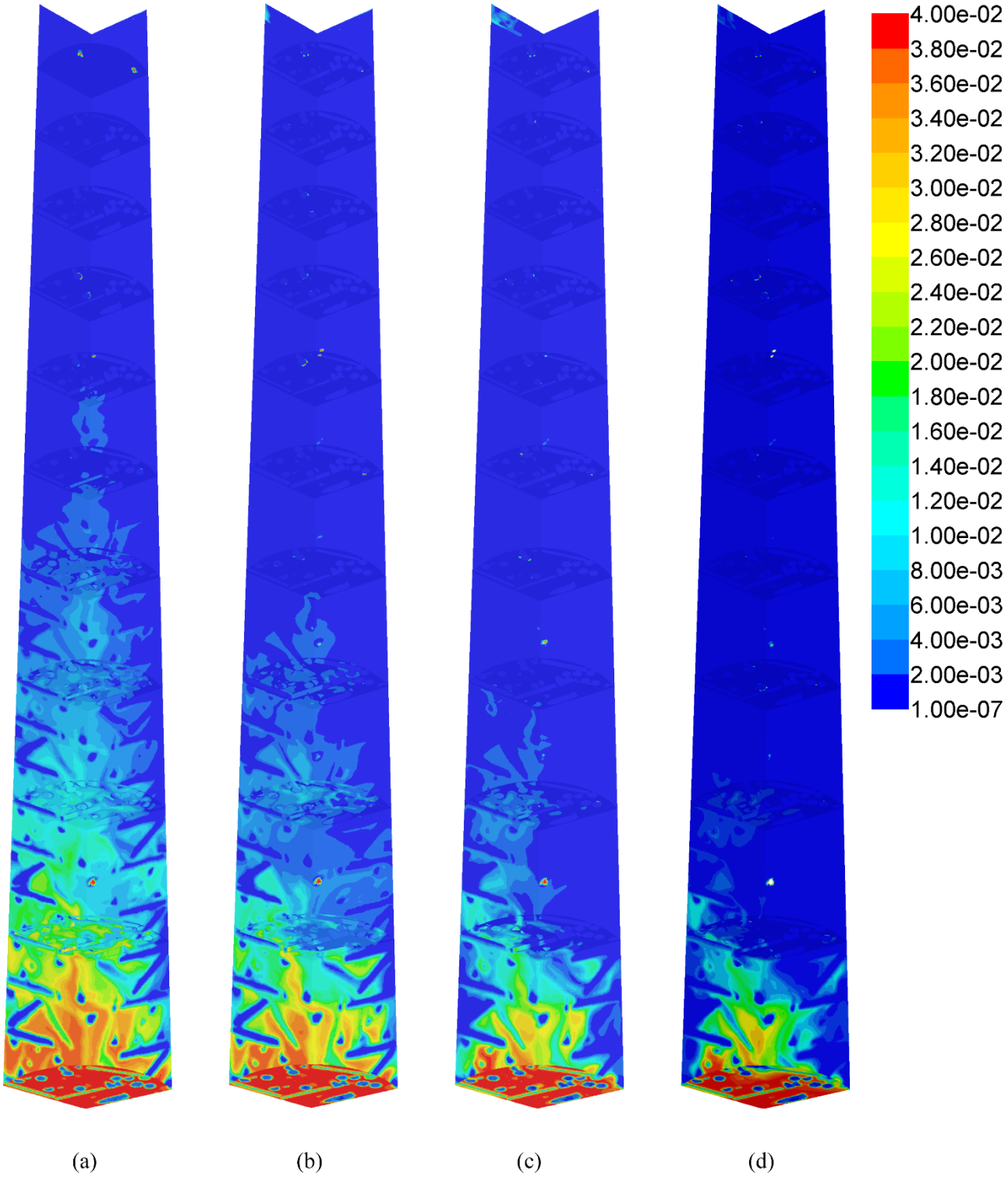

Figure 7-8 Concentration contours of triolein on radial and axial planes in packed bed for three-step reaction kinetics at 453K for space-times (a)30sec (b)60sec (c)130sec and (d)210 sec

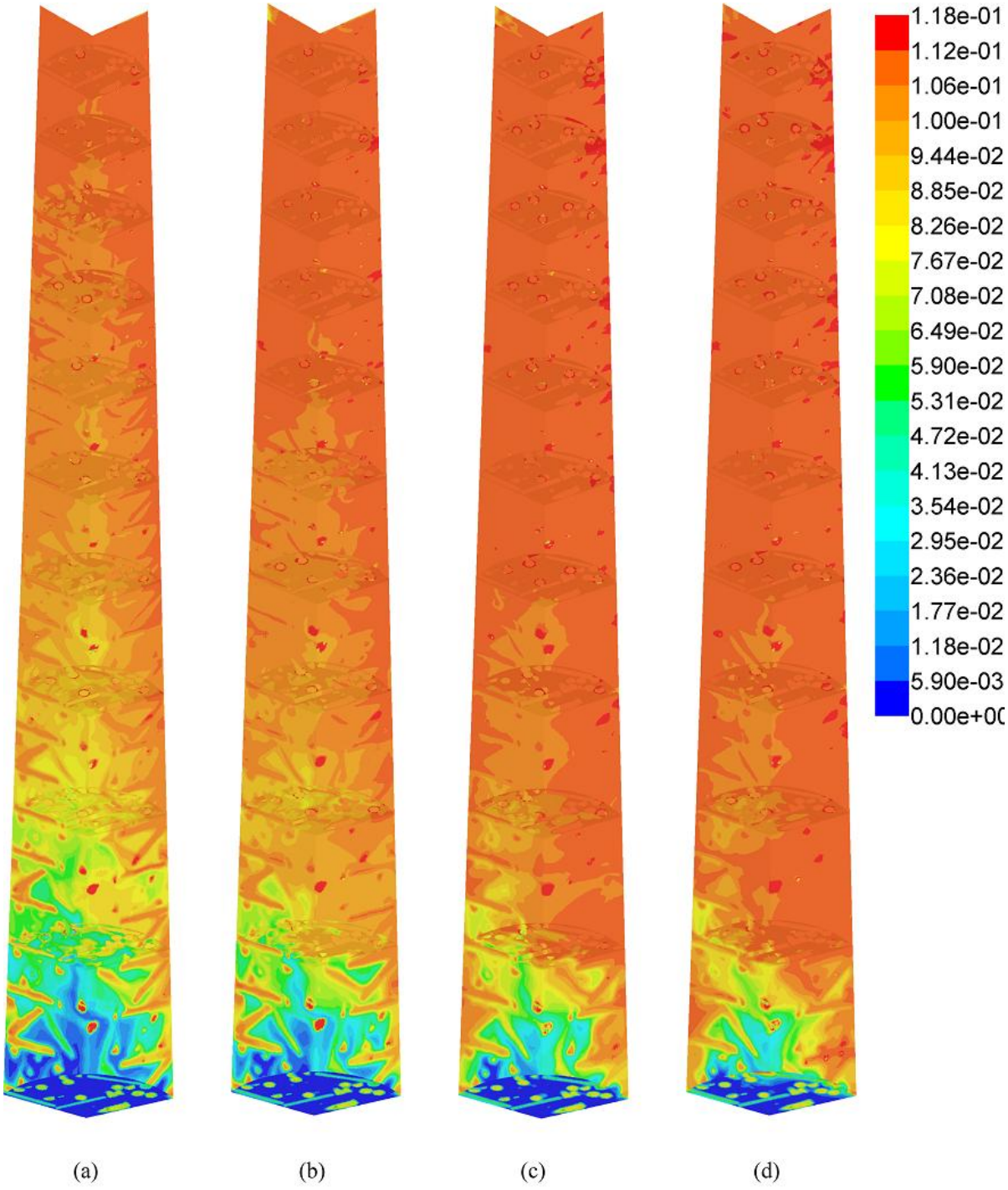

Figure 7-9 Concentration contours of fatty acid methyl esters on radial and axial planes in packed bed for three-step reaction kinetics at 453K for space-times (a)30sec (b)60sec (c)130sec and (d)210 sec

The local axial concentration profiles of FAME are shown in *Figure 7-10* for 453 K and in *Figure 7-11* for 478 K. At lengths nearer to the inlet, the concentration is fluctuating due to the high concentration of FAME on the catalyst surface, while it is lower in the other regions on the axial line where catalyst influence is less. This high concentration of FAME on particle surface near the inlet can also be seen in FAME concentration contours in *Figure 7-9*. These concentration variations, cause high density gradients near the reactor inlet. For high pressure

simulations the presence of large density gradients cause numerical instability in the results and may result in convergence problems solving the momentum, continuity and pressure equations (Lakshminarayana, 1991). This numerical instability on the axial line near the entrance of the bed can be observed in Figure 7-10 and Figure 7-11. In Figure 7-11, the data for 30s space-time is not included, although within range, it appeared be erroneously fluctuating.

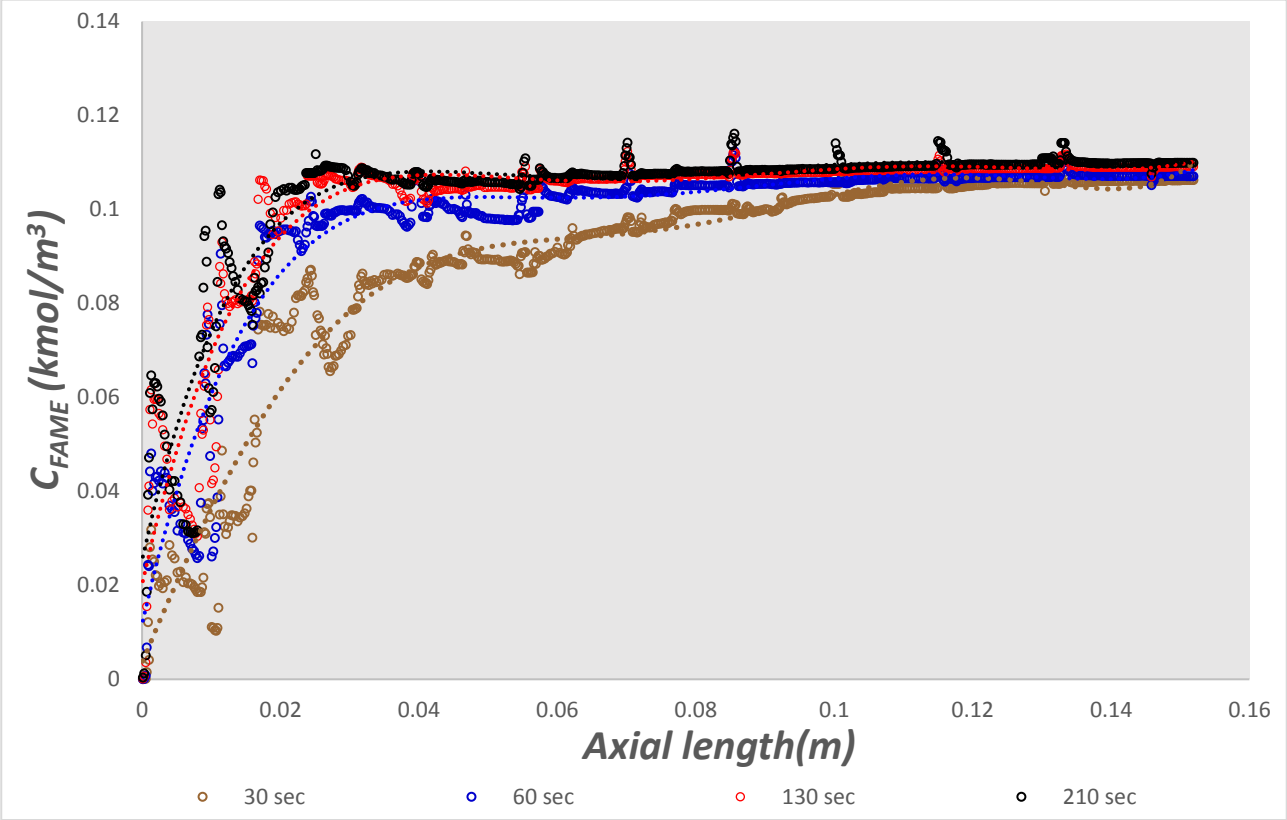

Figure 7-10 Local values of FAME concentration along axial line in reactor for three-step kinetics and 453 K

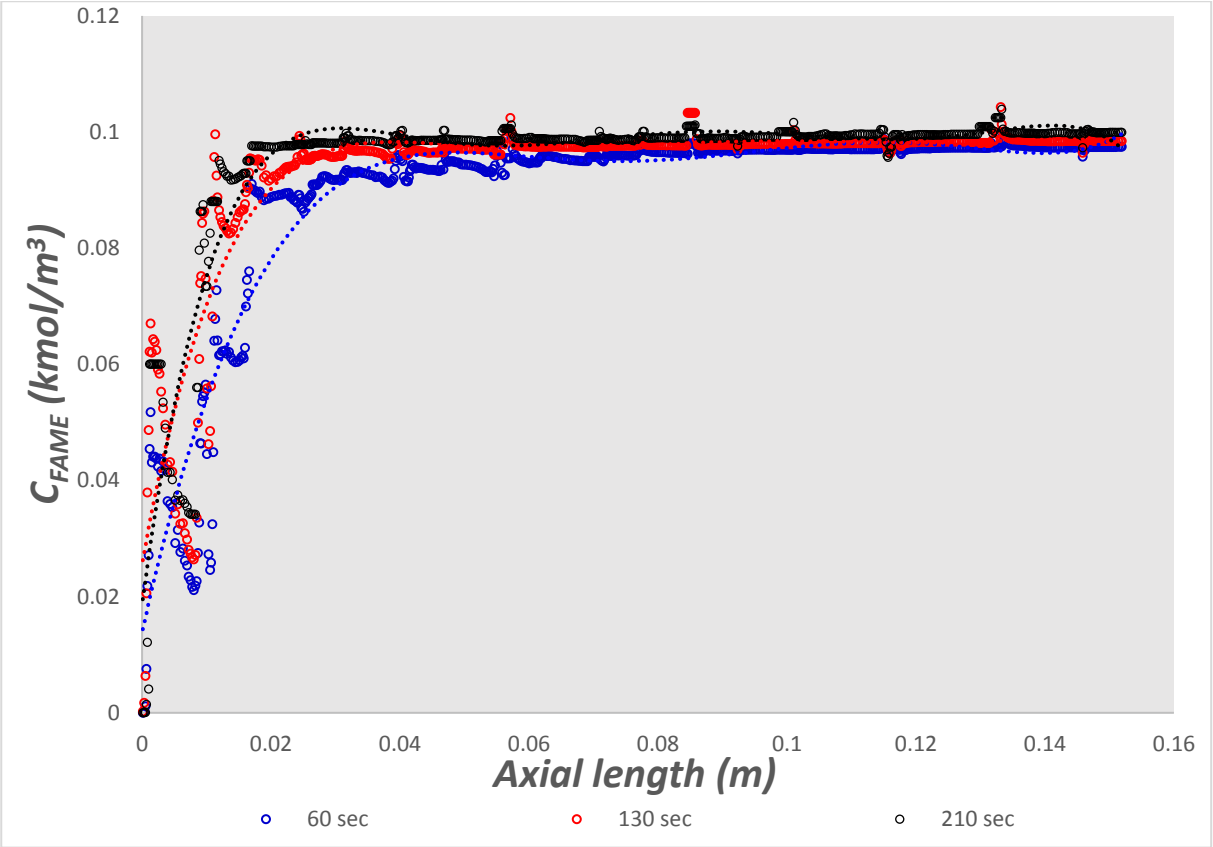

Figure 7-11 Local values FAME concentration along axial line in reactor for three-step kinetics and 478 K

7.3.2 Temperature profiles

Temperature contours for the cases of 453 K inlet temperature and 478 K inlet temperature are shown in *Figure 7-12*. In these cases, the reactor walls are maintained at zero heat flux boundary condition, assuming perfectly insulated adiabatic wall. For 453 K inlet temperature, the temperature in the reactor is increased 8° up to 461 K and for 478 K inlet temperature the temperature increased 10° up to 488 K. This increase in temperature is due to slightly exothermic nature of the reaction.

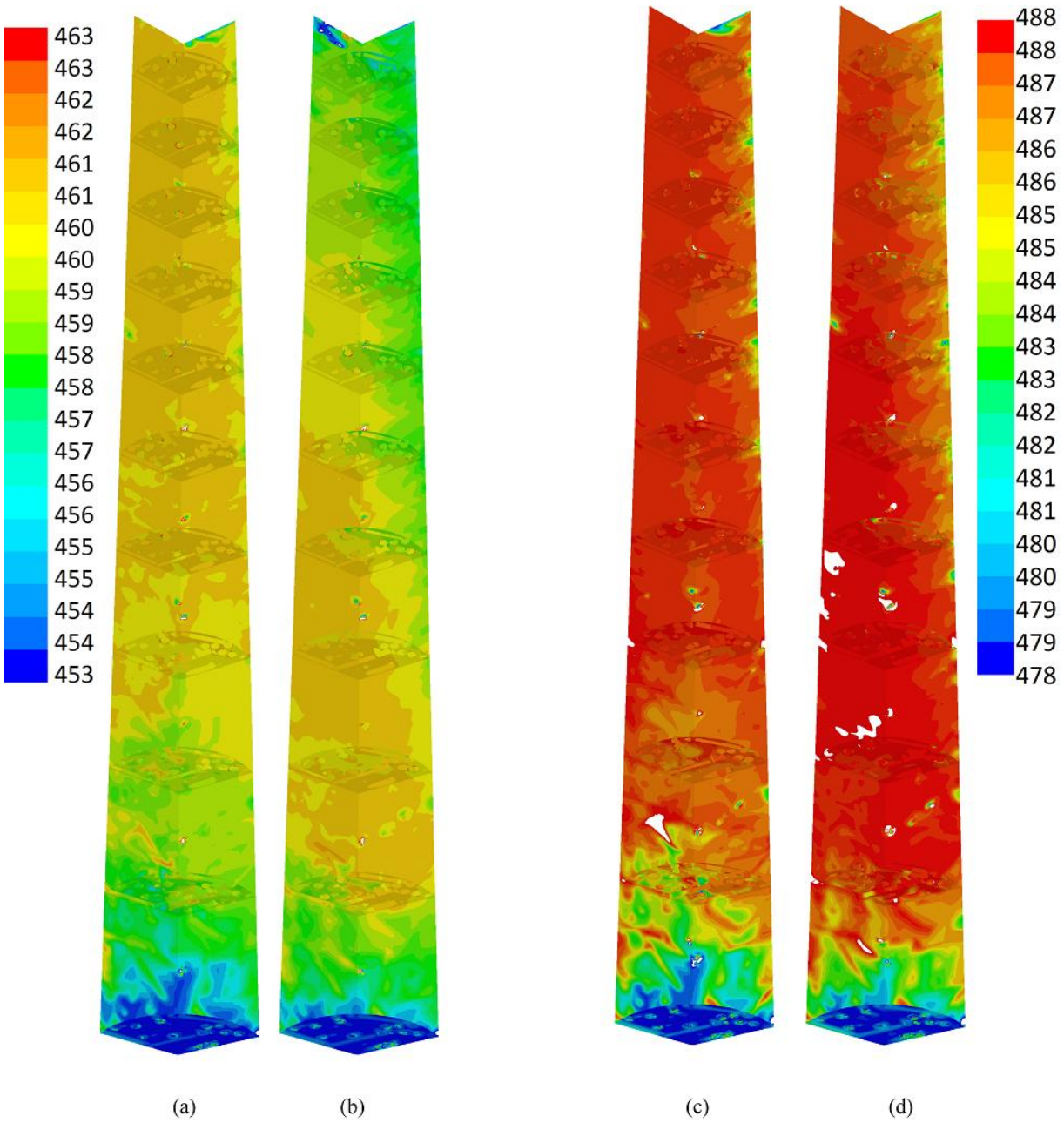

Figure 7-12 Temperature (K) contours on radial and axial planes in packed bed for (a) one-step reaction kinetics at inlet temperature 453K for space-times (a)60sec (b)120sec and for three-step reaction kinetics at inlet temperature 478 K for space-times (c)60 sec and (d)120 sec

Two cases of simulations of three-step kinetics and 453 K for 120 sec and 210 sec space-time are performed with constant wall temperature of 453 K are shown in *Figure 7-13* (c) and (d). This has put the average temperature in the reactor at 455 K, while for a same case with one-step kinetics, and zero wall heat flux boundary condition, the average temperature in the reactor is 459 K. This variation of temperature has slight effect in the yield of FAME, which can be seen in *Figure 7-2*, where the FAME concentration decreased from 0.112kmol/m^3 for 60s to 0.109kmol/m^3 for 120s, while for the same case in one-step kinetics in which zero heat flux

boundary condition on the wall is used, the concentration increased from 0.129kmol/m^3 to 0.132kmol/m^3

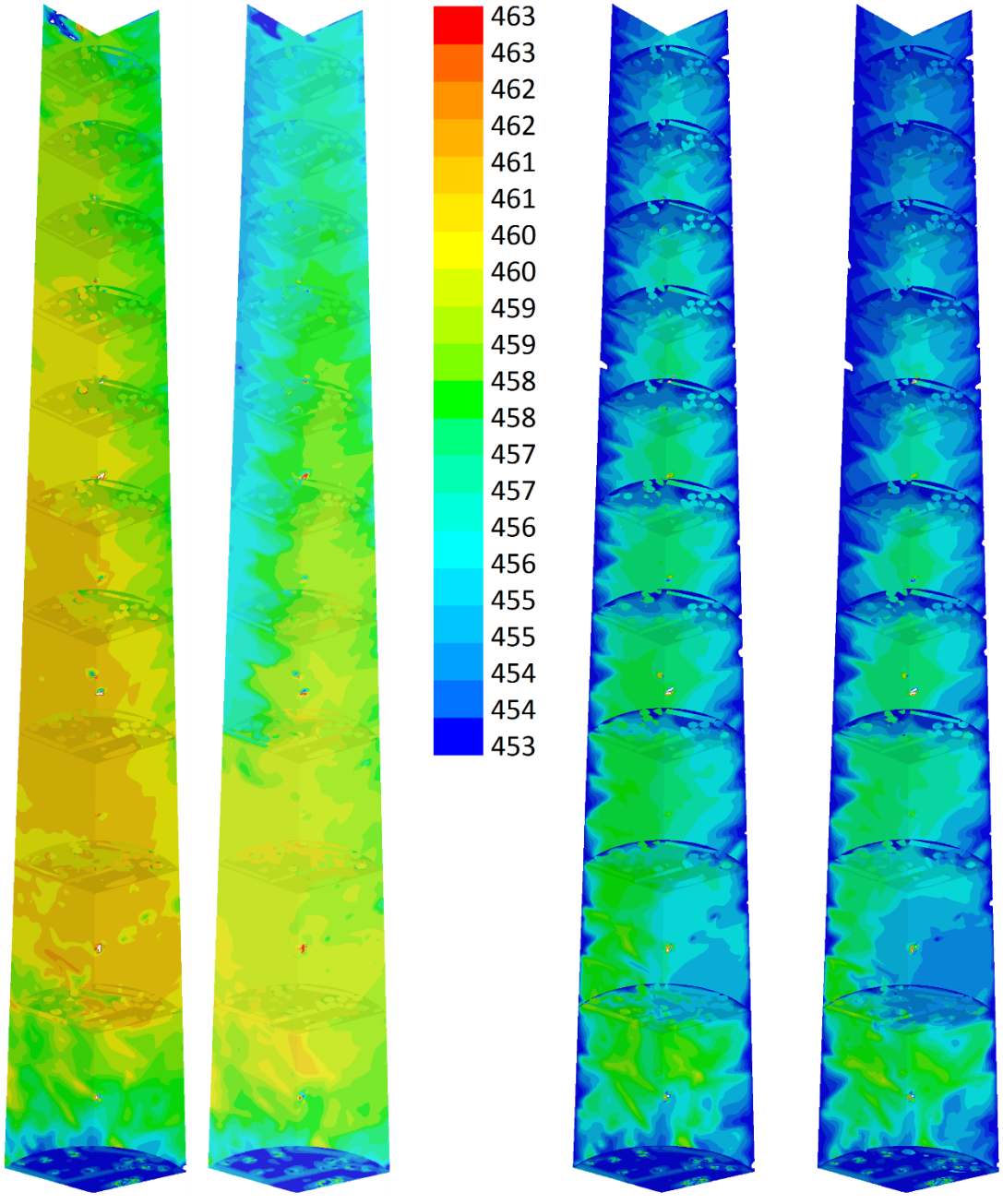

Figure 7-13 Temperature (K) contours on radial and axial planes in packed bed for (a) one-step reaction kinetics at inlet temperature 453K for space-times (a)120sec (b)210sec and for three-step reaction kinetics at inlet temperature 453 K for space-times (c)120sec and (d)210sec

7.3.3 Natural and Forced Convection effects

Mixed convection mass transfer may occur especially in case of high pressure flows, hence the effects of density, flow velocities on mass transfer are studied. The numerical results obtained for mass transfer were compared against the experimental results presented by (Stüber et al., 1996).

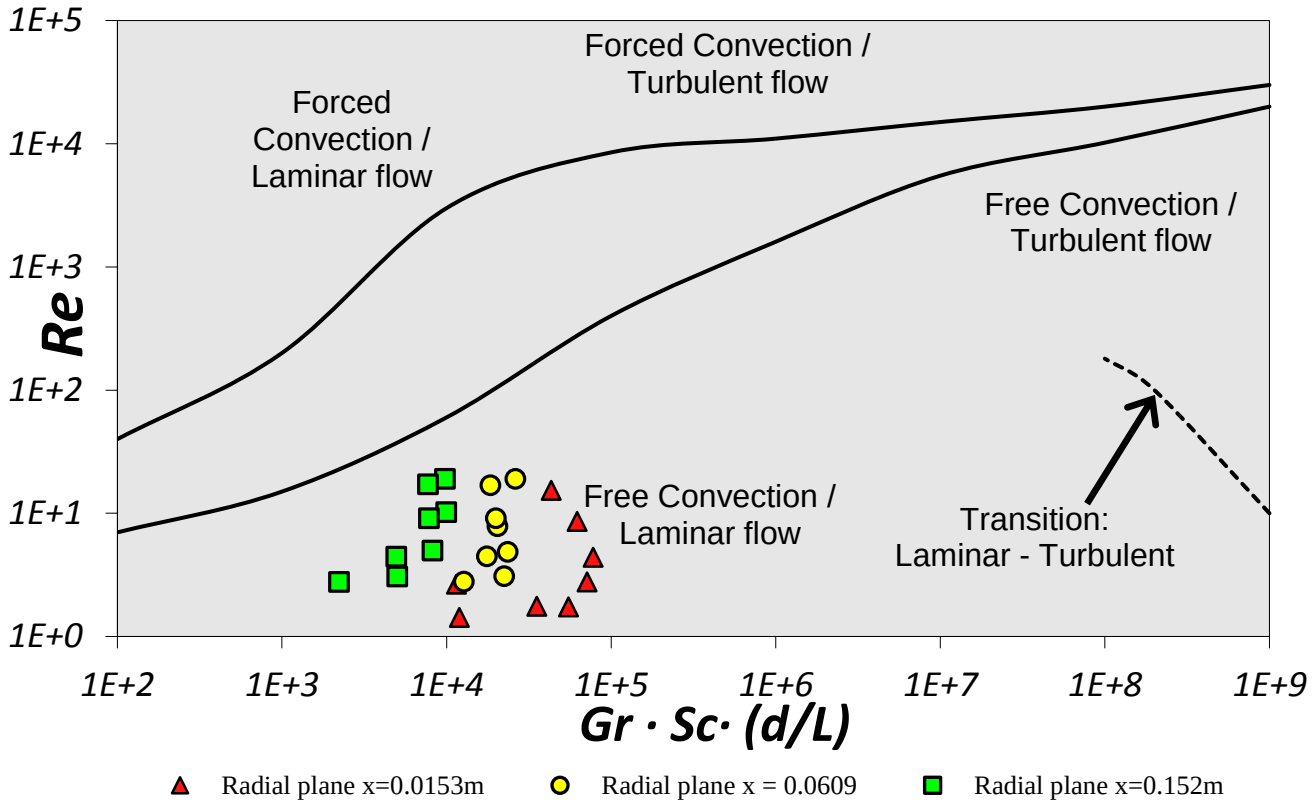

Figure 7-14 Simulation data for one-step kinetics compared with Metais-Eckert maps for different flow rates with data from radial planes at three different locations into the packed bed

For the simulations runs specified in *Table 7-3* gravitational acceleration was used in the operating conditions of the model, so the flow is up flow / opposing flow in which greater amount of free/natural convection is found due to the presence of high density gradients leading to the formation of hydrodynamic instabilities (i.e., counter current flow, recirculation, stream differentiation) which are caused by buoyancy effects. (Benneker et al., 1998)

For the different simulations, local values of Gr, Sc and Re values are calculated on the radial planes and on points on axial line in order to verify transport mechanism inside the packed bed at different locations. The obtained values are plotted on Metais-Eckert maps (Metais and Eckert, 1964). *Figure 7-14* shows the values plotted for local values of one-step kinetics on

radial planes at different lengths into the reactor in axial direction. All the points lie in the free-convection laminar region. The values near the inlet of reactor at x=0.0153 are more randomly placed indicating high density gradients in this region, due to the presence of unreacted triolein, and high concentrations of FAME on the catalysts surface.

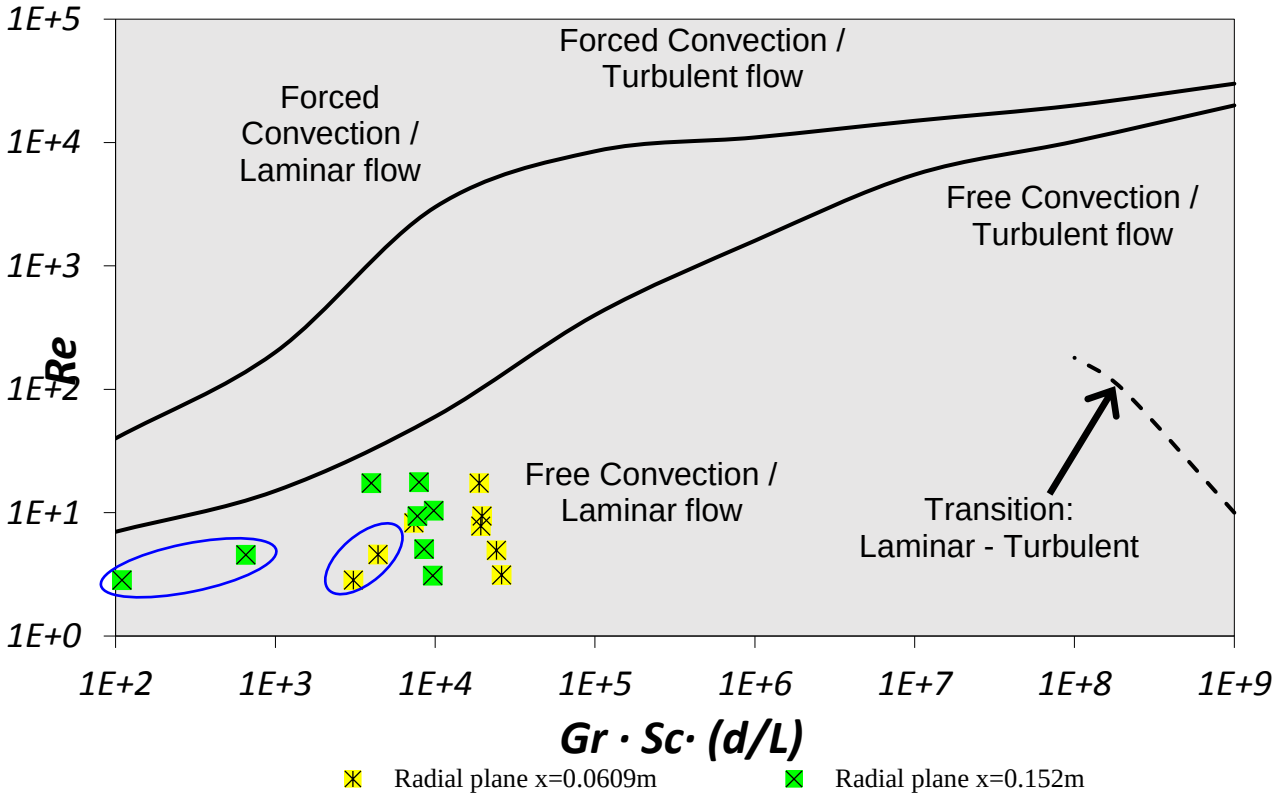

Figure 7-15 Simulation data compared with Metais-Eckert maps for three-step kinetics at different flow rates with data from radial planes at three different locations into the packed bed

The three step kinetics shown in *Figure 7-15* have similar behaviour compared to the one-step kinetics data. And for the simulation runs in which wall temperature is kept constant at 453 K, for which the points in the plot are circled show a deviation, with low Gr, due to high densities as seen in *Figure 7-16* (c) and (d) as a result of dropped temperatures.

At low velocities, fluid movement is controlled by the density gradients. It has been reported well that density and viscosity variations in porous media cause hydrodynamic instabilities (Benneker et al., 1998; Homsy, 1978; Manickam and Homsy, 1998) proving that these instabilities caused by buoyancy effects in the packed bed when density increases lead to a substantial increase in the flow axial dispersion within the bed. In *Figure 7-16* (b), high densities are observed near the walls compared to *Figure 7-16* (a), these density gradients in

(b) are due to buoyancy effects as a result of reduced flow rate (space-time of 210 sec). Also indicating channelling in the region near axis of the reactor.

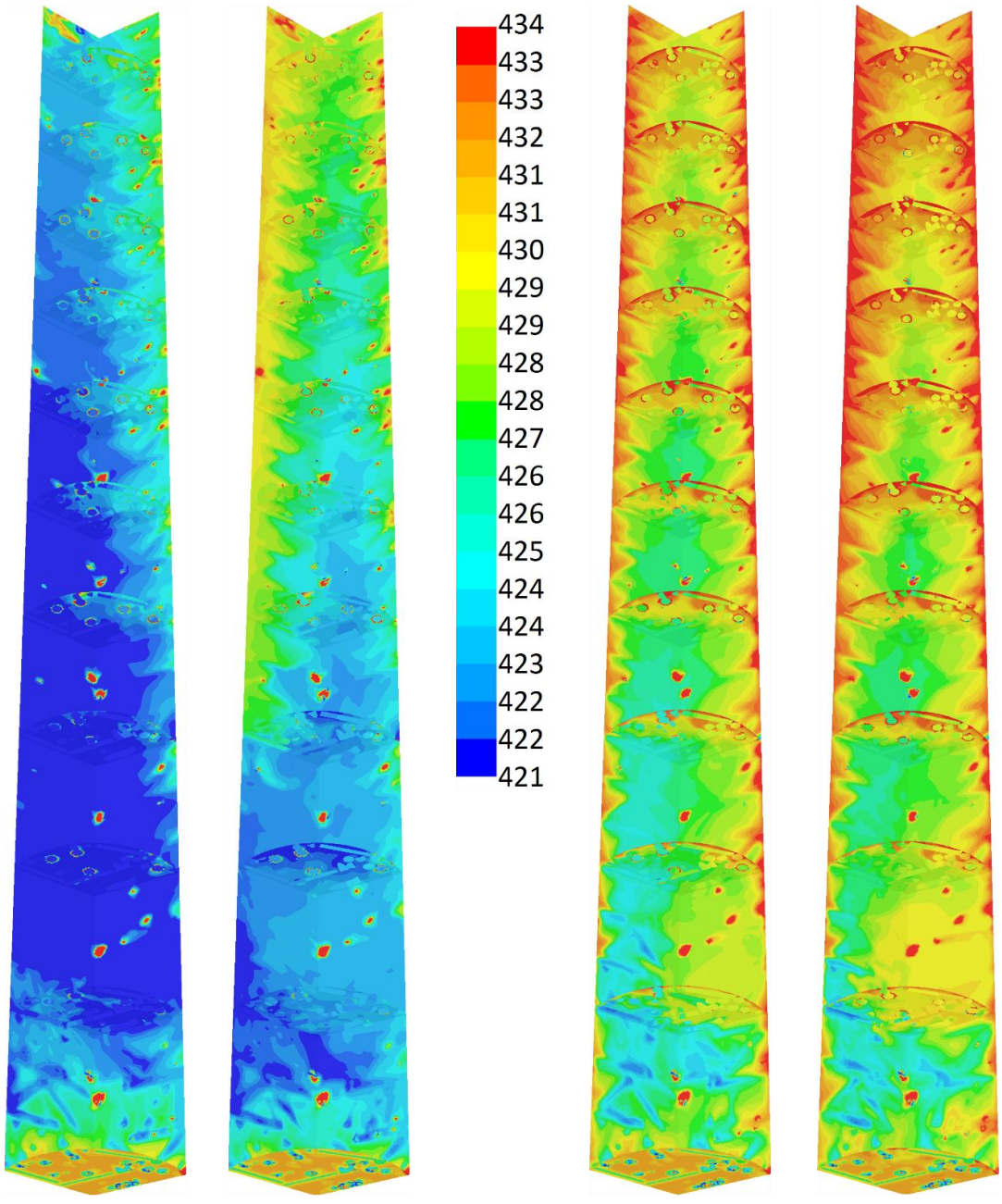

Figure 7-16 Density (kg/m3) contours on radial and axial planes in packed bed at 453 K for (a) one-step reaction kinetics zero heat flux on walls for space-times (a)120 sec (b)210 sec and for three-step reaction kinetics with constant wall temperature of 453 K for space-times (c)120 sec and (d)210 sec

Some of the simulation data of local values of Gr, Sc and Re on the axial line of the reactor are plotted on the Metais-Echert maps in *Figure 7-17* and in *Figure 7-18*. As it can be observed,

the main transport mechanism on the axial lines for different simulation conditions is the free convection in laminar flow regime.

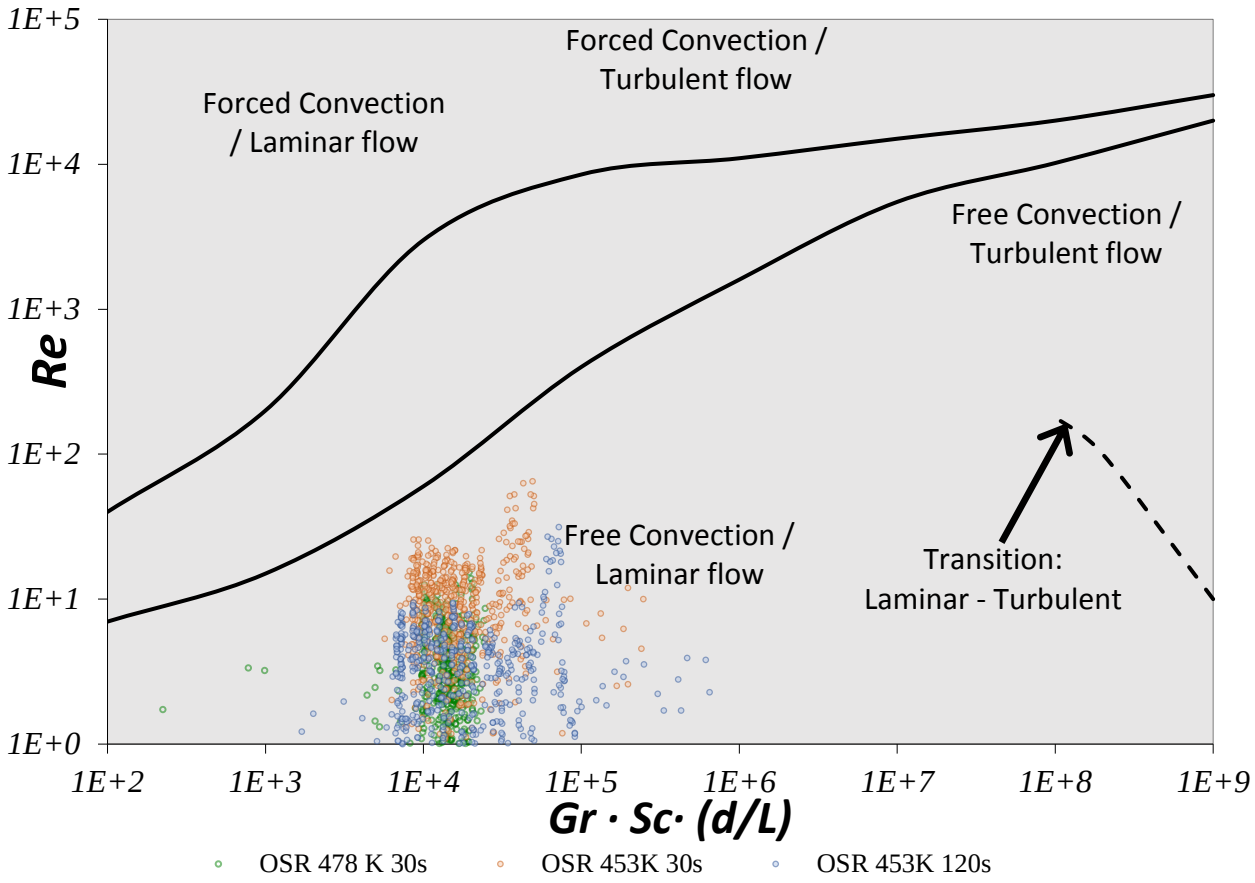

Figure 7-17 Simulation data compared with Metais-Eckert maps for one-step kinetics with data from corresponding axial lines

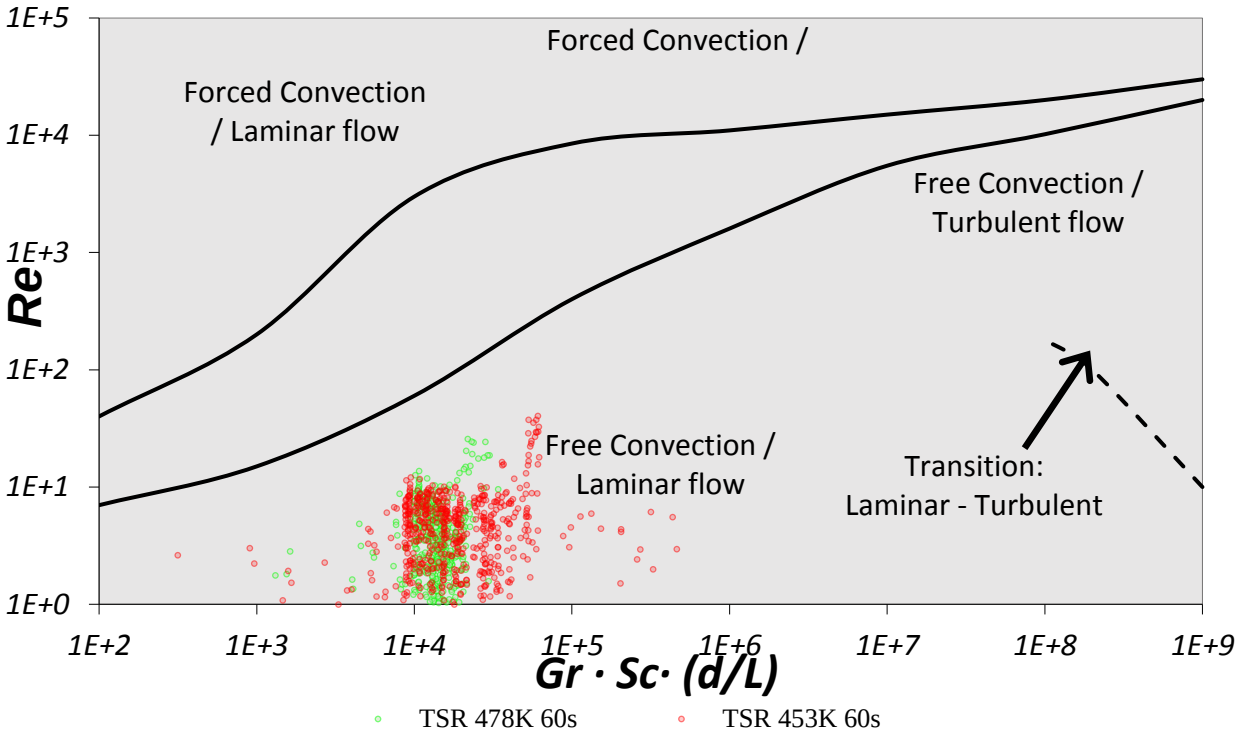

Figure 7-18 Simulation data compared with Metais-Eckert maps for three-step kinetics at two temperatures with data from corresponding axial lines

Figure 7-19 shows velocity contours for different flow rate situations for two temperatures. For (a) and (c) the space-times are equal at 30sec but the velocities at 478 K are slightly higher (as can be seen) due to the lower density at higher temperature. The velocities at some regions in the bed reached to about 10 times the inlet velocity, this can be observed in red regions in (b) and (d) where inlet velocity is about 0.00075 m/s.

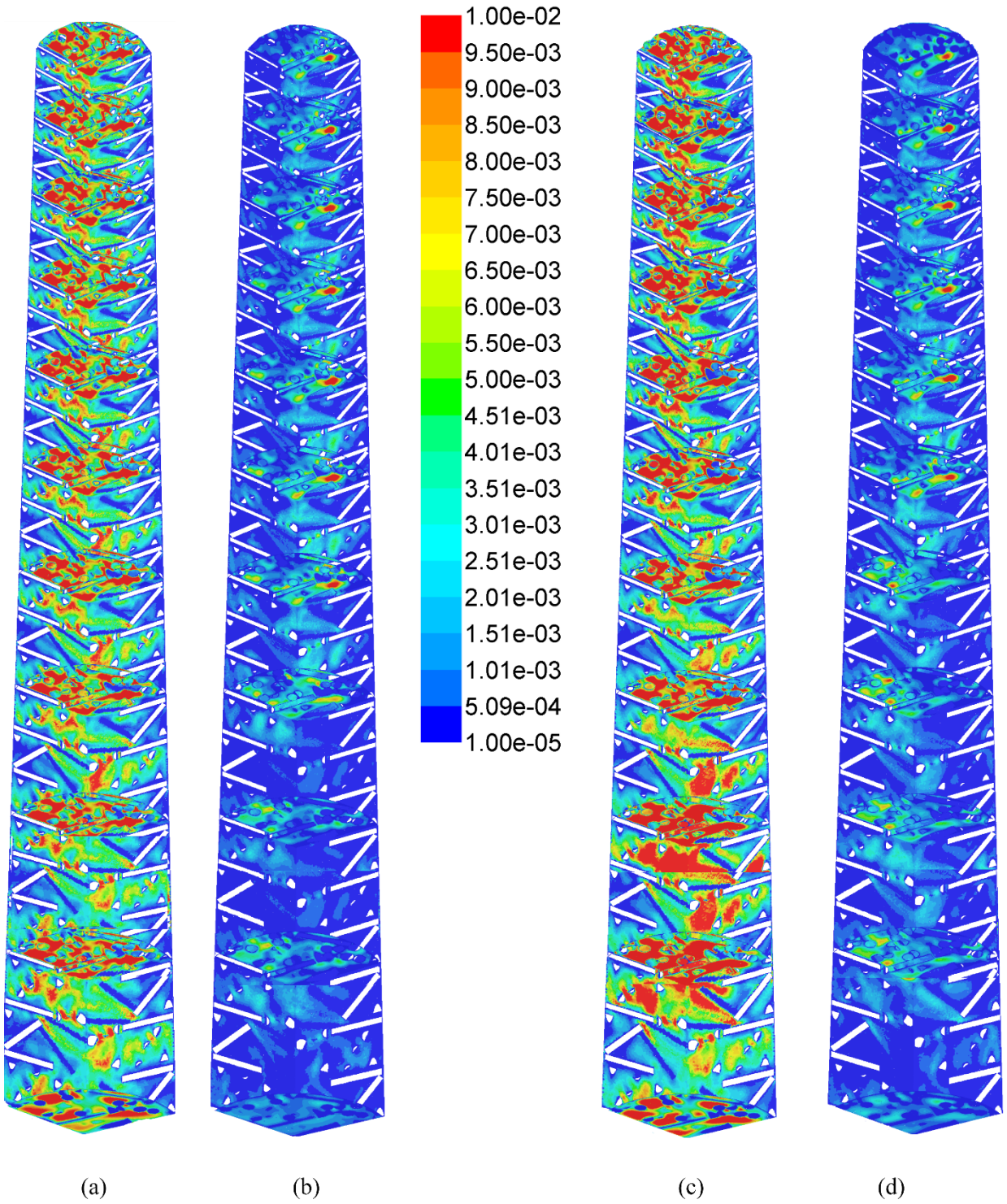

Figure 7-19 Velocity (m/s) contours on radial and axial planes in packed bed for one-step reaction kinetics at for space-times (a)30sec 453 K (b)210 sec at 453 K, and for three-step kinetics space-times (c)30 sec at 478 K and (d)210 sec at 478 K.

As indicated in the previous chapters and numerous authors (Guardo et al., 2007b; Stüber et al., 1996), flow velocity is directly proportional to mass transfer when forced convection takes place. An increase in velocity leads to better mixing and higher mass transfer coefficients. Analysing the mixed convection the results indicate the although the forced convection

component follows this behaviour, the natural convection component is almost constant for all the case as seen in *Figure 7-20* indicating that the free convection is intrinsically related to density and temperature fields and not effected by velocity. Hence when describing natural convection, the dominant dimensionless group used is Gr instead of Re. For both the one-step kinetics and three step kinetics, the natural convection effects were almost similar, indicating less effect due to the presence of monoglyceride and diglyceride on the overall density gradients.

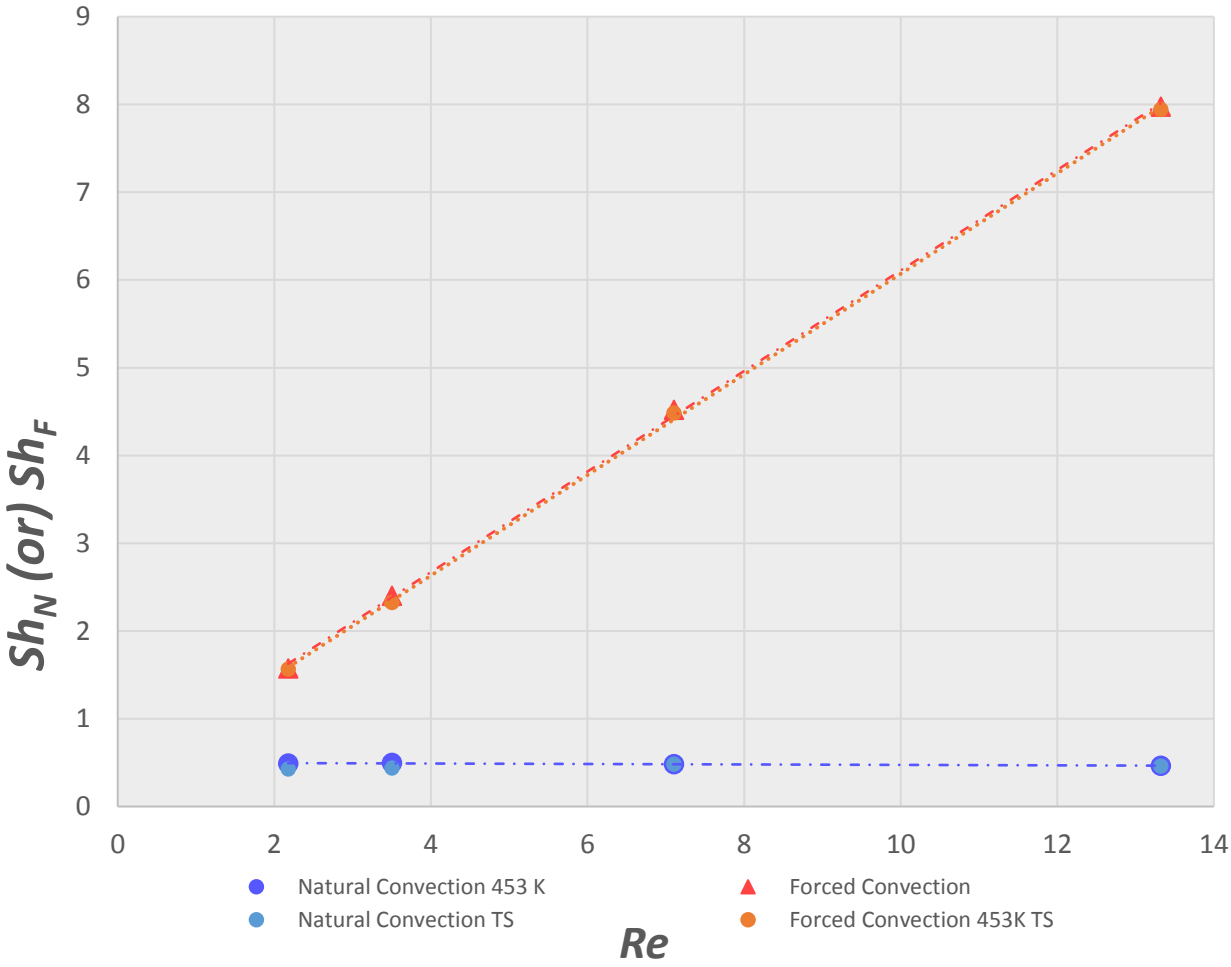

Figure 7-20 Sherwood number vs Reynolds number for free and forced convection

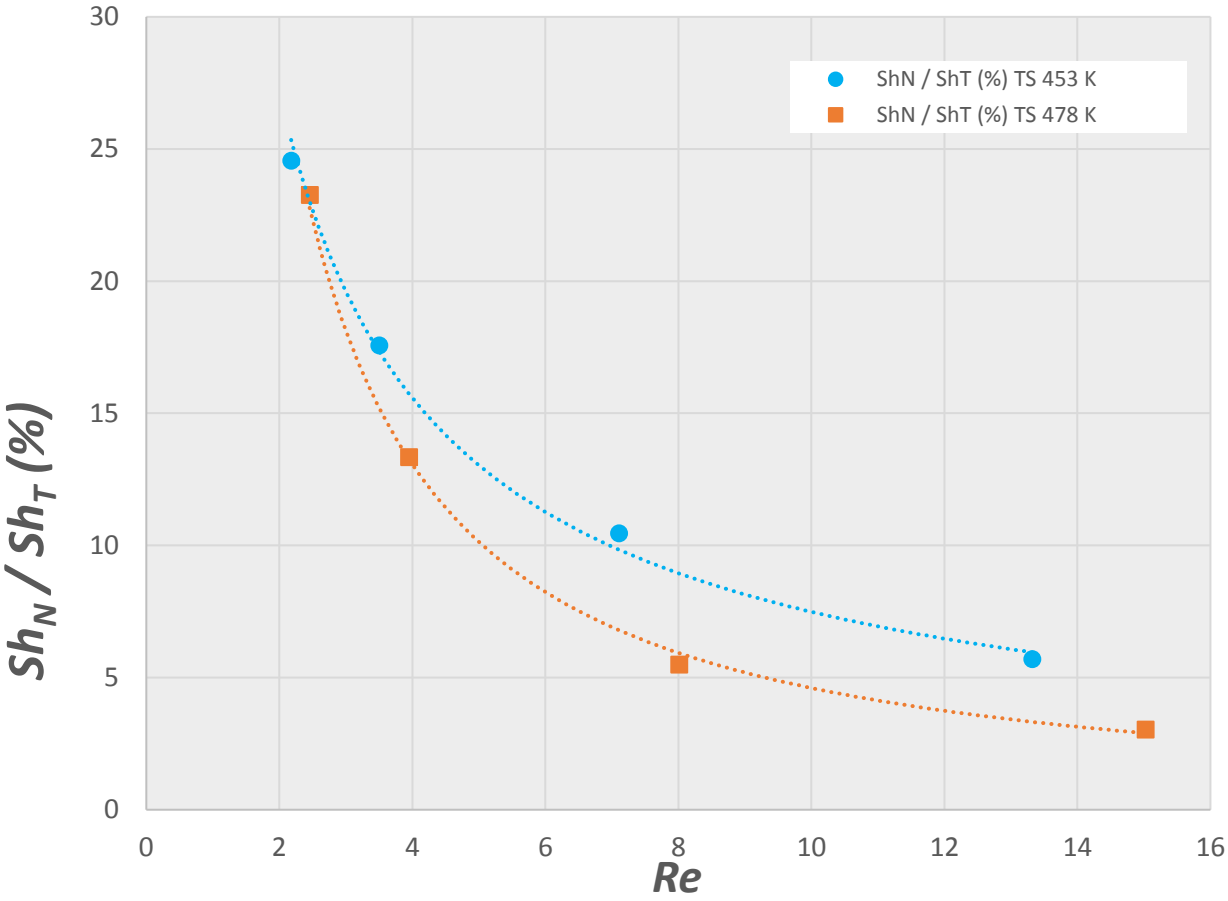

Figure 7-21 Contribution of natural convection to total mass transfer vs. Reynolds number

The contributions of free and forced convection to mass transfer could be assessed following the suggestions of Stüber et al., (1996). *Figure 7-21* shows the contribution of natural convection to the mass transfer with Re, which is decreasing with the increase in Re. It can be observed from the figure that higher contribution to total mass transfer by natural convection is found for lower temperature, as density is higher at this temperature of 453 K. With the decrease in flow rate, this difference is reduced. *Figure 7-22* contribution of forced convection to the total convection is plotted which increased with Re as expected. The numerical results are also in concordance with the experimental results by Stüber et al., (1996) reported in that paper as shown in *Figure 7-22*.

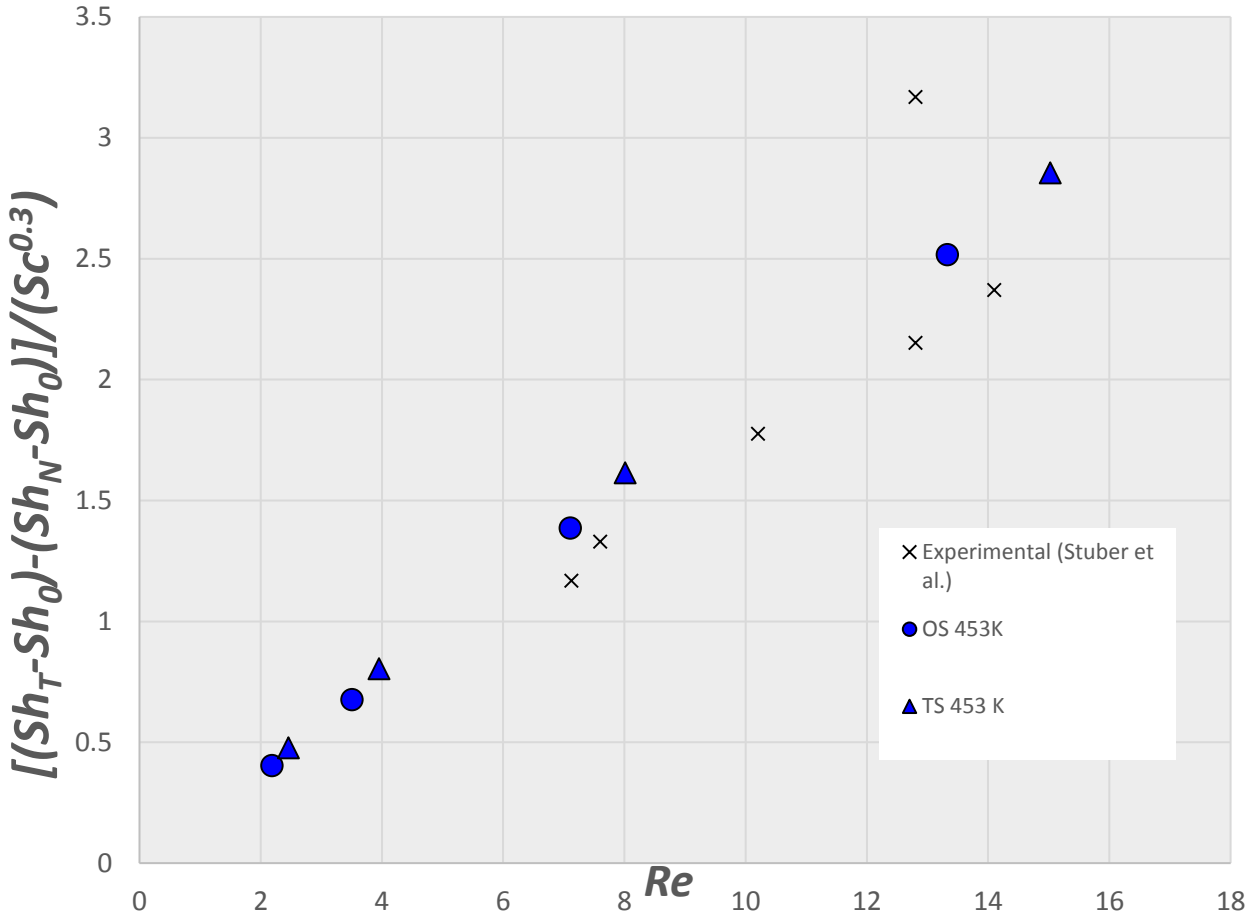

Figure 7-22 CFD obtained contribution of forced convection to total mass transfer vs. Reynolds number and comparison against experimental data presented by Stüber et al., (1996)

7.3.4 Reaction rates and conversion of triolein

In a transesterification reaction, one mole of triglyceride reacts with three moles of alcohol to form one mole of glycerol and three moles of fatty acid alkyl ester. In order to shift the equilibrium to the right, ensure full solubility of triolein and keep the viscosity of reaction mixture low, methanol is added in excess over the stoichiometric amount. The minimum amount of methanol to oil molar ratio commercially used is about 6:1 Some amount of catalyst has to be present to achieve high ester yields.

In catalytic reactions, no matter how active the catalyst is, it can be only effective if the reactants reach the external and internal catalyst surface. In various physical and chemical steps in a catalytic process, the steps involving intra-particle diffusion are (a)transfer of the reactants into porous catalyst (internal diffusion) and (b)adsorption of the reactants (c) surface reaction and then (d)desorption and transfer of the products. (Baiker, 1999). These mass-transfer resistances occur in the interior of the catalyst particles and are not represented in the simulations.

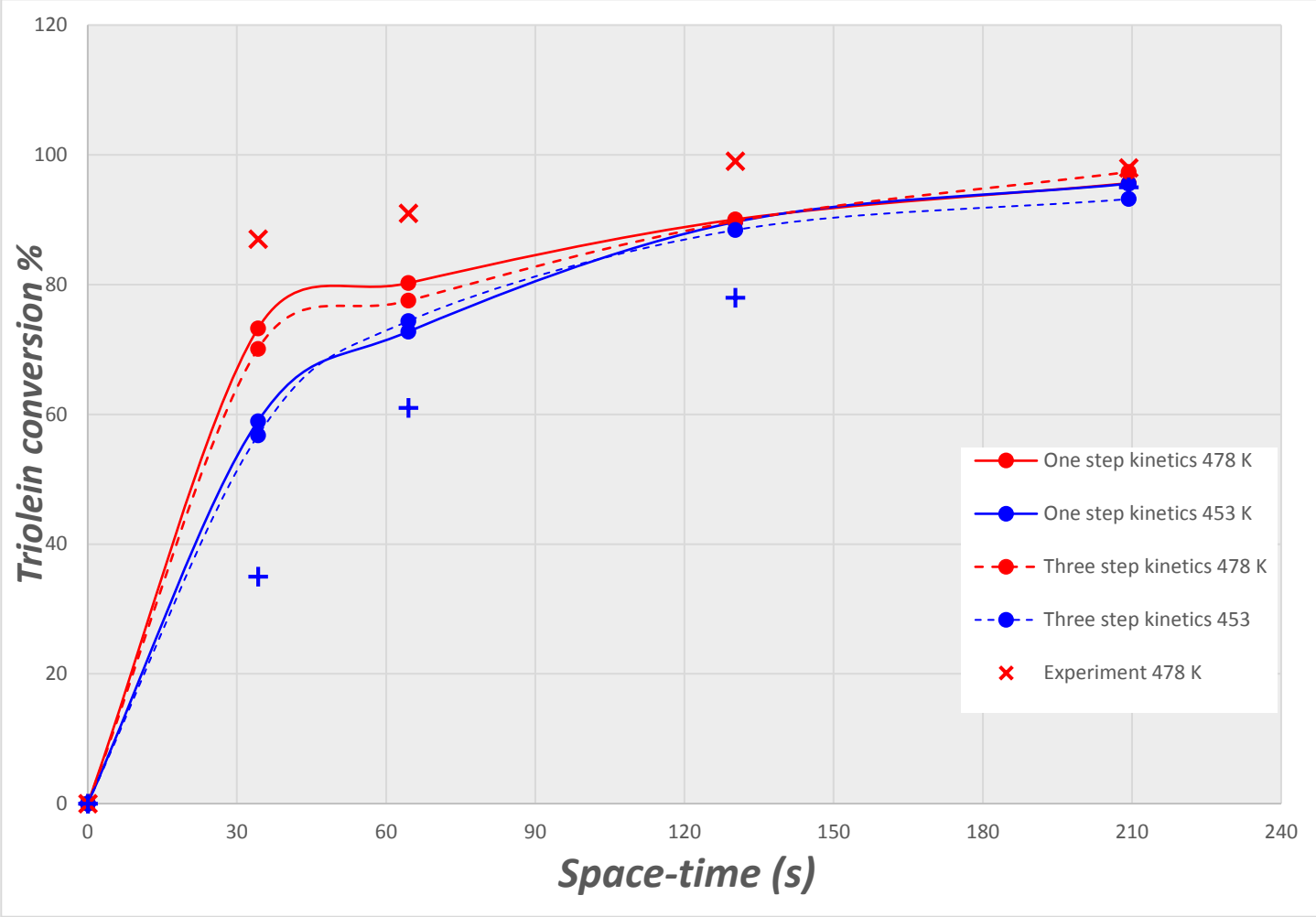

Figure 7-23 Triolein conversion for one-tenth length for one-step and three step kinetics simulations compared against experimental data for 478 K and 453 K.

For the simulations done, triolein concentration data is recorded on radial planes at various lengths into the packed bed, to estimate conversion. The nearly complete conversion obtained was about 99.9 % compared to 99.3 % conversion attained for experiments at 478 K and 2 min space-time conducted in our research group. As the mass transfer resistances are not represented in the simulations, high conversions of triolein are observed. However, for the one-tenth length of the reactor, the observed conversions have a similar trend to that of the experimental results, indicating the use of possible correcting factors to make the simulations more useful for predicting conversions upon the availability of kinetic data.

From the experimental data presented in *Figure 7-23*, it can be seen that the conversion of triglycerides increased with temperature and with space-time.

The high conversion in simulations are obtained even for lower space-times. This high conversion is due to absence of mass-transfer

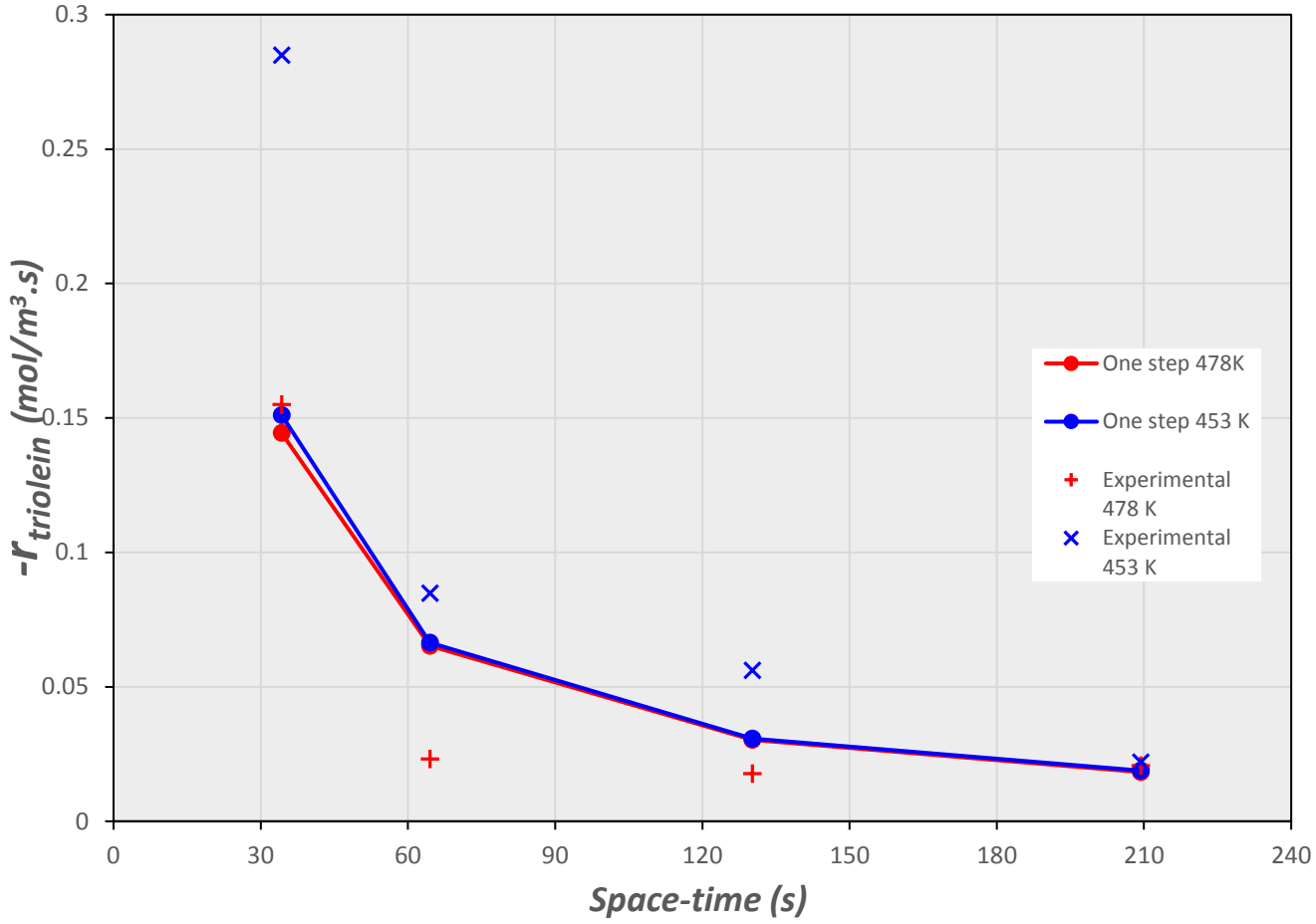

Figure 7-24 Reaction rates obtained for full length reactor compared against experimental obtained rates

The reaction rates are estimated from one-step kinetics data. Higher reaction rates are observed for lower space-times as expected. The obtained reaction rates are compared against experimental data from our research group, verifying the simulation data. For reaction rate for 30 sec space-time at 453 K however, the experimental value is high at 0.27 mol/m^3.s while for simulation is 0.15 mol /m^3.s. For 210 sec space-time flow rate, the experimental data and simulation data are almost equal.

7.4 CONCLUSIONS

Transesterification reaction in the presence of supercritical solvent occurring in a heterogeneous reactor is modelled in a geometrical packed bed model with randomly packed cylindrical catalysts, with the reaction occurring on the surface of the catalysts. A full-length wall segment geometric model with extensions at the inlet ant outlet has been used. Two reaction kinetic

models – one step irreversible reaction and a three step reversible reactions were compared for two temperatures.

Concentration, density, temperature and velocity profiles in the reactor are obtained and analysed. The concentration profiles at the initial lengths of the bed were comparable with the experimental data. The conversions obtained at these lengths were analogous to the experiments. Higher yield of FAME was observed for lower temperature of 453 K. The three-step kinetics showed lower yield, which is more accurate due to the formation of intermediate reaction species, monoglyceride and diglyceride. However, both the kinetics showed a similar trend in the concentration profiles verifying the applicability of the one-step irreversible kinetic model. The reaction showed exothermic effect with increased temperature, this effect is more visible when zero heat flux boundary condition is applied on the wall.

Mass transfer by free and forced convection occurring in the reactor is analysed. Local values of Gr, Sc and Re on radial planes and axial line are estimated and plotted on Metais-Eckert maps, which show the mass transfer occurring by free convection, which can be substantiated by the presence of density gradients throughout the reactor. For both the one-step kinetics and three step kinetics, the natural convection effects were almost similar, indicating less effect due to the presence of monoglyceride and diglyceride on the overall density gradients. The contribution of forced convection to mass transfer obtained was comparable to the published experimental data.

High conversions of triolein was observed for simulations for higher space-time and for longer length into the packed bed. The conversion of triolein for 478 K compared to 453 K was observed in both simulations and published experimental data. Very high conversions for full-length packed bed observed in simulations, as the reaction occurs directly on the particle surface, while the intra-particle mass-transfer resistances are not modelled in the simulations. For further investigation, intra-particle mass transfer resistances can be modelled. The reaction rates are estimated from one-step kinetics data. Higher reaction rates are observed for lower space-times as expected. The obtained reaction rates are compared against experimental data obtained at our research group lab, verifying the simulation data.

Computational Fluid Dynamics proves to be a valuable tool for study of heterogeneous catalytic transesterification of oils in the presence of supercritical solvent. With the increase in computational capabilities year after year, this computational technique allows to obtain in a fast and economical way data that otherwise is very complicated and expensive to obtain experimentally.

In view of the results, it can be suggested that the addition of the reactants to the packed bed is new to the products of the packed bed. The temperature 453 K is found to be sufficient for higher space-times, but for lower space-time (higher flow rates) higher temperature of 478 K has significant conversion compared to 453K.

For further investigation, the properties data at supercritical conditions can be used for simulation for at various other operating conditions or geometrical design. The method for geometrical design can be used to obtain needed geometry. With the standard reaction conditions simulated can help further researchers to have an idea of the various conditions of temperature or oil to alcohol ratio to use in order to obtain the required yield. Also, the length of the reactor, can be optimized for the required yield. The use of wall-segment packed bed reactor has been proved useful.

REFERENCES

Baiker, A., 1999. Supercritical fluids in heterogeneous catalysis. Chem. Rev. 99, 453–473. doi:10.1021/cr970090z

Benneker, a. H., Kronberg, a. E., Westerterp, K.R., 1998. Influence of buoyancy forces on the flow of gases through packed beds at elevated pressures. AIChE J. 44, 263–270. doi:10.1002/aic.690440205

Demirbaş, A., 2009. Progress and recent trends in biodiesel fuels. Energy Convers. Manag. 50, 14–34.

Dixon, A.G., Taskin, M.E., Hugh Stitt, E., Nijemeisland, M., 2007. 3D CFD simulations of steam reforming with resolved intraparticle reaction and gradients. Chem. Eng. Sci. 62, 4963–4966. doi:10.1016/j.ces.2006.11.052

Freedman, B., Butterfield, R.O., Pryde, E.H., 1986. Transesterification Kinetics of Soybean Oil. J. Am. Oil Chem. Soc. 63.

Freund, H., Zeiser, T., Huber, F., Klemm, E., Brenner, G., Durst, F., Emig, G., 2003. Numerical simulations of single phase reacting flows in randomly packed fixed-bed reactors and experimental validation. Chem. Eng. Sci. 58, 903–910. doi:10.1016/S0009-2509(02)00622-X

Guardo, A., Casanovas, M., Ramìrez, E., Recasens, F., Magaña, I., Martínez, D., Larrayoz, M.A., 2007a. CFD modeling on external mass transfer and intra-particle diffusional effects on the supercritical hydrogenation of sunflower oil. Chem. Eng. Sci. 62, 5054–5061. doi:10.1016/j.ces.2007.01.080

Guardo, A., Coussirat, M., Recasens, F., Larrayoz, M.A., Escaler, X., 2007b. CFD studies on particle-to-fluid mass and heat transfer in packed beds: Free convection effects in supercritical fluids. Chem. Eng. Sci. 62, 5503–5511. doi:10.1016/j.ces.2007.02.040

Homsy, G.M., 1978. Viscous fingering in porous media. Annu. Rev. Fluid Mech. 19, 271–

311.

Kusdiana, D., Saka, S., 2001. Kinetics of transesterification in rapeseed oil to biodiesel fuel as treated in supercritical methanol. Fuel 80, 693–698. doi:10.1016/S0016-2361(00)00140-X

Lakshminarayana, B., 1991. An Assesment of CFD Techniques in the Analysis and Design of Turbomachinery.pdf. J. Fluids Eng. 113, 315–352.

Lotero, E., Liu, Y., Lopez, D., Suwannakarn, K., Bruce, D., Goodwin, J., 2005. No Title. Ind. Eng. Chem. Res. 44, 5353.

Ma, F., Hanna, M.A., 1999. Biodiesel production : a review. Bioresour. Technol. 70, 1–15.

Maçaira, J., Santana, A., Recasens, F., Angeles Larrayoz, M., 2011. Biodiesel production using supercritical methanol/carbon dioxide mixtures in a continuous reactor. Fuel 90, 2280–2288. doi:10.1016/j.fuel.2011.02.017

Manickam, O., Homsy, G.M., 1998. Fingering instabilities in vertical miscible displacement flows through porous media. J. Fluid Mech. 288, 75–102.

Metais, B., Eckert, E.R.G., 1964. Forced, Mixed, and Free Convection Regimes. J. Heat Transfer 86, 295.

Noureddini, H., Gao, X., Philkana, R., 2005. Immobilized Pseudomonas cepacialipase for biodiesel fuel production from soybean oil. Bioresour. Technol. 96, 769–77.

Pinnarat, T., Savage, P., 2008. Assessment of noncatalytic biodiesel synthesis using supercritical reaction conditions. Ind. Eng. Chem. Res. 47, 6801.

Poling, B.E., Prausnitz, J.M., 2001. THE PROPERTIES OF GASES AND LIQUIDS, McGraw-Hill. McGraw-Hill. doi:10.1036/0070116822

Portha, J.F., Allain, F., Coupard, V., Dandeu, A., Girot, E., Schaer, E., Falk, L., 2012. Simulation and kinetic study of transesterification of triolein to biodiesel using modular reactors. Chem. Eng. J. 207-208, 285–298. doi:10.1016/j.cej.2012.06.106

Schwab, A.W., Bagby, M.O., Freedman, B., 1987. Preparation and properties of diesel fuels from vegetable oils. Fuel 66, 1372–1378. doi:http://dx.doi.org/10.1016/0016-2361(87)90184-0

Stüber, F., Vazquez, A.M., Larrayoz, M.A., Recasens, F., 1996. Supercritical Fluid Extraction of Packed Beds : External Mass Transfer in Upflow and Downflow Operation. Ind. Eng. Chem. Res. 35, 3618–3628.

Varma, M.N., Deshpande, P. a., Madras, G., 2010. Synthesis of biodiesel in supercritical alcohols and supercritical carbon dioxide. Fuel 89, 1641–1646. doi:10.1016/j.fuel.2009.08.012

Wehinger, G.D., Eppinger, T., Kraume, M., 2015. Detailed numerical simulations of catalytic fixed-bed reactors : Heterogeneous dry reforming of methane. Chem. Eng. Sci. 122, 197–209. doi:10.1016/j.ces.2014.09.007

Yuen, E.H.L., Sederman, A.J., Sani, F., Alexander, P., Gladden, L.F., 2003. Correlations Between Local Conversion and Hydrodynamics in a 3-D Fixed-Bed Esterification Process: An MRI and Lattice-Boltzmann Study. Chem. Eng. Sci. 58, 613–619.

Zimmermann, S., Taghipour, F., 2005. CFD Modeling of the Hydrodynamics and Reaction Kinetics of FCC Fluidized-Bed Reactors. Ind. Eng. Chem. Res. 44, 9818–9827.

CHAPTER VIII

8. CONCLUSIONS AND FUTURE WORK

8.1 WALL-TO-FLUID HEAT TRANSFER

Heating of reactor walls is necessary to maintain the reactor under specified reaction conditions. A wall-segment packed bed model is created with randomly packed cylindrical particles. It is possible to model a realistic case of packed bed of cylinders including the contact point within the surfaces involved in the geometry. Computational grids of different mesh densities and element size are generated for the geometric model and checked for their independence. The simulation model is set up for high pressure supercritical conditions with tertiary mixture fluid. The use of CFD for studying the wall-to-fluid heat transfer in packed bed assessed. Flow, energy and species mathematical models have been solved for the setup.

CFD simulations were done for two cases of methanol to oil molar ratios in two different packed bed geometries of one-tenth WS model and full-length WS model. Velocity, density and temperature profiles are obtained on radial, axial planes and axis of the packed bed. The temperature profiles showed higher temperature for lower *Re*. Velocity vector fields show higher velocities near the exit end of the bed. Higher density at lower *Re* can be observed, which is due to accumulation of methanol in the bed at this *Re*, although there is higher temperature at lower Re. However, for full-length bed (oil to alcohol ratio of 25), the density is as expected. Large density gradients are observed for lower Re and near to the outlet of the packed bed, resulting in free convection in these regions.

Mixed convection at high pressure in a packed bed was also analysed. For a supercritical fluid in laminar flow regime, it was possible to study the effects of density gradient, velocity over mass transfer. The density gradients observed neat the outlet of the packed bed and for lower Re number, generated hydrodynamic instabilities leading to convection due to natural convection as observed in the Metais-Eckert maps.

Values of wall Nusselt number and effective radial thermal conductivity are estimated for different Re are obtained with data of temperature profiles along the axis of the bed. The results show a trend of increase with Reynolds number for wall Nusselt number. Higher heat transfer is observed than what is predicted by some empirical correlations, which signifies the higher heat transfer for supercritical fluids. The Nu_w almost increases linearly with Re number for full

length packed bed, along with some empirical correlation, validating the numerical results for higher Re. But for Re<10, the simulation results are not linear.

Hence, CFD proves to be a reliable tool for modelling convective wall-to-fluid heat transfer in high pressure supercritical conditions for species mixtures in complex geometries. Free/Forced convection situations in the packed bed can be analysed.

8.2 PARTICLE-TO-FLUID HEAT TRANSFER

Heat transfer from particle to bulk fluid in a packed bed is studied. A geometric model of packed bed is created with cylindrical packing particles with tube-to particle diameter ratio of about 9. Full-length and half-length wall segment models have been used. The simulations model was set up for high-pressure and temperature supercritical conditions with tertiary mixture. Flow, energy and species mathematical models have been solved for the setup.

Mixed convection at high pressure in a packed bed was also analysed. For a supercritical fluid in laminar flow regime, it was possible to study the effects of density gradient, velocity over heat transfer. Large density gradients were observed near the inlet of the packed bed. These density gradients generated hydrodynamic instabilities leading to convection due to natural convection as observed in the Metais-Eckert maps.

For very low Re, the equilibrium temperature is achieved at shorter lengths of the packed bed. Hence for a given requirement, low Re conditions, shorted packed bed is sufficient.

Heat balance equation, which takes into consideration the axial dispersion is used for estimating heat transfer coefficients. The influence of velocity over the heat transfer is analysed and plotted. The value of Nu increases almost linearly with the increase in velocity. The simulation data agrees with many empirical correlations for predicting particle-to-fluid heat transfer. The heat transfer coefficients decreased with increase in length into the packed bed.

Computational fluid dynamics proved to be a reliable tool for modelling convective heat transfer in high pressure supercritical conditions for species mixtures in complex geometries. Free/Forced convection situations in the packed bed can be analysed at different locations in the packed bed. The obtained results can be compared qualitatively and quantitatively with previously published data.

8.3 PARTICLE-TOFLUID MASS TRANSFER

CFD proves to be a reliable tool for modelling convective mass transfer in high pressure supercritical conditions for species mixtures in complex geometries. Free/Forced convection situations in the packed bed can be analysed at different locations into the packed bed. The obtained results can be compared qualitatively and quantitatively with previously published data.

Mass transfer from particle surface to bulk fluid in a packed bed is studied. Diffusion of triolein from particle (oil extraction) to bulk fluid mixture of methanol and carbon dioxide is simulated. A geometric model of packed bed is created with randomly packed cylindrical packing particles. A half-length wall segment models have been used. The simulations model was set up for high-pressure and temperature supercritical conditions with tertiary mixture. Flow, and species mathematical models have been solved for the setup.

Mixed convection at high pressure in a packed bed was also analysed. For a supercritical fluid in laminar flow regime, it was possible to study the effects of density gradient, velocity over mass transfer. Large density gradients were observed near the inlet of the packed bed. These density gradients generated hydrodynamic instabilities leading to convection due to natural convection as observed in the Metais-Eckert maps.

Mass balance equation, which takes into consideration the axial dispersion is used for estimating heat transfer coefficients. The influence of velocity over the mass transfer is analysed and plotted. The value of Sh increases almost linearly with the increase in velocity. The simulation data agrees with many empirical correlations for predicting particle-to-fluid heat transfer. The mass transfer coefficients decreased with increase in length into the packed bed.

8.4 REACTIVE FLOW MODELLING OF TRANSESTERIFICATION REACTION

Transesterification reaction in the presence of supercritical solvent occurring in a heterogeneous reactor is modelled in a geometrical packed bed model with randomly packed cylindrical catalysts, with the reaction occurring on the surface of the catalysts. A full-length wall segment geometric model with extensions at the inlet ant outlet has been used. Two reaction kinetic models – one step irreversible reaction and a three step reversible reactions were compared for two temperatures.

Concentration, density, temperature and velocity profiles in the reactor are obtained and analysed. The concentration profiles at the initial lengths of the bed were comparable with the experimental data. The conversions obtained at these lengths were analogous to the experiments. Higher yield of FAME was observed for lower temperature of 453 K. The three-step kinetics showed lower yield, which is more accurate due to the formation of intermediate reaction species, monoglyceride and diglyceride. However, both the kinetics showed a similar trend in the concentration profiles verifying the applicability of the one-step irreversible kinetic model. The reaction showed exothermic effect with increased temperature, this effect is more visible when zero heat flux boundary condition is applied on the wall.

Mass transfer by free and forced convection occurring in the reactor is analysed. Local values of Gr, Sc and Re on radial planes and axial line are estimated and plotted on Metais-Eckert maps, which show the mass transfer occurring by free convection, which can be substantiated by the presence of density gradients throughout the reactor. For both the one-step kinetics and three step kinetics, the natural convection effects were almost similar, indicating less effect due to the presence of monoglyceride and diglyceride on the overall density gradients. The contribution of forced convection to mass transfer obtained was comparable to the published experimental data.

High conversions of triolein was observed for simulations for higher space-time and for longer length into the packed bed. The conversion of triolein for 478 K compared to 453 K was observed in both simulations and published experimental data. Very high conversions for full-length packed bed observed in simulations, as the reaction occurs directly on the particle surface, while the intra-particle mass-transfer resistances are not modelled in the simulations. For further investigation, intra-particle mass transfer resistances can be modelled. The reaction rates are estimated from one-step kinetics data. Higher reaction rates are observed for lower space-times as expected. The obtained reaction rates are compared against experimental data from our research group, verifying the simulation data.

In view of the results, it can be suggested that the addition of the reactants to the packed bed is new to the products of the packed bed. The temperature 453 K is found to be sufficient for higher space-times, but for lower space-time (higher flow rates) higher temperature of 478 K has significant conversion compared to 453K.

Computational Fluid Dynamics proves to be a valuable tool for study of heterogeneous catalytic transesterification of oils in the presence of supercritical solvent. With the increase in computational capabilities year after year, this computational technique allows to obtain in a

fast and economical way data that otherwise is very complicated and expensive to obtain experimentally.

8.5 FUTURE WORK

For the improvement of the current work, some aspects can be modified, or added. Conduction of the solid catalyst has to be examined in order to have more accurate effective thermal conductivity in the packed bed. It could be used for developing an intra-particle to fluid heat and mass transfer models, to see it effectiveness in modelling mass transfer resistances that exist in porous catalyst. The data could be used for developing a theoretical model for heat/mass transfer coefficients. As having a intra particle grid, and simulations are computational effort intensive, more optimization techniques for such studies have to be developed.

Various packing building methods can be utilized to generate different packed bed models in order to develop most effective catalyst design. A comparison of spherical and cylindrical particle, or other shaped particles could be examined. The influence of the packing arrangement, void distribution.

The influence of buoyancy on the flow in packed bed under supercritical can be further analysed by doing a comparative study of gravity opposing and gravity assisting flows. Natural and forced convection heat and mass transfer can be analogously analysed and compared. And thereby development of an empirical correlation that could be used.

A through energy balance of the transesterification can be done to accesses the exothermic/ endothermic effects of the reaction in supercritical conditions. The heat effects in the reactor could be concurrently studied for wall-to-fluid heat transfer, thereby analysing the effect of reaction the wall-to-fluid heat transfer coefficients.

In the reactive flows study, having a solid catalyst in order to account for mass-transfer resistances is essential in order to have accurate description of the physical process. The current results show very high conversions for simulations compared to experimental values is due to lack of any mass transfer resistances in the surface of particles in packed bed model as discussed in the chapter. This would help in developing more accurate kinetics for the transesterification reaction. CFD simulations are very much advantageous especially for the complex situations involving supercritical fluids which are expensive to conduct in order to analyse the reaction kinetics.

For further investigation, the properties data at supercritical conditions can be used for simulation for at various other operating conditions or geometrical design. The method for geometrical design can be used to obtain needed geometry. With the standard reaction conditions simulated can help further researchers to have an idea of the various conditions of temperature or oil to alcohol ratio to use in order to obtain the required yield. Also, the length of the reactor, can be optimized for the required yield. The use of wall-segment packed bed reactor has been proved useful.

APPENDICES

A. PHYSICAL PROPERTIES ESTIMATION AT SUPERCRITICAL CONDITIONS

A.1 DENSITY AT HIGH PRESSURE CONDITIONS

The density of supercritical CO_2 for pressures 150 to 400bar and temperatures 315 to 588 K was defined by Redlich-Kwong cubic equation of state (Redlich and Kwong, 1949).

$$\rho = \frac{p_{op} M_w}{zRT} \tag{A-1}$$

Density is computed from the cubic equation of state, where the compressibility factor (z) is estimated from the cubic EOS in general form as

$$z^3 - \left(1 + B^* - uB^*\right) z^2 + (A^* + wB^{*2} - uB^* - uB^{*2}) z - \left(A^* B^*\right) - wB^{*2} - wB^{*3} = 0 \tag{A-2}$$

Where

$$A^* = \frac{aP}{R^2 T^2} \tag{A-3}$$

$$B^* = \frac{bP}{RT} \tag{A-4}$$

Here, *u = 1*; *w = 0*; $b = \frac{0.08664 RT_c}{P_c}$; and $a = \frac{0.42748 R^2 T_c^{2.5}}{P_c T^{0.5}}$

The Redlich-Kwong EOS was used in estimating the density of CO_2. The density is calculated as a function of temperature for particular pressures which are called user defined equations (UDE), that are fed into the CFD solver, for the substance of interest. The following algorithm is used in estimating the density of CO_2.

Methanol density data is taken from NIST data (Xiang et al., 2006). In which the correlation is developed from experimental data. Viscosity and density are presented as a function of temperature and pressure.

The densities of triolein ($C_{57}H_{104}O_6$), di-glyceride ($C_{39}H_{72}O_5$), mono-glyceride ($C_{21}H_{40}O_4$) and glycerol ($C_3H_8O_3$) at high temperatures is calculated through Rackett Equation in which Rackett proposed that saturated liquid volumes can be calculated by Equation (A-5) (Poling and Prausnitz, 2001) with reference triolein density of 0.915 kg/m^3 at 15ºC. For di-glyceride the reference density of 0.93 kg/m^3 at 20°C, for mono-glyceride 0.95 kg/m^3 at 15°C and for glycerol 1.26 kg/m^3 at 20°C.

$$V_s = V_s^R Z_c^{\phi} \tag{A-5}$$

Where, V_s = saturated liquid volume, V_s^R = experimental value at a reference temperature T^R, Z_c = critical compressibility factor. And $\varphi = (1 - T/T_c)^{2/7} - (1 - T^R/T_c)^{2/7}$.

The high pressure densities for triolein, diglyceride, mono-glyceride were correlated from with the Tait equation (Equation A-6), with known high temperature densities from Rackett Equation (Acosta et al., 1996)

$$v = v_o \left[1 + c \ln \left(\frac{P + B}{P_o + B} \right) \right] \tag{A-6}$$

Where c is a constant, $B(T)$ is a temperature dependent constant. v_o and P_o are reference specific volume and pressure respectively at a known condition. The known values of specific volume and pressure are taken from that calculated at the prevailing temperature and atmospheric pressure using Rackett equation. The model parameters are available in Acosta et al., 1996. For higher temperatures the constant $B(T)$ is extrapolated exponentially.

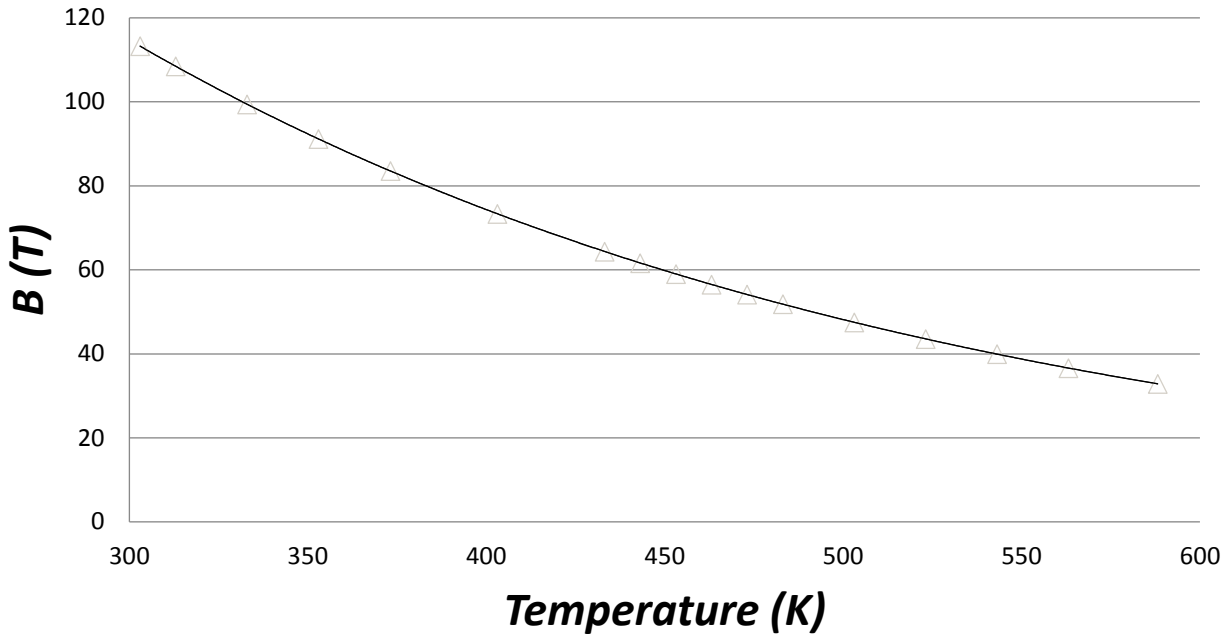

Figure A-1 Extrapolated (exponentially) temperature dependent constant B(T) in Tait equation

A.1.1 Density of mixture

The mixture density is estimated by the CFD solver by volume-weighted mixing rule Equation (4-7), which is for non-ideal gas mixtures and assumes no molecular interactions.

$$\rho = \frac{1}{\sum_i \frac{Y_i}{\rho_i}} \tag{A-7}$$

For the estimation of physical properties of viscosity, thermal conductivity, specific heat and viscosity for a mixture of carbon dioxide, methanol, and triolein a cylindrical model (2D) of length 1m and 0.1m diameter was made. Carbon dioxide is fed from one side of the pipe in laminar flow regime of Re 100 at a temperature of 423.15K. Methanol and triolein were imposed from the walls with equal mass fractions of 0.49 at temperature of 473.15K. *Figure A-2* the temperature profiles along the axis of the cylinder obtained. The under-relaxation factors for the pressure, density, body forces, momentum, methanol, triolein and energy have been set to 0.3, 1, 1, 0.7, 1, 1 and 1 respectively. Temperature, velocity, and mass fractions were checked for convergence.

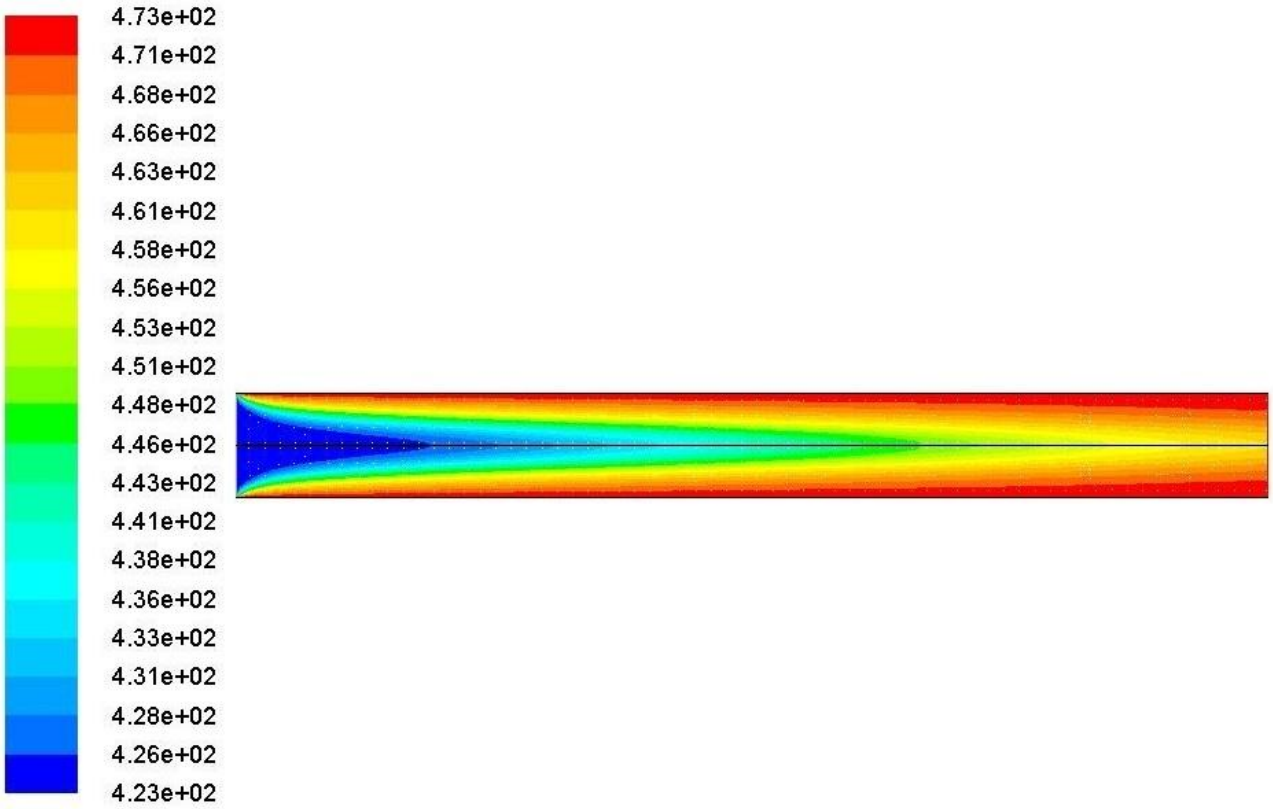

Figure A-2 Temperature (K) contours on cross-section of the cylinder along axis

Figure A-3 shows the variation of mixture density at 200 bar with temperature on the cylinder axis along the length. The composition of the mixture (mass fractions) is also shown. A comparison was made of correlations of the properties of a tertiary mixture of carbon dioxide, methanol and triolein with data from the CFD solver. A parity plot for this is shown in *Figure A-4*. The densities calculated by both ways have error of less than 1%, showing low discrepancy in property polynomials and laminar flow model used in estimating the flows.

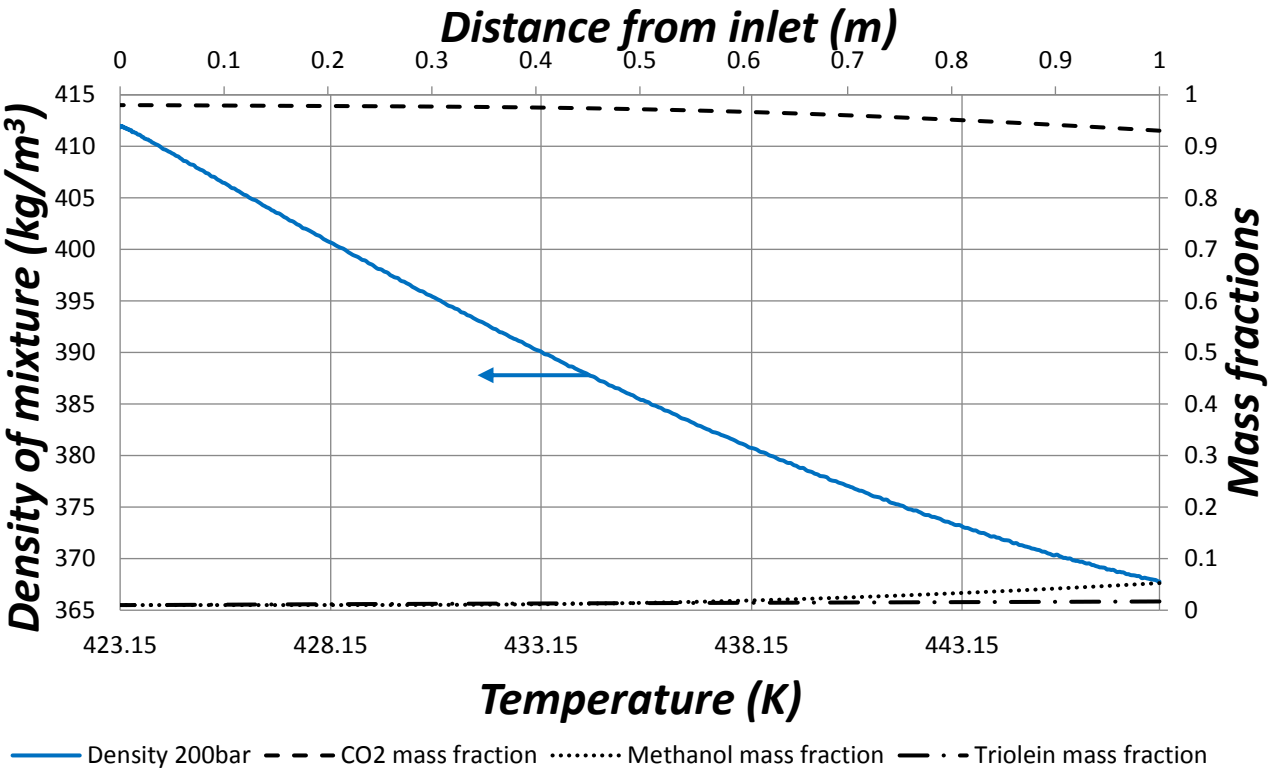

Figure A-3 CFD estimated mixture densities along the cylinder axis

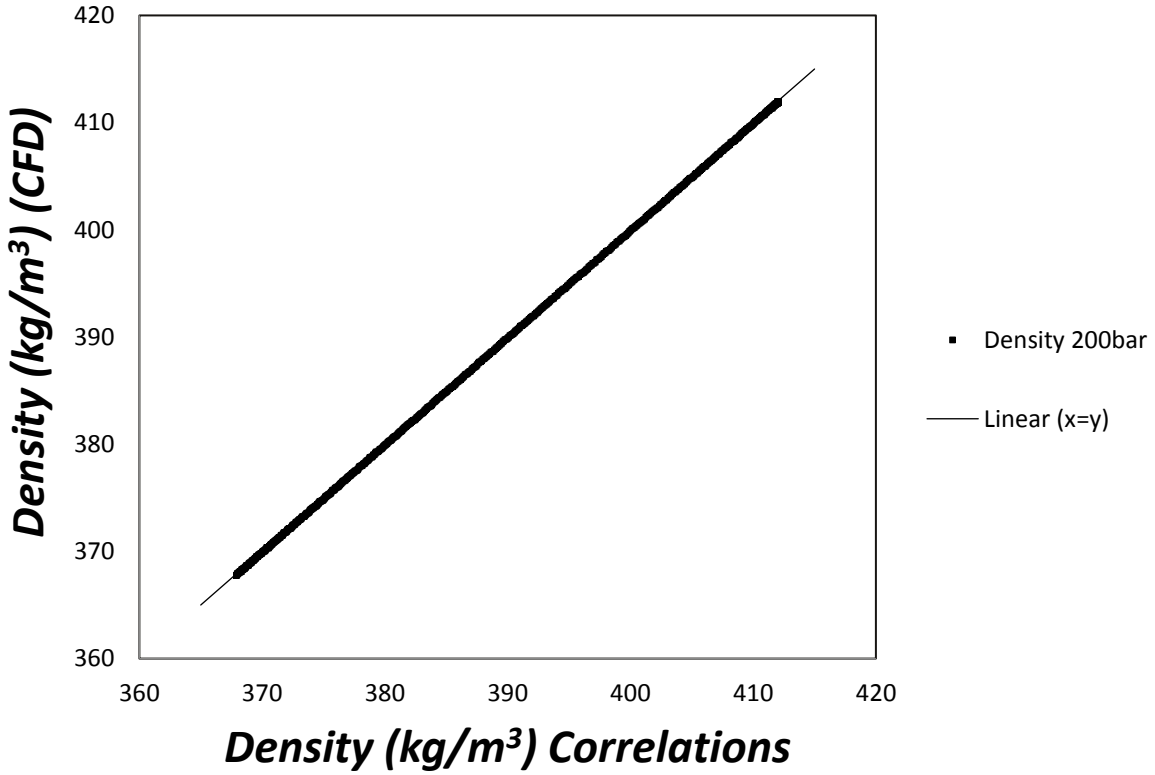

Figure A-4 Parity plot for densities obtained using CFD and densities obtained using the models for pure components, both methods use volume-weighted mixing rule.

A.2 VISCOSITY AT HIGH PRESSURE CONDITIONS

The viscosity of CO_2 at supercritical conditions is calculated by a technique proposed by Lucas, (1980), in which, for a reduced temperature of interest, parameters Z_1 and Z_2 are calculated

$$Z_1 = (0.807T_r^{0.618} - 0.357e^{-0.449T_r} + 0.340e^{-4.058T_r} + 0.018)F_P^0 F_Q^0 = \mu^0 \xi \quad \text{(A-8)}$$

Where F_P^0 and F_Q^0 are low pressure polarity and quantum correction factors determined as shown in Equations (A-10) and (A-11) respectively. To obtain the first of the mentioned correction factors, a reduced dipole moment is required. Lucas defined this quantity as

$$\sigma_r = 1.75216 \times 10^{-29} \frac{\sigma^2 P_c}{T_c^2} \quad \text{(A-9)}$$

Then F_P^0 values are found as:

$$\begin{aligned} F_P^0 &= 1 && 0 \le \sigma_r < 0.022 \\ F_P^0 &= 1 + 30.55(0.292 - z_c)^{1.72} && 0.022 \le \sigma_r < 0.075 \\ F_P^0 &= 1 + 30.55(0.292 - z_c)^{1.72} \left|0.96 + 0.1(T_r - 0.7)\right| && 0.075 \le \sigma_r \end{aligned} \quad \text{(A-10)}$$

The factor F_Q^0 is used only for quantum gases He, H_2 and D_2.

$$F_Q^0 = 1.22Q^{0.15}\left\{1 + 0.00385\left[(T_r - 12)^2\right]^{1/M_w}\left|T_r - 12\right|\right\} \quad \text{(A-11)}$$

For Non Quantum gases, $F_Q^0 = 1$

If $(1 < T_r < 40)$ and $(0 < P_R \le 100)$, then

$$Z_2 = \mu^0 \xi \left[1 + \frac{aP_r^e}{bP_r^f + (1 + cP_r^d)^{-1}}\right] \quad \text{(A-12)}$$

where $\mu^\circ\xi$ is found from Equation (A-8). The values of the constants in Equation (A-12) are defined as follows:

$$a = \frac{1.245\times10^{-3}}{T_r} e^{5.1726 T_r^{-0.3286}}$$
$$b = a\left(1.6553 T_r - 1.2723\right)$$
$$c = \frac{0.4489}{T_r} e^{3.0578 T_r^{-37.7332}}$$
$$d = \frac{1.7368}{T_r} e^{2.2310 T_r^{-7.6351}} \quad \text{(A-13)}$$
$$e = 1.3088$$
$$f = 0.9425 e^{-0.1853 T_r^{0.4489}}$$

After computing Z_1 and Z_2, we define

$$Y = \frac{Z_2}{Z_1} \quad \text{(A-14)}$$

And the correction factors F_P and F_Q

$$F_P = \frac{1+(F_P^0-1)Y^{-3}}{F_P^0} \quad \text{(A-15)}$$

$$F_Q = \frac{1+(F_Q^0-1)\left[Y^{-1}-0.007(\ln Y)^4\right]}{F_Q^0} \quad \text{(A-16)}$$

Finally, the dense gas viscosity is calculated as

$$\mu = \frac{Z_2 F_P F_Q}{\xi} \quad \text{(A-17)}$$

Where

$$\xi = 0.176\left(\frac{T_c}{M_w^3 P_c^4}\right)^{1/6} \quad \text{(A-18)}$$

Methanol density data is taken from NIST data (Xiang et al., 2006), where viscosity is presented as a function of temperature.

Increasing the pressure over a liquid results in an increase in viscosity. The viscosities of triolein, diglyceride, mono-glyceride, glycerol and fatty acid methyl esters at high pressures are estimated by high-pressure liquid Lucas method (Lucas, 1981). In which data of a reference viscosity at atmospheric pressure is used. The change may be estimated by the

$$\frac{\eta}{\eta_{SL}} = \frac{1 + D(\Delta P_r / 2.118)^A}{1 + C\omega\Delta P_r} \quad \text{(A-19)}$$

Where

η = viscosity of the liquid at a high pressure P

η_{SL} = viscosity of saturated liquid at atmospheric pressure

$\Delta P_r = (P - P_{vp}) / P_c$

The reference viscosity for diglyceride is calculated by Joback and Reid, (1987) method. The reference data for each of the species is given in The viscosity data at high pressures are estimated as a function of temperature to up to about 523 K.

Compound	**Reference viscosity (Pa.s)**	**Temperature (K)**	**Reference**
Triolein	0.00494	373.15	(Anitescu and Bruno, 2012)
Diglyceride	0.007434	373.15	(Joback and Reid, 1987)
Mono-glyceride	0.00088442	373.15	(DIPPR, 2010)
Glycerol	0.01483	373.15	(Cheng, 2008)
Fatty acid methyl esters	0.00159	373.15	(Yuan et al., 2003)

Table A-1 Reference viscosity data for the high pressure Lucas method

A.2.1 Mixture viscosity

The mixture density is estimated by the CFD solver by mass fraction average of pure species viscosities Equation (A-7), which is for non-ideal gas mixtures and assumes no molecular interactions.

$$\mu = \sum_i Y_i \mu_i \quad \text{(A-20)}$$

For the flow through cylinder with conditions mentioned earlier in this chapter, with temperature profiles shown in *Figure A-2*. The *Figure A-5* shows the variation of mixture density at 200 bar with temperature on the cylinder axis along the length. The composition of

the mixture (mass fractions) is also shown. A comparison was made of correlations of the properties of a tertiary mixture of carbon dioxide, methanol and triolein with data from the CFD solver. A parity plot for this is shown in *Figure A-6*

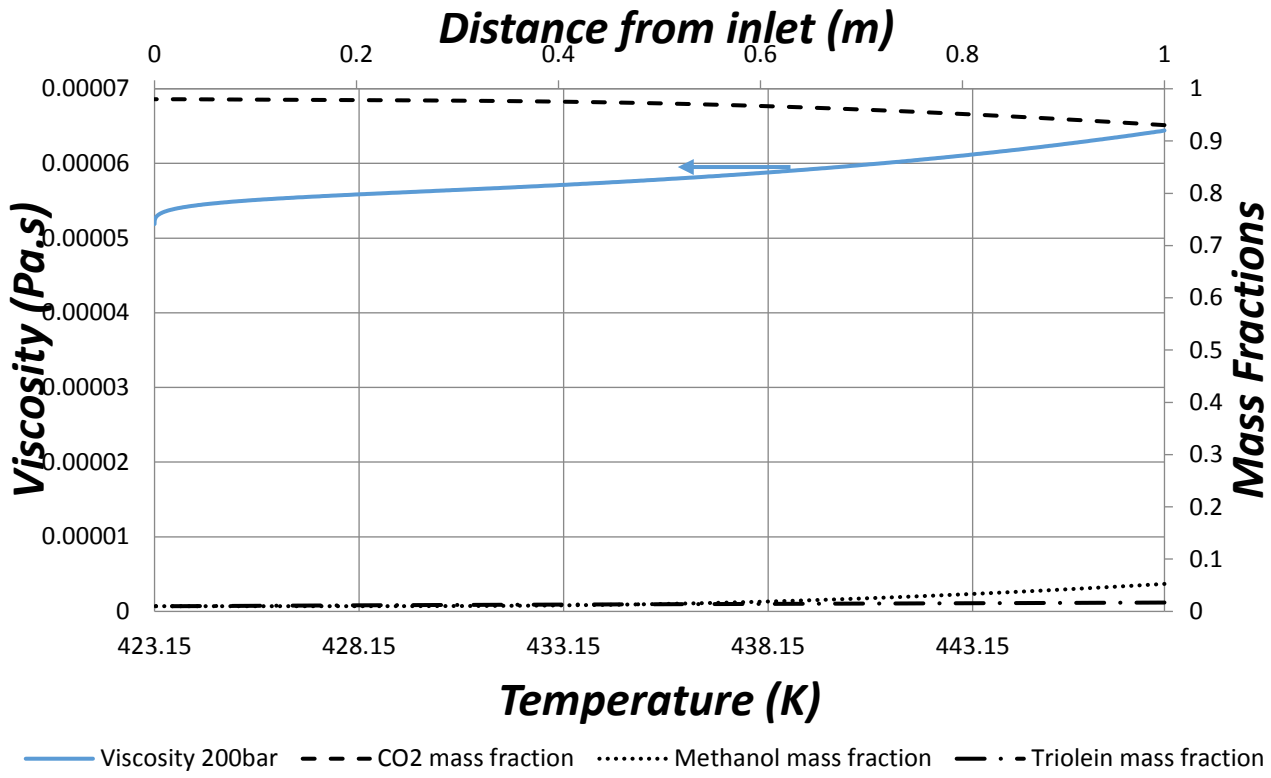

Figure A-5 CFD estimated mixture viscosities along the cylinder axis

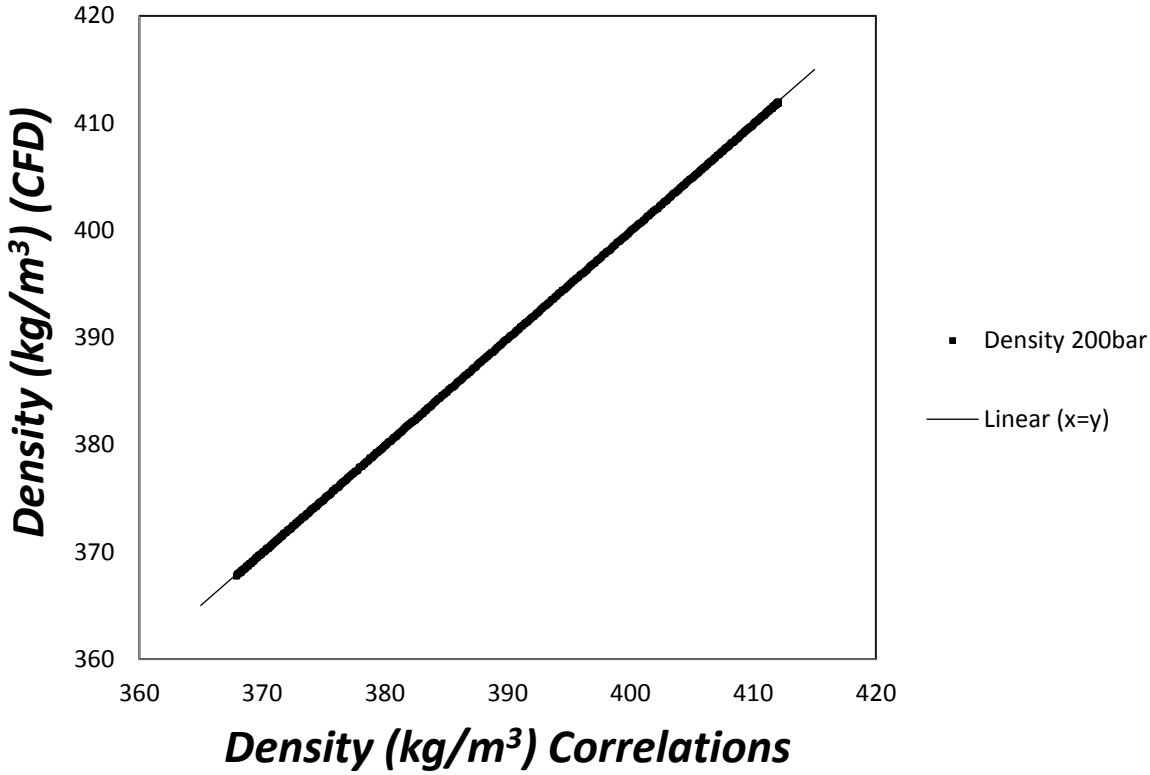

Figure A-6 Parity plot for viscosities obtained using CFD and viscosities obtained using the models for pure components, both methods use volume-weighted mixing rule.

A.3 SPECIFIC HEAT ESTIMATION

For high pressures it was chosen to define the heat capacity relating it to the value in the ideal-gas state, at the same temperature and composition:

$$C_p = C_p^0 + \Delta C_p \tag{A-21}$$

Where

C_p^0 = ideal gas heat capacity constant

ΔC_p = residual heat capacity, is determined by Equation (A-22) (Modell and Reid, 1983)

$$\Delta C_p = T\int_{\infty}^{V}\left(\frac{\partial^2 P}{\partial T^2}\right)dV - \frac{T\left(\partial P/\partial T\right)_V^2}{\left(\partial P/\partial V\right)_T} - R \tag{A-22}$$

The specific heat capacity data for methanol is from Goodwin, (1987) in which computations for thermal properties were made in the homogeneous domain with ideal gas state function at zero domain, and then numerically integrated along isotherms using an equation of state for change in heat capacity.

Heat capacities for triolein, diglyceride, mono-glyceride, glycerol, and fatty acid methyl esters is calculated by a group contribution method by Ruzicka and Domalski, (1993).

$$C_{pL} = R\left[A + B\frac{T}{100} + D\left(\frac{T}{100}\right)^2 \right] \tag{A-23}$$

Where R is the gas constant and T is temperature in K. The parameters A, B, and D are obtained from

$$A = \sum_{i=1}^{k} n_i a_i \qquad B = \sum_{i=1}^{k} n_i b_i \qquad D = \sum_{i=1}^{k} n_i d_i \tag{A-24}$$

Where n_i is the number of groups of type *i*, *k* is the total number of different types of groups, and the parameters a_i, b_i, and d_i are group specific and obtained from Ruzicka and Domalski, (1993)

The ideal-gas specific heat is obtained at atmospheric pressure and by corresponding states method for liquid C_p

$$\frac{C_p - C_p^o}{R} = 1.586 + \frac{0.49}{1-T_r} + \omega\left[4.2775 + \frac{6.3(1-T_r)^{1/3}}{T_r} + \frac{0.4355}{1-T_r} \right] \tag{A-25}$$

For higher pressures, the specific heat is obtained from the ΔC_p, residual heat capacity Equation (A-25). The mixture specific heat capacity, in the CFD solver is calculated by the mass fraction average of pure species heat capacities, given by the

$$C_p = \sum_i Y_i C_{pi} \tag{A-26}$$

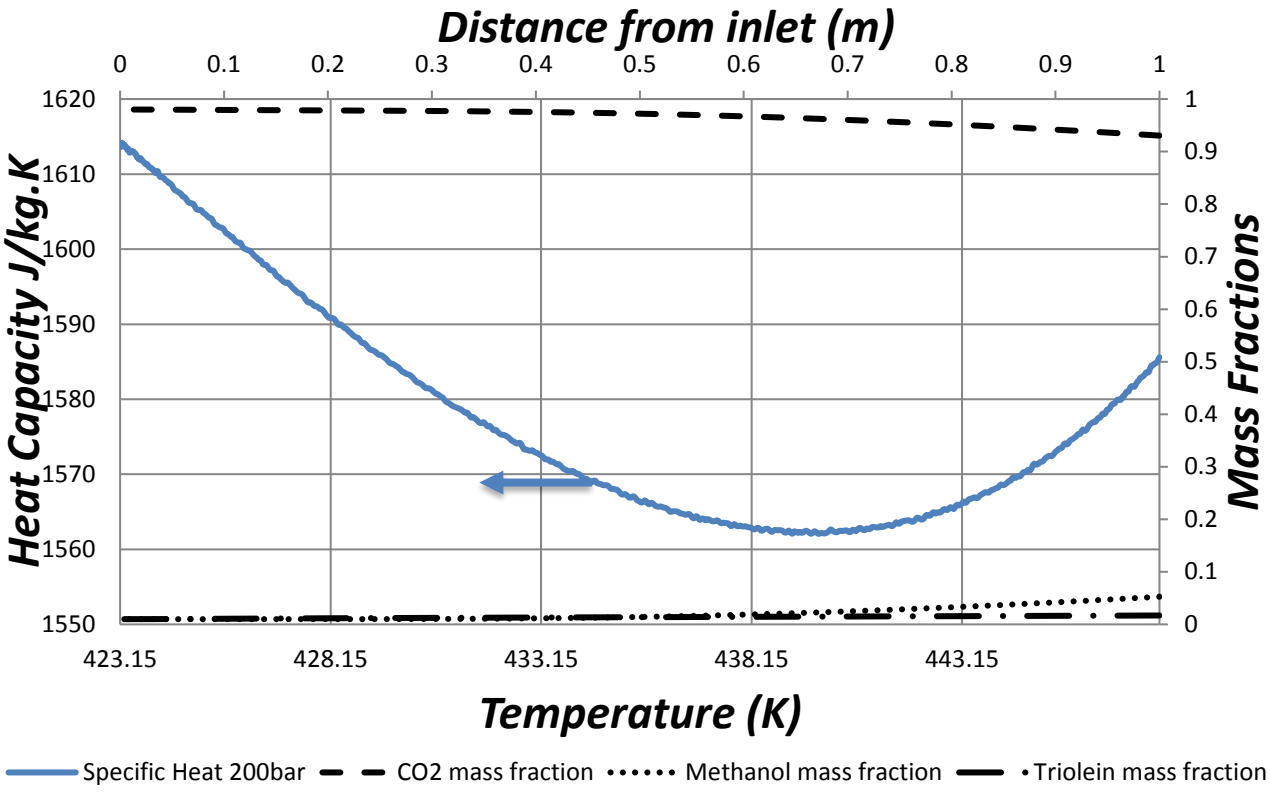

Figure A-7 CFD estimated tertiary mixture heat capacities along the cylinder axis

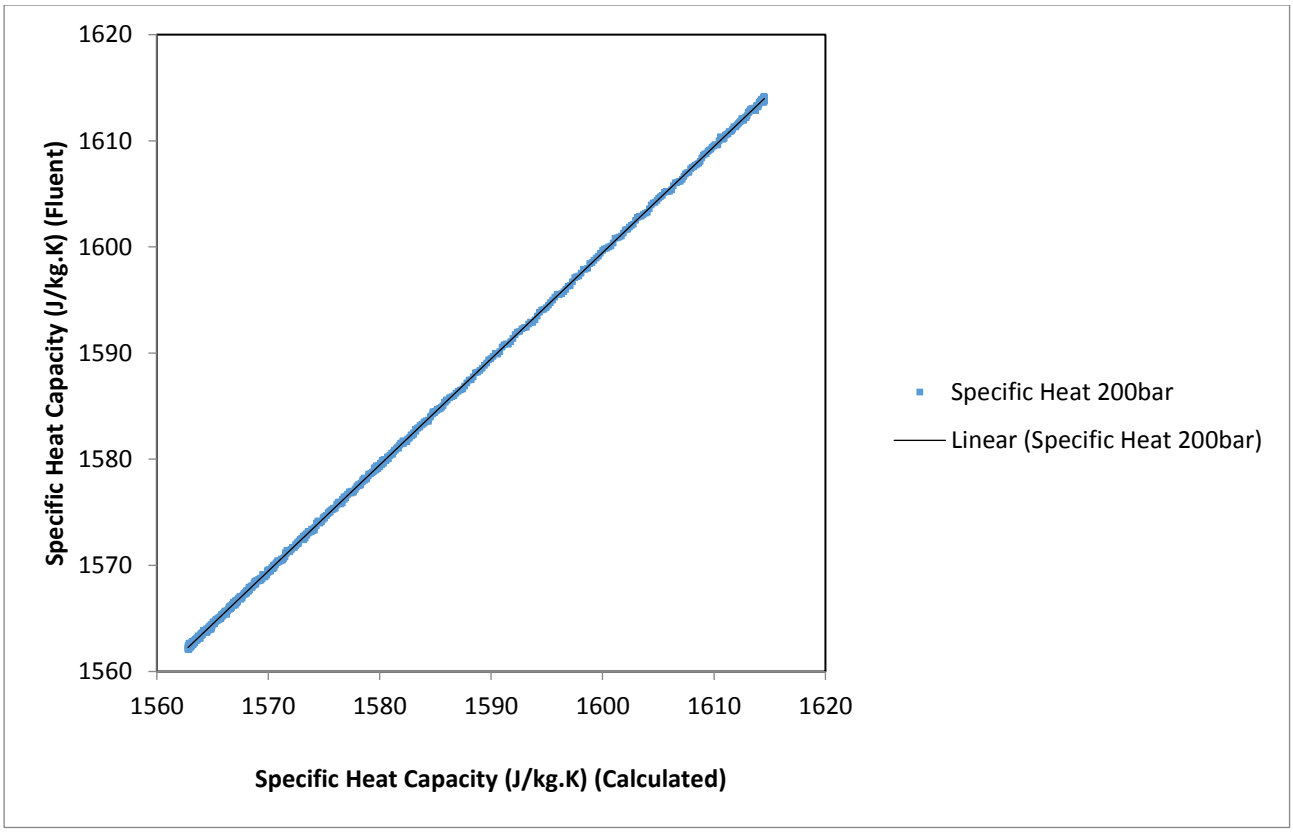

Figure A-8 Parity plot of heat capacities obtained using CFD and densities obtained using the models for pure components

A.4 THERMAL CONDUCTIVITY FOR HIGH PRESSURES

For supercritical fluids the thermal conductivity is estimated using excess thermal correlations (Stiel and Thodos, 1964), which depends on reduced density:

$$\left(k-k^0\right)\Gamma z_c^5 = 1.22\times10^{-2}\left(e^{0.535\rho_r}-1\right) \qquad \rho_r < 0.5 \qquad \text{(A-27)}$$

$$\left(k-k^0\right)\Gamma z_c^5 = 1.14\times10^{-2}\left(e^{0.67\rho_r}-1.069\right) \qquad 0.5 < \rho_r < 2.0 \qquad \text{(A-28)}$$

$$\left(k-k^0\right)\Gamma z_c^5 = 2.60\times10^{-3}\left(e^{1.155\rho_r}+2.016\right) \qquad 2.0 < \rho_r < 2.8 \qquad \text{(A-29)}$$

where

$$\Gamma = \left[\frac{T_c M_w^3 N_0^2}{R^5 P_c^4}\right]^{1/6} \qquad \text{(A-30)}$$

At atmospheric pressure, for methanol, triolein, diglyceride, mono-glyceride, glycerol, and fatty acid methyl esters, the thermal conductivity at atmospheric pressure is estimated by a method proposed by Latini and coworkers (Baroncini et al., 1980):

$$\lambda_L = \frac{A(1-T_r)^{0.38}}{T_r^{1/6}} \qquad \text{(A-31)}$$

Where

$$A = \frac{A^* T_b^{\alpha}}{M^{\beta} T_c^{\gamma}} \qquad \text{(A-32)}$$

λ_L = thermal conductivity of the liquid, W/(m.K)

T_b = normal boiling point (at 1 atm), K

T_c = critical temperature, K

M = molecular weight, g/mol

$T_r = T/T_c$

And the parameters A^*, α, β, and γ are specific for various classes of organic compounds.

For effect of pressure on thermal conductivity, Missenard, (1970) has proposed a simple correlation for λ_L

$$\frac{\lambda_L(P_r)}{\lambda_L(lowpressure)} = 1 + QP_r^{0.7} \quad \text{(A-33)}$$

λ_L *(Pr)* λ_L (low pressure) refer to the liquid thermal conductivities at high and low pressures. The values of Q are dependent on reduced temperature and reduced pressure, are shown in

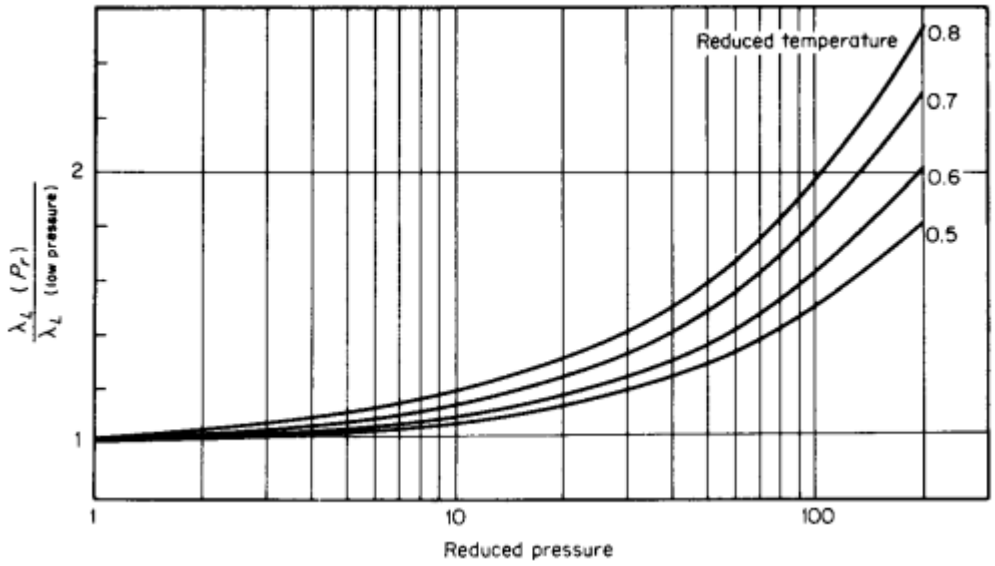

Figure A-9 Missenard, (1970) correlation for liquid thermal conductivities at higher pressures

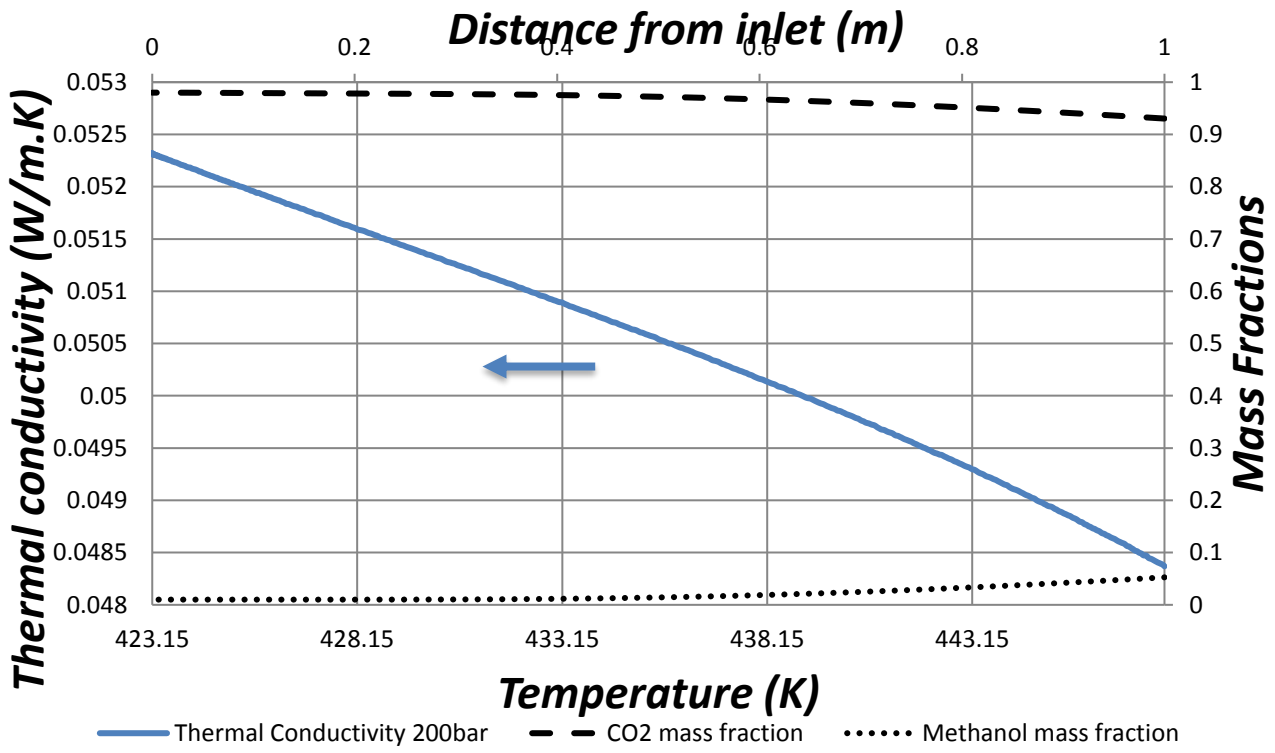

Figure A-10 CFD estimated tertiary mixture thermal conductivities along the cylinder axis at 200 bar

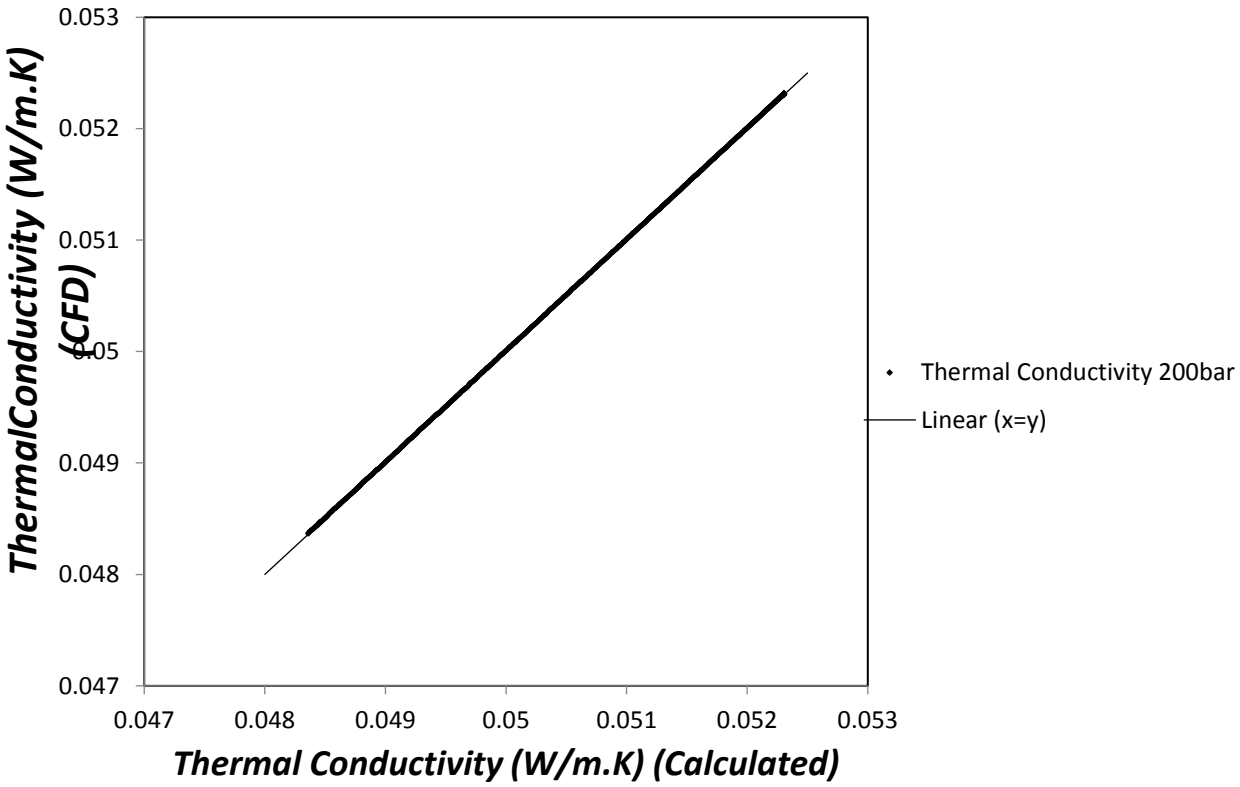

Figure A-11 Parity plot of thermal conductivities obtained using CFD and using the models for pure components

A.5 DIFFUSION COEFFICIENTS

The knowledge of binary diffusion coefficients of solutes in liquid or supercritical solvent is required for any equipment design and process development. When there is lack of data especially at high pressures and temperatures for supercritical solvents, it's important to be able to make a good estimate of the diffusion coefficients.

In estimating the mass diffusivities for the transesterification system, it was chosen to have dilute approximation diffusivity coefficients in which CO_2 is taken as the "carrier" fluid, which is in higher concentrations relative to the other component species.

The diffusion of solute (2) into supercritical solvent CO_2 (1) is given by an equation (A-34)for infinite-dilution mass diffusion coefficients in supercritical solvents proposed by (He and Yu, 1998).

$$D_{21} = A * 10^{-9} \sqrt{\frac{T}{M_2}} \exp\left(-\frac{\gamma' V^*}{V_1 - 0.23 V_{c_1}}\right) \quad \text{(A-34)}$$

Where

M_2 = molecular mass of solute

γ' = numerical factor to correct for overlap of free volume

V^* = critical hole volume

V_1 = molar volume of solvent

V_{c_1} = critical molar volume of solvent

The parameters A and $\gamma' V^*$ must be related to the solute-solvent properties. By analysis, these could be approximated as:

$$\gamma' V^* = 0.3889 V_{c_1} \quad \text{(A-35)}$$

$$A = 14.882 + 5.9081k + 2.0821k^2 \quad \text{(A-36)}$$

$$k = \frac{T_{c_1} V_{c_1}}{1000 M_1} \quad \text{(A-37)}$$

The molar volume V_1 for CO_2 at supercritical conditions is estimated from compressibility factor of Redlich-Kwong equation of state shown in Equation (A-2).

Diffusivity of triolein to near critical CO_2 by this method for 251 bar and 308.1K as 3.621E-9m^2/s was compared against experimental data 3.55±0.37E-9m^2/s (Owen J. Catchpole and King, 1994). And the error estimated as 1.97%.

$$Error\% = \left(\frac{3.62 - 3.55}{3.55}\right) * 100 = 1.97\% \quad \text{(A-38)}$$

The diffusion coefficients of solutes to supercritical solvent CO_2 estimated for 250 bar pressure are tabulated below in *Table A-2*.

	478.15 K	**453.15 K**	**423.15 K**
Methanol	5.0470E-08	4.6235E-08	4.0604E-08
Triolein	9.6053E-09	8.7993E-09	7.7277E-09
Glycerol	2.9769E-08	2.7271E-08	2.3950E-08
Mono-glyceride	1.5129E-08	1.3860E-08	1.2172E-08
Diglyceride	1.1464E-08	1.0502E-08	9.2232E-09
Fatty acid methyl esters	1.6591E-08	1.5199E-08	1.3348E-08

Table A-2 Diffusion coefficients (m^2/s) estimated for 250 bar by He and Yu, (1998) equation

REFERENCES

Acosta, G.M., Smith, R.L., Arai, K., 1996. High-Pressure PVT Behavior of Natural Fats and Oils , Trilaurin , Triolein , and n-Tridecane from 303 K to 353 K from Atmospheric Pressure to 150 MPa. J. Chem. Eng. Data 9568, 961–969. doi:10.1021/je960006x

Anitescu, G., Bruno, T.J., 2012. Fluid properties needed in supercritical transesterification of triglyceride feedstocks to biodiesel fuels for efficient and clean combustion – A review. J. Supercrit. Fluids 63, 133–149. doi:10.1016/j.supflu.2011.11.020

Baroncini, C., Filippo, P. Di, Latini, G., Pacetti, M., 1980. An improved correlation for the calculation of liquid thermal conductivity. Int. J. Thermophys. 1, 159–175. doi:10.1007/BF00504518

Catchpole, O.J., King, M.B., 1994. Measurement and Correlation of Binary Diffusion Coefficients in Near Critical Fluids. Ind. Eng. Chem. Res. 33, 1828–1837. doi:10.1021/ie00031a024

Cheng, N.-S., 2008. Formula for the Viscosity of a Glycerol−Water Mixture. Ind. Eng. Chem. Res. 47, 3285–3288. doi:10.1021/ie071349z

DIPPR, 2010. (Design Institute for Physical Property Data) - full version [Internet]. Am. Inst. Chem. Eng.

Goodwin, R.D., 1987. Methanol Thermodynamic Properties From 176 to 673 K at Pressures to 700 Bar. J. Phys. Chem. Ref. Data 16, 799–892.

He, C.-H., Yu, Y.-S., 1998. New Equation for Infinite-dilution diffusion coefficients in supercritical and high-temperature liquid solvents. Ind. Eng. Chem Res. 37, 3793–3798. doi:10.1016/S0378-3812(98)00239-8

Joback, K.G., Reid, R.C., 1987. ESTIMATION OF PURE-COMPONENT PROPERTIES FROM GROUP-CONTRIBUTIONS. Chem. Eng. Commun. 57, 233–243.

Lucas, K., 1981. No Title. Chem. Ing. Tech 53, 959.

Lucas, K., 1980. Phase Equilibriua and Fluid Properties in the Chemical Industry, in: Dechema, Frankfurt. p. 573.

Missenard, A., 1970. No Title. Rev. Gen. Thermodyn 101, 649.

Modell, M., Reid, R.C., 1983. Thermodynamics and its Applications.

Poling, B.E., Prausnitz, J.M., 2001. THE PROPERTIES OF GASES AND LIQUIDS, McGraw-Hill. McGraw-Hill. doi:10.1036/0070116822

Redlich, O., Kwong, J., 1949. On the thermodynamics of solutions V: an equation of state. Fugacities of gaseous solutions. Chem. Revews 44, 233–244.

Ruzicka, V., Domalski, E.S., 1993. No Title. J. Phys. Chem. Ref. Data 22, 597.

Stiel, L.I., Thodos, G., 1964. The thermal conductivity of nonpolar substances in the dense gaseous and liquid regions. AIChE J. 10, 26–30.

Xiang, H.W., Laesecke, A., Huber, M.L., 2006. A New Reference Correlation for the Viscosity of Methanol. J. Phys. Chem. Ref. Data 35, 1597. doi:10.1063/1.2360605

Yuan, W., Hansen, A.C., Zhang, Q., 2003. Predicting the Physical Properties of Biodiesel For Combustion Modeling. Trans. ASAE 46, 1487–1493.

B. CONFERENCE PROCEEDINGS

8th European Congress of Chemical Engineering

CFD Study on Flow Effects in the Production of Biodiesel Using a Dense Gas as Solvent Media – Preliminary Flow Results

Samuel Mekala, Alfredo Guardo, M. Angels Larrayoz.

Berlin, September 2011

Abstract

Biodiesel production processes are traditionally carried out using a base (KOH, NaOH) or an acid (H_2SO_4) as homogeneous catalysts. Usually these processes are performed in batches and they require of different separation stages (glycerol, catalyst, etc.) until obtaining the Fatty Acid Methyl Esters (FAMEs) that compose the biodiesel; in addition, these FAMEs in the presence of a basic catalyst can produce soap, reducing the reaction yield and difficulting the separation processes.

Carrying out the biodiesel production reaction using a solid acid catalyst (SAC-13) and a dense gas, composed by a mixture of CO_2/Methanol (75/25 w/w), as a solver in a fixed bed reactor allows to eliminate different separation stages, obtaining FAMEs reaction yields of 86% and with a glycerol content lower than the provided by the legal regulations.

Flow effects are of primal importance when dealing with a dense gas. The aim of this work is to study the effects of the flow pattern over catalyst particles in the production of biodiesel by means of Computational Fluid Dynamics (CFD). The effect of flow velocity and direction over reaction rates and yields are analyzed. Reaction kinetics used in the computational model were obtained from previous experimental work. Properties for the dense gas (density, viscosity) and diffusion coefficients are estimated from empirical correlations and built into the computational model via user defined functions.

10th Conference on Supercritical Fluids and their Applications

Evaluation of Physical Properties of a Supercritical Tertiary Mixture Using CFD

Samuel Mekala, Alfredo Guardo, M. Angels Larrayoz.

Naples, May 2013

Abstract

Computational fluid dynamics (CFD) methods for simulating flow conditions in contacting equipment have proven to be sufficiently accurate in modeling their performance. The extension of this method to supercritical flow conditions and mixtures of chemically reactive species is useful for wide applications.

The mixture of CO_2-methanol-triolein at supercritical conditions, where CO_2 acts as a cosolvent to reduce operating conditions such as pressure and temperature, is mainly of interest in trans-esterification reactions. Preliminarily, estimation of the physical properties of this mixture using CFD may help asset the viability of this using it in simulating the packed-bed reactor required for the aforementioned reaction.

In this work, physical properties of a tertiary supercritical mixture of CO_2, methanol and triolein were obtained using a CFD pipe flow model. Supercritical CO_2 (at reaction pressure and temperature) was taken to be the circulating fluid. Methanol and triolein diffusive flows were imposed through the pipe walls.

Navier-Stokes equations along with an equation of state and the pure species physical properties and diffusion models were solved by the finite volumes algorithm. The fluid was considered to be Newtonian, compressible and in laminar regime.

Values obtained using the CFD model were compared against the mixture properties estimated using a cubic equation of state and suitable correlations for obtaining physical property values in supercritical conditions, obtaining a good agreement as a result.

68th Annual Session of Indian Institute of Chemical Engineers

Wall-to-Fluid Heat transfer in a catalytic reactor under supercritical conditions

Samuel Mekala, Alfredo Guardo, M. Angels Larrayoz.

Guwahati, December 2015

Abstract

Packed beds are widely used in chemical industries due to their simplicity in structure and effectiveness in terms of providing abundant contact area for surface reaction or for heat or

mass transfer area. The study of heat transfer rate in packed beds is important not only important for design of heat exchangers but also for catalytic reactors.

For a cylindrical packed bed operated as a steady-state heat exchanger, the steady state temperatures at different locations in the bed can be described by a two-dimensional pseudo-homogeneous model,

The use of computational fluid dynamics to simulate the fluid flow and heat transfer phenomena is becoming a standard approach for fluid flow phenomena. Finite volumes methods CFD codes are accurate in application to complex geometries like packed beds. Derkx and Dixon, (1996) have used CFD in a packed bed by solving 3D Navier-Stokes equations, reporting Nuw values. Guardo et al., (2006) have done similar studies for randomly packed beds later. CFD method can also be used for the development of heterogeneous model as a replacement for the pseudo-continuum idealization (Pedernera et al., 2003). Fixed bed models have been usually developed for high tube-to-particle diameter ration (N) beds, in which temperature gradients are less and could be averaged.

The fluid, mixture of carbon dioxide (CO_2), methanol (CH_3OH) and triolein ($C_{57}H_{104}O_6$), (reactants for transesterification reaction with supercritical solvent CO2) is flown into the packed bed at 250 bar, is taken to be Newtonian, in laminar flow. Pure component properties are taken at this pressure as a function of temperature. The mixture properties are based volume weighted for density and specific heat, and mass weighted average for thermal conductivity and viscosity. The fluid mixture enters at temperature 473.15K and the wall is heated at temperature 483.15K. The heat transfer coefficient is correlated in terms of Nusselt number. Figure (2). Wall Nusselt numbers are plotted against Re for different flow rates, and compared against empirical models.